CORA Cork Open Research Archive
Cartlann Taighde Oscailte Chorcaí

Title	The design, synthesis and characterisation of selected chitosan-based thin films and studies of their use as materials for antimicrobial, heavy metal adsorption, and wound dressing applications
Authors	Pemble, Oliver James
Publication date	2022-09
Original Citation	Pemble, O. J. 2022. The design, synthesis and characterisation of selected chitosan-based thin films and studies of their use as materials for antimicrobial, heavy metal adsorption, and wound dressing applications. PhD Thesis, University College Cork.
Type of publication	Doctoral thesis
Rights	© 2022, Oliver James Pemble. - https://creativecommons.org/publicdomain/zero/1.0/
Download date	2026-11-07 02:13:34
Item downloaded from	https://hdl.handle.net/10468/14519

UCC
University College Cork, Ireland
Coláiste na hOllscoile Corcaigh

Ollscoil na hÉireann, Corcaigh

National University of Ireland, Cork



The Design, Synthesis and Characterisation of Selected Chitosan-Based Thin Films and Studies of their use as Materials for Antimicrobial, Heavy Metal Adsorption, and Wound Dressing Applications

Thesis presented by

Oliver James Pemble, MSc

for the degree of

Doctor of Philosophy

University College Cork

School of Chemistry

Head of School/Department: Dr Humphrey Moynihan

Supervisor(s): Dr Maria Bardosova, Dr Ian Povey

2022

Table of Contents

1. Introduction 1

1.1 What is chitosan? Classification and properties 1

1.1.1 Properties of chitosan 2

1.1.2 Determination of degree of deacetylation 4

1.1.3 Determination of molecular weight 7

1.1.3.1 Static light scattering 7

1.1.3.2 Viscometry 8

1.1.3.3 Gel permeation chromatography 8

1.1.4 Viscosity 9

1.1.5 Solubility 10

1.1.5.1 Solution pH 10

1.1.5.2 Molecular weight 11

1.1.5.3 Number of N-acetyl-glucosamine units 11

1.2 How chitosan is made 12

1.2.1 Industrial synthesis of chitosan 12

1.3 Modifications of chitosan 16

1.3.1 Interpenetrating Polymer Networks and polymer blends 16

1.3.2 History of IPNs 18

1.3.3 Applications of IPNs 19

1.3.3.1 Biomedical research 19

1.3.3.2 Sorptive materials 19

1.4 Applications of chitosan and chitosan-based films 21

1.4.1 Chitosan in heavy metal sorption 22

1.4.2 Biological activities of chitosan 27

1.4.2.1 Antimicrobial activity 27

1.4.2.2 Antioxidant activity 30

1.4.2.3 Biomedical applications of chitin and chitosan 30

1.5 Preamble to the remaining sections of this thesis 32

References 33

2. Materials and Methods 50

2.1 Hydrogel recipes and ratios 50

2.1.1 Preparation of chitosan-based hydrogels 50

2.1.1.1 Chi-TEOS 51

2.1.1.2 Chi-GA 53

2.1.1.3 Chi-APTES 57

2.1.1.4 Chi-PAM 59

2.1.2 Preparation, casting and drying of films 61

2.1.2.1 Drop-casting films 61

2.1.2.2 Preparation of films using a slot-die method (refer to Chapter 4) 62
2.2 Analysis and characterisation 64
2.2.1 Spectroscopy 64
2.2.2 Mechanical strength 64
2.3 Heavy metal adsorption studies (performed in conjunction with staff and students from the Faculty of Natural Sciences at Comenius University, Bratislava - see Chapter 5) 66
2.3.1 Swelling characteristics 66
2.3.2 Adsorption capacity 66
2.4 Antimicrobial studies (performed in conjunction with staff and students from the Microbiology Department at UCC - see Chapter 6) 67
2.4.1 Materials 67
2.4.2 Method 67
2.4.2.1 LB broth 67
2.4.2.2 Brain Heart Infusion broth 68
2.4.3 T-streak method 68
2.4.3.1 Inoculation of chitosan samples 69
2.4.4 Optical Density measurements 70
2.5 Wound dressing design and testing (performed in conjunction with staff from the National Institute for Materials Science, Tsukuba - see Chapter 7) 71
2.5.1 Sample preparation and thickness measurements 71
2.5.2 Photonic crystal film fabrication 73
References 75
3. The Structural and Mechanical Characterisation of Chitosan-Based Films 78
3.1 Film appearance and composition 79
3.2 FT-IR spectroscopic analysis of chitosan-based films 82
3.2.1 Chitosan and Chi-TEOS 83
3.2.2 Chi-GA 84
3.2.3 Chi-APTES 85
3.2.4 Chi-PAM 85
3.3 Mechanical strength tests 86
3.3.1 Stress-strain curve 86
3.3.2 Tensile strength results 88
3.3.2.1 Chitosan 91
3.3.2.2 Chi-TEOS 92
3.3.2.3 Chi-APTES 94
3.3.2.4 Chi-GA 95
3.3.2.5 Chi-PAM 96
3.4 Discussion 99
3.5 Conclusions 101
References 102

4. A Slot-Die Technique for the Preparation of Continuous, High-Area, Chitosan-Based Thin Films 105
4.1 Introduction 105
4.2 Materials and Methods 108
4.2.1 Slot-die casting via a doctor blade apparatus 108
4.2.2 The preparation of chitosan-based hydrogels 109
4.2.3 Tensile strength tests 113
4.3 Results 114
4.3.1 Slot-die film casting 114
4.3.2 Tensile strength tests 115
4.4 Discussion 118
4.5 Conclusions 121
References 122
5.1 Introduction 126
5.1.1 Heavy metal pollution 126
5.1.2 Chitosan-based materials for heavy metal adsorption 127
5.2 Methods 129
5.2.1 Swelling characteristics 129
5.2.2 Adsorption experiments 129
5.3 Results 132
5.3.1 Evaluation of swelling characteristics 132
5.3.2 Evaluation of the optimum pH for the $^{99m}TcO_4^-$ adsorption process 134
5.3.3 Adsorption of pertechnetate ions 136
5.3.4 Adsorption Isotherms and possible adsorption mechanisms 140
5.3.4.1 Langmuir Isotherm straight-line plot derivation 143
5.3.4.1 Freundlich Isotherm straight-line plot derivation 144
5.4 Conclusions 147
References 149
6. A preliminary study on the antibacterial properties of selected chitosan-based films 153
6.1 Introduction 153
6.1.1 Bacteria 153
6.1.1.1 Bacterial growth and attachment 154
6.1.1.2 Bacteria subgroups 155
6.1.2 Antibacterial materials 158
6.1.3 Chitosan antibacterial activity 159
6.2 Methods 161
6.2.1 Basic methodology for antimicrobial studies 161
6.2.2 Determination of bacteriological activity using Optical Density measurements 161
6.3 Results and discussions 162
6.3.1 pH of bacterial cultures 162

6.3.2 Optical Density measurements ... 163
6.3.3 Bacterial attachment ... 164
6.3.4 Bacterial growth ... 166
6.4 Conclusions ... 168
References ... 170
7. Demonstration of a Chitosan-Based, pH-Responsive, Smart Material for Potential Wound Dressing Applications ... 178
7.1 Introduction ... 178
7.2 Introduction to smart wound dressings ... 178
7.2.1 What are smart wound dressings? ... 179
7.2.2 Chronic wounds ... 179
7.2.3 Ideal properties of smart wound dressings ... 181
7.2.4 Scope of this work ... 182
7.3 Synthesis and characterisation of the chitosan films ... 184
7.3.1 Swelling tests of free-standing drop-cast films ... 186
7.3.2 Synthesis of the flexible polystyrene colloidal photonic crystal films ... 187
7.3.3 Proposed mechanism of colour change, flexible photonic crystals ... 188
7.3.4 Characterisation of the test structures ... 191
7.4 Sensor testing ... 193
7.4.1 Optical spectroscopy ... 194
7.5 Results – Observed variations in stop band ... 195
7.5.1 Chitosan films – neutral pH ... 195
7.5.2 Chi-APTES (2:1) – variation in stop band position as a function of pH ... 197
7.5.3 Chi-GA (8:1) – variation in stop band position as a function of pH ... 199
7.6 Conclusions ... 201
References ... 202
8. Conclusions and suggestions for further work ... 208
8.1 Summary of work presented, and conclusions drawn ... 208
8.2 Suggestions for further work ... 211
Appendix ... 213
A.1 Chapter 2: Schematic of all chitosan film composites ... 213
A.2 Chapter 5: Swelling percentages ... 214
A.2.1 Chi-TEOS (1:1) ... 215
A.2.2 Chi-APTES (2:1) ... 215
A.2.3 Chi-GA (8:1) ... 216
A.2.4 Chi-PAM (1:1) ... 216
A.3 Chapter 5: Sorption efficiency on sample size and pH ... 217
A.3.1 Sample size ... 217
A.4 Chapter 5: Langmuir and Freundlich straight-line graphs ... 218
A.4.1 Langmuir straight-line graphs ... 218

A.4.1.1 Chi-TEOS 218
A.4.1.2 Chi-APTES 218
A.4.1.3 Chi-GA 219
A.4.1.4 Chi-PAM 219
A.4.2 Freundlich straight-line graphs 220
A.4.2.1 Chi-TEOS 220
A.4.2.2 Chi-APTES 220
A.4.2.3 Chi-GA 221
A.4.2.4 Chi-PAM 221
A.5 Chapter 6: Optical Density measurements 222
A.5.1 Chi-TEOS 1:1 222
A.5.2 Chi-APTES 2:1 222
A.5.3 Chi-PAM 1:1 223
A.5.4 Chi-GA 8:1 223
A.6 Chapter 7: Stop band peak centres 224
A.6.1 Chi-APTES 224
A.6.2 Chi-GA 227

Declaration

This is to certify that the work I am submitting is my own and has not been submitted for another degree, either at University College Cork or elsewhere. All external references and sources are clearly acknowledged and identified within the contents. I have read and understood the regulations of University College Cork concerning plagiarism and intellectual property.

Acknowledgments

I would like to sincerely thank my supervisors Dr Maria Bardosova and Dr Ian Povey for giving me the opportunity to pursue this PhD within the Advanced Materials and Surfaces Group at Tyndall National Institute. I would also like to thank my colleagues Dr Tomas Kohoutek, Dr Catherine Dwyer, and Dr Mikhail Parchine for their support and patience in the labs. I would like to express my gratitude to all associated research staff, postdocs, and students with whom I have worked with on various projects, particularly Dr Olga Rosskopfová and Andrea Hamárová from Comenius University Bratislava, Dr David Clarke, Rebecca Quinlan, and Ina Bremenkamp from University College Cork, and Dr Hiroshi Fudouzi from the National Institute for Materials Science in Tsukuba.

A very special thank you to my father, Prof Martyn Pemble, whose guidance and wisdom has kept me motivated throughout this PhD, I wouldn't have been able to do this without you.

Finally, a big thank you to my family and friends for always believing in me when I did not. To my sister, Daisy, whom I look up to, you inspire me. To my mother, Julie, who can always distil my anxieties, you never fail to cheer me up. To my wonderful fiancé, Liam, whose unrivalled positivity lights up my days, I cannot wait to marry you.

Abstract

Chitosan is a naturally-derived polymer, sourced from the chitin present in crustacean shells and insect exoskeletons. It is a highly diverse molecule, with heavy metal adsorption, antibacterial and pH-based swelling properties. However, these properties may be hindered by the lack of strength of a singular polymer structure. Chitosan has the ability to cross-link with other polymers or reagents to create interpenetrating polymer networks (IPNs) and blends to improve the mechanical strength or application mechanisms. These composites can be cast into films which have superior properties for the applications listed above.

The first half of this PhD thesis sets out to describe the process of synthesising thin films made from combining chitosan with cross-linking reagents and other polymer networks. These materials comprise two siloxane networks Tetraethyl-orthosilicate (TEOS) and 3-aminopropyltriethoxysilane (APTES), glutaraldehyde (GA), and the polymer polyacrylamide (PAM). Aqueous acidic solutions of low molecular weight chitosan were made and combined with one of the four materials at different ratios to produce hydrogels that could then be cast into thin films. These chitosan-based films were characterised as to their molecular structures via FT-IR spectroscopy and their mechanical elasticity/plasticity via tensile strength tests.

The method of casting the films was primarily drop-casting in a Petri dish and drying for 24 hours, but an alternative procedure that utilises a doctor blade slot-die head was also developed. This novel method was studied in-depth, and the findings were published. For this reason, the results of the slot-die casting studies are presented in their published form. Briefly, the slot-die casting technique produced high quality thin films of chitosan-based composites in under 2 hours. Further, there was no influence of the direction of travel of the films during deposition on their mechanical properties. This study served as a proof-of-concept that high volumes of chitosan-based films could be made quickly, cheaply, and reproducibly.

The second half of this thesis explores the applications of the composite chitosan-based films, by use of their adsorption, antimicrobial, and swelling abilities.

The adsorption of radioactive technetium pertechnetate $^{99m}TcO_4^-$ ions via chelation from solution was evaluated and correlated based on the Langmuir and Freundlich

isotherms. It was found that the chitosan-glutaraldehyde films showed the best ability to adsorb $^{99m}TcO_4^-$ ions and that a Langmuir-type, monolayer-based adsorption process was most likely in operation.

A preliminary study of the antimicrobial properties of the chitosan-based films was undertaken via Gram-negative and Gram-positive bacterial growth and attachment assays. The intent of the study was to test the antibacterial abilities of the films while also speculating as to the mechanism of said abilities. The chitosan-tetraethyl-orthosilicate films were found to be the most effective against both types of bacterial growth and attachment. However, the chitosan-glutaraldehyde films showed little-to-no antibacterial ability, suggesting the antibacterial mechanism may be affected by the cross-linking reagent.

Finally, a prototype for a smart wound dressing device that incorporates a pH sensitive sensor for chronic wounds was designed and developed using the chitosan-based films. The device utilised chitosan's natural swelling ability and colloidal photonic crystal technology to create an indicator that produced a visual colour change in response to fluctuating pH levels, which may occur in chronic wounds. The mechanism was based on the distortion of photonic crystal layers by the swelling of the chitosan-based films to give a distinct red to green colour change. This preliminary study shows the potential of chitosan /photonic crystal-based sensors for use in medical devices that do not require an external power source to operate.

1. Introduction

1.1 What is chitosan? Classification and properties

Chitosan is a non-toxic, semicrystalline, [1] and biodegradable [2, 3] commercially available polysaccharide that is derived from the deacetylation of the naturally occurring compound chitin. Chitin, (poly (1-4)-N-acetyl-D-glucosamine)), is a material that occurs as ordered crystalline microfibrils and is one of the primary components of arthropod exoskeletons due to its relatively resilient and pliable nature. [1] It is one of the most abundant natural polysaccharides in the world, second only to cellulose. [4] Chitin is a hard, white solid that is hydrophobic, insoluble in most organic solvents, has a low toxicity and is inert in the gastrointestinal tract of mammals; it is biodegradable. These properties allow the material to be applied in many areas of food science such as the immobilisation of enzymes and whole cells for fruit juice and milk processing. [1, 5] It has also been utilised in medical and pharmaceutical fields in the form of films and fibres for wound dressing materials and controlled drug release. [6, 7] However, chitin may be limited in application due to its poor solubility and is often converted to its deacetylated derivative, chitosan. [1, 8]

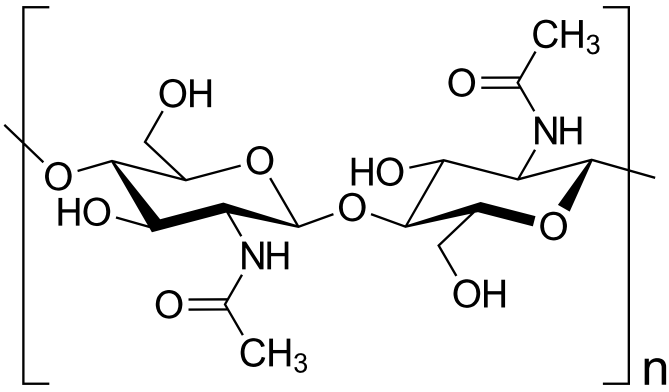


Figure 1.1: chemical structure of the chitin molecule showing the repeating N-acetyl-glucosamine units that form long chains.

1.1.1 Properties of chitosan

Chitosan is a polycation whose charge density depends on the degree of deacetylation and pH of the environment. Chitosan chains are able to interact electrostatically with negatively charged molecules such as nucleic acids [9] or polyphosphates. [10] These polycationic properties have paved the way for chitosan's application in biomedical and pharmaceutical fields, [11] such as drug delivery systems and tissue engineering. [12, 13] Moreover, the positive charge gives chitosan good mucoadhesive properties, [14] haemostatic properties that make it a good material for wound dressings, [15, 16] and antibacterial properties that limit the risk of infection. [16] In general, chitosan produced from chitin that is sourced from fungi present a narrow molecular weight distribution compared to chitosan produced from crustacean shells, and a non-animal source is considered to be safer for biomedical applications. [17, 18]

Chitin and chitosan are of commercial interest due to their high percentage of nitrogen compared to synthetically substituted cellulose. Unlike starch and cellulose, the chitosan macromolecule consists of such repeating units of 2-acetamido-2- deoxy-β-D-glucopyranose and 2-amino-2-deoxy- β-D-glucopyranose. These fragments connect each other across the β(1→4)-glucoside bonds. That is, chitosan is a poly(amino saccharide). [19]

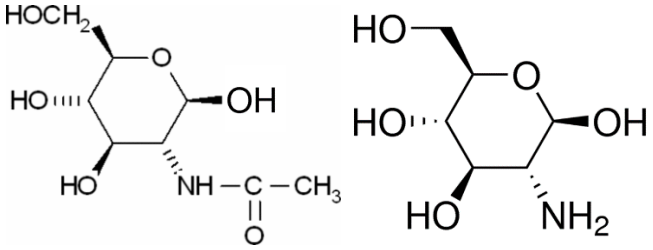


Figure 1.2: 2-acetamido-2- deoxy-β-D-glucopyranose unit (left) and 2-amino-2-deoxy- β-D-glucopyranose unit (right)

Few biological polymers have such a high content of primary amines and hydroxyl groups which can be used for chemical modification. Chemical modifications of chitin are generally difficult owing to the lack of solubility, so with regard to developing advanced functions, chitosan is the primary focus. [20] Figure 1.3 shows the growing interest in chitosan research compared to chitin, taken from the SCOPUS database.

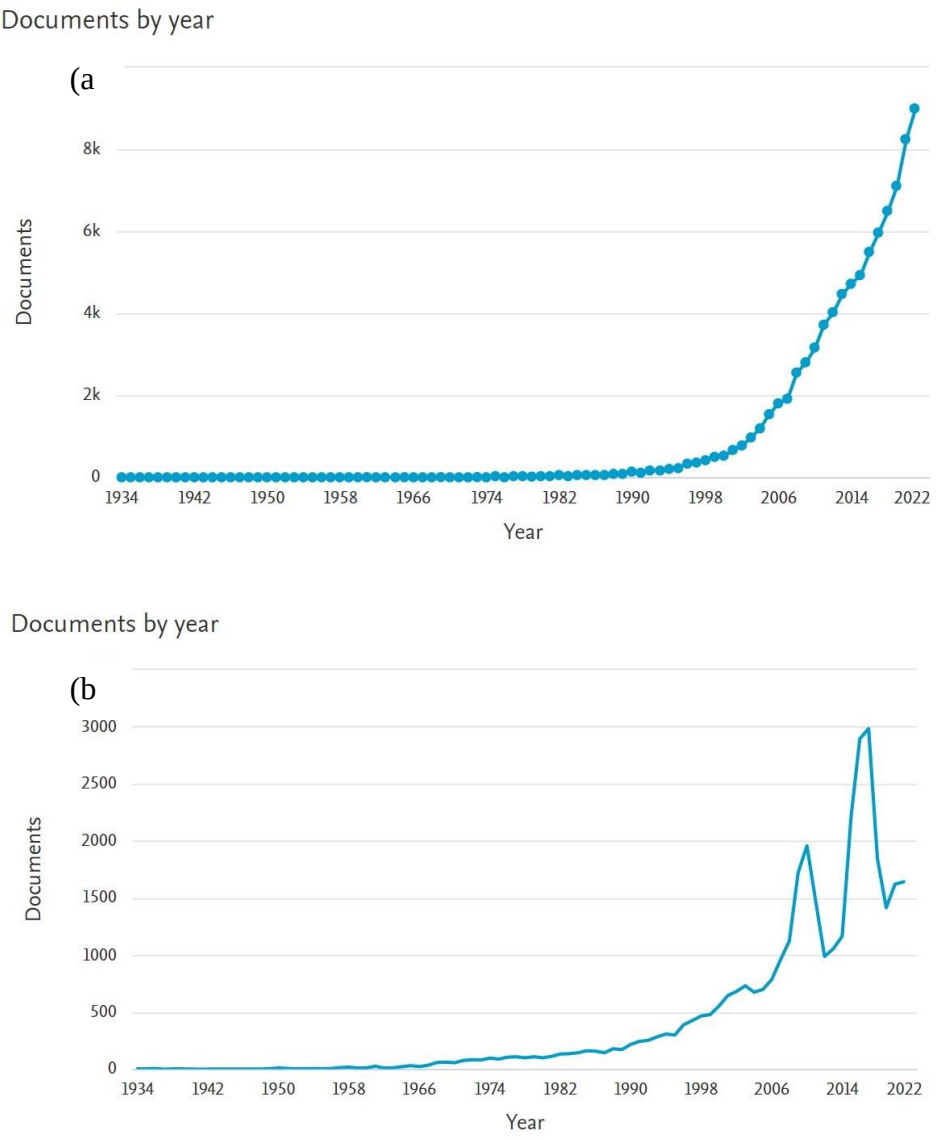


Figure 1.3 Scopus data graph of publications that mention (a) chitosan and (b) chitin.

The trend in chitin and chitosan research is clear, though much of the research may overlap, it is the superior properties of chitosan which makes it a diverse molecule for research in many fields of study.

The chemical and physical properties of chitosan depend on a number of factors, deacetylation degree, molecular weight, viscosity, and solubility. These factors and their methods of characterisation are discussed in the following sections.

1.1.2 Determination of degree of deacetylation

If chitin undergoes deacetylation in the presence of basic hydroxides it forms chitosan. Chitosan is produced on an industrial level by chemical or enzymatic deacetylation of chitin using sodium hydroxide or lysozyme and chitin deacetylase respectively. [21] The overall outline of the chemical synthesis of chitosan from chitin is described as follows: chitin is depolymerised in the presence of a strong base to produce monomeric N-acetyl-glucosamine units. These units are then deacetylated by the same strong base to produce monomeric D-glucosamine units. The subsequent polymerisation of these two-unit types lead to the formation of polymeric chitosan. The ratio of N-acetyl-glucosamine units and the D-glucosamine units is known as the deacetylation degree (DD).

Some reports in the literature refer to the percentage of N-acetylated-glucosamine units as the degree of acetylation, with the designation DA. When expressed as a percentage relative to DD this parameter becomes DD = 100 – DA (%). [22] For the purposes of clarity, this thesis will only refer to the degree of deacetylation (DD) in the chitin/chitosan chains. That is, the DD is the percentage of the active -NH_2 units that allow chitosan specifically to have superior and diverse properties over chitin.

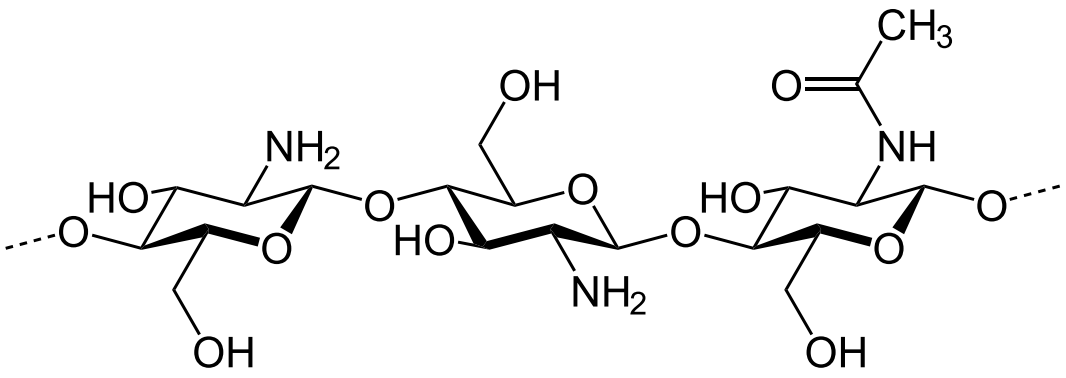


Figure 1.4: Chemical structure of the chitosan molecule showing randomly distributed D-glucosamine and N-acetyl-glucosamine units.

The deacetylation degree (DD) is an important parameter that determines the percentage of free amine groups present and the distinction between chitosan or chitin. [23] The presence of amino groups in chitosan gives the polymer many advantageous properties over chitin. The D-glucosamine residues may be protonated, providing solubility in acidic aqueous solutions [24] and selective complexation with protein macromolecules. [25]

Table 1.1 and table 1.2 summarises several commonly used analytical methods to determine the DD in chitin and chitosan samples. Although the list is not exhaustive, it is intended to be an overview of the techniques used, so as to aid in choosing the best method to suit specific requirements. The preferred method is often influenced by the solubility of the sample or availability of instruments or equipment. Therefore, the methods have been divided into two categories, namely those that are ideal for samples in solution or solid states. As such, due to the poor solubility of chitin, the methods that analyse solid samples are best suited. For typical analytical purposes of soluble chitosan, measuring the N-acetyl-glucosamine units by first derivative UV methods gives very good results. [26, 27] FT-IR spectroscopy however remains to be the most reliable method for solid samples of both chitin and chitosan. [28-30]

Insoluble samples:		
Method	**Analytical conditions**	**Description**
FT-IR spectroscopy	Powder samples are mixed with dry KBr, thin films can be cast	Assigning bands from references calibrated with NMR, UV spectroscopy and potentiometry methods [28-30]
Elemental analysis	Powder analysed directly	Calculated from the Carbon Nitrogen ratio [31]
Thermal analysis	Powder analysed directly	Based on enthalpy of degradation of sample [32]
HPLC	Sample hydrolysed with H_2SO_4	Based on the measure of freed acetyl groups [33]

Table 1.1: Various characterisation methods for determining the degree of deacetylation in chitin and chitosan for insoluble samples

Soluble samples:		
Method	**Analytical conditions**	**Description**
1H NMR spectroscopy	Depolymerised chitosan samples dissolved in D_2O at 90 °C	DD is calculated from the relative area of H-1 resonances of N-acetylglucosamine and/or D-glucosamine in combination with N-acetyl group resonances to the total area of resonances [34]
UV spectroscopy	Chitosan dissolved in acetic acid	First derivative of absorbance is recorded at point of null contribution of acetic acid ($\lambda \sim 200$ nm) [26, 27]
Potentiometry	Chitosan dissolved in HCl	Titration with NaOH to measure the HCl needed to protonate NH2 groups [35]
Enzymatic method	Chitosan dissolved in acetic acid and incubated with β-D-glucosaminidase, β-N-acetylhexosaminidase and chitosanase	Freed D-glucosamine and N-acetyl-glucosamine monosaccharides are measured via colorimetric HPLC methods [36]

Table 1.2: Various characterisation methods for determining the degree of deacetylation in chitin and chitosan for soluble samples

A deacetylation degree of ≥40% defines chitosan [37] and plays a significant role in determining the possible applications due to the influences on the physical and chemical properties. These influences include the tensile strength of films [38] and the ability to chelate metal ions. [39] The DD determines the fraction of active amino groups that will be available for protonation or interactions with metal ions. Infra-red spectroscopy and NMR analysis are the most common methods to evaluate the deacetylation degree. [40]

1.1.3 Determination of molecular weight

The molecular weight and distribution of that weight influences the chemical, biological, and physical properties of chitosan such as: (i) mechanical properties of films and hydrogels, (ii) membrane pore size, [41] (iii) antimicrobial activity, [16] and particle size and drug release effectiveness. [42] Therefore, the molecular mass directly affects how chitosan is used in the pharmaceutical, food, and biomedical industries. Chitosan molecular weight can be classified into three categories, low molecular weight (LMW) at <50 kDa, medium molecular weight (MMW) at 50-250 kDa and high molecular weight (HMW) at >250 kDa. Several reports have noted that LMW chitosan shows enhanced properties such as antibacterial, [43] mucoadhesive [44] and antitumor properties. [45]

The typical methods used for determining the molecular weight of chitosan are the same as used for any polymer. Commonly used methods include static light scattering, viscometry, and gel permeation chromatography, these are briefly discussed in the following subsections.

1.1.3.1 Static light scattering

Static light scattering (SLS) directly determines the polymers weight-average molecular weight without the need of calibration. [46] Although it is an absolute method that can determine important information about the polymer, including the conformation, interaction with environment and chain stiffness, the use of SLS is limited due to the requirement of fully soluble polymers, expensive equipment and strict experimental conditions. [47] The principle of this method uses the relationship between the molecular weight of a molecule and the intensity of the light scattered by it, described by the Rayleigh theory. This theory says that larger molecules scatter more light than smaller ones, and the intensity of light is proportional to the molecular weight of the molecule.

A polymer that is dissolved in a solution becomes a colloidal suspension, where the material is evenly dispersed throughout the solvent. [48] Light scattering takes place when the colloidal molecules absorb incident light of a certain frequency and emits light of the same frequency in all directions. Under atmospheric pressure and low, constant temperature, this type of light scattering is known as static light scattering. [49, 50]

1.1.3.2 Viscometry

The simplicity of viscosimetry makes it is the most widely used technique for determining the molecular weight of chitosan, despite its disadvantage of not being absolute. It relies on the correlation between the values of molecular weight and intrinsic viscosity, determined by an absolute method for fractions of a particular polymer, as shown in the Mark-Houwink-Sakurada equation (Eqn. 1.1): [51]

$$[\eta] = KM_{\upsilon}^{\alpha} \qquad \text{Eqn. 1.1}$$

Where M_υ is the viscosimetric-average molecular weight and K and α are constants that depend on the nature of the polymer, temperature, and solvent. The DD and polydispersion must be known for the calibration, as chitosan has a tendency to form aggregates. [52]

1.1.3.3 Gel permeation chromatography

Size exclusion chromatography and gel permeation chromatography can determine not only the molecular weight of a polymer but its polydispersity, i.e., the degree of non-uniformity of the polymer chain. The polymer is dissolved in a suitable solvent and eluted through a column made of organic and inorganic material grafted on an inorganic surface such as silica (stationary phase). Solvents may include acetic acid, sodium acetate or ammonium acetate buffer. [53] With the addition of a refractive index detector to a high-performance size exclusion liquid chromatography system, it is possible to determine the amount of polymer eluted at any given retention time or volume. Smaller molecular weight polymer chains have a higher attraction toward the column materials than larger ones. Because of this, higher molecular weight polymers have lower retention times that smaller ones. However, this system must be calibrated in terms of expected retention volume of a polymer fraction of a known molecular weight in order to calculate the known molecular weight. Since there are no standards for chitosan, to construct a calibration curve, pullulan polysaccharide standards of narrow molecular weight distribution are used. [54]

1.1.4 Viscosity

One of the most unique properties of chitosan is its polycationic nature. When dissolved in an acidic solution (pKa = 6.0) it forms a viscous solution. The viscosity is affected by the molecular weight, degree of deacetylation, concentration, temperature, and pH of the solution. At the molecular level, the viscosity is a direct measure of the volume of polymer molecules in the chain, which as mentioned above, can be used in the Mark-Houwink-Sakurada equation (Eqn. 1.2) to determine the average molecular weight. The intrinsic viscosity can be calculated from the following equation:

$$[\eta] = \frac{(\eta - \eta_s)}{(\eta_s C)} \qquad \text{Eqn. 1.2}$$

Where η is the solution viscosity in dLg^{-1}, η_s is the reference solvent viscosity and C is the solution concentration. [55] Generally, the viscosity and flow of chitosan solution increases with increasing DD due to the elongated conformation and more flexible chain structure. When the DD is decreased, the molecule may take a spiral shape due to the low charge density in the polymeric chain. In aqueous solutions chitosan is stabilised by intra- and intermolecular hydrogen bonds between the amino and hydroxyl groups. Therefore, less deacetylated chitosan has a lower density of hydrogen bonds and produces a less viscous solution. [56]

Intrinsic viscosity [η] (dLg-1)	**Molecular weight (Da)**
9.40	654,127
4.72	285,231
2.55	135,839
1.50	71,676
0.54	20,698

Table 1.3: Intrinsic viscosity and average molecular weight of different chitosan samples. [57]

1.1.5 Solubility

Chitin has a three-dimensional crystal matrix consisting of strong hydrogen bonds between acetyl, hydroxyl, and amine functional groups. Pure chitin contains about 90% N-acetyl groups in its chain which contribute to intra- and intermolecular bonds, making chitin highly aggregated. Therefore it is mostly insoluble in many regular solvents such as water, mild acid/basic solutions and organic solvents. [58] The first study on chitin solubility was done by Austin, who tested chitin in different organic solvents such as dichloroacetic and trichloroacetic acids, alcohols and lithium chloride / dimethylacetamide mixtures. [59] Following this initial research, many other studies were conducted with the same intention of finding a suitable solvent for chitin. These solvents included N-methyl-2-pyrrolidone, [60] phosphoric acid, [61] lithium thiocyanate, [62] and hexafluoro-isopropyl alcohol. [1, 63] Although the dissolution of chitin was possible with these solvents, many of them were highly toxic, mutagenic, corrosive, or scarcely degradable. The choice of an appropriate solvent for chitin is important for lab scale research and industrial practices.

With the removal of at least 40% of the acetyl groups on chitin, the polymer becomes more soluble in the form of chitosan. The active amino groups in chitosan contribute the most to the polysaccharide's solubility. They may react with aldehyde or ketone groups, or take part in short-range primary and secondary electrostatic interactions or hydrogen bonding to affect the overall solubility. [58] The factors that affect the solubility and aggregation of chitosan are (i) solution pH, (ii) molecular weight, and (iii) number of N-acetyl-glucosamine units, all of which will be briefly discussed.

1.1.5.1 Solution pH

The level of aggregation for chitosan can be strongly influenced by the solvent pH. Generally, chitosan is ionised at pH 6.0 and below, via the protonation of the amino groups. The exhibited positive surface charge helps to resist aggregation of the molecule due to coulombic repulsion forces, but when the DD value decreases, aggregation begins to take over. This is the mechanism behind the acid sensitive swelling behaviour of chitosan. [64] The pH value at which the net charge of the chitosan solution prevents aggregation is called the critical pH. [58] At a pH value higher than the critical pH, the number of deprotonated species in the solution rises, and aggregation changes to agglomeration due to hydrogen bonding between neutralised amino groups. [65]

1.1.5.2 Molecular weight

Chitosan solubility increases with decreasing molecular weight, that is, the tendency towards aggregation decreases. [65, 66] The formation of aggregates is a process of a loss of entropy. Shorter molecular chains mean higher loses of entropy and reduced hydrogen bond interactions due to the decrease in number of associated amino groups. Consequently, the soluble-insoluble transition takes place at a higher pH, where the hydrogen bond interactions are enhanced and drive aggregation. When the molecular weight of chitosan decreases, aggregates cannot form, even when the amino groups are not charged, thus making it water-soluble. [66]

1.1.5.3 Number of N-acetyl-glucosamine units

The two monomer units that are present in chitin and chitosan are N-acetyl-glucosamine and D-glucosamine, which exist in different fractions. As mentioned previously, the degree of deacetylation determines the ratio of acetyl and amino groups present in the polymer, thus defining it as chitin or chitosan. Naturally if the number of amino groups outweigh the number of acetyl groups, the polymer becomes hydrophilic, positively charged in acidic solution and more soluble as a result. [58] Therefore, chitosan becomes more soluble with decreasing N-acetyl-glucosamine groups and increasing D-glucosamine groups.

1.2 How chitosan is made

Chitin was first isolated from mushrooms in the early 1800s, and a decade later was discovered in the shells of insects. [67] In 1859 chitosan was isolated by boiling chitin in potassium hydroxide solution to deacetylate it. [68] Today, chitosan is produced on an industrial scale using a range of chemical and biological methods. Chitin represents an essentially inexhaustible, permanently available source of chitosan, arthropods alone constitute the majority of that source. [69] The following section discusses the chemical and enzymatic methods of producing chitosan on an industrial scale.

1.2.1 Industrial synthesis of chitosan

A promising option for producing chitosan on a large scale is to use the abundance of waste lobster, crab and shrimp shells from fisheries. [70] Marine crustacean shells are the preferred source of chitin over fungi, algae and yeasts due to the high availability from the seafood industry. [71]

The general process for the extraction of chitin from crustacean shells has two main steps: deproteinization with alkali treatments and demineralisation with acidic treatments. The order of these two steps can be interchangeable depending on the proposed use of the chitin or its source. [72] Figure 1.5 shows a basic scheme of the preparation of both chitin and chitosan via chemical methods.

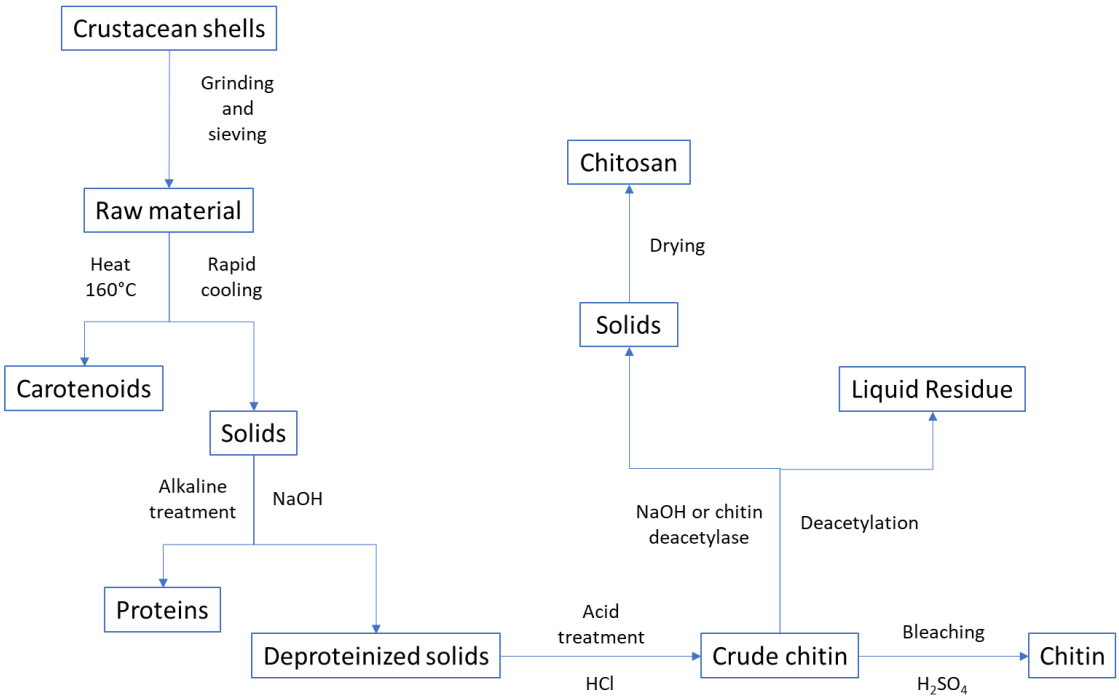


Figure 1.5: scheme of chitin and chitosan preparation via chemical methods. [73]

The processing conditions can significantly affect the molecular weight and DD of chitosan. The stronger the acid used for the demineralisation stage, the lower the molecular weight of the final product. [74] In the deproteinization stage however, the alkaline treatment has been shown to be less damaging to the structure of the final product. [23]

Unfortunately, chemical methods of chitin and chitosan extraction and purification are very energy consuming and hazardous to the environment with high waste processing costs. [75] The deacetylation process requires large amounts of alkaline treatments and washes. [76] Prolonged exposure to the alkaline and acid treatments can cause depolymerisation of the polysaccharide. Additionally, alkali recovered proteins have a low biological value which limits their use in the animal feed industry. [72] To address these particular problems, biological and environmentally friendly alternatives have been proposed by use of proteases for the deproteinization steps in place of harsh alkaline treatments. Proteases have been used for deproteinization and demineralisation of crustacean shells [77] and lactic acid bacteria has been used as a fermentation agent for the extraction of chitin from crab shells. [78] Several commercial proteases have been assessed for crustacean shell protein extraction, and alcalase is the most effective of them all. [79-81] Although the deproteinization levels

are generally lower than those obtained through alkaline treatments, these ecologically friendly alternatives produce nutritionally valuable protein alongside chitin. [80] Figure 1.6 shows a brief scheme of the extraction of chitin and the synthesis of chitosan via environmentally friendly methods.

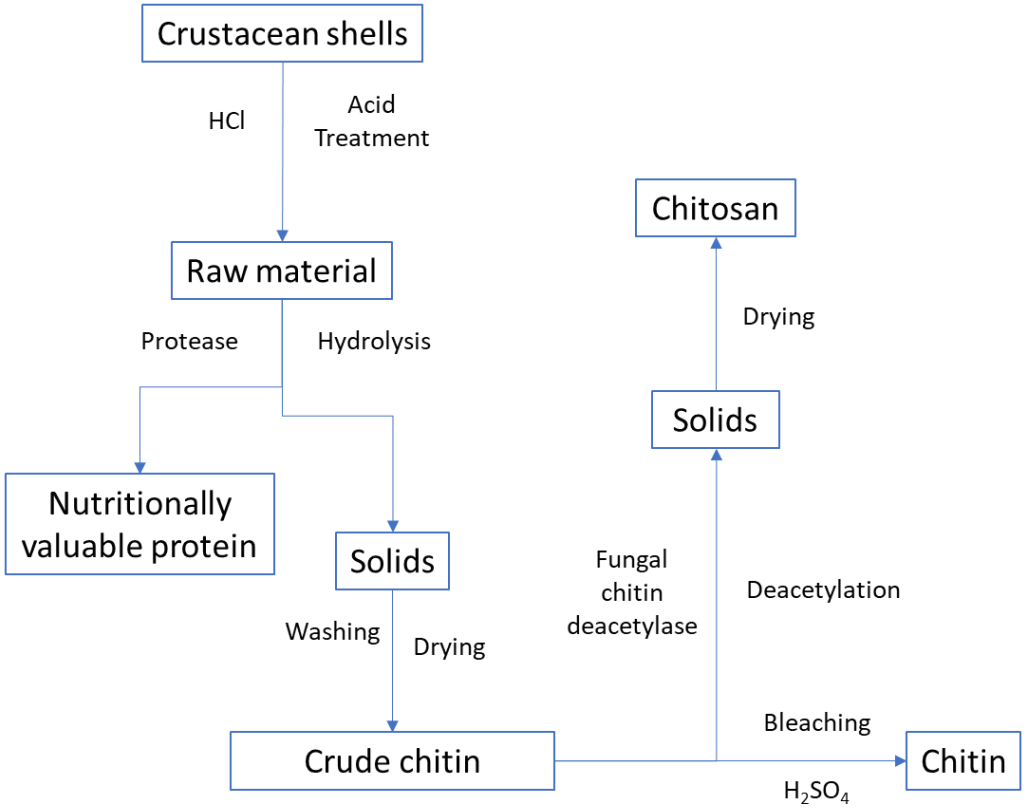


Figure 1.6: Scheme of chitin and chitosan production using only eco-friendly methods. [73]

The use of a strong base solution such as NaOH and high temperatures to convert chitin into chitosan can cause variability in the final product properties, decrease the quality and increase processing costs. [82]

Fungal cell walls are an alternative source of chitin and chitosan, as well as acid polysaccharides. Chitosan is a constituent of the cell walls, so its production is coupled with growth of the fungus. One such fungus is Mucor rouxii which has been extensively studied over the years. [72, 83-86] Chatterjee et al. found that chitosan with more consistent physio-chemical properties can be obtained by altering the culture media and fermentation conditions. Among the three culture media, molasses

salt, potato dextrose broth and yeast extract peptone glucose, chitosan made from molasses salt was more crystalline and less polydispersed which indicates a higher quality polymer. [83] Aside from the reduced use of chemicals in its production, there are two advantages of fungal chitin and chitosan: lower heavy metal content and a lower molecular weight. [86]

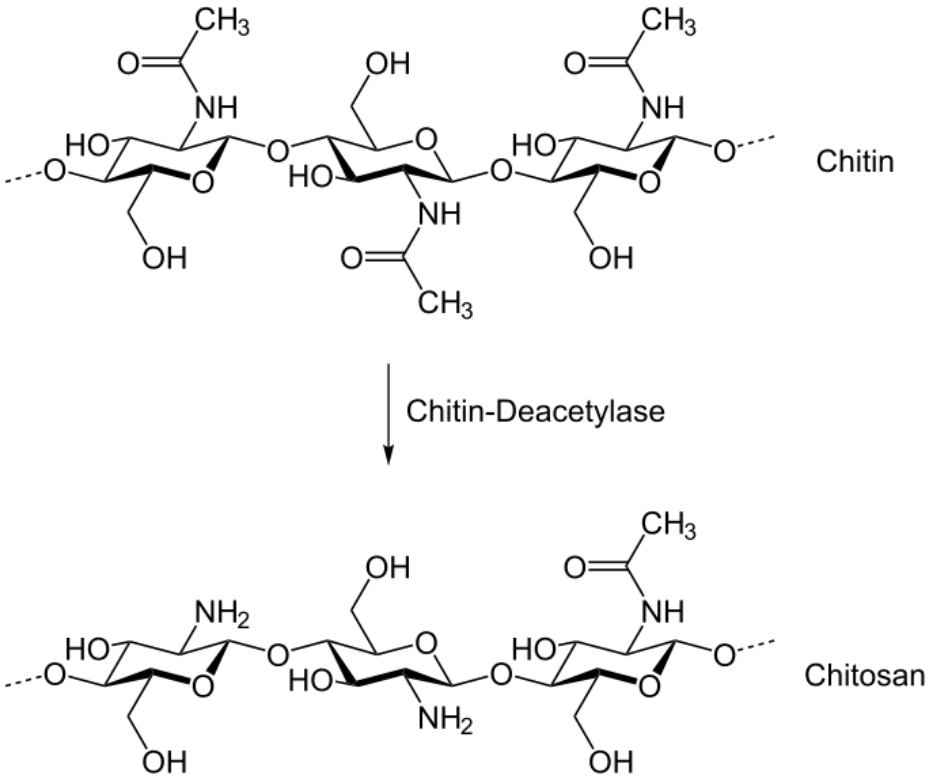


Figure 1.7: Chemical structure of chitin and the enzyme-based deacetylation reaction that forms the linear polysaccharide chitosan. [87]

1.3 Modifications of chitosan

1.3.1 Interpenetrating Polymer Networks and polymer blends

Interpenetrating Polymer Networks (IPNs) can be defined as a combination of two or more polymer networks that have been crosslinked or synthesised in the immediate presence of each other. IPNs are different from simple polymer blends in that they can swell, have no melting point and are not soluble in solvents. [88] The insolubility of IPNs is due to their cross-linked nature, which affects the entire morphology of the substance. They often take the form of a hydrogel which can then be solidified to form a film.

A chemical cross-link is a bond that links one polymer chain to another to create a longer chain or a complex network. They are formed by chemical reactions initiated by heat, pressure, or pH change with the use of crosslinking agents. By cross-linking one polymer with another, the properties of the resulting polymer network will change to create a generally more robust product that is resistant to heat, pressure, extreme pH conditions and mechanical stress.

IPNs may be synthesised by several different methods, the two main ones being:

Sequential: A polymer network is made and a monomer, crosslinker and activator are swollen into the network in situ. The synthesis of one network leads to the synthesis of the other.

Simultaneous: The monomers, activators and crosslinkers of all networks are mixed at the same time and the reaction takes place simultaneously.

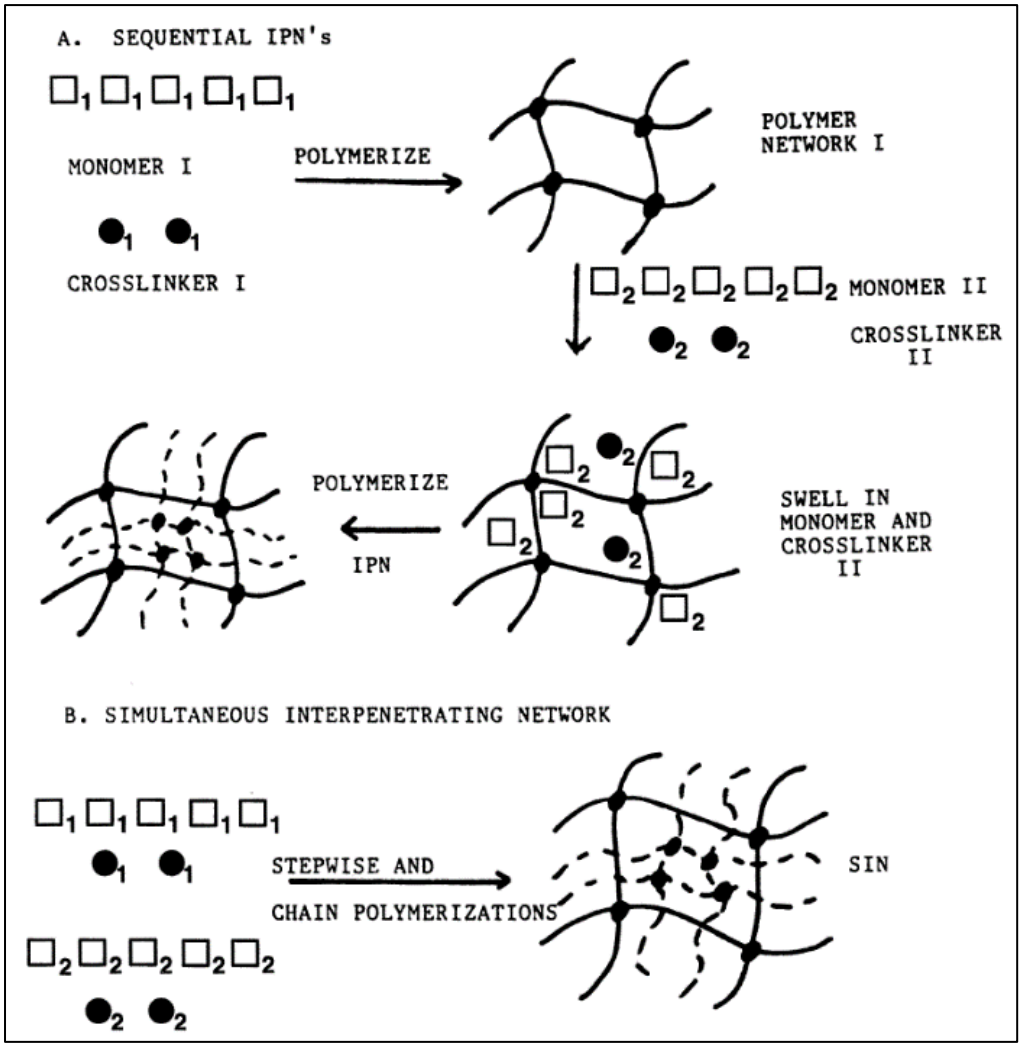


Figure 1.8: Basic synthesis methods for IPNs. A: Sequential synthesis in which the synthesis of one polymer leads to the synthesis of another which is crosslinked into the network. B; Simultaneous synthesis in which all the components for the chosen polymers are mixed together in situ and are crosslinked at the same time. [89]

Chitosan membranes can be cross-linked with reagents such as tetraethyl-orthosilicate (TEOS) to improve their mechanical properties and overall stability. [90] A chitosan – tetraethyl-orthosilicate (TEOS) IPN contains chitosan as an individual polymer chain and the monomer TEOS which forms a siloxane polymer chain from hydrolysis and subsequent condensation. The two chains crosslink to form a chitosan-TEOS interpenetrating polymer network (Chi-TEOS IPN). The synthesis of this particular IPN combination was first described by Park et al. [90]

1.3.2 History of IPNs

The first known synthesis of an IPN was by Jonas Aylsworth, Thomas Edison's chief chemist, who in 1914 combined phenol-formaldehyde compositions with natural rubber and sulphur. [91] The phenol-formaldehyde was sourced from Edison himself as he was using the new phenol-formaldehyde resin. Edison was then working in West Orange, New Jersey and the inventor of phenol-formaldehyde resins, Leo Baekeland was working across the river in Yonkers, New York. By combining natural rubber and sulphur, Aylsworth made the world's first rubber-toughened plastic, decades before rubber-toughened styrenes were commercial. The patent [91], however, does not mention IPNs or polymer networks. This was six years prior to H. Staudinger's macromolecular hypothesis, the first statement that certain colloids had long chain structures.

The next known discovery of IPNs was by Staudinger and Hutchinson as revealed in a patent with a 1941 application date. [92] In order to smooth the surfaces of transparent plastic sheeting, Staudinger and Hutchinson took sheets of cross-linked polystyrene and swelled them with the same monomer mix. After polymerization, they were stretched to reduce the surface imperfections of the original material.

The next independent invention of IPNs was by Solt in 1955. [93] Solt made cationic-anionic ion exchange resins with oppositely charged networks. The idea of both charges on the same particle was that the exchange efficiency would be improved if both charges were in juxtaposition, but still separated in space.

The term "Interpenetrating Polymer Networks" was coined by Millar in 1960. [94] However, several teams found IPNs independently in the 1960s; Shibayama and Suzuki, [95] Lipatov and Sergeeva [96] and Frisch et al. [97]Sperling and Friedman founded the field of IPNs, setting the pace for modern development. [98]

1.3.3 Applications of IPNs

IPNs exhibit a range of interesting and varied properties, while they can be used in many applications such as biomedical research and sorptive materials, as described in the following sections:

1.3.3.1 Biomedical research

Various IPN hydrogels made from chitosan have been synthesised for their biomedical applications such as pH/temperature responsive drug delivery systems. Guo *et al.* have reported a method to obtain thermo and pH responsive chitosan based IPN hydrogels that control the release rate of a coenzyme as a function of temperature. [99, 100]

Kim *et al.* prepared a semi-IPN composed of chitosan and poloxamer, a non-ionic copolymer composed of a central hydrophobic chain flanked by two hydrophilic chains. Their freeze-drying strategy allowed them to obtain sponge type hydrogels. These IPN composite hydrogels had water adsorption properties, interconnected pores and high mechanical strength which suggested to the authors that they could lead to their use as wound dressing material. [101]

Cryogels are three dimensional macroporous gels prepared below the freezing point of the solvent. [101-106] They possess a capillary network through which a solvent can flow, a high mechanical strength and osmotic stability. Based on these properties, Kumar et al. developed cryogel IPNs to be used as flexible scaffolds for biomaterials. [102, 103]

1.3.3.2 Sorptive materials

Water pollution with heavy metal species is becoming a huge environmental problem due to wastewater from power plants containing heavy metal ions such as Technetium and Caesium. Alongside heavy metals, dyes also pose a threat to the environment with many products from plastic, textiles and paper industries containing non-biodegradable and toxic effluents. Many conventional methods of removing these pollutants such as coagulation/flocculation, solvent extraction and chemical precipitation are not always effective. Adsorption is considered an effective and economical method of removing high concentrations of pollutant due to its reusability. [107, 108] Therefore, over the past decade there has been interest in finding sorbents with high adsorption capacities, fast adsorption/ desorption rates, and easy separation and regeneration. [109, 110]

To evaluate the sorption capacity for ionic species such as dyes and heavy metals, the behaviour of various IPNs need to be evaluated in batch mode. By determining the residual concentration of the ionic species, the adsorption capacity q, expressed by Eqn. 1.3, and the removal efficiency R%, expressed by Eqn. 1.4 can be calculated.

$$q_e = \frac{(C_o - C_e)V}{W} \quad \text{(mg/g)} \quad \text{Eqn. 1.3}$$

$$R = \frac{(C_o - C_e)}{C_o} \times 100 \quad (\%) \quad \text{Eqn. 1.4}$$

Where C_o and C_e are the initial and final concentrations, respectively, V is the volume of the aqueous phase (L), and W is the weight of the dried composite gel or IPN film (g). [99]

The main factors which influence the sorption capacity on IPNs, and hydrogels are pH, sorbent dosage, temperature, and the initial concentration of solute. Interference with other ionic species should be also considered.

1.4 Applications of chitosan and chitosan-based films

A large interest in chitosan has arisen due to the presence in its repeating units of hydroxyl and amino groups. The amino groups give chitosan unique chelating and electrostatic properties allowing it to readily complex with heavy metal ions. [111, 112] The amino groups on the ring are available for protonation, which makes the compound acid sensitive. The chitosan structure can swell in acidic conditions. This phenomenon has been extensively researched with controlled drug-release systems in mind. [113] From a food industry perspective, chitosan has distinct fat-binding functionality by way of the fat molecules getting embedded in the long chains of the chitosan structure. [114] The antimicrobial activity of chitosan has also been studied extensively. One such example is the preparation of films to be used as packaging material for a variety of foods. [115] Table 1.4 describes some of the many potential applications for chitosan. This material has a number of beneficial properties that may be applied in biomedical and environmental fields, it is one of the most versatile macromolecules due to its amphiphilic structure.

Potential Applications	**Principal Characteristics**	**Refs**
Food and beverage	Cross-linked chitosan is not digestible by humans, Preservative, Lipid binding, Antibacterial and anti-fungal coatings	[116-119]
Biopharmaceutics	Healing and bacteriostatic, Immunologic, and anti-tumour properties, Haemostatic, and anticoagulant	[120-124]
Agriculture	Time release of fertilizers in soil, Frost protection coating on seeds, Boost plant defence mechanisms and plant growth	[125-128]
Cosmetics	Acne treatment, Oral care (toothpaste), Skin moisturizer, Hair maintenance	[129-132]
Water and waste treatment	Removal of metal ions, Odour reduction, Flocculent for clarification of water	[108, 133-135]

Table 1.4: Potential applications of chitosan, highlighting the main characteristics that would be relevant to each application. [1]

1.4.1 Chitosan in heavy metal sorption

Chitosan has received a lot of attention and interest for use in heavy metal removal due to its excellent metal binding properties and relatively low cost compared to other absorbent materials such as activated carbon. [136] The long chain of active primary amino groups, hydroxyl groups and overall flexibility means that chitosan is a perfect choice for metal ion complexation and sorption. [137-139] Generally metal sorption on chitosan or chitosan-based derivatives occurs through several interactions of coordination, chelation, ion exchange or electrostatic interactions. [137, 140] However the exact type of metal-polymer interactions depends on the metal ion, the pH, and the chemical nature of the polymer. In a single system, complexation, adsorption and precipitation can occur at the same time, such as the interaction between Pb(II) in solution and chitosan. [141, 142] The research carried out by Muzzarelli et al. in 1969 described the synthesis and adsorption capacity of chitin and chitosan based chelating supports for the removal of metal ions from sea water. [143] Since then, numerous papers have been published discussing the use of chitosan as an effective sorbent for pollutants (either organic or inorganic) in wastewaters. The growing interest in this subject can be seen by following the published works on the "SCOPUS" database over several time periods (using the terms "chitosan" in combination with "adsorption" or "removal").

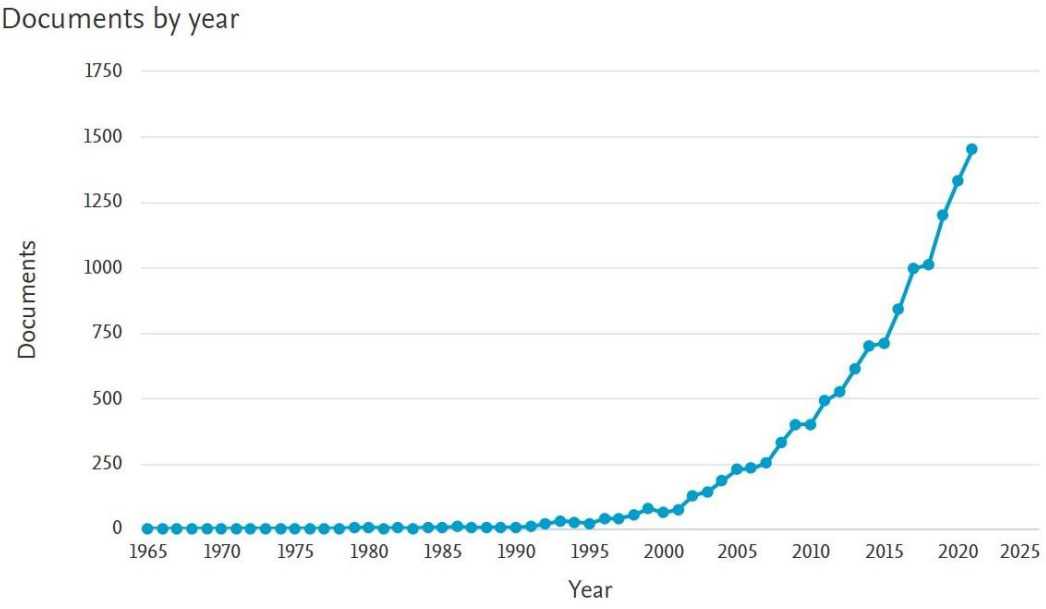


Figure 1.9: Number of publications with keywords "chitosan" and "adsorption" or "removal" in Scopus database.

The major advantage of chitosan is the ability to modify its chemical structure. This is done by either cross-linking reactions or grafting functional groups to form derivatives that have superior properties such as resistance to extreme conditions and enhanced adsorption capacities.

The number of research articles published in recent years that discuss the use of chitosan-based adsorbents for metals and ions removal from aqueous solution is much greater than those for dye removal. This may be because metals and ions represent a larger range of pollutants that are more toxic, thus the need for such adsorbents is higher. The mechanism in which the metals and ions are adsorbed is chelation, which occurs readily to bind the pollutants. Chelation is defined as: "The formation or presence of bonds (or other attractive interactions) between two or more separate binding sites within the same ligand and a single central atom". [144] Various papers that describe metal and ion adsorption onto modified chitosan are discussed below:

Chitosan-modified multiwalled carbon nanotubes (MWCNT-CS) were utilized by Chen et al. to remove uranium VI from wastewater. [145] Uranium is a major component of nuclear waste that can significantly impact the environment. When paired with certain products such as phosphate or calcium, it can lead to radiological pollution or direct damage to biological organisms. [146, 147] The danger of radionucleotides to human health has led many countries such as China, Brazil, USA, and India to search for effective ways of removing uranium VI from wastewater. There is insufficient data regarding the carcinogenicity of uranium in humans and experimental animals. The guideline value for the chemical toxicity of uranium was derived using a TDI (tolerable daily intake) approach and WHO recommends that uranium VI concentration in drinking water should be below 15 $\mu g L^{-1}$. [148] Chen et al. found that the MWCNT-CS sorption was dependant on pH and independent on ionic strength. The grafted chitosan improved the sorption capacity of the MWCNT-CS to a maximum of 40mg g^{-1}. [145]

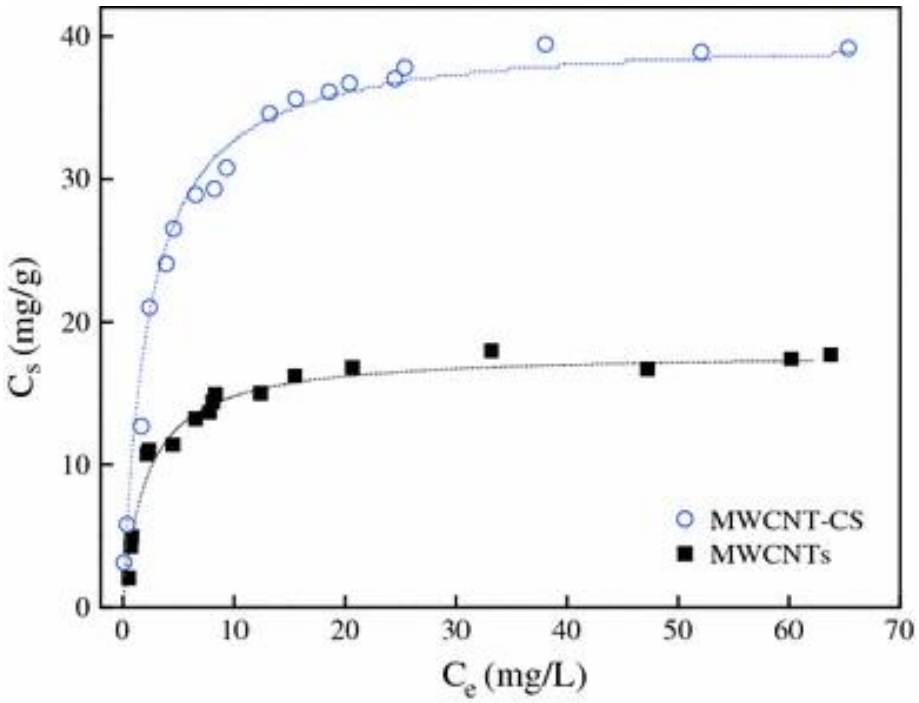


Figure 1.10: Sorption isotherms of UO_2^{2+} from solution on MWCNTs (non-modified), and MWCNT-CS (modified) over 48 hours at room temperature at pH 5, taken from Chen et al. [145] The sorption isotherms are well fitted by the Langmuir model. The maximum sorption capacities of uranium VI calculated from the Langmuir model are ~17 mg/g for MWCNTs, and ~41 mg/g for MWCNT-CS.

Arvand et al. recognised that chitosan powder swelled in an aqueous medium, so it was unsuitable for use in an adsorption column. They proposed that the adsorption capacity of chitosan can be enhanced by spreading it on physical supports, increasing the availability of the active metal binding sites on the molecule. A modified product was made from chitosan, 3,4-dimethyloxybenzaldehyde (DMB) and bentonite and used as an absorbent for the removal of cadmium II ions from water. [149] The synthesis of this new product was confirmed by FT-IR and SEM before and after the adsorbent testing. During the pH experiments an increase in metal uptake was observed with increasing pH levels up to nine. Cadmium started to precipitate from the solution at pH levels higher than seven, so the optimum value selected was 6.5. After running the Langmuir Isotherm model for the experiment, the maximum adsorption at monolayer coverage for the chitosan/DMB/bentonite product was found to be 217.4 mg g^{-1}. [149]

A magnetically-modified chitosan resin was prepared by Elwakeel et al. by cross-linking chitosan with glutaraldehyde in the presence of magnetite and chemically reacting with tetraethylenepentamine (TEPA). [150] This amine bearing chitosan modification showed a higher affinity to the uptake of UO^{2+} ions from aqueous solution than unmodified chitosan. The sorption isotherm was modelled by the Langmuir equation and the maximum sorption capacity reached 1.67 mmol g^{-1}. The advantage to preparing this kind of material for sorption is that the methods are scalable and cheap. Magnetic resins can be easily collected from aqueous solutions by use of an external magnetic field. [151] Magnetic separation technique is ideal for heavy metal ion removal as it reduces the need for centrifugation or filtration and thus reduces the chance of coming into contact with radioactive material. Moreover, methods that involve magnetism are more suitable for automation. [151]

Suc and Ly modified chitosan flakes with citric acid and cross-linked with glutaraldehyde and applied it to the removal of Pb(II) ions from aqueous solutions. [152] The adsorption experiments were run at a pH of five to avoid any precipitation of $Pb(OH)_2$. The maximum sorption capacity for Pb(II) was found to be 101.7 mg g^{-1}.

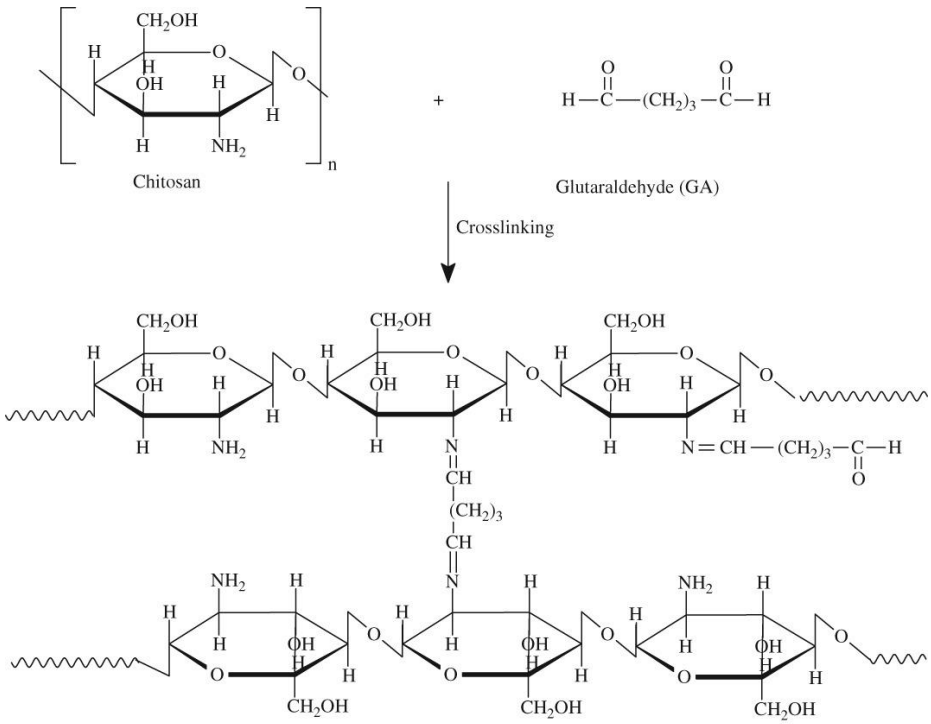


Figure 1.11: Reaction of chitosan and glutaraldehyde cross-linking. [152]

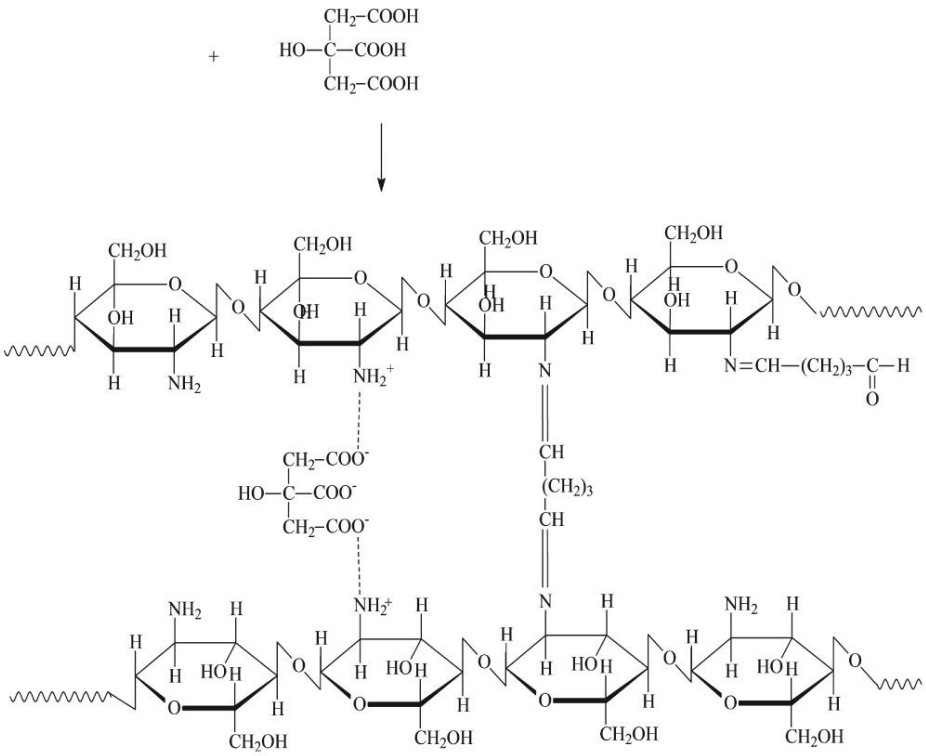


Figure 1.12: Reaction of glutaraldehyde cross-linked chitosan with citric acid. [152]

Their rationale for grafting citric acid to glutaraldehyde cross-linked chitosan was that the adsorption capacities of heavily cross-linked chitosan are reduced. This is due to the active functional groups becoming inaccessible because of the cross-linked polymer network. [153, 154] The solution they proposed was to graft new functional groups onto the polymer via citric acid and create a more suitable environment for the sorption of heavy metal ions. [155]

1.4.2 Biological activities of chitosan

Chitosan and its derivatives possess a number of beneficial biological properties such as biocompatibility and biodegradability and as such have gained a lot of attention from the biomedical, food, pharmaceutical and biotechnology fields. [156, 157] These activities and others will be discussed below in greater detail. In particular, the food preservation and packaging industry has recognised the use of chitosan-based antimicrobial films. The antimicrobial and antioxidant properties paired with the film forming nature of chitosan makes it an ideal material for this application. [158-160] In this present thesis a similar study has been done in chapter 6 where the antibacterial activity of chitosan-based films was evaluated.

Alishahi and Aider [160] found that using chitosan-based films in packaging cause a resistance to selective gas permeability and fat diffusion from the foods. However, due to the strong hydrophilic properties of chitosan, it was not very resistant to water vapour transmission. For this reason, the use of polymer blending or biocomposites have considerable potential in the preparation of chitosan-based films for food packaging. Friedman et al [158] studied the antimicrobial properties of chitosan powders, coating and edible films against pathogenic viruses, spoilage bacteria and fungi. The food categories chosen were dairy, meats, fish, cereal, and fruit juices. They suggest that lower molecular weight chitosan at a pH of six or below presents the optimal conditions for the desired antimicrobial and antioxidant effects on these food groups.

1.4.2.1 Antimicrobial activity

Chitosan has been shown to have some advantages over conventional disinfectants, possessing a higher antimicrobial activity and a lower toxicity towards mammalian cells. [72, 161] Many studies have demonstrated that chitosan has effective antimicrobial properties, but the mechanism(s) as to how it achieves this is not yet fully understood. One of the most likely hypotheses is that the positively charged active sites on the polysaccharide changes the cell permeability of the bacteria. The inhibition of bacterial growth is caused by the active sites affecting the anionic components such as N-acetylmuramic acid or sialic acid on the cell surface. This can result either the prevention of essential material from entering the cell or leakage of the cells contents. [162, 163]

Several types of antimicrobial activity have been explored. Sudarshan et al. proposed that low molecular weight chitosan particles can penetrate the bacterial cell wall and prevent DNA transcription by inhibiting mRNA synthesis. [164] Chung et al found that the antibacterial mechanism of chitosan involves the adsorption of chitosan onto the cell. The cell wall hydrophilicity and the negative charge were higher in Gram-negative bacteria than Gram-positive bacteria. In acidic conditions the more negatively charged surface of the cell wall interacted with the positive chitosan active sites and thus inhibiting the bacteria. [165] The antibacterial activity of chitosan can be more effective for Gram-negative bacteria than Gram-positive bacteria- indeed a number of other studies have confirmed this, [166-168] However other studies have concluded the opposite. [169] It is most likely a case-by-case basis. Moreover, the adsorption of chitosan is increased at a lower pH level, lower molecular weight, and higher degree of deacetylation. [170]

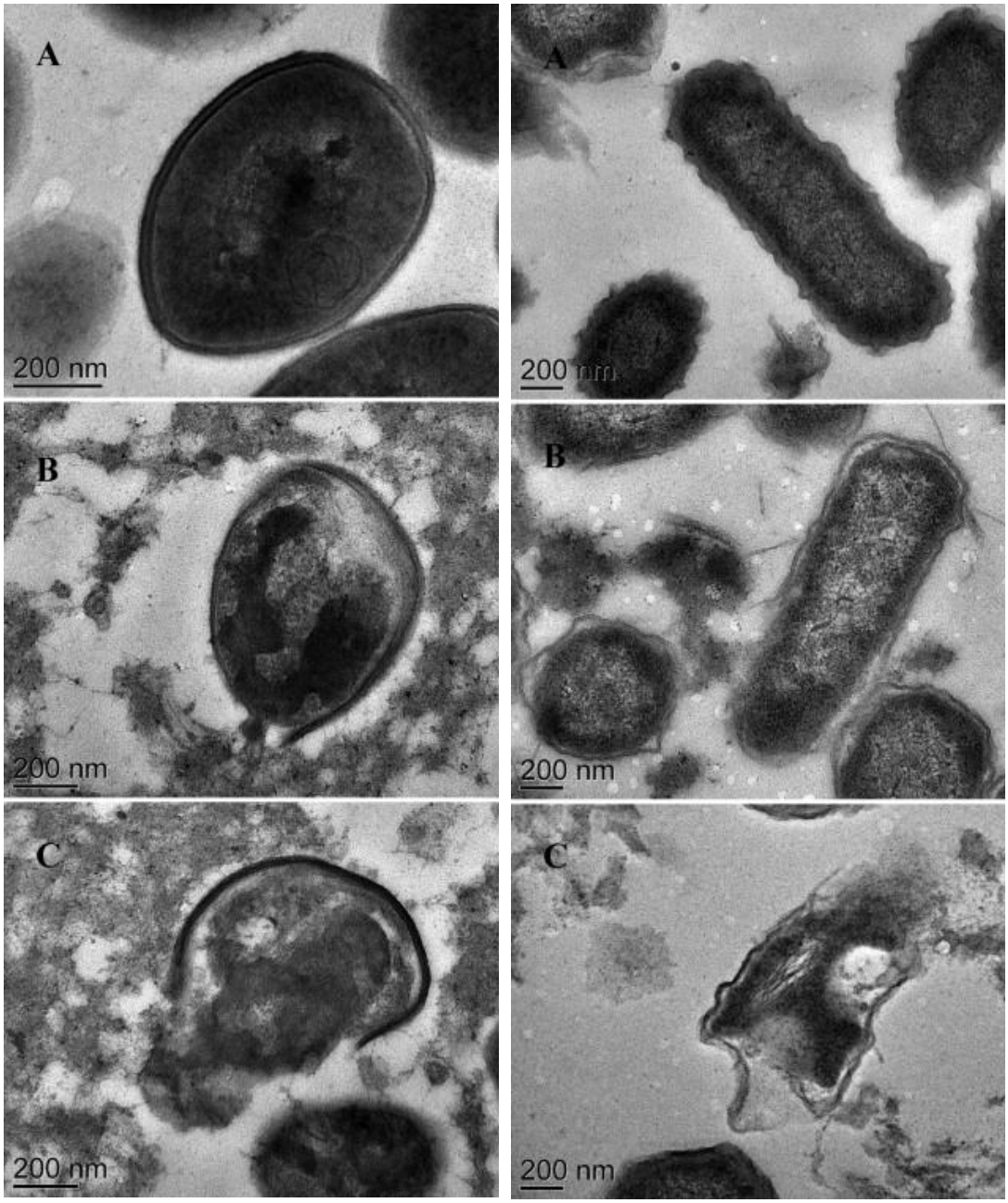


Figure 1.13: Transmission electron micrographs of S. *aureus* (left) and P. aeruginosa (right) treated with chitosan for 0 min (A), 20 min (B) and 2 h (C). After 20 minutes some ruptures which could cause some slight leakages of cellular cytoplasmic contents, were observed. Two hours of treatment later, the cytoplasmic membranes of chitosan-treated cells completely collapsed. [169]

Regarding the antifungal properties of chitosan, it has been reported that chitosan can reduce the infection of Fusarium oxysporum f. sp. apii in celery and inhibit the spread of Botrytis cinerea on cucumber plants. [171, 172] The mechanism by which this is achieved is by the formation of a gas permeable film around the plant which controls the oxygen and carbon dioxide permeability. This can directly interfere with fungal growth while keep the rest of the plant untouched. [173]

1.4.2.2 Antioxidant activity

Chitosan and its derivatives have been reported to act like antioxidants by scavenging oxygen radicals such as hydroxyl and alkyl radicals just as well as stable 2,2-diphenyl-1-picrylhydrazyl (DPPH) scavenging radicals when tested in vitro. [174] Much like the antibacterial properties mentioned in section 1.4.2.1, this radical scavenging process is dependent on the chitosan molecular weight and degree of deacetylation. Park et al. demonstrated that low molecular weight chitosan has a higher potential to collect different radicals. [174] The influence of molecular weight was also studied by Kwung et al, who looked at the antioxidant activity of chitosan on salmon skin. They found that chitosan with a molecular weight of 30-kDa had a higher salmon lipid oxidation reduction rate. [175] Even though the exact mechanism of chitosan-based radical scavenging is not yet fully understood, it can be attributed to the active amino and hydroxyl groups. This activity may be remarkably similar with how chitosan adsorbs heavy metal ions, as discussed previously.

1.4.2.3 Biomedical applications of chitin and chitosan

The most noteworthy properties of chitin and chitosan for biomedical purposes are biocompatibility, non-toxicity, [176] biodegradability in the body, [177] and non-allergenicity. Additionally, due to their beneficial biological activities (antibacterial, antifungal, antioxidant) and bio-adhesivity, [178] they are widely used as hydrating and adsorption agents, as well as for wound healing and film production. [1, 179-182] Both chitosan and chitin may be synthesised into different forms such as beads, powders, fibres, films, and gels. [159] In fibre or film state, chitosan and chitin can be applied to tissue engineering or wound dressing. [183-185] Indeed, chitosan may be used in oral or nasal routes for drug delivery due to the transmucosal absorption promoter effect, delivering vaccines and drugs to peptides in the body. [186, 187] Some of the most promising developments in the pharmaceutical and biomedical fields have been chitin or chitosan based over the years. [180, 188-194]

Chitin applications are less developed compared to those of chitosan due to its insolubility and processing difficulties. Because of this, chitin is often combined with chitosan or its derivatives for these applications. Flexible chitin films have been utilized as wound dressing materials and displayed accelerated wound healing properties. Yusof et al. compared chitin-based wound dressings to commercial dressings made from conventional materials and found that the chitin wound dressings displayed an improved infection-free healing rate. Additionally they did not observe any abnormally high inflammatory response, which is usually expected from a biodegradable material. [7] A mixture of chitin nanofibrils, chitosan glycolate and chlorhexidine was manufactured into a gel, spray, and gauze for wound treatment. When testing on mice wound models, Muzzarelli et al. found that the spray could be used on bleeding abrasions as a first aid tool, the gel could be used on thin epidermal layers to enhance physiological repair and the gauze was superior to other dressings made of conventional materials as no scar remained on the skin afterwards. [195]

Chitosan-based films, like other polysaccharide-based films, have a resistance to selective gas permeability and fat diffusion but they perform relatively poorly in terms of preventing water vapour transmission. This is due to their hydrophilic character which leads to increased water molecule interactions. [196] To overcome this problem, biocomposites and polymer blends can be used for preparing chitosan-based stable coatings.

Chitosan and its derivatives have mucoadhesive properties that are proven to enhance the adsorption of drugs at neutral pH. N-lauryl-carboxymethyl-chitosan (LCC) was synthesised by Miwa et al. by attaching lauryl groups to the amino sites and carboxymethyl groups to the hydroxyl sites to provide both hydrophobic and hydrophilic moieties. This allowed for the effective solubilisation of the chemotherapy drug taxol by forming micelles. The membrane toxicity was tested and found to be safe and that the micelle-entrapped taxol was more efficient than free taxol in an in vitro assay. [197] Modified chitosan has also been used for genetic transfection - the process of introducing nucleic acid into eukaryotic cells to enhance or inhibit specific gene expressions in the cells. N-alkylated chitosan self-aggregates in acetic acid unlike unmodified chitosan due to its strong electrostatic repulsion. The N-alkylated chitosan can complex with DNA more efficiently due to increased entry into the cell facilitated by the hydrophobic interactions. [198]

1.5 Preamble to the remaining sections of this thesis

Having introduced chitosan and chitosan-based films and described some of their applications, this thesis continues with chapter 2 which described the experiment methods conducted over various projects. These projects and their results are described in further detail in their respective chapters. Chapter 3 discusses the formation of chitosan-based thin films and their analysis with regards to film composition, spectroscopy, and mechanical properties. Chapter 4 describes a technique from a previously published work on slot-die based chitosan film casting. The mechanical properties of the films cast via the slot-die technique are also discussed. This is followed by three application-driven chapters that discuss different chitosan mechanisms: sorption, antimicrobial activity, and pH dependant swelling. Chapter 5 explores the use of chitosan-based composite films in the sorption of heavy metals from aqueous solutions. Preliminary adsorption isotherm studies were carried out. In chapter 6, the antibacterial activities of chitosan-based films were tested on both Gram-negative and Gram-positive types of bacteria. The mechanisms of antibacterial activity were discussed based on bacterial growth assay results. Following that, chapter 7 proposed a preliminary design for the foundation of the development of smart wound dressings made from chitosan-based films for chronic wounds. The swelling properties of the films paired with photonic crystal layer deposition were the basis of the colour change design. Finally, chapter 8 concludes the thesis and summarises the results and discussions from each chapter.

References

1. Rinaudo, M., *Chitin and chitosan: Properties and applications.* Progress in Polymer Science, 2006. **31**(7): p. 603-632.
2. Varum, K.M., et al., *In vitro degradation rates of partially N-acetylated chitosans in human serum.* Carbohydrate Research, 1997. **299**(1-2): p. 99-101.
3. Bagheri-Khoulenjani, S., S.M. Taghizadeh, and H. Mirzadeh, *An investigation on the short-term biodegradability of chitosan with various molecular weights and degrees of deacetylation.* Carbohydrate Polymers, 2009. **78**(4): p. 773-778.
4. Jayakumar, R., et al., *Novel chitin and chitosan nanofibers in biomedical applications.* Biotechnology Advances, 2010. **28**(1): p. 142-150.
5. Krajewska, B., *Application of chitin- and chitosan-based materials for enzyme immobilizations: a review.* Enzyme and Microbial Technology, 2004. **35**(2-3): p. 126-139.
6. Kanke, M., et al., *Appilcation of Chitin and Chitosan to Pharmaceutical Preparations. I. : Film Preparation and in Vitro Evaluation.* CHEMICAL & PHARMACEUTICAL BULLETIN, 1989. **37**(2): p. 523-525.
7. Yusof, N.L.B.M., et al., *Flexible chitin films as potential wound-dressing materials: Wound model studies.* Journal of Biomedical Materials Research Part A, 2003. **66A**(2): p. 224-232.
8. Kurita, K., *Controlled functionalization of the polysaccharide chitin.* Progress in Polymer Science, 2001. **26**(9): p. 1921-1971.
9. Guliyeva, U., et al., *Chitosan microparticles containing plasmid DNA as potential oral gene delivery system.* European Journal of Pharmaceutics and Biopharmaceutics, 2006. **62**(1): p. 17-25.
10. Calvo, P., et al., *Novel hydrophilic chitosan-polyethylene oxide nanoparticles as protein carriers.* Journal of Applied Polymer Science, 1997. **63**(1): p. 125-132.
11. Illum, L., *Chitosan and its use as a pharmaceutical excipient.* Pharmaceutical Research, 1998. **15**(9): p. 1326-1331.
12. Park, J.H., et al., *Targeted delivery of low molecular drugs using chitosan and its derivatives.* Advanced Drug Delivery Reviews, 2010. **62**(1): p. 28-41.

13. Madihally, S.V. and H.W.T. Matthew, *Porous chitosan scaffolds for tissue engineering.* Biomaterials, 1999. **20**(12): p. 1133-1142.
14. Duttagupta, D.S., V.M. Jadhav, and V.J. Kadam, *Chitosan: A Propitious Biopolymer for Drug Delivery.* Current Drug Delivery, 2015. **12**(4): p. 369-381.
15. Minagawa, T., et al., *Effects of molecular weight and deacetylation degree of chitin/chitosan on wound healing.* Carbohydrate Polymers, 2007. **67**(4): p. 640-644.
16. Rabea, E.I., et al., *Chitosan as antimicrobial agent: Applications and mode of action.* Biomacromolecules, 2003. **4**(6): p. 1457-1465.
17. Aranaz, I., R. Harris, and A. Heras, *Chitosan Amphiphilic Derivatives. Chemistry and Applications.* Current Organic Chemistry, 2010. **14**(3): p. 308-330.
18. Riva, R., et al., *Chitosan and Chitosan Derivatives in Drug Delivery and Tissue Engineering.* Chitosan for Biomaterials Ii, 2011. **244**: p. 19-44.
19. Farion, I.A., et al., *Functionalization of chitosan with carboxylic acids and derivatives of them: Synthesis issues and prospects of practical use: A review.* Express Polymer Letters, 2018. **12**: p. 1081-1105.
20. Zohuriaan-Mehr, M.J., *Advances in chitin and chitosan modification through graft copolymerization: A comprehensive review*. Iranian Polymer Journal, 2005. **14**(3): p. 235-265.
21. Cai, J., et al., *Enzymatic preparation of chitosan from the waste Aspergillus niger mycelium of citric acid production plant.* Carbohydrate Polymers, 2006. **64**(2): p. 151-157.
22. Peniche, C., W. Arguelles-Monal, and F.M. Goycoolea, *Chitin and Chitosan: Major Sources, Properties and Applications.* Monomers, Polymers and Composites from Renewable Resources, 2008: p. 517-542.
23. Roberts, G.A., *Chitin chemistry*. 1992: Macmillan International Higher Education.
24. Leedy, M.R., et al., *Use of Chitosan as a Bioactive Implant Coating for Bone-Implant Applications*, in *Chitosan for Biomaterials II*, R. Jayakumar, M. Prabaharan, and R.A.A. Muzzarelli, Editors. 2011, Springer Berlin Heidelberg: Berlin, Heidelberg. p. 129-165.

25. Chen, Z.G., et al., *Intermolecular interactions in electrospun collagen-chitosan complex nanofibers.* Carbohydrate Polymers, 2008. **72**(3): p. 410-418.
26. Muzzarelli, R.A.A. and R. Rocchetti, *Determination of the degree of acetylation of chitosans by first derivative ultraviolet spectrophotometry.* Carbohydrate Polymers, 1985. **5**(6): p. 461-472.
27. Tan, S.C., et al., *The degree of deacetylation of chitosan: advocating the first derivative UV-spectrophotometry method of determination.* Talanta, 1998. **45**(4): p. 713-719.
28. Baxter, A., et al., *IMPROVED METHOD FOR IR DETERMINATION OF THE DEGREE OF N-ACETYLATION OF CHITOSAN.* International Journal of Biological Macromolecules, 1992. **14**(3): p. 166-169.
29. Brugnerotto, J., et al., *An infrared investigation in relation with chitin and chitosan characterization.* Polymer, 2001. **42**(8): p. 3569-3580.
30. Duarte, M.L., et al., *An optimised method to determine the degree of acetylation of chitin and chitosan by FTIR spectroscopy.* International Journal of Biological Macromolecules, 2002. **31**(1-3): p. 1-8.
31. Muzzarelli, R.A.A.P.M.G.E.C.S., *Chitin handbook.* 1997, Atec, Grottammare, Italy: European Chitin Society.
32. Alonso, I.G., C. Penichecovas, and J.M. Nieto, *DETERMINATION OF THE DEGREE OF ACETYLATION OF CHITIN AND CHITOSAN BY THERMAL-ANALYSIS.* Journal of Thermal Analysis, 1983. **28**(1): p. 189-193.
33. Sato, H., et al., *Determination of the degree of acetylation of chitin/chitosan by pyrolysis gas chromatography in the presence of oxalic acid.* Analytical Chemistry, 1998. **70**(1): p. 7-12.
34. Varum, K.M., et al., *HIGH-FIELD NMR-SPECTROSCOPY OF PARTIALLY N-DEACETYLATED CHITINS (CHITOSANS) .1. DETERMINATION OF THE DEGREE OF N-ACETYLATION AND THE DISTRIBUTION OF N-ACETYL GROUPS IN PARTIALLY N-DEACETYLATED CHITINS (CHITOSANS) BY HIGH-FIELD NMR-SPECTROSCOPY.* Carbohydrate Research, 1991. **211**(1): p. 17-23.
35. Muzzarelli, R.A.A., *CHAPTER 2 - STEREOCHEMISTRY AND PHYSICAL CHARACTERIZATION*, in *Chitin*, R.A.A. Muzzarelli, Editor. 1977, Pergamon. p. 45-86.

36. Nanjo, F., R. Katsumi, and K. Sakai, *ENZYMATIC METHOD FOR DETERMINATION OF THE DEGREE OF DEACETYLATION OF CHITOSAN.* Analytical Biochemistry, 1991. **193**(2): p. 164-167.
37. Peter, M.G., *Applications and Environmental Aspects of Chitin and Chitosan.* Journal of Macromolecular Science, Part A, 1995. **32**(4): p. 629-640.
38. Mima, S., et al., *Highly deacetylated chitosan and its properties.* Journal of Applied Polymer Science, 1983. **28**(6): p. 1909-1917.
39. Miyoshi, H., et al., *Characterization of Some Fungal Chitosans.* Bioscience, Biotechnology, and Biochemistry, 1992. **56**(12): p. 1901-1905.
40. Domszy, J.G. and G.A.F. Roberts, *Evaluation of infrared spectroscopic techniques for analysing chitosan.* Die Makromolekulare Chemie, 1985. **186**(8): p. 1671-1677.
41. Tsaih, M.L. and R.H. Chen, *Molecular weight determination of 83% degree of decetylation chitosan with non-gaussian and wide range distribution by high-performance size exclusion chromatography and capillary viscometry.* Journal of Applied Polymer Science, 1999. **71**(11): p. 1905-1913.
42. Janes, K.A. and M.J. Alonso, *Depolymerized chitosan nanoparticles for protein delivery: Preparation and characterization.* Journal of Applied Polymer Science, 2003. **88**(12): p. 2769-2776.
43. Bano, I., et al., *Chitosan: A potential biopolymer for wound management.* International Journal of Biological Macromolecules, 2017. **102**: p. 380-383.
44. Luo, K., et al., *Mucoadhesive and elastic films based on blends of chitosan and hydroxyethylcellulose.* Macromolecular Bioscience, 2008. **8**(2): p. 184-192.
45. Song, M.J., et al., *Drug-eluting bead loaded with doxorubicin versus conventional Lipiodol-based transarterial chemoembolization in the treatment of hepatocellular carcinoma: a case-control study of Asian patients.* European Journal of Gastroenterology & Hepatology, 2011. **23**(6): p. 521-527.
46. Chu, B., *VIII - CHARACTERIZATION OF POLYMER MOLECULAR-WEIGHT DISTRIBUTION (PARTICLE SIZING)*, in *Laser Light Scattering (Second Edition)*, B. Chu, Editor. 1991, Academic Press. p. 283-319.
47. Anthonsen, M.W., et al., *AGGREGATES IN ACIDIC SOLUTIONS OF CHITOSANS DETECTED BY STATIC LASER-LIGHT SCATTERING.* Carbohydrate Polymers, 1994. **25**(1): p. 13-23.

48. Slomkowski, S., et al., *Terminology of polymers and polymerization processes in dispersed systems (IUPAC Recommendations 2011).* Pure and Applied Chemistry, 2011. **83**(12): p. 2229-2259.
49. Ghazy, A., et al., *Determination of Chitosan Scattering Parameters by Using Multi Angle Static Laser Light Scattering(MASLLS).* Delta J. Sci, 2016. **37**: p. 71-80.
50. Debye, P.P., *Light Scattering in Solutions.* Journal of Applied Physics, 1944. **15**: p. 338-342.
51. Kasaai, M.R., J. Arul, and C. Charlet, *Intrinsic viscosity-molecular weight relationship for chitosan.* Journal of Polymer Science Part B-Polymer Physics, 2000. **38**(19): p. 2591-2598.
52. Rinaudo, M., M. Milas, and P. Ledung, *CHARACTERIZATION OF CHITOSAN - INFLUENCE OF IONIC-STRENGTH AND DEGREE OF ACETYLATION ON CHAIN EXPANSION.* International Journal of Biological Macromolecules, 1993. **15**(5): p. 281-285.
53. Jiang, X., et al., *Chitosan-g-PEG/DNA complexes deliver gene to the rat liver via intrabiliary and intraportal infusions.* Journal of Gene Medicine, 2006. **8**(4): p. 477-487.
54. Hasegawa, M., A. Isogai, and F. Onabe, *MOLECULAR-MASS DISTRIBUTION OF CHITIN AND CHITOSAN.* Carbohydrate Research, 1994. **262**(1): p. 161-166.
55. Kumari, S. and R. Kishor, *Chapter 1 - Chitin and chitosan: origin, properties, and applications*, in *Handbook of Chitin and Chitosan*, S. Gopi, S. Thomas, and A. Pius, Editors. 2020, Elsevier. p. 1-33.
56. Budishevska, O., et al., *Chapter 12 - Formation of three-dimensional polymer structures through radical and ionic reactions of peroxychitosan*, in *Studies in Natural Products Chemistry*, R. Atta Ur, Editor. 2020, Elsevier. p. 365-390.
57. Chattopadhyay, D.P. and M.S. Inamdar, *Aqueous Behaviour of Chitosan.* International Journal of Polymer Science, 2010. **2010**.
58. Jagadish, C.R.a.F.S.a.S.G.a.A.F., *Solubility of Chitin: Solvents, Solution Behaviors and Their Related Mechanisms*, in *Solubility of Polysaccharides*, X. Zhenbo, Editor. 2017, IntechOpen: Rijeka.

59. Austin, P.R., Wilmington, and Del, *Solvents for and purification of chitin*, in *United States Patent*, N. University of Delaware, Editor. 1976, University of Delaware, Newark: US. p. 2.
60. Popa-Nita, S., et al., *Continuum of Structural Organization from Chitosan Solutions to Derived Physical Forms.* Biomacromolecules, 2010. **11**(1): p. 6-12.
61. Philippova, O.E., et al., *Aggregation of some water-soluble derivatives of chitin in aqueous solutions: Role of the degree of acetylation and effect of hydrogen bond breaker.* Carbohydrate Polymers, 2012. **87**(1): p. 687-694.
62. Ma, G.P., et al., *Synthesize and properties of photosensitive organic solvent soluble acylated chitosan derivatives (2).* Carbohydrate Polymers, 2011. **84**(1): p. 681-685.
63. Tamura, H., T. Hamaguchi, and S. Tokura, *Destruction of rigid crystalline structure to prepare chitin solution.* Advances in Chitin Science, 2004. **7**: p. 84-87.
64. Luo, Y.C. and Q. Wang, *Recent development of chitosan-based polyelectrolyte complexes with natural polysaccharides for drug delivery.* International Journal of Biological Macromolecules, 2014. **64**: p. 353-367.
65. Philippova, O.E. and E.V. Korchagina, *Chitosan and its hydrophobic derivatives: Preparation and aggregation in dilute aqueous solutions.* Polymer Science Series A, 2012. **54**(7): p. 552-572.
66. Tian, M., et al., *Molecular weight dependence of structure and properties of chitosan oligomers.* Rsc Advances, 2015. **5**(85): p. 69445-69452.
67. Braconnot, H., *Sur la nature des champibnons.* Ann Chi, 1881. **79**: p. 265-304.
68. Rouget, C., *Des substances amylacées dans les tissus des animaux, spécialement des Articulés (chitine).* Comp. Rend, 1859. **48**: p. 792-795.
69. Abdou, E.S., K.S.A. Nagy, and M.Z. Elsabee, *Extraction and characterization of chitin and chitosan from local sources.* Bioresource Technology, 2008. **99**(5): p. 1359-1367.
70. Wu, F.-C., R.-L. Tseng, and R.-S. Juang, *Comparative adsorption of metal and dye on flake- and bead-types of chitosans prepared from fishery wastes.* Journal of Hazardous Materials, 2000. **73**(1): p. 63-75.
71. Kurita, K., *Chitin and chitosan: Functional biopolymers from marine crustaceans.* Marine Biotechnology, 2006. **8**(3): p. 203-226.

72. Synowiecki, J. and N.A. Al-Khateeb, *Production, properties, and some new applications of chitin and its derivatives.* Critical Reviews in Food Science and Nutrition, 2003. **43**(2): p. 145-171.
73. Vazquez, J.A., et al., *Chondroitin Sulfate, Hyaluronic Acid and Chitin/Chitosan Production Using Marine Waste Sources: Characteristics, Applications and Eco-Friendly Processes: A Review.* Marine Drugs, 2013. **11**(3): p. 747-774.
74. Percot, A., C. Viton, and A. Domard, *Optimization of chitin extraction from shrimp shells.* Biomacromolecules, 2003. **4**(1): p. 12-18.
75. Jung, W.J., et al., *Production of chitin from red crab shell waste by successive fermentation with Lactobacillus paracasei KCTC-3074 and Serratia marcescens FS-3.* Carbohydrate Polymers, 2007. **68**(4): p. 746-750.
76. Healy, M., A. Green, and A. Healy, *Bioprocessing of marine crustacean shell waste.* Acta Biotechnologica, 2003. **23**(2-3): p. 151-160.
77. Jo, G.H., et al., *Screening of protease-producing Serratia marcescens FS-3 and its application to deproteinization of crab shell waste for chitin extraction.* Carbohydrate Polymers, 2008. **74**(3): p. 504-508.
78. Bautista, J., et al., *Preparation of crayfish chitin by in situ lactic acid production.* Process Biochemistry, 2001. **37**(3): p. 229-234.
79. Valdez-Pena, A.U., et al., *Screening of industrial enzymes for deproteinization of shrimp head for chitin recovery.* Food Science and Biotechnology, 2010. **19**(2): p. 553-557.
80. Synowiecki, J. and N. Al-Khateeb, *The recovery of protein hydrolysate during enzymatic isolation of chitin from shrimp Crangon crangon processing discards.* Food Chemistry, 2000. **68**(2): p. 147-152.
81. De Holanda, H.D. and F.M. Netto, *Recovery of components from shrimp (Xiphopenaeus kroyeri) processing waste by enzymatic hydrolysis.* Journal of Food Science, 2006. **71**(5): p. C298-C303.
82. Synowiecki, J. and N. AlKhateeb, *Mycelia of Mucor rouxii as a source of chitin and chitosan.* Food Chemistry, 1997. **60**(4): p. 605-610.
83. Chatterjee, S., et al., *Chitosan from Mucor rouxii: production and physico-chemical characterization.* Process Biochemistry, 2005. **40**(1): p. 395-400.

84. Sandipan, C., B. Chatterjee, and A. Guha, *Kinetics of Mucor rouxii fermentation in relation to chitosan production.* Research Journal of Microbiology, 2010. **5**(7): p. 696-700.
85. Martinou, A., et al., *Mode of action of chitin deacetylase from Mucor rouxii on partiality N-acetylated chitosans.* Carbohydrate Research, 1998. **311**(1-2): p. 71-78.
86. Trutnau, M., et al., *Enhanced chitosan production and modeling hyphal growth of Mucor rouxii interpreting the dependence of chitosan yields on processing and cultivation time.* Engineering in Life Sciences, 2009. **9**(6): p. 437-443.
87. NEUROtiker, *By NEUROtiker - Own work, Public Domain,* *https://commons.wikimedia.org/w/index.php?curid=3534135*. https://en.wikipedia.org/wiki/Chitosan, 18/09/2017.
88. Sperling, L.H., *Interpenetrating polymer networks and related materials*. 1981: Plenum Press.
89. Sperling, L.H., *Interpenetrating Polymer Networks: An Overview*, in *Interpenetrating Polymer Networks*. 1994, American Chemical Society. p. 3-38.
90. Park, S.-B., et al., *A novel pH-sensitive membrane from chitosan — TEOS IPN; preparation and its drug permeation characteristics.* Biomaterials, 2001. **22**(4): p. 323-330.
91. Aylsworth, *J. W. U.S. Patent* 111, 1914. **284**(1).
92. Staudinger, J.J.P.H., *H. M. U.S. Patent 2.* 539, 1951. **377**(1).
93. Solt, G.S., *British Patent.* 728, 1955. **508**(1).
94. Millar, J.R., *J. Chem. Soc.* 1311., 1960.
95. Shibayama, K.S., Y. , *Rubber Chem. Tech.* 40, 1967.
96. Lipatov, Y.S.S., *C. M. Russ. Chem. Rev.* 45, 1967. **1**(63).
97. Frisch, H.L., D. Klempner, and Frisch, *K. C. J. Polym. Sci., Polym. Phys. Ed. 7.* 1969. **11**(755).
98. Sperling, L.H.F., *D. W. J. Polym. Sci. .* A-2, 1969. **7**(425).
99. Dragan, E.S., *Design and applications of interpenetrating polymer network hydrogels. A review.* Chemical Engineering Journal, 2014. **243**: p. 572-590.

100. Guo, B., et al., *Preparation and release profiles of pH/temperature-responsive carboxymethyl chitosan/P(2-(dimethylamino) ethyl methacrylate) semi-IPN amphoteric hydrogel.* Colloid and Polymer Science, 2007. **285**(6): p. 665-671.
101. Kim, I.-Y., et al., *Preparation of semi-interpenetrating polymer networks composed of chitosan and poloxamer.* International Journal of Biological Macromolecules, 2006. **38**(1): p. 51-58.
102. Jain, E. and A. Kumar, *Designing Supermacroporous Cryogels Based on Polyacrylonitrile and a Polyacrylamide–Chitosan Semi-interpenetrating Network.* Journal of Biomaterials Science, Polymer Edition, 2009. **20**(7-8): p. 877-902.
103. Tripathi, A. and A. Kumar, *Multi-Featured Macroporous Agarose–Alginate Cryogel: Synthesis and Characterization for Bioengineering Applications.* Macromolecular Bioscience, 2010. **11**(1): p. 22-35.
104. Lozinsky, V.I., et al., *Polymeric cryogels as promising materials of biotechnological interest.* Trends in Biotechnology, 2003. **21**(10): p. 445-451.
105. Artyukhov, A.A., et al., *Macroporous polymeric hydrogels formed from acrylate modified polyvinyl alcohol macromers.* Journal of Polymer Research, 2011. **18**(4): p. 667-673.
106. Plieva, F.M., et al., *Pore structure in supermacroporous polyacrylamide based cryogels.* Soft Matter, 2005. **1**(4): p. 303-309.
107. Crini, G. and P.-M. Badot, *Application of chitosan, a natural aminopolysaccharide, for dye removal from aqueous solutions by adsorption processes using batch studies: A review of recent literature.* Progress in Polymer Science, 2008. **33**(4): p. 399-447.
108. Wan Ngah, W.S., L.C. Teong, and M.A.K.M. Hanafiah, *Adsorption of dyes and heavy metal ions by chitosan composites: A review.* Carbohydrate Polymers, 2011. **83**(4): p. 1446-1456.
109. Dalaran, M., et al., *Study on a novel polyampholyte nanocomposite superabsorbent hydrogels: Synthesis, characterization and investigation of removal of indigo carmine from aqueous solution.* Desalination, 2011. **279**(1): p. 170-182.
110. Huang, X.-Y., et al., *Chemical modification of chitosan by tetraethylenepentamine and adsorption study for anionic dye removal.* Carbohydrate Research, 2011. **346**(10): p. 1232-1240.

111. Adewuyi, S., I.O. Bisiriyu, and C.A. Akinremi, *ZINC (II) METAL ION COMPLEXES OF CHITOSAN: TOWARD HETEROGENEOUS-ACTIVE CATALYSTS FOR THE POLYMERIZATION OF VINYL ACETATE*. IJS, 2015. **III**: p. 749-754.
112. ELmezayyen, A.S. and F.M. Reicha, *Preparation of Chitosan Copper Complexes: Molecular Dynamic Studies of Chitosan and Chitosan Copper Complexes.* Open Journal of Applied Sciences, 2015. **Vol.05No.08**: p. 14.
113. Qu, X., A. Wirsén, and A.C. Albertsson, *Novel pH-sensitive chitosan hydrogels: swelling behavior and states of water.* Polymer, 2000. **41**(12): p. 4589-4598.
114. Zhang, J.L., et al., *Chitosan Modification and Pharmaceutical/Biomedical Applications.* Marine Drugs, 2010. **8**(7): p. 1962-1987.
115. Fajardo, P., et al., *Evaluation of a chitosan-based edible film as carrier of natamycin to improve the storability of Saloio cheese.* Journal of Food Engineering, 2010. **101**(4): p. 349-356.
116. McConnell, E.L., S. Murdan, and A.W. Basit, *An investigation into the digestion of chitosan (noncrosslinked and crosslinked) by human colonic bacteria.* Journal of Pharmaceutical Sciences, 2008. **97**(9): p. 3820-3829.
117. Hu, Z.Y. and M.G. Ganzle, *Challenges and opportunities related to the use of chitosan as a food preservative.* Journal of Applied Microbiology, 2019. **126**(5): p. 1318-1331.
118. Muzzarelli, R.A.A., et al., *Chitosan taurocholate capacity to bind lipids and to undergo enzymatic hydrolysis: An in vitro model.* Carbohydrate Polymers, 2006. **66**(3): p. 363-371.
119. Devlieghere, F., A. Vermeulen, and J. Debevere, *Chitosan: antimicrobial activity, interactions with food components and applicability as a coating on fruit and vegetables.* Food Microbiology, 2004. **21**(6): p. 703-714.
120. Liu, L., et al., *Preparation and properties of chitosan-based bacteriostatic agents and their application in strawberry bacteriostatic preservation.* Journal of Food Science, 2021. **86**(10): p. 4611-4627.
121. Patrulea, V., et al., *Chitosan as a starting material for wound healing applications.* European Journal of Pharmaceutics and Biopharmaceutics, 2015. **97**: p. 417-426.

122. Roy, K., et al., *Oral gene delivery with chitosan-DNA nanoparticles generates immunologic protection in a murine model of peanut allergy.* Nature Medicine, 1999. **5**(4): p. 387-391.
123. Wu, J.W., et al., *Chitosan Nano Carriers Loading Anti-tumor Drugs.* Journal of Nano Research, 2015. **32**: p. 113-U159.
124. Wang, Q.Z., et al., *Preparation and blood coagulation evaluation of chitosan microspheres.* Journal of Materials Science-Materials in Medicine, 2008. **19**(3): p. 1371-1377.
125. Araujo, B.R., et al., *Evaluation of the interactions between chitosan and humics in media for the controlled release of nitrogen fertilizer.* Journal of Environmental Management, 2017. **190**: p. 122-131.
126. El Hadrami, A., et al., *Chitosan in Plant Protection.* Marine Drugs, 2010. **8**(4): p. 968-987.
127. Hadwiger, L.A., *Multiple effects of chitosan on plant systems: Solid science or hype.* Plant Science, 2013. **208**: p. 42-49.
128. Kashyap, P.L., X. Xiang, and P. Heiden, *Chitosan nanoparticle based delivery systems for sustainable agriculture.* International Journal of Biological Macromolecules, 2015. **77**: p. 36-51.
129. Sungkharak, S., et al., *Antibacterial Activity Against Acne Involved Bacteria of Chitosan in a Soluble State and as Nanoparticles.* Chiang Mai Journal of Science, 2016. **43**(5): p. 1149-1158.
130. Resende, A.H.M., et al., *Application of biosurfactants and chitosan in toothpaste formulation.* Colloids and Surfaces B-Biointerfaces, 2019. **181**: p. 77-84.
131. Chaiwong, N., et al., *Synergistics of Carboxymethyl Chitosan and Mangosteen Extract as Enhancing Moisturizing, Antioxidant, Antibacterial, and Deodorizing Properties in Emulsion Cream.* Polymers, 2022. **14**(1).
132. Matos, B.N., et al., *Chitosan nanoparticles for targeting and sustaining minoxidil sulphate delivery to hair follicles.* International Journal of Biological Macromolecules, 2015. **75**: p. 225-229.
133. Fast, S.A., B. Kokabian, and V.G. Gude, *Chitosan enhanced coagulation of algal turbid waters - Comparison between rapid mix and ultrasound coagulation methods.* Chemical Engineering Journal, 2014. **244**: p. 403-410.

134. Zeng, D., J. Wu, and J.F. Kennedy, *Application of a chitosan flocculant to water treatment.* Carbohydrate Polymers, 2008. **71**(1): p. 135-139.
135. Vakili, M., et al., *Application of chitosan and its derivatives as adsorbents for dye removal from water and wastewater: A review.* Carbohydrate Polymers, 2014. **113**: p. 115-130.
136. Babel, S. and T.A. Kurniawan, *Low-cost adsorbents for heavy metals uptake from contaminated water: a review.* Journal of Hazardous Materials, 2003. **97**(1-3): p. 219-243.
137. Guibal, E., *Interactions of metal ions with chitosan-based sorbents: a review.* Separation and Purification Technology, 2004. **38**(1): p. 43-74.
138. Monteiro, O.A.C. and C. Airoldi, *Some thermodynamic data on copper-chitin and copper-chitosan biopolymer interactions.* Journal of Colloid and Interface Science, 1999. **212**(2): p. 212-219.
139. Wang, X., Y.M. Du, and H. Liu, *Preparation, characterization and antimicrobial activity of chitosan - Zn complex.* Carbohydrate Polymers, 2004. **56**(1): p. 21-26.
140. Gandhi, M.R., et al., *Sorption behaviour of copper on chemically modified chitosan beads from aqueous solution.* Carbohydrate Polymers, 2011. **83**(3): p. 1082-1087.
141. Muzzarelli, R.A.A., *Potential of chitin/chitosan-bearing materials for uranium recovery: An interdisciplinary review.* Carbohydrate Polymers, 2011. **84**(1): p. 54-63.
142. Ngah, W.S.W. and S. Fatinathan, *Pb(II) biosorption using chitosan and chitosan derivatives beads: Equilibrium, ion exchange and mechanism studies.* Journal of Environmental Sciences, 2010. **22**(3): p. 338-346.
143. Muzzarelli, R.A. and O. Tubertini, *CHITIN AND CHITOSAN AS CHROMATOGRAPHIC SUPPORTS AND ADSORBENTS FOR COLLECTION OF METAL IONS FROM ORGANIC AND AQUEOUS SOLUTIONS AND SEA-WATER.* Talanta, 1969. **16**(12): p. 1571-+.
144. Muller, P., *Glossary of terms used in physical organic chemistry (IUPAC Recommendations 1994).* Pure and Applied Chemistry, 1994. **66**(5): p. 1077-1184.

145. Chen, J.H., et al., *Removal of U(VI) from aqueous solutions by using MWCNTs and chitosan modified MWCNTs.* Journal of Radioanalytical and Nuclear Chemistry, 2013. **295**(3): p. 2233-2241.
146. Singh, A., K.U. Ulrich, and D.E. Giammar, *Impact of phosphate on U(VI) immobilization in the presence of goethite.* Geochimica Et Cosmochimica Acta, 2010. **74**(22): p. 6324-6343.
147. Stewart, B.D., M.A. Mayes, and S. Fendorf, *Impact of Uranyl-Calcium-Carbonato Complexes on Uranium(VI) Adsorption to Synthetic and Natural Sediments.* Environmental Science & Technology, 2010. **44**(3): p. 928-934.
148. World Health, O., *Uranium in drinking-water: background document for development of WHO guidelines for drinking-water quality*. 2004, World Health Organization: Geneva.
149. Arvand, M. and M.A. Pakseresht, *Cadmium adsorption on modified chitosan-coated bentonite: batch experimental studies.* Journal of Chemical Technology and Biotechnology, 2013. **88**(4): p. 572-578.
150. Elwakeel, K.Z., A.A. Atia, and E. Guibal, *Fast removal of uranium from aqueous solutions using tetraethylenepentamine modified magnetic chitosan resin.* Bioresource Technology, 2014. **160**: p. 107-114.
151. Donia, A.M., A.A. Atia, and K.Z. Elwakeel, *Selective separation of mercury(II) using magnetic chitosan resin modified with Schiff's base derived from thiourea and glutaraldehyde.* Journal of Hazardous Materials, 2008. **151**(2-3): p. 372-379.
152. Suc, N.V. and H.T.Y. Ly, *Lead (II) removal from aqueous solution by chitosan flake modified with citric acid via crosslinking with glutaraldehyde.* Journal of Chemical Technology and Biotechnology, 2013. **88**(9): p. 1641-1649.
153. Ngah, W.S.W., S. Ab Ghani, and L.L. Hoon, *Comparative adsorption of lead(II) on flake and bead-types of chitosan.* Journal of the Chinese Chemical Society, 2002. **49**(4): p. 625-628.
154. Merrifield, J.D., et al., *Uptake of mercury by thiol-grafted chitosan gel beads.* Water Research, 2004. **38**(13): p. 3132-3138.
155. Honary, S., B. Hoseinzadeh, and P. Shalchian, *The Effect of Polymer Molecular Weight on Citrate Crosslinked Chitosan Films for Site-Specific Delivery of a Non-Polar Drug.* Tropical Journal of Pharmaceutical Research, 2010. **9**(6): p. 525-531.

156. Farkas, V., *FUNGAL CELL-WALLS - THEIR STRUCTURE, BIOSYNTHESIS AND BIOTECHNOLOGICAL ASPECTS.* Acta Biotechnologica, 1990. **10**(3): p. 225-238.
157. Fleet, G.H. and H.J. Phaff, *Fungal Glucans — Structure and Metabolism*, in *Plant Carbohydrates II: Extracellular Carbohydrates*, W. Tanner and F.A. Loewus, Editors. 1981, Springer Berlin Heidelberg: Berlin, Heidelberg. p. 416-440.
158. Friedman, M. and V.K. Juneja, *Review of Antimicrobial and Antioxidative Activities of Chitosans in Food.* Journal of Food Protection, 2010. **73**(9): p. 1737-1761.
159. Navard, P., *The European Polysaccharide Network of Excellence (EPNOE): research initiatives and results*. 2012: Springer Science & Business Media.
160. Alishahi, A. and M. Aider, *Applications of Chitosan in the Seafood Industry and Aquaculture: A Review*. Food and Bioprocess Technology, 2012. **5**(3): p. 817-830.
161. Franklin, T.J. and G.A. Snow, *Biochemistry of antimicrobial action*. 2013: Springer.
162. Chen, C.S., W.Y. Liau, and G.J. Tsai, *Antibacterial effects of N-sulfonated and N-sulfobenzoyl chitosan and application to oyster preservation.* Journal of Food Protection, 1998. **61**(9): p. 1124-1128.
163. Jung, B.O., et al., *Preparation of amphiphilic chitosan and their antimicrobial activities.* Journal of Applied Polymer Science, 1999. **72**(13): p. 1713-1719.
164. Sudarshan, N.R., D.G. Hoover, and D. Knorr, *ANTIBACTERIAL ACTION OF CHITOSAN.* Food Biotechnology, 1992. **6**(3): p. 257-272.
165. Chung, Y.C., et al., *Relationship between antibacterial activity of chitosan and surface characteristics of cell wall.* Acta Pharmacologica Sinica, 2004. **25**(7): p. 932-936.
166. Jeon, Y.J., P.J. Park, and S.K. Kim, *Antimicrobial effect of chitooligosaccharides produced by bioreactor.* Carbohydrate Polymers, 2001. **44**(1): p. 71-76.
167. Muzzarelli, R., et al., *ANTIMICROBIAL PROPERTIES OF N-CARBOXYBUTYL CHITOSAN.* Antimicrobial Agents and Chemotherapy, 1990. **34**(10): p. 2019-2023.

168. Rhoades, J. and S. Roller, *Antimicrobial actions of degraded and native chitosan against spoilage organisms in laboratory media and foods.* Applied and Environmental Microbiology, 2000. **66**(1): p. 80-86.
169. Tao, Y., L.H. Qian, and J. Xie, *Effect of chitosan on membrane permeability and cell morphology of Pseudomonas aeruginosa and Staphyloccocus aureus.* Carbohydrate Polymers, 2011. **86**(2): p. 969-974.
170. Younes, I., et al., *Influence of acetylation degree and molecular weight of homogeneous chitosans on antibacterial and antifungal activities.* International Journal of Food Microbiology, 2014. **185**: p. 57-63.
171. Bell, A.A., et al., *Effects of chitin and chitosan on the incidence and severity of Fusarium yellows of celery.* Plant Disease, 1998. **82**(3): p. 322-328.
172. Ben-Shalom, N., et al., *Controlling gray mould caused by Botrytis cinerea in cucumber plants by means of chitosan.* Crop Protection, 2003. **22**(2): p. 285-290.
173. Bai, R.K., M.Y. Huang, and Y.Y. Jiang, *SELECTIVE PERMEABILITIES OF CHITOSAN-ACETIC ACID COMPLEX MEMBRANE AND CHITOSAN-POLYMER COMPLEX MEMBRANES FOR OXYGEN AND CARBON-DIOXIDE.* Polymer Bulletin, 1988. **20**(1): p. 83-88.
174. Park, P.J., J.Y. Je, and S.K. Kim, *Free radical scavenging activity of chitooligosaccharides by electron spin resonance spectrometry.* Journal of Agricultural and Food Chemistry, 2003. **51**(16): p. 4624-4627.
175. Kim, K.W. and R.L. Thomas, *Antioxidative activity of chitosans with varying molecular weights.* Food Chemistry, 2007. **101**(1): p. 308-313.
176. Kumar, M., et al., *Chitosan chemistry and pharmaceutical perspectives.* Chemical Reviews, 2004. **104**(12): p. 6017-6084.
177. Patil, R.S., V. Ghormade, and M.V. Deshpande, *Chitinolytic enzymes: an exploration.* Enzyme and Microbial Technology, 2000. **26**(7): p. 473-483.
178. Venter, J.P., et al., *Synthesis and evaluation of the mucoadhesivity of a CD-chitosan derivative.* International Journal of Pharmaceutics, 2006. **313**(1-2): p. 36-42.
179. Rinaudo, M., *Main properties and current applications of some polysaccharides as biomaterials.* Polymer International, 2008. **57**(3): p. 397-430.

180. Sarmento, B. and J. das Neves, *Chitosan-based systems for biopharmaceuticals: delivery, targeting and polymer therapeutics*. 2012: John Wiley & Sons.
181. Stevens, C.V., *Bio-based plastics: materials and applications*. 2013: John Wiley & Sons.
182. Khor, E., *Chitin: a biomaterial in waiting.* Current Opinion in Solid State & Materials Science, 2002. **6**(4): p. 313-317.
183. Maeda, Y., et al., *Synthesis, characterization and bioactivity studies of novel beta-chitin scaffolds for tissue-engineering applications.* International Journal of Biological Macromolecules, 2008. **42**(5): p. 463-467.
184. Nagahama, H., et al., *Novel biodegradable chitin membranes for tissue engineering applications.* Carbohydrate Polymers, 2008. **73**(2): p. 295-302.
185. Yang, T.L., *Chitin-based Materials in Tissue Engineering: Applications in Soft Tissue and Epithelial Organ.* International Journal of Molecular Sciences, 2011. **12**(3): p. 1936-1963.
186. Mi, F.L., et al., *Chitin/PLGA blend microspheres as a biodegradable drug-delivery system: phase-separation, degradation and release behavior.* Biomaterials, 2002. **23**(15): p. 3257-3267.
187. Dumitriu, S., *Polysaccharides: structural diversity and functional versatility*. 2004: CRC press.
188. Kumirska, J., et al., *Biomedical Activity of Chitin/Chitosan Based Materials-Influence of Physicochemical Properties Apart from Molecular Weight and Degree of N-Acetylation.* Polymers, 2011. **3**(4): p. 1875-1901.
189. Jayakumar, R., et al., *Biomedical applications of chitin and chitosan based nanomaterials-A short review.* Carbohydrate Polymers, 2010. **82**(2): p. 227-232.
190. Aranaz, I., et al., *Functional characterization of chitin and chitosan.* Current chemical biology, 2009. **3**(2): p. 203-230.
191. Dutta, P.K., J. Dutta, and V.S. Tripathi, *Chitin and chitosan: Chemistry, properties and applications.* Journal of Scientific & Industrial Research, 2004. **63**(1): p. 20-31.
192. Park, B.K. and M.M. Kim, *Applications of Chitin and Its Derivatives in Biological Medicine.* International Journal of Molecular Sciences, 2010. **11**(12): p. 5153-5165.

193. Cheba, B.A., *Chitin and chitosan: marine biopolymers with unique properties and versatile applications.* Global Journal of Biotechnology & Biochemistry, 2011. **6**(3): p. 149-153.
194. *Chitin and Chitosan Derivatives: Advances in Drug Discovery and Developments.* Chitin and Chitosan Derivatives: Advances in Drug Discovery and Developments, 2014: p. 1-492.
195. Muzzarelli, R.A.A., et al., *Chitin nanofibrils/chitosan glycolate composites as wound medicaments.* Carbohydrate Polymers, 2007. **70**(3): p. 274-284.
196. Bordenave, N., et al., *Water and moisture susceptibility of chitosan and paper-based materials: Structure-property relationships.* Journal of Agricultural and Food Chemistry, 2007. **55**(23): p. 9479-9488.
197. Miwa, A., et al., *Development of novel chitosan derivatives as micellar carriers of taxol.* Pharmaceutical Research, 1998. **15**(12): p. 1844-1850.
198. Liu, W.G., et al., *N-alkylated chitosan as a potential nonviral vector for gene transfection.* Bioconjugate Chemistry, 2003. **14**(4): p. 782-789.

2. Materials and Methods

2.1 Hydrogel recipes and ratios

2.1.1 Preparation of chitosan-based hydrogels

Based on the information available from the literature [1-3], the chitosan chosen for this work had a lower molecular weight (50,000–190,000 Da, Sigma Aldrich Ireland) with a DD of 75–85 % to help facilitate the dissolving of the crystalline solid in aqueous acid solution. Tetraethyl-orthosilicate (≥99 %), glutaraldehyde solution (25 %), 3-aminopropyltriethoxysilane (99 %) polyacrylamide solution (≥99 %), hydrochloric acid (37 %), acetic acid (≥99 %) and ethanol (≥99 %) were purchased from Sigma-Aldrich (Ireland). Millipore deionized water (18 MΩ) was used to prepare aqueous solutions. All materials were used as received. Five types of chitosan-based hydrogel were synthesized and made into to (a), chitosan-only films, (b), chitosan-TEOS IPNs, (c), chitosan-glutaraldehyde cross-linked films, (d), chitosan-APTES IPNs and (e), chitosan-PAM polymer blends. The general syntheses of all these types of films have been reported previously in the literature [4-13] and served as benchmarks for the synthesis, characterisation and discussion of the film made here.

For all films studied, the dissolution of the chitosan was initially performed as follows: low molecular weight chitosan (50,000–190,000 Da, 0.005 mol, 1.04 g) was dissolved in Millipore deionized H_2O (65 mL and acetic acid (0.32 mL, 1% wt.)), covered with Parafilm and left to continuously stir at room temperature overnight. The chitosan solid began to dissolve once the acid was added as a result of protonation of the amine groups on the chitosan, as shown in scheme 2.1 below:

$$Chi - NH_2 + H_3O^+ \leftrightarrow Chi - NH_3^+ + H_2O \qquad \text{scheme 2.1}$$

2.1.1.1 Chi-TEOS

For the synthesis of the chitosan-tetraethyl-orthosilicate IPN films (Chi-TEOS), hydrogels were prepared in mildly acidic conditions to facilitate cationic polymerization. The procedure was based on that described by Park et al. [14] TEOS (≥99%, 0.005 mol, 1.11 mL) was dissolved in filtered ethanol (15 mL) and allowed to continuously stir at room temperature for 30 minutes. Next, HCl (0.0274 mL), filtered ethanol (10 mL) and Millipore deionized water (25 mL) were added to a beaker and allowed to stir continuously at room temperature for 30 minutes. After 30 minutes the HCl solution was slowly added to the TEOS solution, dropwise, with continuous stirring. The mixture was covered with Parafilm and allowed to continuously stir at room temperature for 24 hours. The acidic TEOS solution was then slowly added to the chitosan solution dropwise, with continuous stirring. The resulting Chi-TEOS (1:1) mixture was covered with Parafilm and allowed to continuously stir at room temperature for a further 48 hours. The mixture was observed to become more viscous over the 48-hour period. The hydrogel was then stored in a fridge until removed for use. A series of Chi-TEOS (2:1) films were also synthesised for tensile strength tests.

It is known that this process results in the formation of an IPN between the chitosan and the siloxane polymer that forms when TEOS is hydrolysed. [14-16] The first step in the formation of the IPN involves the hydrolysis of the TEOS. Figure 2.1 shows the accepted mechanism of the formation of the siloxane polymer via the hydrolysis and condensation of TEOS, based on the mechanism presented in [17]:

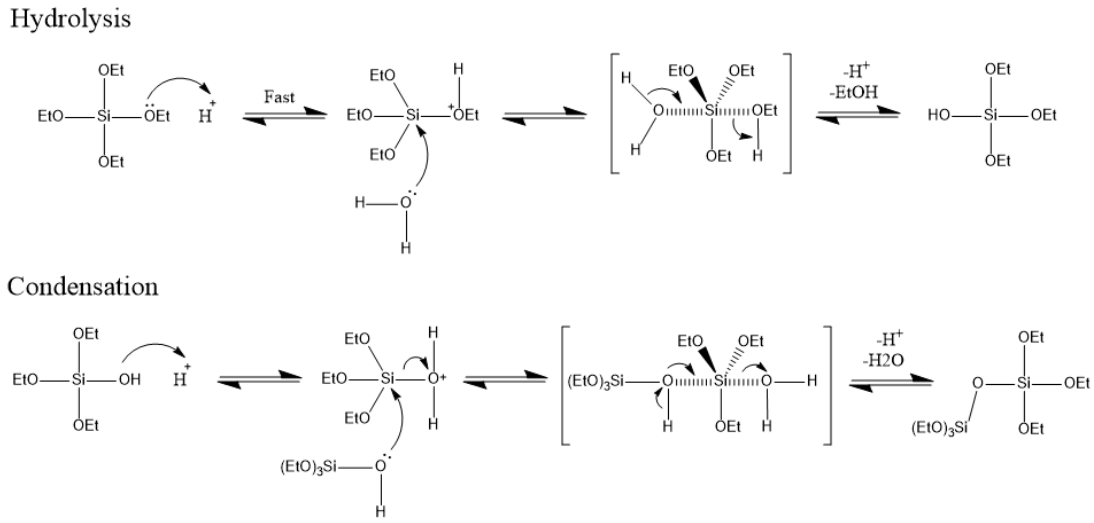


Figure 2.1: Hydrolysis and condensation reactions of TEOS precursors to form a siloxane polymer chain and subsequent network. [17]

The chitosan network itself is held together with hydrogen bonds, as shown in Figure 2.2. When this solution is added to the solution containing the siloxane polymer, mixing occurs, and the chitosan chains form their hydrogen-bonded network around the covalently bonded siloxane chains. The cross-linking between the two components thus occurs non-covalently by intermolecular hydrogen bonding in the polymer networks between the polar hydroxyl and amino functional groups of the chitosan polymer network and the polar hydroxyl groups of the TEOS network, as shown in Figure 2.2.

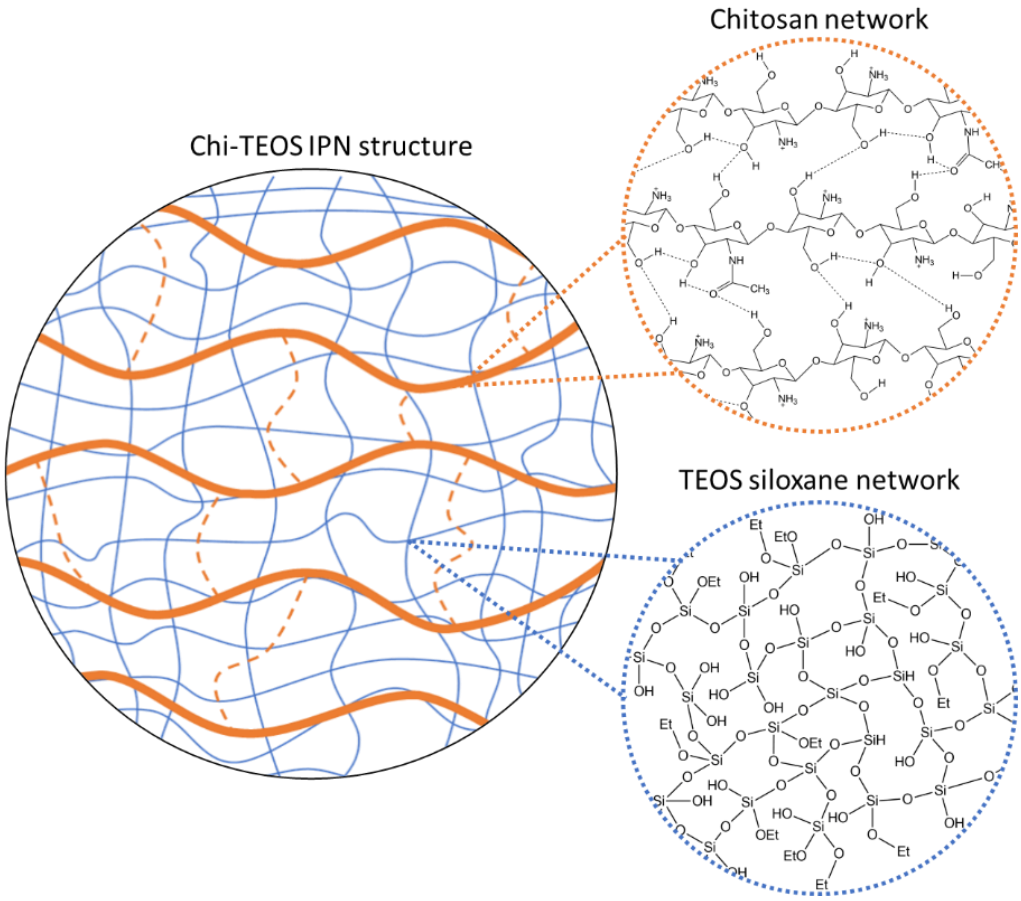


Figure 2.2: A schematic representation of the formation of a Chi-TEOS IPN.

2.1.1.2 Chi-GA

For the synthesis of the chitosan-glutaraldehyde, cross-linked hydrogels glutaraldehyde solution (GA) (25%, 0.12 mL) was mixed with filtered ethanol (15 mL) and allowed to continuously stir at room temperature for 30 minutes. Next, HCl (0.0274 mL), filtered ethanol (10 mL) and Millipore deionized water (25 mL) were added to a beaker and allowed to stir continuously at room temperature for 30 minutes.

After 30 minutes, the two solutions were mixed slowly, dropwise, with continuous stirring. The resulting Chi-GA (8:1) mixture was then covered with Parafilm and allowed to continuously stir at room temperature for 24 hours, before being added slowly dropwise to the chitosan solution, with continuous stirring. The resulting mixture was covered with Parafilm and al-lowed to continuously stir at room temperature for a further 48 hours. The mixture was observed to become viscous. The hydrogel was stored in a fridge at 4 °C prior to use.



Figure 2.3: Photograph of the Chi-GA hydrogel at a higher concentration ratio than (8:1). The high viscosity deemed it unsuitable to produce a uniform film.

Unlike the formation of the Chi-TEOS IPN, the reaction cross-linking the chitosan chains with glutaraldehyde molecules is a single step process in which the chitosan hydrogel is first prepared and then glutaraldehyde is added to the gel, which subsequently undergoes a covalent Schiff base reaction. Schiff bases are synthesized from an aliphatic or aromatic amine and a carbonyl compound by nucleophilic addition, followed by a de-hydration to generate an imine, [18] as shown schematically in Figure 2.4 below.

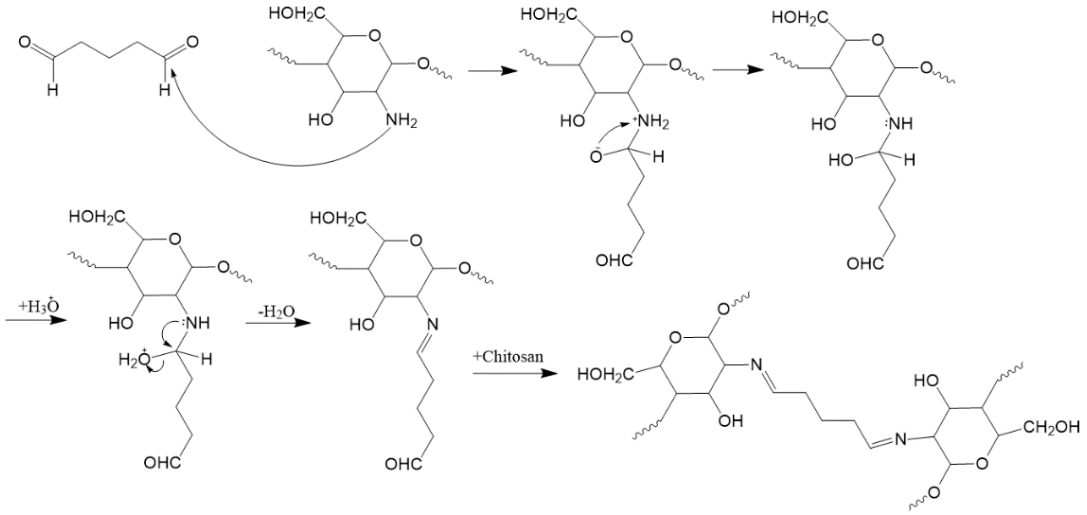


Figure 2.4: The formation of glutaraldehyde-based cross-links between chitosan chains via the formation of Schiff base imine functionalities. The chitosan polymer chains are chemically bonded by Schiff base imine bridges via cross-linking, creating a sterically more rigid structure. [19]

The ratio of (8:1) was chosen based on a previous study whereby the range of possible Chi-GA ratios were tested. It was found that the hydrogels that had higher concentrations of glutaraldehyde were unsuitable for films synthesis due to the increased viscosity and faster cross-linking reaction times. The same concentration of chitosan was used for each film, the ratio notation refers to the concentration of the cross-linking agent only. Therefore, for the sake of simplicity, Chi-GA (1:0.0125) may be written as Chi-GA (8:1).

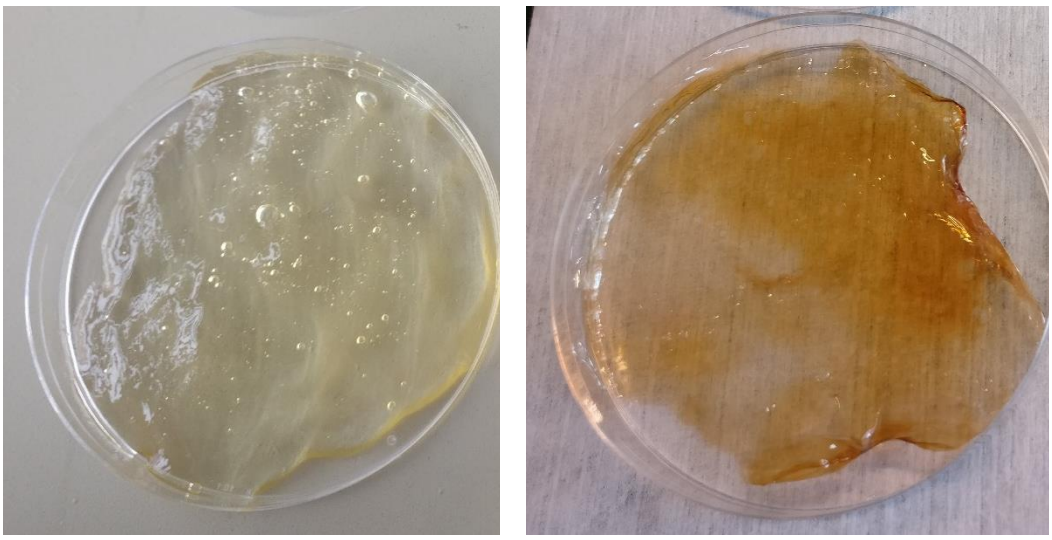


Figure 2.5: Chitosan-glutaraldehyde 4:1 concentration hydrogel (left) and dried film (right). The viscosity of the hydrogel was too high to flow naturally and fill the Petri dish, resulting in an uneven dry film.

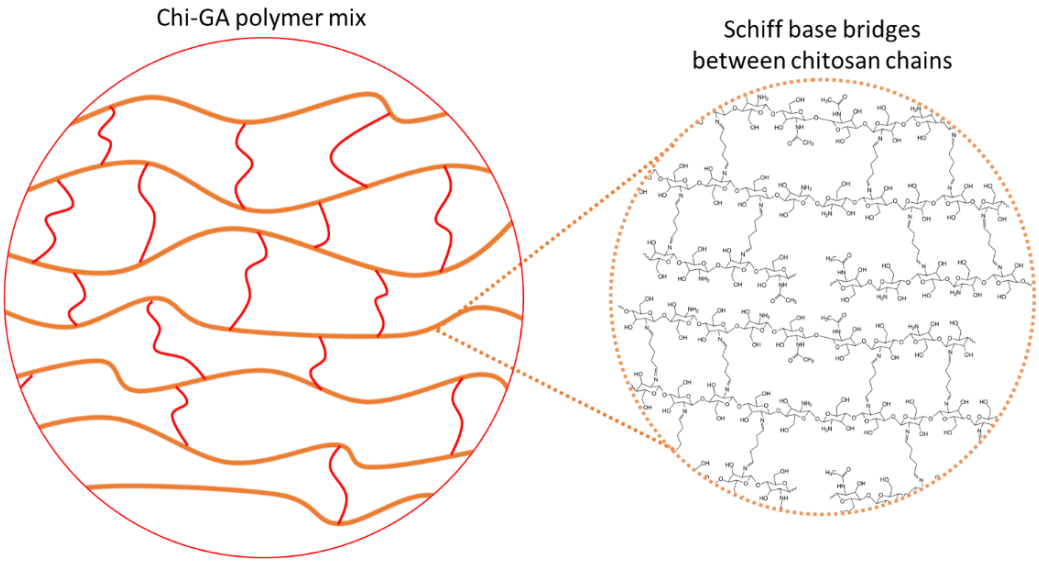


Figure 2.6: A schematic representation of the formation of a Chi-GA IPN

2.1.1.3 Chi-APTES

The synthesis of the chitosan-3-aminopropyltriethoxysilane (Chi-APTES) films is similar to the Chi-TEOS films. The hydrogels were prepared in mildly acidic conditions to facilitate cationic polymerization. The procedure was based on that described by Park et al. [14] and Chen et al. [20]; APTES (99%, 0.55 mL) was dissolved in filtered ethanol (15 mL) and allowed to continuously stir at room temperature for 30 minutes.

The ratio of (2:1) (Chi-APTES) was chosen due to the unsuitable state of the (1:1) ratio films. The (1:1) films showed signs of flaking after drying and were difficult to peel off the Petri dish in one free standing piece.

HCl (0.0274 mL), filtered ethanol (10 mL) and Millipore deionized water (25 mL) were added to a beaker and allowed to stir continuously at room temperature for 30 minutes. After 30 minutes the HCl solution was slowly added to the APTES solution, dropwise, with continuous stirring. The mixture was covered with Parafilm and allowed to continuously stir at room temperature for 24 hours. The acidic APTES solution was then slowly added to the chitosan solution dropwise, with continuous stirring. The resulting Chi-APTES (2:1) mixture was covered with Parafilm and allowed to continuously stir at room temperature for a further 48 hours. The mixture was observed to become more viscous over the 48-hour period. The hydrogel was then stored in a fridge until removed for use.

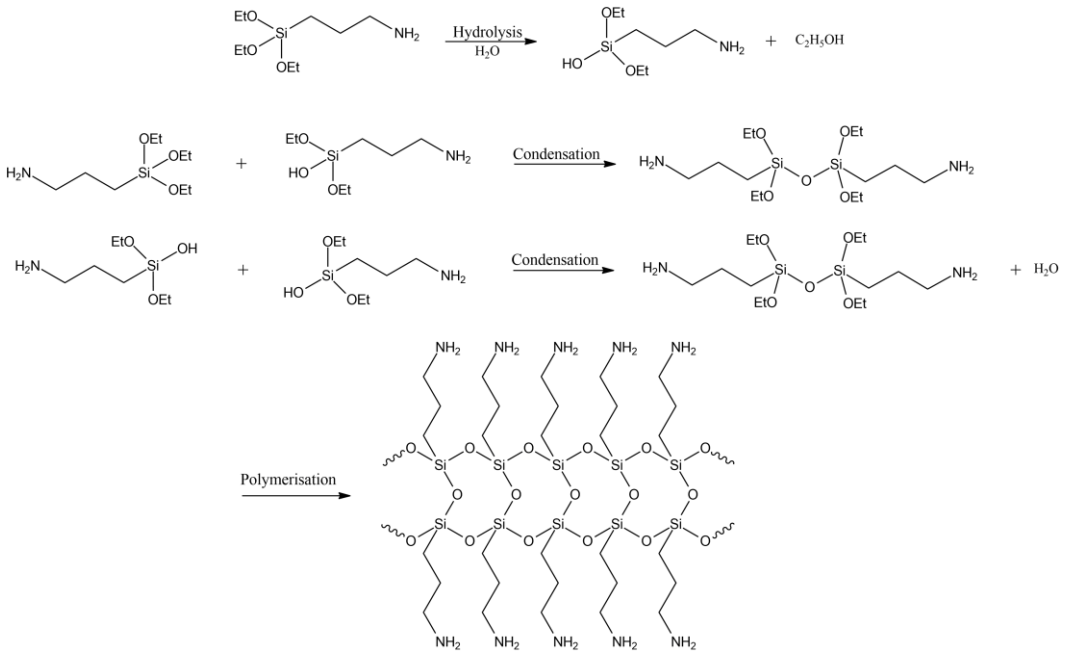


Figure 2.7: Hydrolysis and condensation reactions of APTES to form a continuous polymer chain.

The accepted mechanism of cross-linking between APTES and chitosan is as follows: APTES was hydrolysed in the presence of an acid (HCl) forming silanol groups. Siloxane bonds were formed between silanol groups and the hydroxyl groups via condensation. This created a siloxane chain polymer with branching amine groups, see figure 2.7 above. The amine and hydroxyl groups of the siloxane polymer chain undergo hydrogen bonding with the amine and hydroxyl groups of the chitosan polymer chain. It may be stated that the crystallinity of the chitosan polymers decreases by the introduction of the APTES siloxane chain, because the chains were disturbed and previously formed intra- or inter-molecular hydrogen bonds between the NH_2 and OH groups were broken. [13]

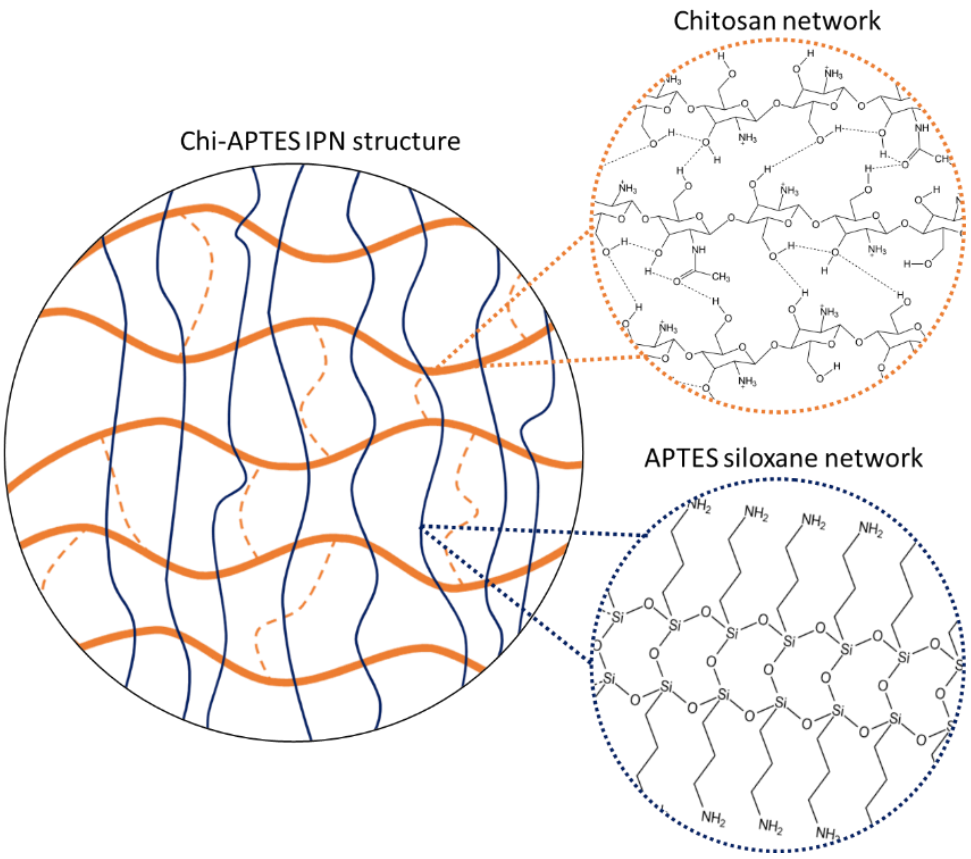


Figure 2.8: A schematic representation of the formation of a Chi-APTES IPN

2.1.1.4 Chi-PAM

Polyacrylamide (1.04 g) was dissolved in Millipore deionized H_2O (65 mL and acetic acid (0.32 mL, 1% wt.)), covered with Parafilm and left to continuously stir on a gentle heat overnight. The polyacrylamide solid began to dissolve after 2-3 hours of stirring.

After 24 hours of continuous stirring on a gentle heat, the polyacrylamide solution was added slowly dropwise to the chitosan solution. The resulting Chi-PAM (1:1) mixture was then stirred for a further 48 hours to ensure maximum heterogeneity. A series of Chi-PAM (2:1) and Chi-PAM 1:2 films were also made for tensile strength tests. Polyacrylamide is highly soluble in water, so the formation of the hydrogel blend was relatively easy compared to the other reagents. Water molecules form hydrogen bond with the hydrophilic NH_2 and C=O functional groups of the polyacrylamide chain as shown in figure 2.9. [21]

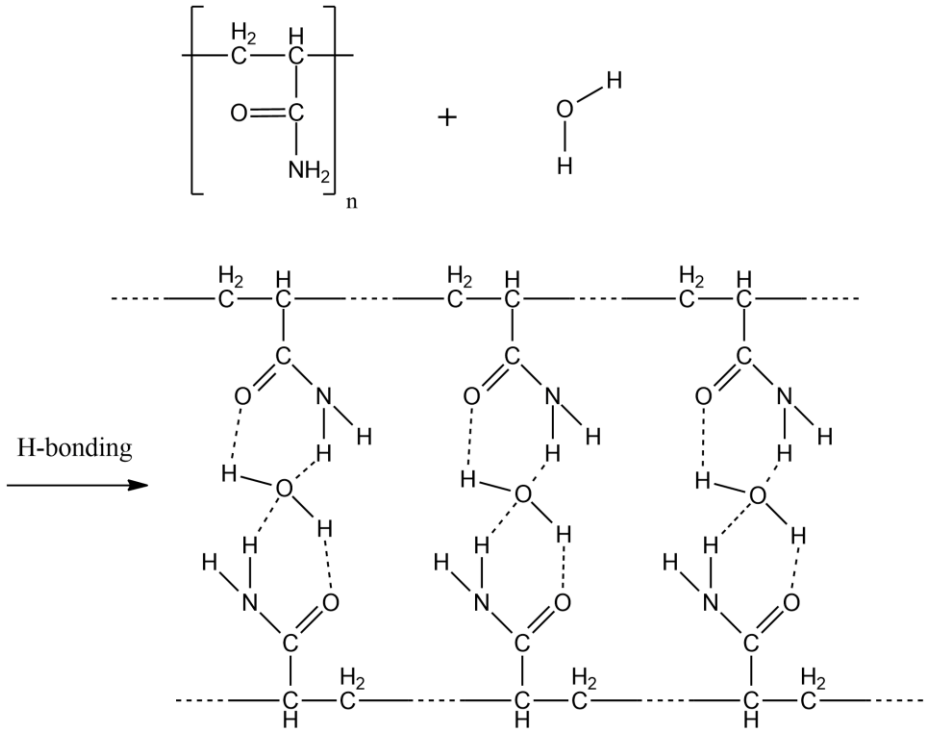


Figure 2.9: Polyacrylamide in water to form hydrogen bonded polymer chains. [21]

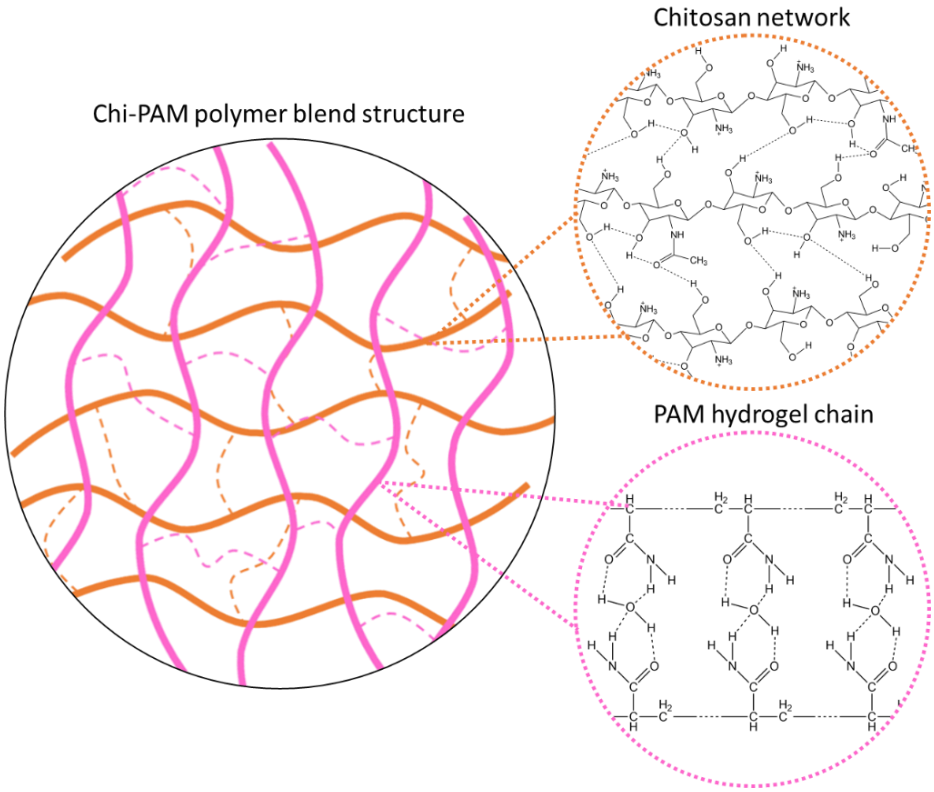


Figure 2.10: A schematic representation of the formation of a Chi-PAM IPN

A summary of all chitosan film schematics and molecular structures can be found in the appendix section A.1.

2.1.2 Preparation, casting and drying of films

Films were prepared using two different approaches- via a drop-cast method and via the use of a slot-die apparatus. These are described in the following sections although a more detailed description of the slot-die approach is given in Chapter 4, which is essentially a transcript of a publication arising from this work.

2.1.2.1 Drop-casting films

Several films were prepared using the basic Petri dish drop cast method. In this method, the hydrogel (15 mL) was cast into a Petri dish (100 mm diameter) ensuring a minimum production of bubbles and was spread thinly to cover the surface uniformly. The Petri dish was allowed to dry uncovered on a level surface in an oven at 40 °C for 24 hours. Once dry, the films were peeled off the surface of the Petri dish in one piece (where possible) and stored at room temperature. Examples of the resulting free-standing thin films made from chitosan, Chi-TEOS, Chi-APTES, Chi-PAM, and Chi-GA are presented in figures 2.11 and 2.12 below. It may be seen that these films were transparent, slightly yellow in tone and flexible.

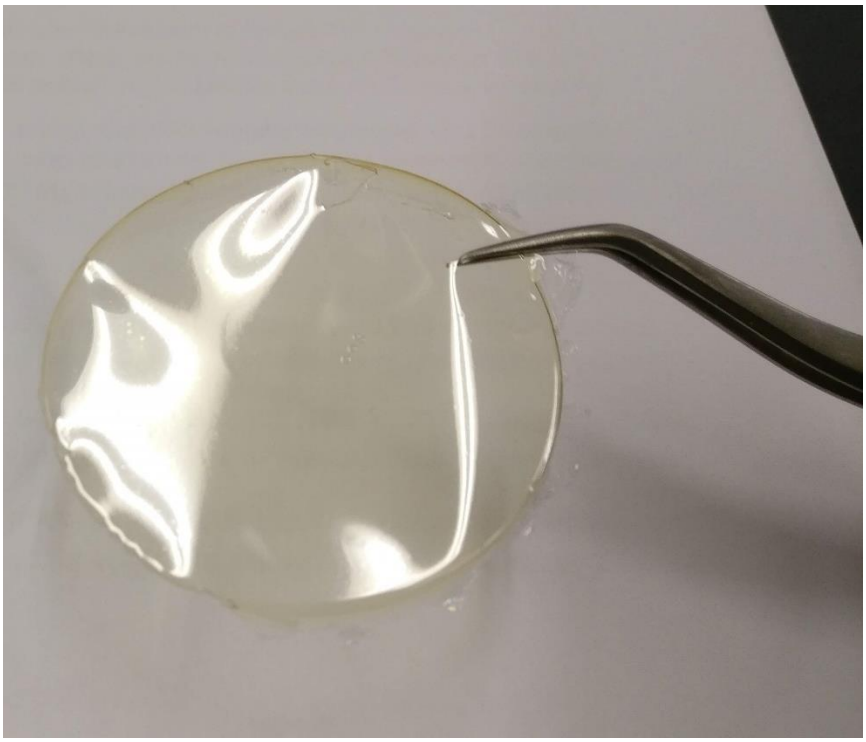


Figure 2.11: Photograph of a dry free-standing chitosan film

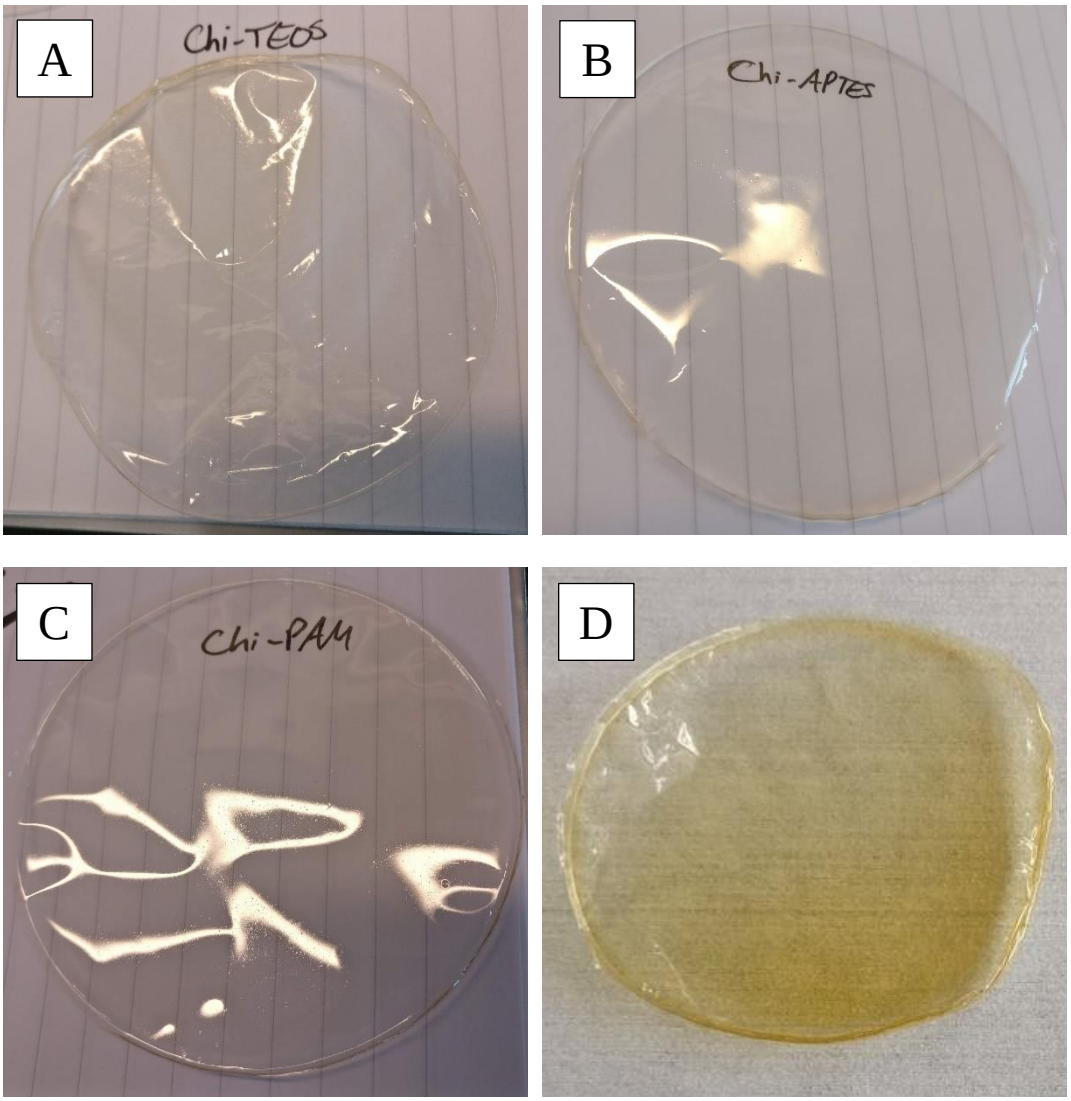


Figure 2.12: Photographs of all dry composite film types. (A) Chitosan-TEOS (1:1), (B) Chitosan-APTES (2:1), (C) Chitosan-PAM (1:1), and (D) Chitosan-GA (8:1)

2.1.2.2 Preparation of films using a slot-die method (refer to Chapter 4)

The slot-die casting apparatus consists of two rollers 50 cm apart with a flat hotplate set to 50°C in between the rollers, figure 2.13. This apparatus was constructed by the group of Professor Roberto M. Faria at IFSC USP Brazil. The direction of travel of the film formed via the extrusion of the hydrogel through the slot is marked by an arrow in figure 2.13.

A PET foil substrate (175 µm thick) was plasma-cleaned using an Expanded Tabletop oxygen plasma cleaner (PDC-002) with a PlasmaFlo gas flow mixer and pressure monitor (PDC-FMG-2). The plasma-treated film was then wrapped around the rollers and stretched flat on the hotplate. The doctor blade slot-die head was positioned above

the PET foil on an adjustable horizontal bar that spanned the width of the foil. The slot-die nozzle opening was 2 cm in length with the width of the slot set to 2 mm and was angled 2 mm above the PET substrate at 45 degrees.

A syringe pump with a 3 cm diameter syringe was attached to the slot-die head via a thin flexible tubing. The rate of deposition and movement of the substrate were 1 mL/min and 1 cm/min, respectively. Approximately 20 – 25 mL of gel was cast onto the PET substrate over 20 minutes. The gel was left to dry on the PET under an extraction fan. A thin transparent film formed over the course of an hour. It was then carefully peeled off the PET and allowed to air dry for a further hour. The film was then cut into 1 cm x 4 cm pieces with a rolling blade and stored in an airtight container.

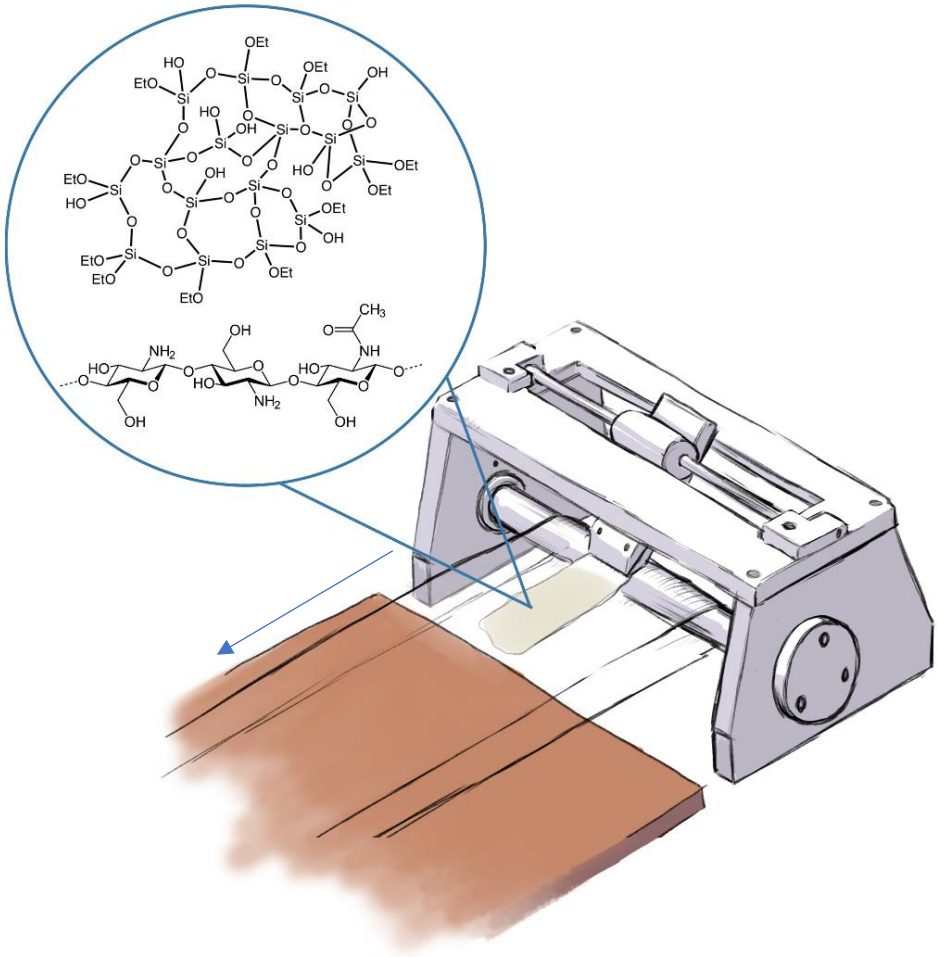


Figure 2.13: Artist's rendition of the slot-die apparatus. As the PET film travels in the direction of the arrow, the chitosan-TEOS hydrogel is deposited in a uniform layer and dried over a hotplate. Drawn by Mr Liam Cuthbert. See Chapter 4 for more details of this approach.

2.2 Analysis and characterisation

2.2.1 Spectroscopy

An infrared vibrational spectroscopic analysis was carried out on free-standing thin film samples using a Bruker Alpha FT-IR spectrometer in single reflection ATR mode which utilizes a platinum diamond crystal. This technique allows for the structural identification of various functional groups present in the films.

2.2.2 Mechanical strength

A TA.HDplusC Texture Analyser from Stable Micro Systems and Instron 5565 Universal Testing Machine were used to carry out tensile strength tests. The Instron was calibrated periodically using a set of reference weights that were certified annually by the National Metrology Lab, Dublin. In terms of standardizing the tensile strength tests performed using this type of instrument, there is no material with a known stress-strain graph that can be used repeatedly without suffering fatigue itself. Such a material would make the calibration temperature sensitive, as it would be likely to exhibit different stress strain characteristics at different ambient temperatures. Therefore, the only standards measured for the Instron are force, displacement, and time. This factor was taken into consideration when collecting the tensile strength data.

The thin films were cut using a rotary cutter into strips 40 mm to 10 mm in dimension. The samples were clamped in between PDMS supports and provided a gauge length of 20 mm. The strips were pulled apart along the 20 mm edge until they broke cleanly in the middle. [22] Test conditions at room temperature included a load of 5 kN, clamp speed of 0.5 $mm.min^{-1}$ and data acquisition rate of 10 Hz.

For the films prepared using the slot-die approach, an evaluation of possible anisotropy in the mechanical strength of the films in relation to the direction of travel of the film was performed using strips that were cut both parallel and at perpendicular right angles to this direction.

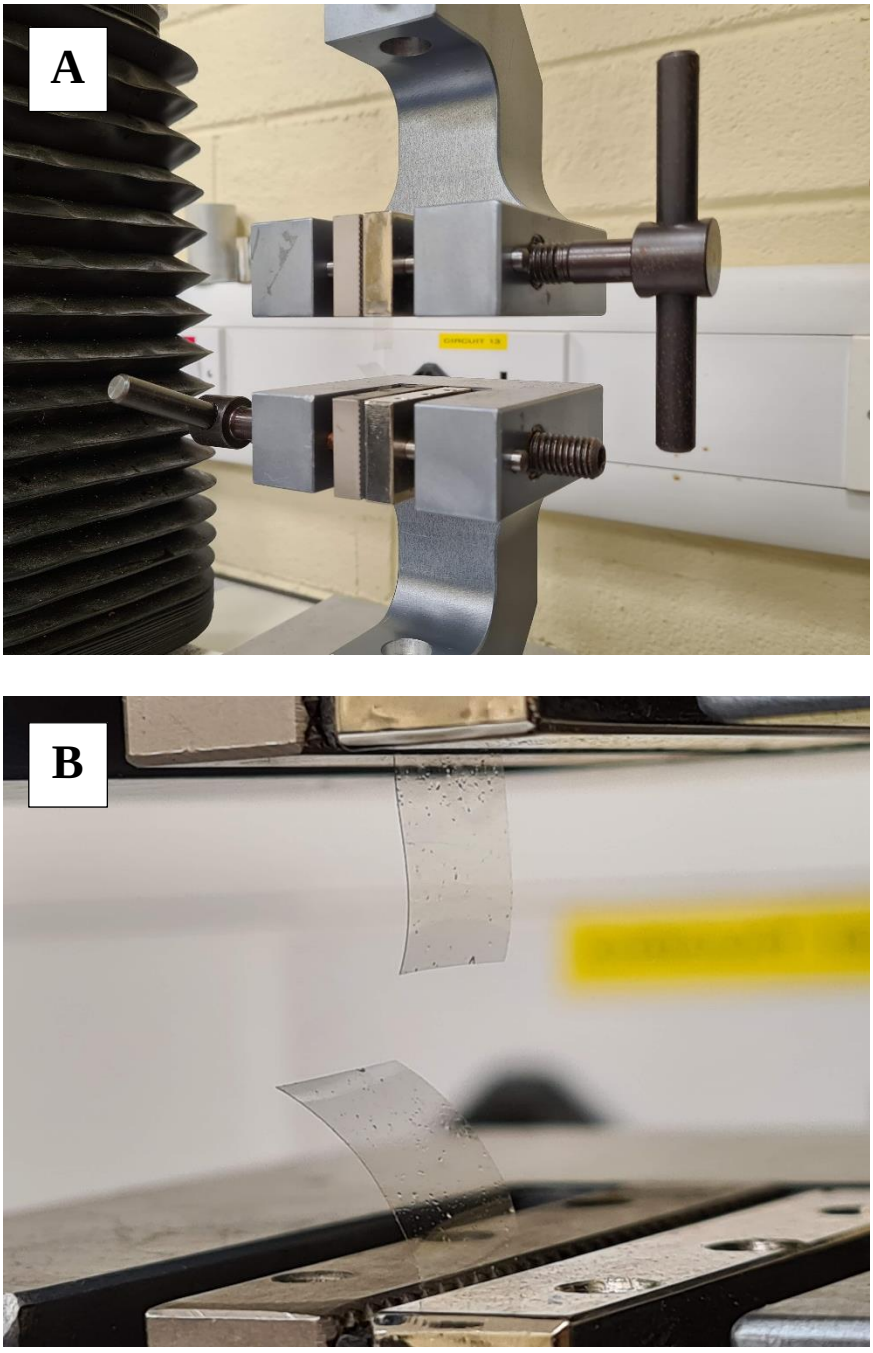


Figure 2.14: (A) TA.HDplusC Texture Analyser with tensile strength clamp peripherals. (B) Enhanced detail of a film sample split evenly down the middle during a tensile test.

2.3 Heavy metal adsorption studies (performed in conjunction with staff and students from the Faculty of Natural Sciences at Comenius University, Bratislava - see Chapter 5)

2.3.1 Swelling characteristics

The swelling characteristics of chitosan-based films were determined by immersing pre-weighed samples in an aqueous acidic medium and allowing them to swell over 60 minutes. The film samples were then removed, dried, and weighed. The full method is described in chapter 5, section 5.2.1.

2.3.2 Adsorption capacity

The pertechnetate anion absorption capacities of the chitosan-based films were determined by the radioisotope indication method with the radioisotope ^{99m}Tc and the radio-indicator $^{99m}TcO_4^-$. The films were mixed with the anion solution and placed in a constant temperature vibration shaker until adsorption reached equilibrium. Adsorption rate, capacity and distribution rate were calculated.

The linear Langmuir and Freundlich isotherm models were used to describe the adsorption of $^{99m}TcO_4^-$ onto the chitosan-based films. The Langmuir isotherm is theoretical model used to graph monolayer adsorption onto a surface and the Freundlich isotherm is an experimental model for multilayer adsorption onto a surface. [23] The full method is described in chapter 5, section 5.2.2.

2.4 Antimicrobial studies (performed in conjunction with staff and students from the Microbiology Department at UCC - see Chapter 6)

2.4.1 Materials

All nutrient broths were purchased from Oxoid Ltd.

- 400 mL Lysogeny Broth (LB) in H_2O – Peptone (10 gL^{-1}), Yeast extract (5 gL^{-1}), NaCl (10 gL^{-1}), LB Agar (15 gL^{-1})
- 400 mL Brain Heart Infusion Broth (BHIB) in H_2O – Beef heart infusion solids (12.5 gL^{-1}), Proteose Peptone (10 gL^{-1}), Glucose (2 gL^{-1}), NaCl (5 gL^{-1}), disodium phosphate (2.5 gL^{-1})
- Crystal Violet stain dye.
- Bacteria:
    - Gram negative (-): Escherichia coli (*E. coli*)
    - Gram positive (+): Staphylococcus (*S. aureus*)

2.4.2 Method

For bacteria to be successfully cultured, they must be grown in the appropriate media. Lysogeny Broth (LB) is a nutrient rich broth that is a standard for culturing *E. coli*, as it allows for quick growth and high yields. Brain heart Infusion Broth (BHIB) is a liquid medium rich in nutrients, suitable for the cultivation of several strains of bacteria, such as Staphylococcus (*S. aureus*), fungi and yeasts. BHIB is recommended in standard methods for water testing and in antimicrobial susceptibility tests.

2.4.2.1 LB broth

Peptone (4 g), Yeast extract (2 g), NaCl (4 g) and LB Agar (6 g) were weighed out, added to 400 mL distilled H_2O in a clean Pyrex bottle and mixed. The top of the bottle was lightly sealed with aluminium foil, and then it was autoclaved for approximately 20 minutes. After autoclaving, the LB medium was allowed to cool to 55°C before handling. The LB broth was stored in sterile conditions at room temperature. LB Agar was prepared by pouring the LB broth into sterilised Petri dishes and letting them solidify at approximately 30 °C. The LB plates were stored at 4 °C.

2.4.2.2 Brain Heart Infusion broth

Brain Heart Infusion (14.8 g) was suspended in distilled H_2O (400 mL) and dissolved by heating with frequent agitation. Once fully dissolved the solution was transferred to a clean Pyrex bottle, lightly sealed with aluminium foil, and autoclaved for approximately 20 minutes. After autoclaving, the BHIB medium was allowed to cool to 55°C before handling. The BHIB was stored in sterile conditions at room temperature. BHI Agar was prepared by pouring the BHI broth into sterilised Petri dishes and letting them solidify at approximately 30 °C. The BHI plates were stored at 4 °C.

2.4.3 T-streak method

To create isolated colonies of a particular bacteria rapidly, the T-streak method was utilised. Streaking is a method in which the sample/inoculum is diluted across the surface of an agar plate to the point where only one bacterial cell is present every few millimetres. These lone bacterial cells can divide and produce thousands of new bacterial cells; thus, an isolated colony is formed. The inoculating loop was sterilized with a Bunsen burner and allowed it to cool. The loop was inserted into the culture bottle (*E. coli* or *S. aureus*) and immediately streaked across half of the agar plate using a back-and-forth motion (1). The loop was flamed again, inserted into the culture bottle, and streaked across half of the plate but also overlapping the first streak (2). Finally, the loop was flamed, inserted into the culture bottle, and streaked across the remaining quarter of the agar plate (3). The T-streaked plates were incubated for 24 hours (37 °C for *E. coli* and 30 °C for *S. aureus*).

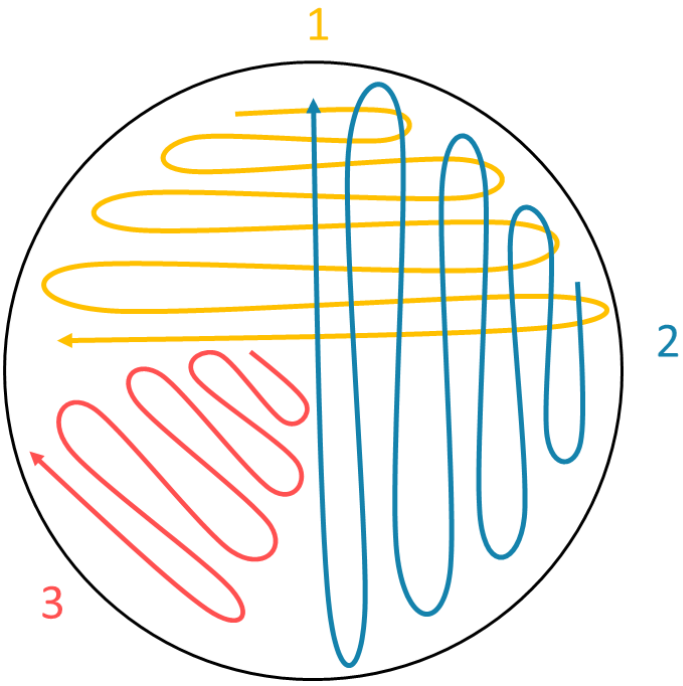


Figure 2.15: Schematic representation of the T-streak method of inoculating an agar plate with a bacterial colony using steps 1, 2 and 3 as described above.

After 24 hours incubation, the bacterial colonies had grown on the agar plate. An inoculating loop was used to transfer a single colony to 5 mL liquid broth (LB or BHIB). These colonies were set aside for overnight incubation (37 °C for *E. coli* and 30 °C for *S. aureus*). After the incubation period, 1 mL of the overnight colonies was withdrawn and transferred to a plastic cuvette. The absorbance or optical density (OD) of the bacterial colonies were measured at a wavelength of 600 nm using a spectrophotometer (Shimadzu UVmini-1240 model).

2.4.3.1 Inoculation of chitosan samples

1 mL of the overnight cultures was withdrawn and then centrifuged at 14000 RPM for 15 minutes to separate the supernatant growth media. The resulting cell pellet was re-suspended in Phosphate Buffered Saline (PBS) to give a final OD_{600nm} = 1. This step is to prevent any further growth of the bacteria so we can accurately measure the OD_{600nm} without risk of it changing overnight.

The chitosan samples were prepared by drop casting the hydrogel in a plasma cleaned Petri dish and dried in an oven for 24 hours at 40 °C. The purpose of the plasma cleaning was to adhere the films to the surface of the Petri dishes so the bacterial growth can be accurately measured on one side of the film. The chitosan samples were

flooded with LB or BHIB broths (5 mL) and inoculated with the re-suspended cultures (50 µL) to create a 1:100 dilution (equivalent to OD_{600nm} = 0.01). The samples were then allowed to incubate for 24 hours (37 °C for *E. coli* and 30 °C for *S. aureus*). Control samples were also prepared using sterile PBS.

2.4.4 Optical Density measurements

After the incubation period, the broth was removed and an OD_{600nm} reading was taken to measure the growth of bacteria in the broth. To remove any cells there were not tightly bound to the surface, the films were washed with distilled water and stained with Crystal Violet (CV) for 15 minutes. The stain was poured off and the plates were washed again with distilled water and allowed to dry. The CV was solubilised in ethanol (10 mL) and the OD_{595} was taken as a quantitative measurement of bacterial attachment on the chitosan films. Further details of OD measurements and principles are discussed in chapter 6.

2.5 Wound dressing design and testing (performed in conjunction with staff from the National Institute for Materials Science, Tsukuba - see Chapter 7)

The aim of this procedure was to design a pH sensor based on a free-standing membrane consisting of photonic crystals embedded in a chitosan-based film. The sensor may change colour when exposed to different acidities. This sensor is being developed as a part of the EU project No 873123 - SWORD (Smart Wound Monitoring Restorative Dressings) under Marie Skłodowska-Curie Actions - Research and Innovation Staff Exchange (RISE) Call:H2020-MSCA-RISE-2019.

2.5.1 Sample preparation and thickness measurements

Chitosan hydrogel samples were prepared according to the usual method described previously in section 2.1.2. Hydrogel was cast into Petri dishes and dried in an oven to produce 100 mm diameter chitosan-based films. Three concentrations were tested to determine the appropriate thickness for the swelling studies: 1.3% w/v, 2.6% w/v and 3.9% w/v. The average thickness was recorded with a handheld micrometer in several areas across the films. Note that hydrogels of a higher concentration than 3.9% w/v were too viscous to form a uniform, solid drop cast film. Hydrogels of Chi-APTES (2:1) and Chi-GA (8:1) were also synthesised via the methods described in section 2.1.1 and drop cast into films for pH-based swelling tests.

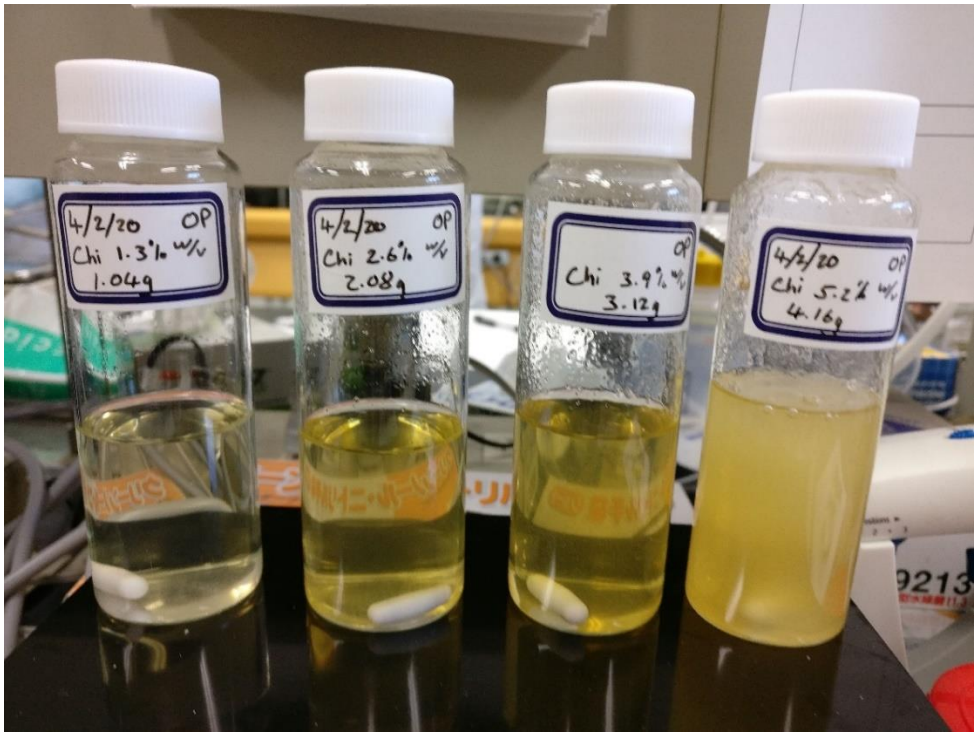


Figure 2.16: Chitosan hydrogel samples increasing in concentration from 1.3% w/v, 2.6% w/v, 3.9% w/v, 5.2% w/v, (left to right).

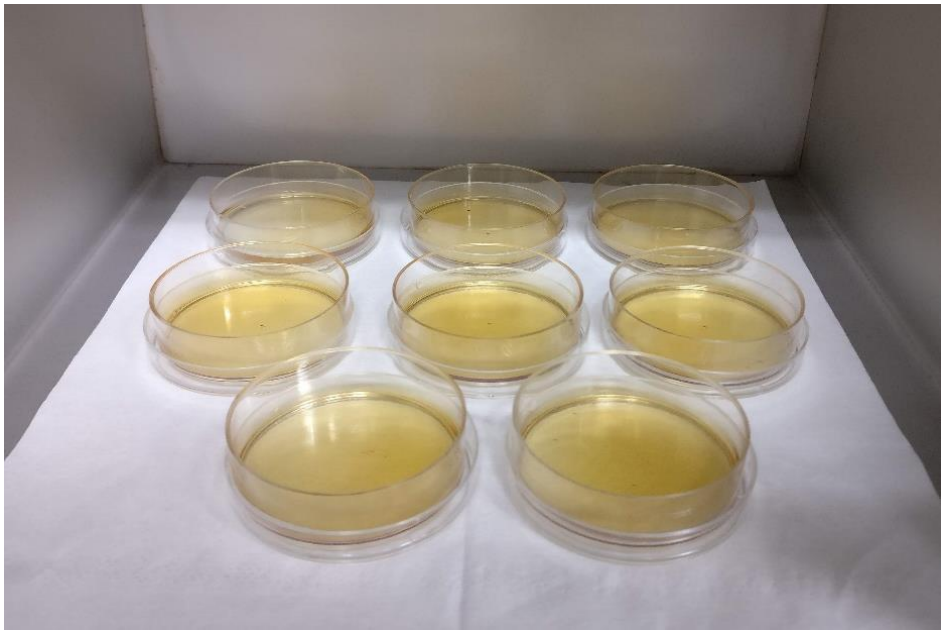


Figure 2.17: Chitosan hydrogel (2.6% w/v) cast in Petri dishes ready to dry in the oven at 40 °C.

2.5.2 Photonic crystal film fabrication

The following procedures were carried out by the members of the Colloidal Crystal Materials Group under the supervision of Dr Hiroshi Fudouzi at the National Institute for Materials Science (NIMS) in Tsukuba, Japan.

Monodisperse 210 nm PS particles were synthesised by emulsion polymerisation of a styrene monomer in the presence of sodium dodecyl sulfate (SDS) as a surfactant. The full procedure is outlined in a previous publication. [24, 25] The flexible rubber substrate that was fixed on a sample holder was immersed vertically into the suspension container filled with the polystyrene (PS) colloid suspension covered with a layer of silicone oil. The vertical stage descended slowly while driven by the stepping motor thus depositing the PS photonic crystal film onto the substrate (see figure 2.18).

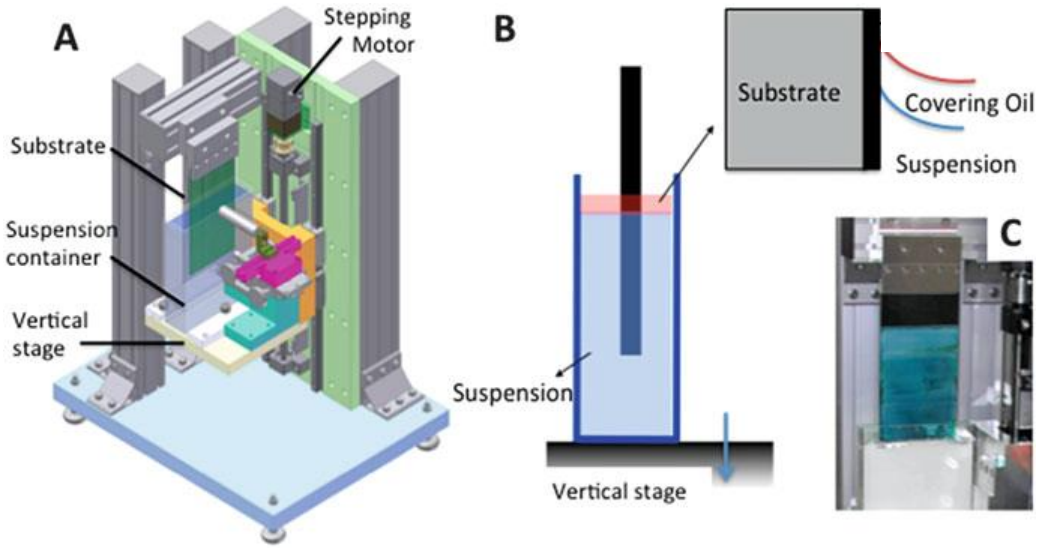


Figure 2.18: Vertical coating opal films by crystal growth under a silicone liquid layer. (A) Schematic drawing of the equipment. The substrate and colloidal suspension container are fixed to the lifting stage. (B) Scheme and photo of the opal film coating system. (C) Black fluororubber (FR) (Tiger Polymers) [26] sheet coated with opal film made of 210 nm PS particles. [25]

The resulting closely packed colloidal crystal film was infiltrated with mixed PDMS precursor liquids, Sylgard 184 (Dow Corning, USA). [27] Two separate liquids consisting of the base material and the curing agent were used. The ratio of base material to curing agent was 10:1 by weight. After curing, PDMS elastomer was

infilled in 3D-arrayed PS colloidal particles. Then, closely packed PS particles were spaced out by additional filling and curing PDMS elastomer.

PDMS precursor was diluted with silicone liquid (0.65 cSt, SH-200 series, i.e., hexamethyldisiloxane, HMDSO) with a (1:1) mass ratio. The PDMS elastomer was polymerized by cross-linking for 12 h at room temperature and 2 h at 60°C. The lattice distance of FCC (111) planes was increased in nanometer scale by repeating infilling PDMS elastomer for several times. This nanoscale spacing allows reversible structural colour change by elastic deformation.

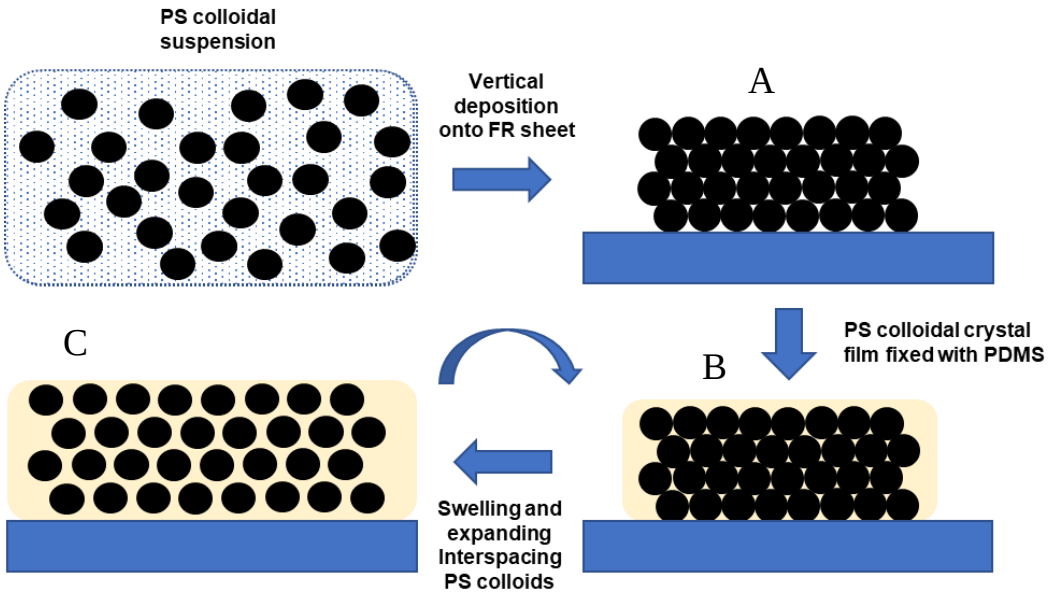


Figure 2.19: Schematic of PS colloidal film deposition procedure. (A) Closely packed colloidal crystal film on a fluororubber sheet. (B) Infilled with PDMS oligomer (Sylgard 184) diluted with a hexamethyldisiloxane, HMDS (0.65cSt silicone oil) by (1:1) wt.%. (C) Infilled with PDMS oligomer (Sylgard 184) diluted with a HDMS (1:1) wt.%. Modified from [25].

The PS colloidal film was utilized in a series of optical spectroscopy tests while swelling under different pH conditions. The full procedure is discussed in more detail in chapter 7. All films were prepared by OJP while the optical measurements were performed by Dr Tomas Kohoutek. Prof Fudouzi and his colleagues provided the polystyrene particles and the fluororubber sheets.

References

1. Kanke, M., et al., *Appilcation of Chitin and Chitosan to Pharmaceutical Preparations. I. : Film Preparation and in Vitro Evaluation.* CHEMICAL & PHARMACEUTICAL BULLETIN, 1989. **37**(2): p. 523-525.
2. Wan Ngah, W.S., L.C. Teong, and M.A.K.M. Hanafiah, *Adsorption of dyes and heavy metal ions by chitosan composites: A review.* Carbohydrate Polymers, 2011. **83**(4): p. 1446-1456.
3. Tripathi, S., G.K. Mehrotra, and P.K. Dutta, *Chitosan based antimicrobial films for food packaging applications.* E-Polymers, 2008.
4. Ligler, F.S., et al., *Development of Uniform Chitosan Thin-Film Layers on Silicon Chips.* Langmuir, 2001. **17**(16): p. 5082-5084.
5. Park, S.B., et al., *A novel pH-sensitive membrane from chitosan - TEOS IPN; preparation and its drug permeation characteristics.* Biomaterials, 2001. **22**(4): p. 323-330.
6. Silva, G.S., et al., *Chitosan/Siloxane Hybrid Polymer: Synthesis, Characterization and Performance as a Support for Immobilizing Enzyme.* Journal of the Brazilian Chemical Society, 2011. **22**(8): p. 1407-1417.
7. Rashidova, S.S., et al., *Bionanocompositional chitosan-silica sorbent for liquid chromatography.* Journal of Chromatography B-Analytical Technologies in the Biomedical and Life Sciences, 2004. **800**(1-2): p. 49-53.
8. Dragan, E.S., *Design and applications of interpenetrating polymer network hydrogels. A review.* Chemical Engineering Journal, 2014. **243**: p. 572-590.
9. Tripathi, S., G.K. Mehrotra, and P.K. Dutta, *Physicochemical and bioactivity of cross-linked chitosan-PVA film for food packaging applications.* International Journal of Biological Macromolecules, 2009. **45**(4): p. 372-376.
10. Tual, C., et al., *Transport properties of chitosan membranes: Influence of cross-linking.* Journal of Polymer Science Part B-Polymer Physics, 2000. **38**(11): p. 1521-1529.
11. Sumayya, et al., *Development and characterization of chitosan and acrylic acid-based novel biodegradable polymeric films for soil conditioning.* International Journal of Biological Macromolecules, 2021. **182**: p. 950-958.

12. Gaabour, L.H., *Spectroscopic and thermal analysis of polyacrylamide/chitosan (PAM/CS) blend loaded by gold nanoparticles.* Results in Physics, 2017. **7**: p. 2153-2158.
13. Zargar, V., M. Asghari, and M. Afsari, *Gas separation properties of swelled nanocomposite chitosan membranes cross-linked by 3-aminopropyltriethoxysilane.* International Journal of Environmental Science and Technology, 2019. **16**(1): p. 37-46.
14. Park, S.-B., et al., *A novel pH-sensitive membrane from chitosan — TEOS IPN; preparation and its drug permeation characteristics.* Biomaterials, 2001. **22**(4): p. 323-330.
15. Ryan, C.C., et al., *Silica-based photonic crystals embedded in a chitosan-TEOS matrix: preparation, properties and proposed applications.* Journal of Materials Science, 2016. **51**(11): p. 5388-5396.
16. Ryan, C.C., M. Bardosova, and M.E. Pemble, *Structural and mechanical properties of a range of chitosan-based hybrid networks loaded with colloidal silica and polystyrene particles.* Journal of Materials Science, 2017. **52**(13): p. 8338-8347.
17. Lofgreen, J.E. and G.A. Ozin, *Controlling morphology and porosity to improve performance of molecularly imprinted sol-gel silica.* Chemical Society Reviews, 2014. **43**(3): p. 911-933.
18. Ostrowska-Czubenko, J., M. Pieróg, and M. Gierszewska, *State of water in noncross-linked and cross-linked hydrogel chitosan membranes - DSC studies.* Progr. Chem. Appl. Chitin Deriv., 2011. **16**: p. 147-156.
19. Luk, C., et al., *A Comprehensive Study on Adsorption Behaviour of Direct, Reactive and Acid Dyes on Cross-linked and Non-cross-linked Chitosan Beads*. 2014.
20. Jian Hua Chen and Qing Lin Liu and Xiu Hua Zhang and Qiu Gen, Z., *Pervaporation and characterization of chitosan membranes cross-linked by 3-aminopropyltriethoxysilane.* Journal of Membrane Science, 2007. **292**(1): p. 125-132.
21. Sekine, Y., et al., *Dependence of structure of polymer side chain on water structure in hydrogels.* Polymer, 2014. **55**(24): p. 6320-6324.
22. Gauthier, M.M. and A.I.H. Committee, *Engineered Materials Handbook, Desk Edition*. 1995: Taylor & Francis.

23. Keller, J.U. and R. Staudt, *Gas Adsorption Equilibria: Experimental Methods and Adsorptive Isotherms*. Gas Adsorption Equilibria: Experimental Methods and Adsorptive Isotherms. 2005: Springer.
24. Furumi, S., H. Fudouzi, and T. Sawada, *Dynamic photoswitching of micropatterned lasing in colloidal crystals by the photochromic reaction.* Journal of Materials Chemistry, 2012. **22**(40): p. 21519-21528.
25. Fudouzi, H. *Colloidal Photonic Crystal Films: Fabrication and Tunable Structural Color and Applications*. in *Nanomaterials and Nanoarchitectures*. 2015. Dordrecht: Springer Netherlands.
26. Corporation, T.P. *FR Sheet (Fluoro rubber)*. https://www.tiger-poly.com/product/detail/9 2017; Accessed on 07/10/2021
27. Dow. *SYLGARD™ 184 Silicone Elastomer Kit*. 2022.

3. The Structural and Mechanical Characterisation of Chitosan-Based Films

In this chapter, results are presented for a series of films produced mainly via drop-casting as described in Chapter 2. The films prepared via the drop-casting approach were chitosan only, Chi-TEOS (1:1), Chi-TEOS (2:1), Chi-APTES (2:1), Chi-PAM (1:1), Chi-PAM (2:1), Chi-PAM (1:2) and Chi-GA (8:1). The same concentration of chitosan was used for each film, the ratio notation refers to the concentration of the cross-linking agent only. Therefore, for the sake of simplicity, Chi-GA 1:0.0125 may be written as Chi-GA (8:1).

Some additional data was then added to the set from selected additional samples prepared using a slot-die, continuous film making process. This latter process is described in more detail in Chapter 4, which presents the text of a paper published in the journal Polymers in 2021 describing the formation and characterisation of chitosan-only, Chi-TEOS (1:1) and Chi-GA (8:1) films by this method demonstrating compatibility with a high-volume manufacturing process.

Importantly, it was found that the structure of the films as measured using FT-IR spectroscopy and the mechanical properties of the films produced were not significantly affected by the choice of preparation method.

3.1 Film appearance and composition

All drop-cast films were transparent, slightly yellow in tone and flexible. The Chi-TEOS (1:1) film appeared to be thinner than the others despite the same volume of hydrogel used in the casting all films. The Chi-GA (8:1) film had a more intense yellow colour and appeared to be more brittle when handling. Both Chi-APTES (2:1) and Chi-PAM (1:1) films appeared to have the same colour tone and flexibility.

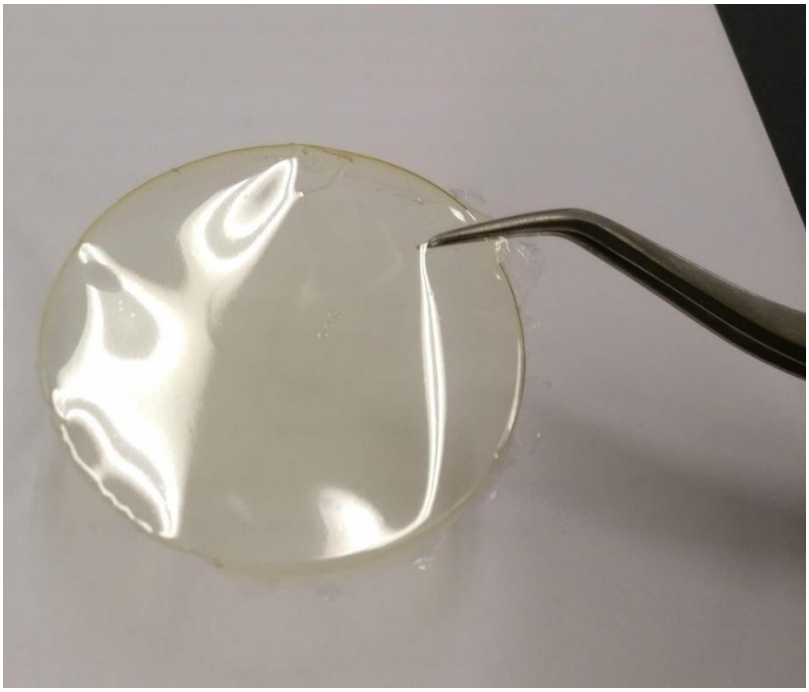


Figure 3.1: Photograph of a dry free-standing chitosan film prepared using the drop-cast method described in Chapter 2

In general, chitosan-based films would have a colourless appearance but that can change depending on the source of the material. Melanin is a tan pigment that is present in some crustacean exoskeletons and insect shells, chitosan from these sources may have a yellow/brown tone in colour. [1, 2] The absence of yellow or brown pigments in shrimp-sourced chitosan is a result of the different mechanisms shrimps use in the production of their exoskeletons. [3] Melanosis is the process in which the surface of a crustacean shell discolours into dark pigments, caused by the enzymatic oxidation of colourless phenols into quinones and subsequent polymerisation. [4] For this reason, an acetone-based decolourisation stage is implemented in the industrial extraction of chitin from crustaceans. [5]

Melanin has a high efficiency in absorbing and scattering photons, especially ones with a higher energy from the ultraviolet part of the light spectrum. [6] This is due to the well-defined π-π conjugated backbone in its molecular structure, see figure 3.2. [7] The yellow/brown tone is due to the conjugated double bonds. Alternating double bonds cause the absorption of the delocalised system to correspond to the wavelengths in the visible region.

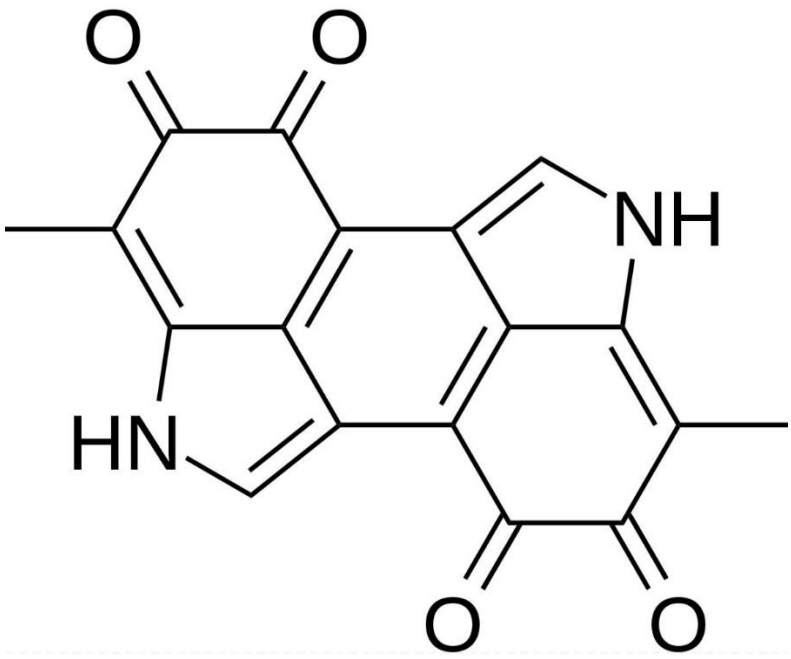


Figure 3.2: Molecular structure of melanin. Note the π electron-rich conjugated formation [8, 9]

Imines can form coloured species and the Schiff base links formed in Chi-GA are examples of imines. Thus, the Chi-GA samples have a more intense colour than the other samples due to the presence of the Schiff base bridges that link the chitosan polymer networks together. It is apparent that the chitosan used in this study was not pure chitosan, owing to the slight yellow/brown colour of the films. Most likely there were some melanin impurities present in the chemical compound which may have not been treated in the decolourisation stage of chitosan processing.

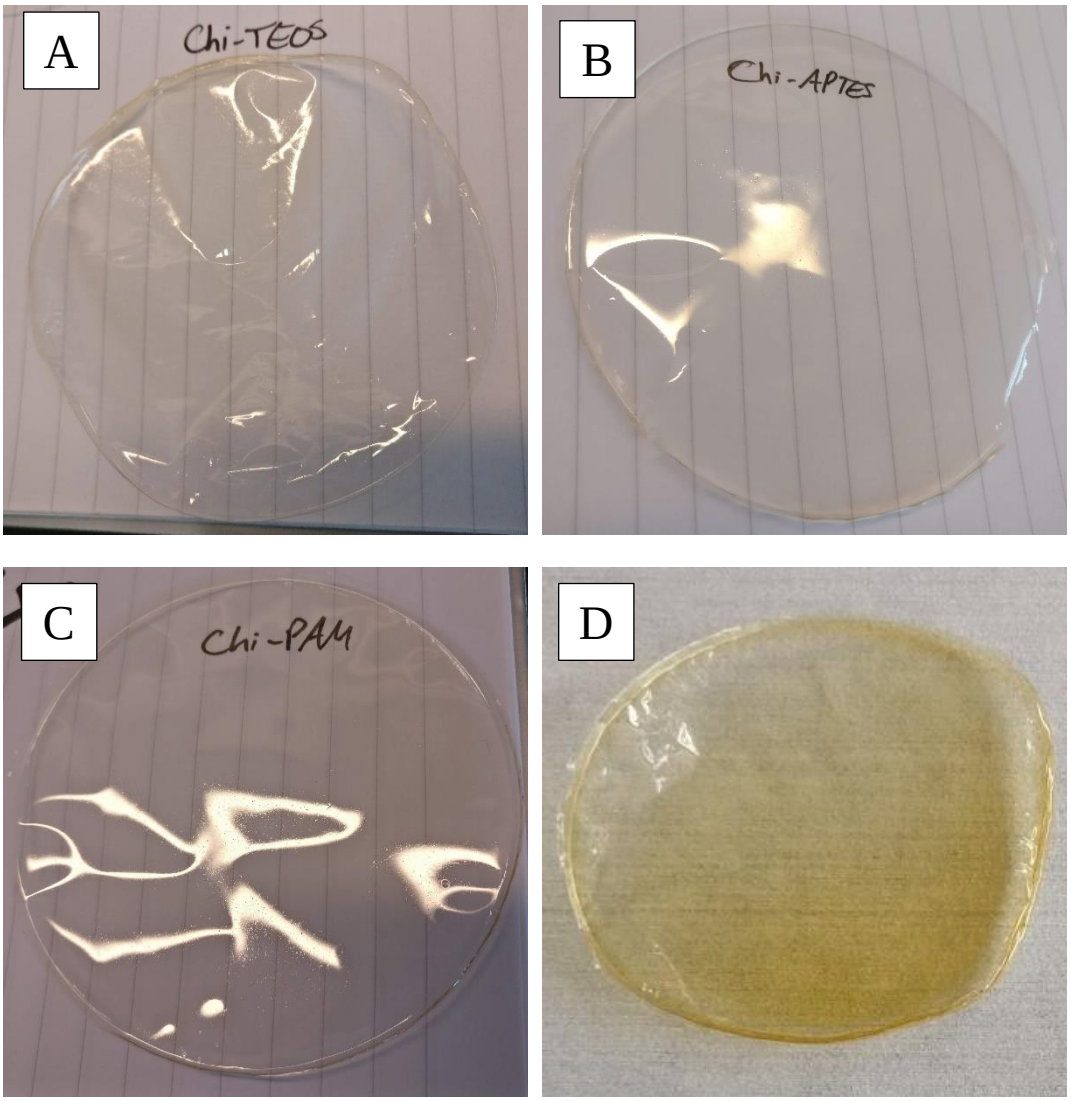


Figure 3.3: Photographs of all four dry, composite film types prepared by drop-casting. (A) Chitosan-TEOS (1:1), (B) Chitosan-APTES (2:1), (C) Chitosan-PAM (1:1), and (D) Chitosan-GA (8:1). Note the distinct yellow colouration associated with the Chitosan-GA (8:1) film as compared to the other films, due to the Schiff base bridges introducing a higher density of π electrons and thus more absorption in the visible region of the light spectrum. [10]

3.2 FT-IR spectroscopic analysis of chitosan-based films

The FT-IR spectra of the drop-cast chitosan membrane films showed important absorption bands to identify the characteristic functional groups which were recorded in the middle infrared range (4000 cm^{-1} to 500 cm^{-1}).

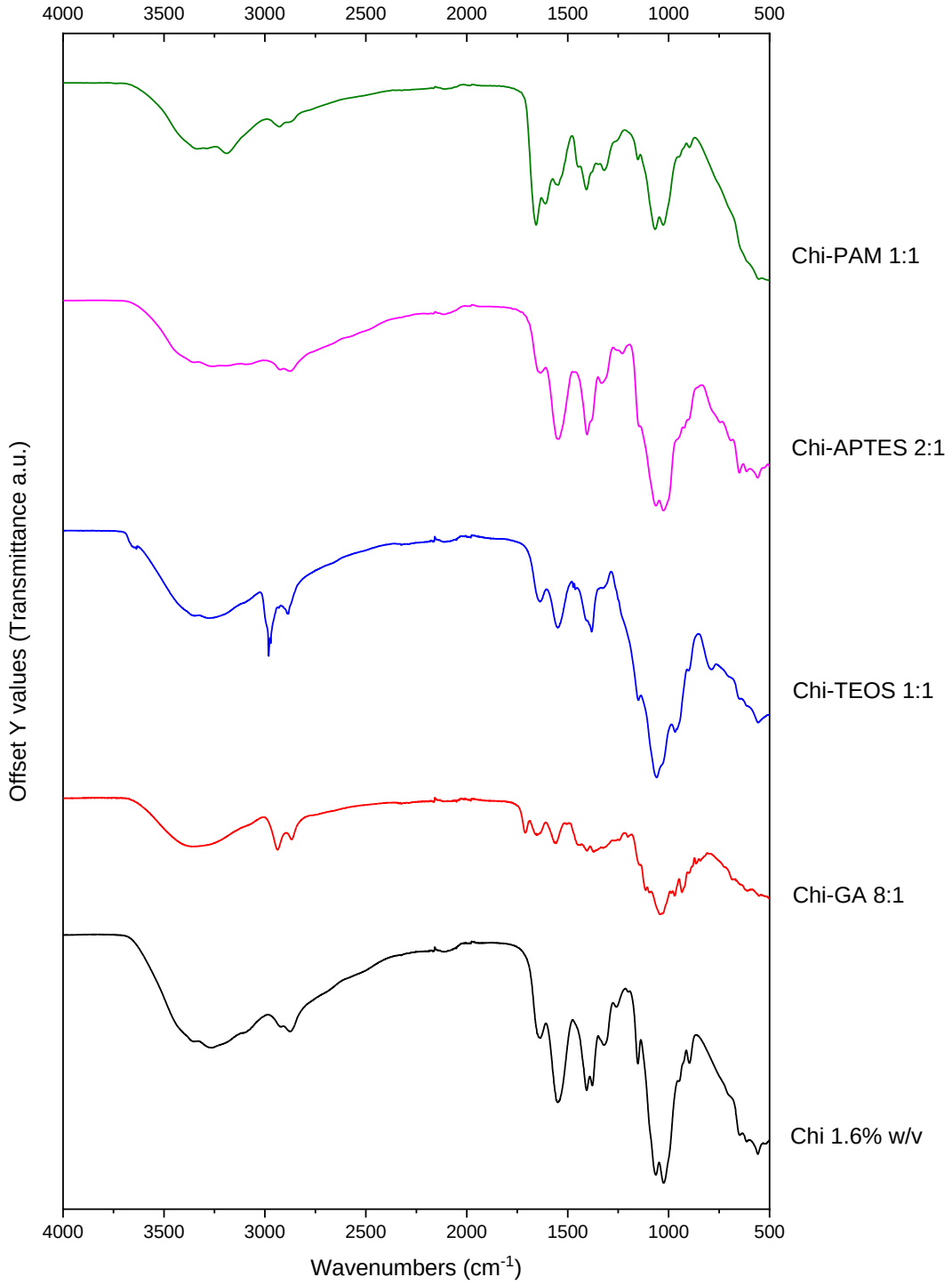


Figure 3.4: FT-IR graphs of chitosan-based composite films: Chi-PAM (1:1), Chi-APTES (2:1), Chi-TEOS (1:1), Chi-GA (8:1), and plain LMW chitosan 1.6% w/v

Practically identical spectra were obtained for the 3 sample types prepared by the slot-die method. The FT-IR spectra of the prepared chitosan-only and Chi-TEOS films, figure 3.4, show important absorption bands in the infrared range (4000 cm^{-1} to 500 cm^{-1}) which may be used to identify the characteristic functional groups. The features shown in the FT-IR spectra of the low molecular weight chitosan-only, Chi-TEOS, Chi-GA, Chi-APTES, and Chi-PAM films as shown in figure 3.4 were assigned as follows:

3.2.1 Chitosan and Chi-TEOS

The broad peaks at 3500–2500 cm^{-1} can be attributed to the stretching vibration of the -OH bond, the broadness indicating that the intermolecular hydrogen bonding between chitosan molecules is present in both types of film. [11] From figure 3.4 it may be seen that the -OH stretching region for the Chi-TEOS film is essentially the same as that for the chitosan film , suggesting that for both films the bulk of hydrogen bonding remains intact, most likely due to interactions via the OH sites as the amino groups are at least partially protonated in the acidic aqueous solution. [12]

The bands at ca. 3000- 2800 cm^{-1} are characteristic C-H vibrations. Figure 3.4 reveals differences in this region between the Chi-TEOS film and the chitosan only film. The Chi-TEOS film gives rise to two relatively sharp C-H vibrations near 3000 cm^{-1} which are not present in the spectrum of the chitosan only film. We propose that this feature may be attributed to the C-H stretching vibrations associated with the ethoxy groups of the TEOS, specifically 2982 cm^{-1} is assigned to CH_3, and 2971 cm^{-1} is assigned to CH_2. [13]

The bands in the region 1500–1600 cm^{-1} can be assigned to N–H bending vibrations of a primary amine. The bands in the region 1350–1450 cm^{-1} are associated with C–H bending vibrations while those in the region 1000–1200 cm^{-1} are associated with the C–N stretching vibrations of an aliphatic amine, overlapping with the anti- symmetric stretching of the C-O-C bridging species. Thus, for both films, the FT-IR data are consistent with the chitosan species remaining essentially chemically unperturbed by film formation.

However, in addition to the extra features in the C-H stretching region there are some other, more subtle differences between the spectra from the two types of film shown in figure 3.4: the bands near 780 cm^{-1} seen in the spectrum of the Chi-TEOS film can

be assigned to deformations in the N–H bonds of the amine groups. [14] The presence of such bending vibrations indicates that there is distortion of the functional group side chains of the chitosan polymer network via, in this case, the functional groups which would be expected to be involved in weak interactions such as H-bonding. The small peak near 440 cm^{-1} indicates the presence of an O-Si-O group, which functions as a bridge in the siloxane polymer network. [15]

Thus, it may be concluded that film formation involving either chitosan alone or in the form of the Chi-TEOS IPN does not significantly alter the molecular structure of the chitosan. In addition, the spectrum for the Chi-TEOS IPN reveals the presence of the second polymer network (the siloxane) and hints at the proposed hydrogen bonding links between the two polymers, as expected. [16]

3.2.2 Chi-GA

The broad bands at 3500-2500 cm^{-1}can once again be attributed to the hydrogen bonded O-H stretching vibrations possibly overlapping with the N-H stretching vibrations which appear in the same spectral region. The bands near 2870 cm^{-1} may be assigned to C-H stretching vibrations of the $-CH_2$ groups present on both the chitosan ring and the Schiff base imine bridges between the chitosan chains. These peaks increase in intensity with the higher concentration of glutaraldehyde, indicating that the assignment is correct and correlates with the amount of Schiff base bridges that are formed. The bands near 1400 cm^{-1} and 1300 cm^{-1} represent the C-H bending vibrations of the bridging alkyl and methyl groups, respectively. Once again, the bands near 1065 cm^{-1} and 1020 cm^{-1} may be attributed to the C-O-C bridging species while it is noteworthy that the amine N-H bending vibration appears at 1630 cm^{-1} - to a lower wavenumber as compared with the N-H bending vibration of the un-cross-linked chitosan. This observation can be attributed to the effective cross-linking of the chitosan hydrogel by the glutaraldehyde, which is expected to occur at the amino groups of the chitosan, forming an imine. [17] The intensity of the amine peak decreases with increasing concentration of glutaraldehyde, indicating that the amine site is being used for the Schiff base, as expected. The peak at 1715 cm^{-1} represents the C=N- stretching vibration of the Schiff base formed at the amine site. Importantly this peak does not appear in the spectra of the chitosan or the Chi-TEOS. Thus, it is proposed that there is considerable evidence for the formation of a chemically cross-linked species with the Chi-GA and that a Schiff base bridge is the method by which

the chitosan chain cross-links with glutaraldehyde. This is further supported by the intense yellow colour of the films, caused by the imine bonds introducing more π electrons and absorbing more visible light.

3.2.3 Chi-APTES

Like Chi-TEOS, the broad peak at 3500–3000 cm^{-1} can be attributed to an overlap of the O–H stretching vibrations of the alcohol and primary and secondary amide N-H group, but the greater intensity of the peak can be attributed to the extra NH_2 group present in APTES. 2900 cm^{-1} was observed to be C-H, 1500–1600 cm^{-1} N–H bending vibrations of primary amine, more intense than Chi-TEOS, again attributed to the amine group on the APTES molecule. 1350–1450 cm^{-1} C–H bending, 1000–1200 cm^{-1} C–N stretch of aliphatic amine overlapped with the anti- symmetric stretching of the C-O-C bridge. The peak at 780 cm^{-1} can be assigned to deformations in N–H groups of the amine groups. The presence of bend deformation vibrations indicates that there is distortion of the functional group side chains of the chitosan polymer network, in this case functional groups which would be expected to be involved in weak interactions such as H-bonding.

3.2.4 Chi-PAM

The absorption bands at 1638 cm^{-1} and 1548 cm^{-1} in chitosan-only films showed significant changes in the spectra of when blended with PAM. With the increase of PAM content, the bands at 1638 cm^{-1} shifted to a lower wavenumber of 1610 cm^{-1}, and the bands at 1548 cm^{-1} shifted to a higher wavenumber of 1656 cm^{-1}. This is attributed to the formation of hydrogen bonds between amino groups in chitosan and amino groups in PAM. [18] In addition, the absorption bands of CH around 3300 cm^{-1}, assigned to the stretching vibration of N-H and O-H, were broadened but their intensity decreased due to the blending of chitosan and PAM. This implies that part of the hydrogen bonds in chitosan were broken by the addition of PAM, and new hydrogen bonds formed between -NH_2, -OH groups in chitosan and -NH_2 groups in PAM.

3.3 Mechanical strength tests

3.3.1 Stress-strain curve

Stress is defined as the ratio of an applied force to the cross-sectional area of the material that it is applied to. [19] The formula for calculating material stress is:

$$\sigma = \frac{F}{A} \qquad \text{Eqn. 3.1}$$

Where F is force (N), A is area (m^2) and σ is stress (N/m^2 or Pa). Stress is understood as the internal force induced in the material in response to an applied external force, resisting any change in dimension caused by the external force.

Strain is defined as the ratio of the change in dimension to the initial dimension of the material and is unitless. [19] Longitudinal strain refers to the change in one dimension, the length. The formula for calculating the strain is:

$$\varepsilon = \frac{(l - l_0)}{l_0} \qquad \text{Eqn. 3.2}$$

Here l_0 is the initial length of the material, and l is the length of the material after applying force. Strain may be positive or negative depending on the direction of the external force. When a load acts on a body, the stress and strain it produces can be graphed as a curve, the shape of which can identify if the material is brittle, ductile or plastic. [20] When a material is pulled apart during a tensile strength test, initially the material follows Hooke's law, that is, stress is directly proportional to strain and the material exhibits elasticity and would spring back to its original shape if the force were to stop, no permanent deformation occurs. [19] As the material is subject to increasing amounts of tensile force, stress increases beyond the proportional limit.

The Young's modulus of elasticity is defined as the ratio of longitudinal stress to strain within the proportional limit of the material. This value is analogous to the stiffness of a spring, and it is necessary to distinguish the modulus of elasticity in different directions for non-isotropic materials such as wood. It is a value used to characterise elastic solids. [19]

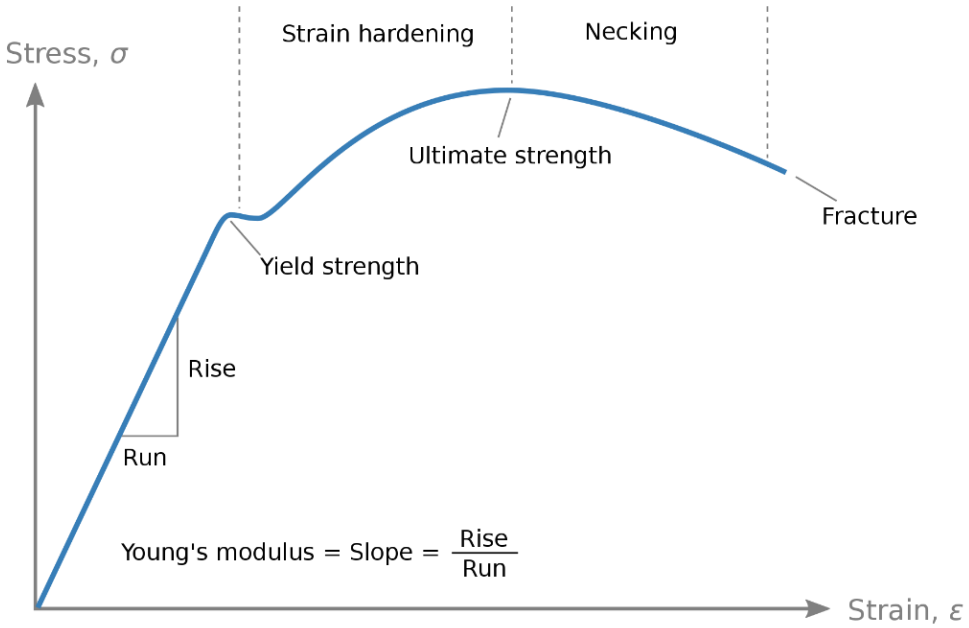


Figure 3.5: An example of a typical stress-strain graph displaying the various stages during a tensile strength test. [21]

The stress-strain relationship deviates from Hooke's law and the strain increases at a faster rate than stress, causing a mild flattening of the curve. This point is known as the yield point, where the elastic limit is reached and the ability to resist a load is measured, since any point beyond causes permanent plastic deformation. Further tensile force on the material results in strain hardening, when the number of dislocations becomes so high, they obstruct each other's movement, and the material is constantly rearranging itself to resist the tension. As plastic deformation continues, the cross section of the material begins to narrow and a thin neck is formed at the weakest point, ultimately resulting in the maximum amount of stress the material can handle and pushes it to breaking point. See figure 3.5 for more details.

All materials studied were ductile materials, with the exception of Chi-GA, which showed some brittleness. For this reason, the values of stress are used for all materials at the point of yield strength beyond which the material undergoes permanent deformation.

3.3.2 Tensile strength results

For all five materials and the various combinations employed, multiple tensile strength tests at varying concentrations were performed until breakage and the displacement of force was recorded for each. Chitosan Chi-TEOS, Chi-APTES and Chi-PAM films were tested 20 times while the Chi-GA films were tested 15 times. The reduced sample number for the Chi-GA films was due to the very brittle nature of these films relative to that of the other films, making them more difficult to handle. The median stress-strain graphs for each material calculated from all measurements taken are shown below in figure 3.6.

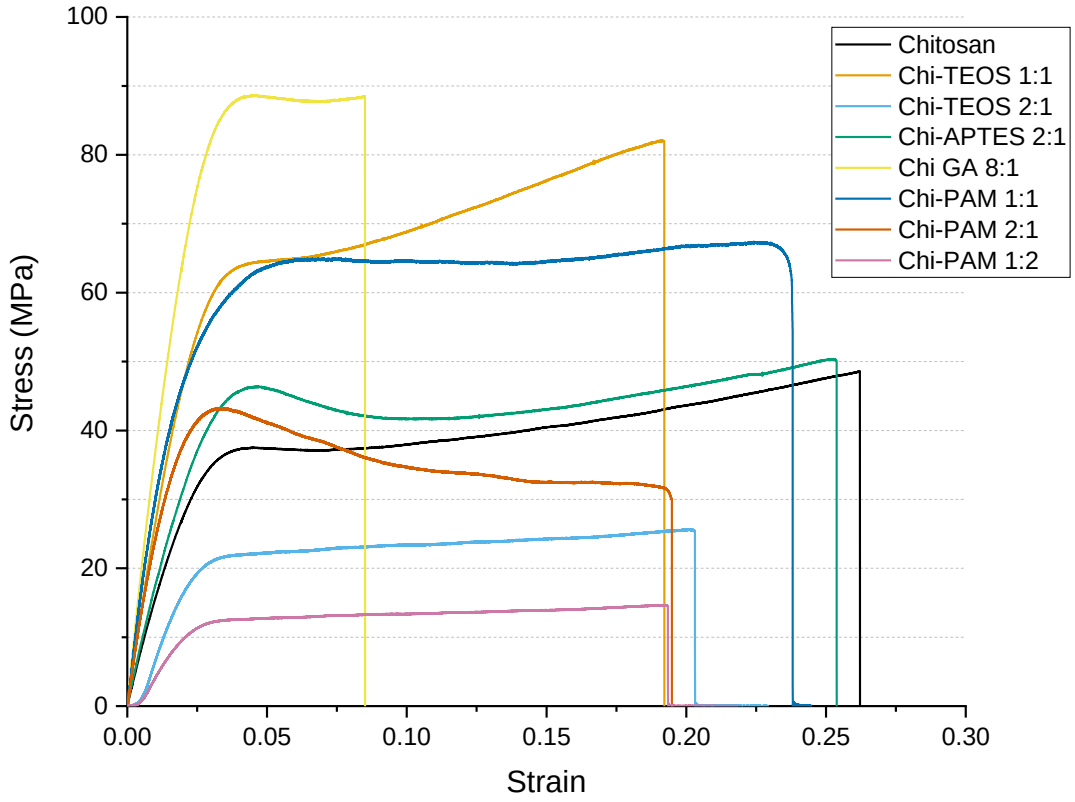


Figure 3.6: Typical stress strain curves recorded for all materials at varying concentrations, adapted and augmented from a previous publication. [22], which is presented in this thesis as Chapter 4.

Sample	Yield Strength (MPa)	Standard Deviation Yield Strength	Young's modulus (MPa)
Chitosan	37.17	2.70	1230.02
Chi-TEOS (1:1)	63.71	3.18	2008.53
Chi-TEOS (2:1)	21.17	1.71	950.41
Chi-APTES (2:1)	46.26	1.31	1341.77
Chi-GA (8:1)	88.36	3.06	2738.94
Chi-PAM 1:2	12.04	1.08	591.69
Chi-PAM (1:1)	64.13	2.21	1742.48
Chi-PAM (2:1)	43.08	2.63	1480.31

Table 3.1: Mean yield strength and Young's modulus of elasticity of each sample

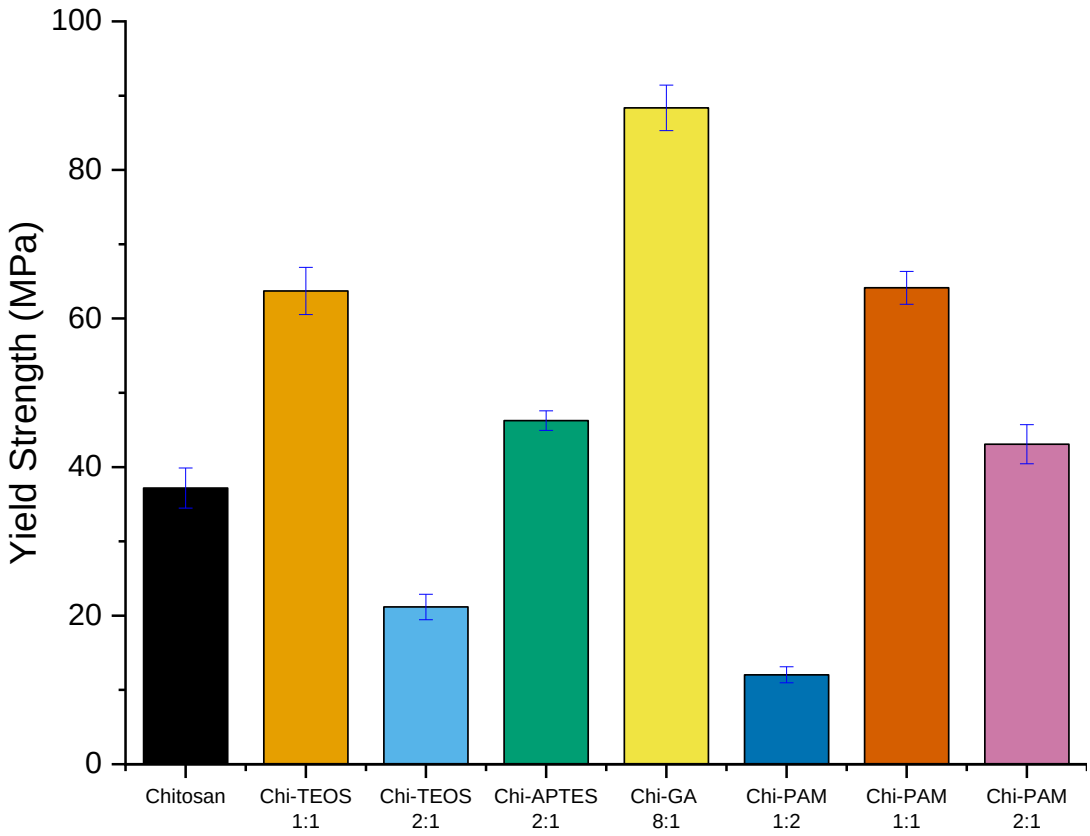


Figure 3.7: Histogram of all films mean tensile strength values expressed in MPa

It was found that there was a considerable sample-to-sample variation in the position of the break point for all the samples studied. However, the position of the initial yield point for the samples was remarkably consistent for each material examined. The yield point is the limit of the elastic region of the material i.e., any strain applied to the material after the yield point results in permanent deformation. During the plastic phase of the stress-strain curve, it is difficult to predict the breakage point due to this permanent deformation, so the yield point of the graphs was used as a more accurate metric for comparison where the strain is at its most uniform. As well as the yield point, the overall shape of the graph shows the type of material the films are plastic or elastic.

The polydispersity Index (PDI) and average molecular weight are the two main factors that affect the mechanical properties of chitosan. Low PDI results in narrower molecular weight distribution which is indicative of the greater uniformity of the polysaccharide structure. With a longer chain length, more molecular entanglement is observed and with a higher molecular weight there is a higher degree of crystallinity. [29] Thus, it is expected that the tensile strength should be enhanced with increased average molecular weight. [25]

3.3.2.1 Chitosan

The average stress yield point for the chitosan-only films was 37.17 MPa which aligns with other chitosan-only films in the literature. [23-25] In this case, the shape of the graphs indicates that material is more ductile than the Chi-GA samples. The initial straight line from the origin point indicates the elastic region with a modulus of elasticity of 1230.02 MPa. The curve represents a full loading of the sample from initial loading to breakage. The shape of the graph shows the material is relatively elastic with minor necking towards the breaking point. The sample remains at an even stress level which being elongated indicated a less crystalline structure than Chi-GA or Chi-TEOS (1:1).

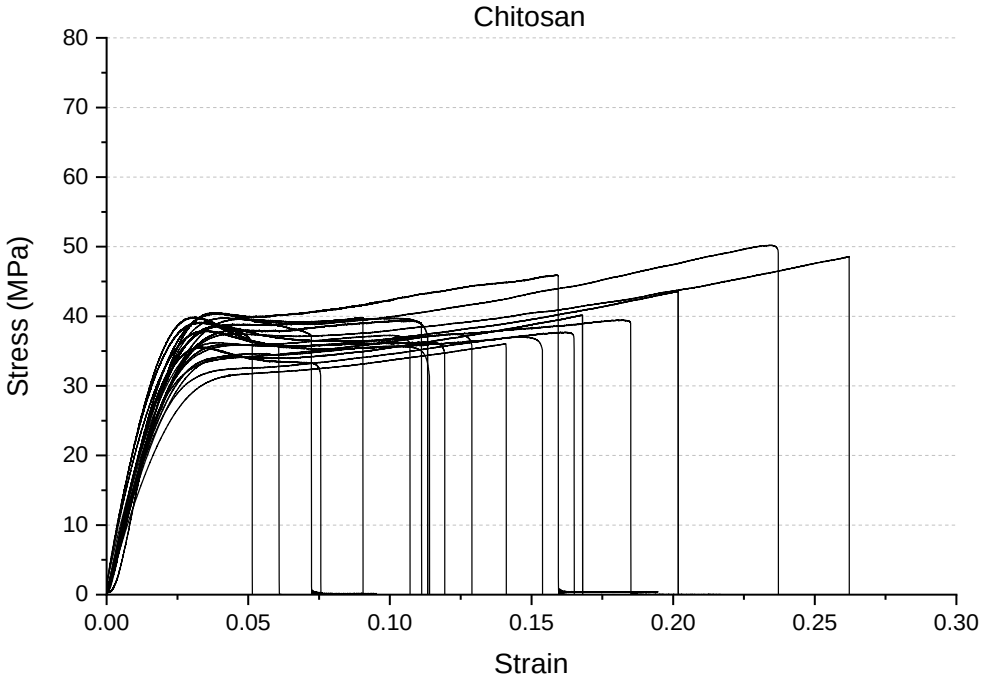


Figure 3.8: Stress-strain curves of the chitosan-only film samples

3.3.2.2 Chi-TEOS

The average stress yield point for the Chi-TEOS (1:1) films was 63.71 MPa which is on par with the literature values for a Chi-TEOS type of film. [25, 26] The initial straight line from the origin point indicates the elastic region with a modulus of elasticity of 2008.53 MPa.

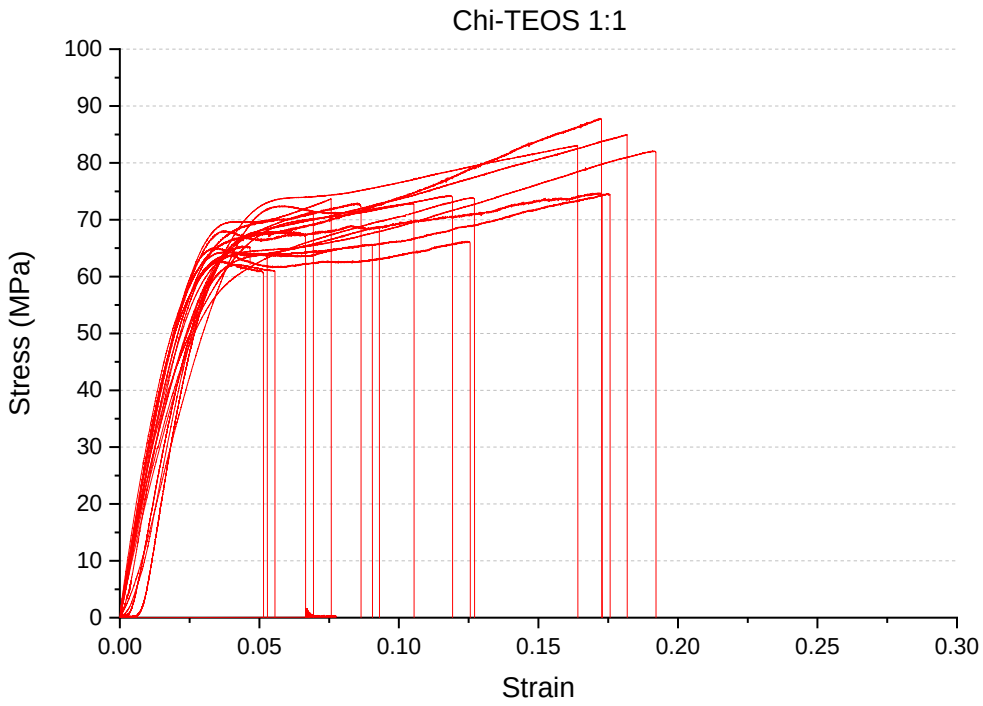


Figure 3.9: Stress-strain curves of the Chi-TEOS (1:1) samples

The average stress yield point for the Chi-TEOS (2:1) films was 21.17 MPa which aligns with similar Chi-TEOS based films in the literature. [27] The initial straight line from the origin point indicates the elastic region with a modulus of elasticity of 950.41 MPa. The shape of the graphs indicates that material is ductile and as an illustration of this, it was observed that a high degree of 'necking' occurred during the testing, as seen by the steep incline of the graph shape after the initial yield point for Chi-TEOS (1:1). The high degree of strain hardening causes strain induced crystallisation. Less necking occurred in the Chi-TEOS (2:1) sample, indicating the material was more ductile and elastic, which is shown by the plateaux shape of the graph and uniform stress values.

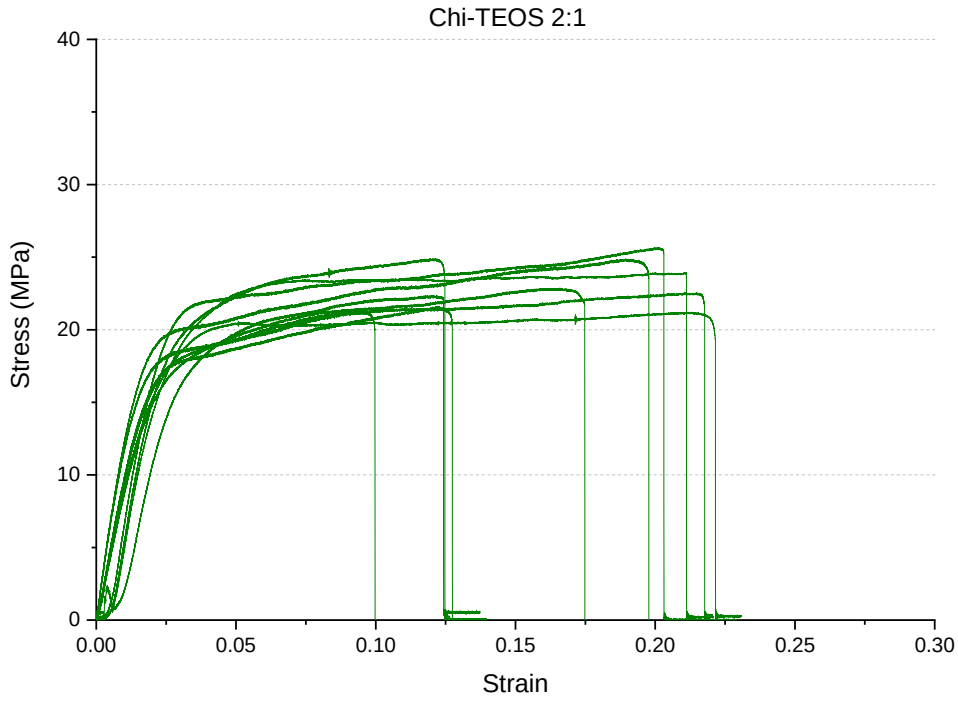


Figure 3.10: Stress-strain curves of the Chi-TEOS (2:1) samples

3.3.2.3 Chi-APTES

The average stress yield point for the Chi-APTES (2:1) films was 46.26 MPa which is similar to other Chi-APTES based films in the literature. [28] The initial straight line from the origin point indicates the elastic region with a modulus of elasticity of 1341.77 MPa. The shape of the graphs indicates this sample is similar to chitosan-only in terms of elasticity but does become more brittle and experiences strain induced crystallisation as shown by the slight incline upwards in the shape of the graph beyond the initial yield point region.

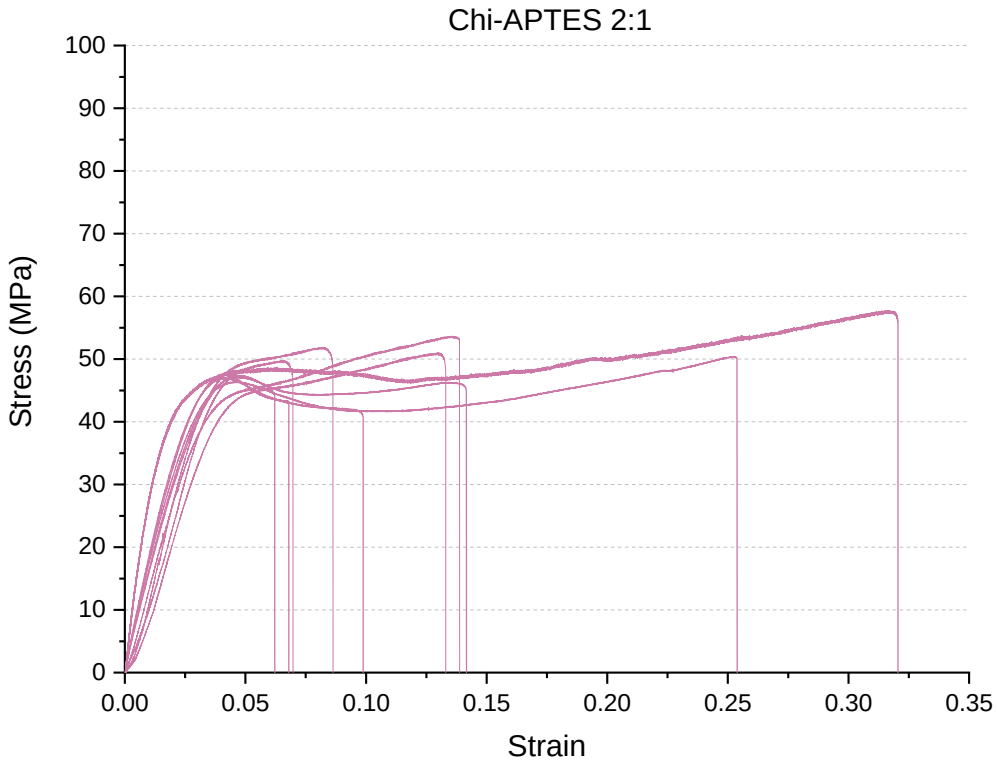


Figure 3.11: Stress-strain curves of the Chi-APTES (2:1) samples

3.3.2.4 Chi-GA

The average stress yield point for the Chi-GA (8:1) films was 88.36 MPa. The initial straight line from the origin point indicates the elastic region with a modulus of elasticity of 2738.94 MPa. The shape of the graphs indicates the material is very brittle with a sharp and tall elastic region. The films break shortly after the initial yield point showing it to be more rigid and crystalline in structure than the more flexible chitosan-only samples. This was noted as the tests were carried out also, the samples appeared to snap and break easily while loading them into the tensile test machine.

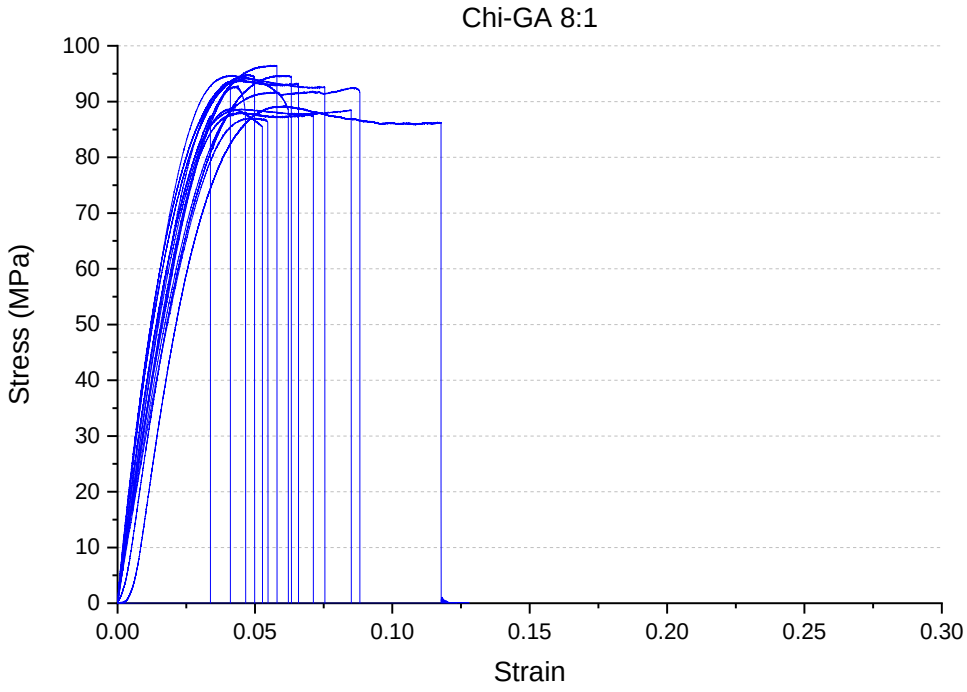


Figure 3.12: Stress-strain curves of the Chi-GA (8:1) samples

3.3.2.5 Chi-PAM

The average stress yield point for the Chi-PAM (1:1) films was 64.13 MPa. The initial straight line from the origin point indicates the elastic region with a modulus of elasticity of 1742.48 MPa. The shape of the Chi-PAM (1:1) graphs indicate the material is similarly elastic to that of chitosan-only or Chi-TEOS (2:1). With no pronounced steep climb or necking, the strain levels remain uniform before breakage.

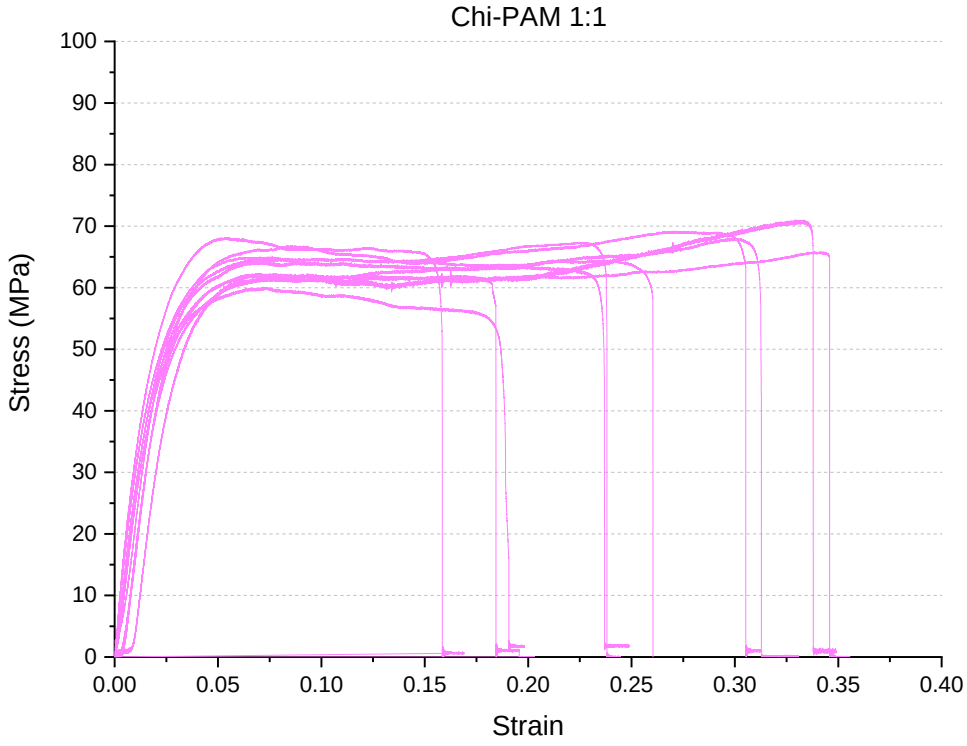


Figure 3.13: Stress-strain curves of the Chi-PAM (1:1) samples

The average stress yield point for the Chi-PAM (2:1) films was 43.08 MPa. The initial straight line from the origin point indicates the elastic region with a modulus of elasticity of 1480.31 MPa. The shape of Chi-PAM (2:1) shows the material is too elastic to the point of degradation when being pulled apart. The elastic region and the initial yield point remain as an indicator of its tensile strength but beyond those points the material begins to degrade as shown by the decline in the curves. Some other samples dip in the middle like Chi-APTES (2:1) but they begin to strengthen and resist tension before the breaking point. However, most Chi-PAM (2:1) samples broke before they could begin to resist further tension.

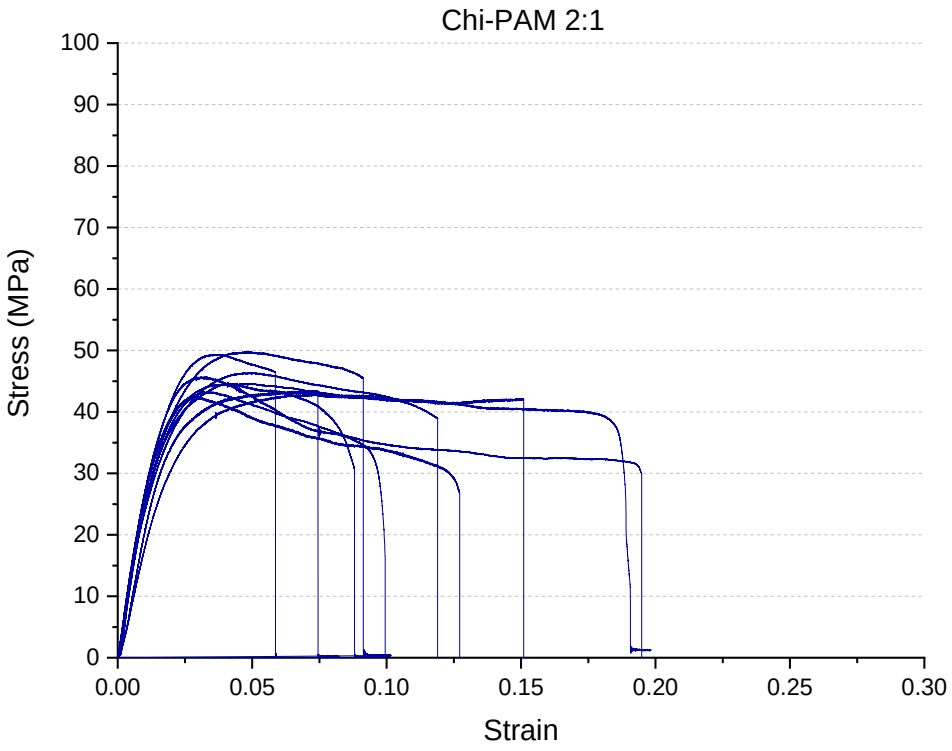


Figure 3.14: Stress-strain curves of the Chi-PAM (2:1) samples

The average stress yield point for the Chi-PAM (1:2) films was 12.04 MPa. The initial straight line from the origin point indicates the elastic region with a modulus of elasticity of 591.69 MPa. The shape of the Chi-PAM 1:2 is similar to Chi-TEOS (2:1) with a very low and flat curve. Even less necking was occurring than Chi-PAM (1:1), showing the film to be rather elastic and pliable but not very mechanically strong compared to other samples.

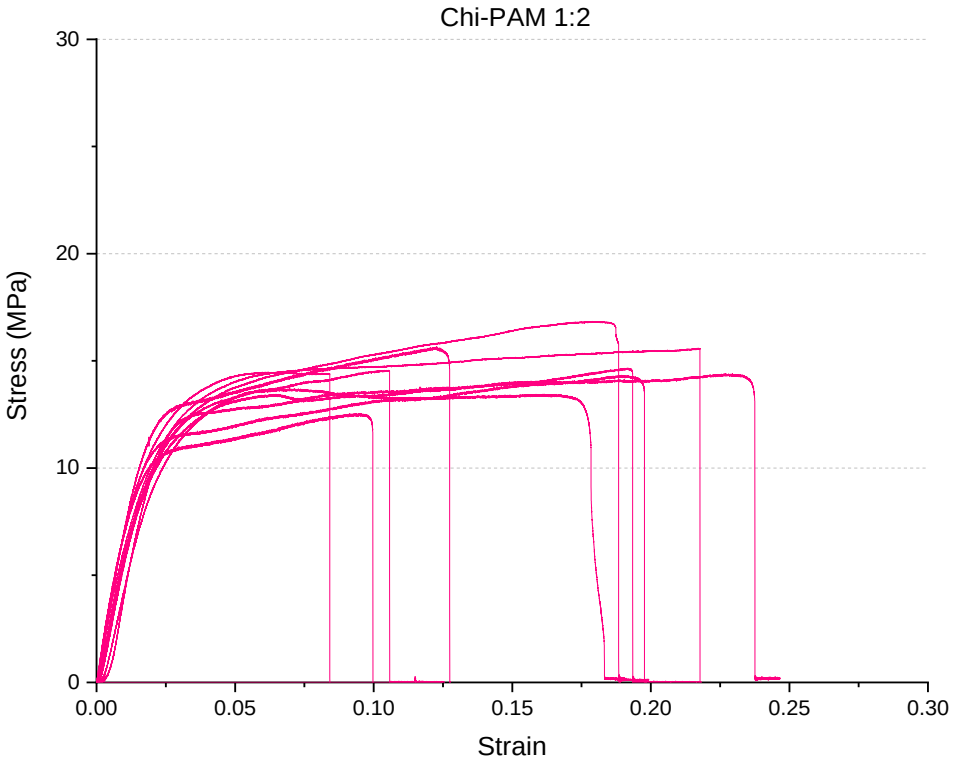


Figure 3.15: Stress-strain curves of the Chi-PAM 1:2 samples

3.4 Discussion

From figure 3.4 and the spectroscopy discussions, it can be seen that the FT-IR spectra of the films made only with chitosan show some evidence of hydrogen bonding between the chitosan chains. The FT-IR spectra of the two siloxane-based IPNs are then seen to be consistent with the formation of true IPNs where the chains of the two polymers concerned are intimately mixed but are not covalently bonded. In contrast the chitosan-GA films show clear evidence of the formation of Schiff base linkages as expected because of the reaction of the amine groups on the chitosan with the glutaraldehyde cross linker. Finally, the polymer blend made with chitosan and PAM is also shown to be consistent with a simple polymeric mixture where the only additional linkages that form as a result of mixing are those due to hydrogen bonding.

The mechanical properties of the films generally vary as might be expected in terms of film composition and proposed structure, but with some notable exceptions. Figure 3.6 and figure 3.7 reveal that perhaps surprisingly, chitosan-only films are not the weakest in terms of mechanical strength. Chi-TEOS (2:1) shows a lower mean yield strength than the chitosan-only films while the Chi-PAM (1:2) film exhibits an even lower mean yield strength, making this film the weakest of all films studied.

Setting these apparently anomalous results to one side for a moment, it may be seen that all other films show a higher mean yield strength value than the chitosan only film, as might be expected, with the highest mean yield strength value being recorded for the Chi-GA (8:1) film which is known to contain covalent linkages between the chitosan chains as a result of cross-linking by the glutaraldehyde.

The next highest mean yield strengths are those associated with the IPN Chi-TEOS (1:1) and the polymer blend, Chi-PAM (1:1), with these samples showing essentially identical average behaviour in terms of mean yields strength, being consistent with an overall increase in robustness that arises from the mixing of two polymeric systems, one resulting in IPN formation (Chi-TEOS (1:1) and the other simply involving chain entanglement Chi-PAM (1:1)).

Next in this series comes the IPN Chi-APTES (2:1) which might be expected to have reduced cross linking between the siloxane chains as a result of exchanging an ethoxy group for the aminopropoxy ligand and the polymer blend Chi-PAM (2:1). Again, these two materials yield similar values of mean yield strength, both higher than that

of the chitosan-only films. The chitosan-only films come next in the series with the two remaining films showing reduced mean yield strength as noted above.

Chi-TEOS (2:1) is still expected to be a true IPN yet it is less mechanically robust than chitosan alone. Similarly, Chi-PAM (1:2) is expected to be a true polymer blend yet it is the weakest film of the series in terms of mean yield strength.

It has been reported in the literature that the tensile strength of chitosan films may be improved by forming composites with TEOS and increasing the cross-linking density to encourage the formation of a dense structure. [26] However, an excess amount of TEOS can cause a decrease in the homogeneity of the film and thus the mechanical strength. Yu et al. [30] found that a TEOS concentration of 5 wt.% or higher in their chitosan membranes resulted in increased rigidness. Massive siloxane aggregates in the polymeric matrix led to looser structured membranes. This was because more of the -OH groups were being used in the condensation stage of polymerisation, resulting in less active sites for hydrogen bonding with the chitosan network. [30, 31] This could provide an explanation as to why the Chi-TEOS (2:1) films are mechanically weaker than Chi-TEOS (1:1) and chitosan-only films. The active -OH and $-NH_2$ sites on the chitosan chain are occupied by hydrogen bonding with a less concentrated siloxane network and thus is less mechanically robust. This leads to the disruption of intramolecular H-bonding within the chitosan network resulting in a less mechanically stable composite.

The Chi-PAM (1:2) films are mechanically weaker than chitosan-only and Chi-PAM (1:1) films due to the increased hygroscopicity from the PAM network. The water absorbed would induce a plasticising effect in the films, increasing elasticity. [18] An excess of water may affect chitosan network by swelling too much and disrupting the intramolecular hydrogen bonds, thus making it weaker than chitosan-only films. As discussed in section 3.3.2.5, this gives the effect of a more pliable film that is not mechanically strong, resulting in a low and flat stress/strain curve after the initial yield point, see figure 3.14. There appears to be a limit for the ratio of chitosan and PAM blends before the mechanical strength starts to decrease due to excessive water content in the films.

3.5 Conclusions

A range of chitosan-based films has been prepared and characterized using FT-IR and mechanical testing. The data obtained are shown to be consistent with the proposed structure of the films (figures 2.2, 2.6, 2.8, and 2.10) although more experiments are required to unequivocally confirm the proposals made. The structure, mechanical properties, and chemistry of the films studied here are key factors that will be considered throughout this thesis. The fundamental properties of the chitosan-based films will remain the same as they are applied to the various different functionalities of roll-to-roll processing (chapter 4), heavy metal adsorption (chapter 5), antibacterial activity (chapter 6), and smart wound dressing design (chapter 7).

References

1. Roy, S., et al., *Preparation and characterization of synthetic melanin-like nanoparticles reinforced chitosan nanocomposite films.* Carbohydrate Polymers, 2020. **231**.
2. Khayrova, A., S. Lopatin, and V. Varlamov, *Obtaining chitin, chitosan and their melanin complexes from insects.* International Journal of Biological Macromolecules, 2021. **167**: p. 1319-1328.
3. Malm, M., et al., *Development of Chitosan Films from Edible Crickets and Their Performance as a Bio-Based Food Packaging Material.* Polysaccharides, 2021. **2**(4).
4. Goncalves, A.A. and A.R.M. de Oliveira, *Melanosis in crustaceans: A review.* Lwt-Food Science and Technology, 2016. **65**: p. 791-799.
5. Kumari, S. and R. Kishor, *Chapter 1 - Chitin and chitosan: origin, properties, and applications*, in *Handbook of Chitin and Chitosan*, S. Gopi, S. Thomas, and A. Pius, Editors. 2020, Elsevier. p. 1-33.
6. Ye, T. and J.D. Simon, *Comparison of the ultrafast absorption dynamics of eumelanin and pheomelanin.* Journal of Physical Chemistry B, 2003. **107**(40): p. 11240-11244.
7. Eom, T. and B.S. Shim. *Natural Melanin Composites by Layer-by-Layer Assembly*. in *Conference on Electroactive Polymer Actuators and Devices (EAPAD)*. 2015. San Diego, CA.
8. contributors, W.C. *File:Melanin.svg*. 19 September 2020 07:25 UTC 18 May 2022 15:51 UTC]; https://commons.wikimedia.org/w/index.php?title=File:Melanin.svg&oldid=464588746].
9. Cao, W., et al., *Unraveling the Structure and Function of Melanin through Synthesis.* Journal of the American Chemical Society, 2021. **143**(7): p. 2622-2637.
10. Cao, W.L., et al., *Effects of the degree of deacetylation on the physicochemical properties and Schwann cell affinity of chitosan films.* Journal of Biomaterials Applications, 2005. **20**(2): p. 157-177.

11. Jennings, K.R., *Spectrometric identification of organic compounds (Fifth Edition) R. M. SILVERSTEIN, G. C. BASSLER AND T. C. MORRILL. Wiley, New York, 1991. No. of pages: 430. ISBN 0471 63404 2. Price: £50.25, $76.10.* Organic Mass Spectrometry, 1991. **26**(9): p. 813-813.
12. Dhanikula, A. and R. Panchagnula, *Development and characterization of biodegradable chitosan films for local delivery of Paclitaxel.* The AAPS journal, 2004. **6**: p. e27.
13. Rubio, F., J. Rubio, and J. Oteo, *A FT-IR study of the hydrolysis of Tetraethylorthoselicate (TEOS).* Spectroscopy Letters, 1998. **31**: p. 199-219.
14. Nunthanid, J., et al., *Physical Properties and Molecular Behavior of Chitosan Films.* Drug Development and Industrial Pharmacy, 2001. **27**(2): p. 143-157.
15. Téllez-Jurado, L., et al., *FT-IR Study of the Hydrolysis and Polymerization of Tetraethyl Orthosilicate and Polydimethyl Siloxane in the Presence of Tetrabutyl Orthotitanate.* Spectroscopy Letters - SPECTROSC LETT, 2006. **37**: p. 11-31.
16. Park, S.-B., et al., *A novel pH-sensitive membrane from chitosan — TEOS IPN; preparation and its drug permeation characteristics.* Biomaterials, 2001. **22**(4): p. 323-330.
17. Akakuru OU, I.B., *Chitosan Hydrogels and their Glutaraldehyde-Cross-linked Counterparts as Potential Drug Release and Tissue Engineering Systems-Synthesis, Characterization, Swelling Kinetics and Mechanism.* J Phys Chem Biophys, 2017. **7**(256).
18. Xiao, C.B., et al., *Blend films from chitosan and polyacrylamide solutions.* Journal of Macromolecular Science-Pure and Applied Chemistry, 2001. **38**(8): p. 761-771.
19. Budynas, R.G. and A.M. Sadegh, *Roark's Formulas for Stress and Strain, 9E*. 2020: McGraw-Hill Education.
20. International, A.S.M., *Atlas of Stress-strain Curves*. 2002: ASM International.
21. *Wikimedia Commons, t.f.m.r. File:Stress strain ductile.svg.* 27 Sep 2020.
22. Pemble, O.J., et al., *A Slot-Die Technique for the Preparation of Continuous, High-Area, Chitosan-Based Thin Films.* Polymers, 2021. **13**(10): p. 13.
23. Shahzadi, K., et al., *Preparation and characterization of bio-based hybrid film containing chitosan and silver nanowires.* Carbohydrate Polymers, 2016. **137**: p. 732-738.

24. Yeng, C.M., S. Husseinsyah, and S.S. Ting, *Corn Cob Filled Chitosan Biocomposite Films.* Multi-Functional Materials and Structures Iv, 2013. **747**: p. 649-+.
25. Ryan, C.C., M. Bardosova, and M.E. Pemble, *Structural and mechanical properties of a range of chitosan-based hybrid networks loaded with colloidal silica and polystyrene particles.* Journal of Materials Science, 2017. **52**(13): p. 8338-8347.
26. Shaari, N.Z.K., N.A. Sulaiman, and N. Abd Rahman, *Thin film composite membranes: Preparation, characterization, and application towards copper ion removal.* Journal of Environmental Chemical Engineering, 2019. **7**(1): p. 7.
27. Sulaiman, N.A., et al. *A Study on Anti - Fouling Behaviour and Mechanical Properties of PVA/Chitosan/TEOS Hybrid membrane in The Treatment of Copper Solution*. in *3rd International Conference on Global Sustainability and Chemical Engineering (ICGSCE)*. 2017. Putrajaya, MALAYSIA: Iop Publishing Ltd.
28. Zimoch, A., et al., *Effect of 3-aminopropyltriethoxysilane on a variability of selected physical properties of chitosan protective coatings.* Przemysl Chemiczny, 2012. **91**(5): p. 1100-1104.
29. Chen, R.H. and H.D. Hwa, *Effect of molecular weight of chitosan with the same degree of deacetylation on the thermal, mechanical, and permeability properties of the prepared membrane.* Carbohydrate Polymers, 1996. **29**(4): p. 353-358.
30. Yu, L.Y., et al., *Preparation and characterization of PVDF-SiO2 composite hollow fiber UF membrane by sol-gel method.* Journal of Membrane Science, 2009. **337**(1-2): p. 257-265.
31. Ogoshi, T. and Y. Chujo, *Synthesis of poly(vinylidene fluoride) (PVdF)/silica hybrids having interpenetrating polymer network structure by using crystallization between PVdF chains.* Journal of Polymer Science Part a-Polymer Chemistry, 2005. **43**(16): p. 3543-3550.

4. A Slot-Die Technique for the Preparation of Continuous, High-Area, Chitosan-Based Thin Films

4.1 Introduction

Chitosan, poly-(D) glucosamine, is a polymer that is derived from the naturally occurring polysaccharide chitin. Chitin, poly (b-(1-4)-N-acetyl-D-glucosamine), is a material that is known for its relatively resilient and pliable nature and is one of the primary components of arthropod exoskeletons. If chitin undergoes deacetylation in the presence of basic hydroxides it forms chitosan which is more soluble and flexible and therefore can be easily applied to the synthesis of a variety of thin films. Chitosan is defined by the degree of deacetylation (DD) of chitin. When this value is at 40% or higher the material is classified as chitosan. [1] Unlike chitosan, chitin is very limited in terms of potential commercial applications due to its poor solubility. The presence of amino groups in chitosan gives the polymer many desirable properties that are not present in chitin. The strong intermolecular hydrogen bonds between the amino and hydroxyl groups of the glucosamine monomers create a rigid crystalline structure. [2] The D-glucosamine residues may be protonated, providing solubility in acidic aqueous solutions. [3] Once dissolved, the chitosan chains form a weak polymeric network due to the intramolecular and intermolecular hydrogen bonding between the hydroxyl groups as seen in figure 4.1. [4-6]

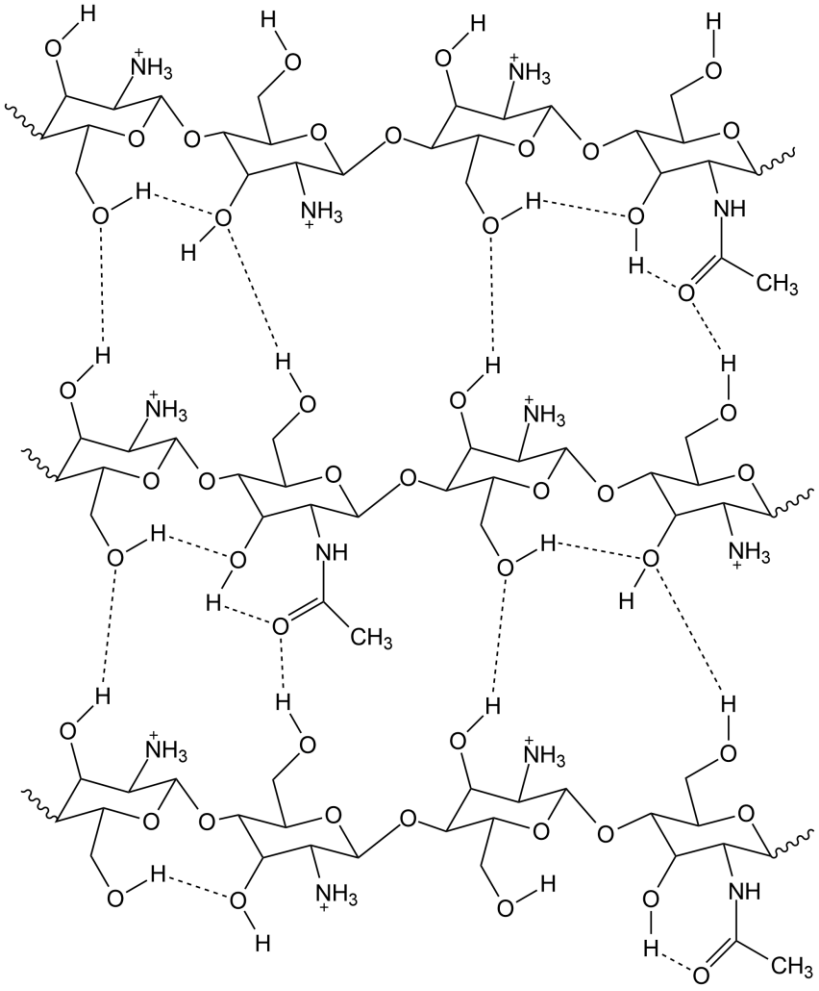


Figure 4.1: The intramolecular and intermolecular hydrogen bonding that occurs in chitosan dissolved in acidic media resulting in the formation of a non-covalently bound network.

In recent years chitosan-based materials have emerged as having many potential uses in areas such as in medical and pharmaceutical applications, for example in the form of fibres for wound dressings [7, 8] and for controlled drug release [9, 10], in food science for use in the immobilisation of enzymes [1] and in water treatment applications for the removal of heavy metal ions. [11] In this latter application it is the presence of the protonated amino groups that allow chitosan to form complexes with heavy metal ions. [1]

In terms of potential high-volume commercial applications of chitosan films, the preparation of antibacterial films for use in food packaging has been demonstrated by creating a chitosan-starch film using microwave treatment without the use of

plasticizers. [12] To date, typical methods of forming chitosan-based films include drop-casting in Petri dishes and drying at room temperature, [13] the layer-by-layer formation of nanostructured films by the Langmuir-Blodgett technique after chemical modification, the layer-by-layer self-assembly via dip coating - a relatively simple technique for producing nanometre scale thin films, [14, 15] and the development of uniform thin chitosan films by spin coating onto silicon discs to achieve a specific thickness. [16]

It is noteworthy that all these methods are essentially batch processes. Although batch processing can be used highly successfully to produce high volumes or high areas of thin film materials, for applications such as packaging it is arguable that a continuous, production process that could accumulate large volumes of coated materials on a roll system would be highly commercially desirable.

This chapter seeks to address this issue directly by demonstrating that a range of reproducible chitosan-based films can be made cheaply and quickly using a simple lab-based slot-die apparatus that is fed directly with the chitosan hydrogel mixture. The apparatus used and its operation is described. It is suggested that it would be a relatively simple step to scale up this equipment to a level required for a real high-volume commercial application. Preliminary mechanical testing on the films produced here have been performed to demonstrate that the results are consistent with those obtained from similar films produced using other methods and are also consistent with the anticipated structure and properties of the films. In addition, since the slot-die process is an example of a polymer extrusion process, some of which are known to influence the structure and properties of the resulting polymer, [17-19] rudimentary assessment of the films in terms of direction of extrusion was performed and no evidence for any such effects was observed.

It is therefore proposed that these findings provide some degree of validation of the slot-die approach for use in potential manufacturing situations.

4.2 Materials and Methods

4.2.1 Slot-die casting via a doctor blade apparatus

The slot-die casting apparatus consists of two rollers 50 cm apart with a flat hotplate set to 50°C in between the rollers, figure 4.2. This apparatus was constructed by the group of Professor Roberto M. Faria at IFSC USP Brazil. The direction of travel of the film formed via the extrusion of the hydrogel through the slot is marked by an arrow.

A PET foil substrate (175 µm thick) was plasma-cleaned using an Expanded Tabletop oxygen plasma cleaner (PDC-002) with a PlasmaFlo gas flow mixer and pressure monitor (PDC-FMG-2). The plasma-treated film was then wrapped around the rollers and stretched flat on the hotplate. The doctor blade slot-die head was positioned above the PET foil on an adjustable horizontal bar that spanned the width of the foil. The slot-die nozzle opening was 2 cm in length with the width of the slot set to 2 mm and was angled 2 mm above the PET substrate at 45 degrees.

A video showing the operation of the slot-die coater is available at this link: https://youtu.be/s042exW21Ho.

A syringe pump with a 3 cm diameter syringe was attached to the slot-die head via a thin flexible tubing. The rate of deposition and movement of the substrate were 1 mL/min and 1 cm/min, respectively. Approximately 20 – 25 mL of gel was cast onto the PET substrate over 20 minutes. The gel was left to dry on the PET under an extraction fan. A thin transparent film formed over the course of an hour. It was then carefully peeled off the PET and allowed to air dry for a further hour. The film was then cut into 1 cm x 4 cm pieces with a rolling blade and stored in an airtight container.

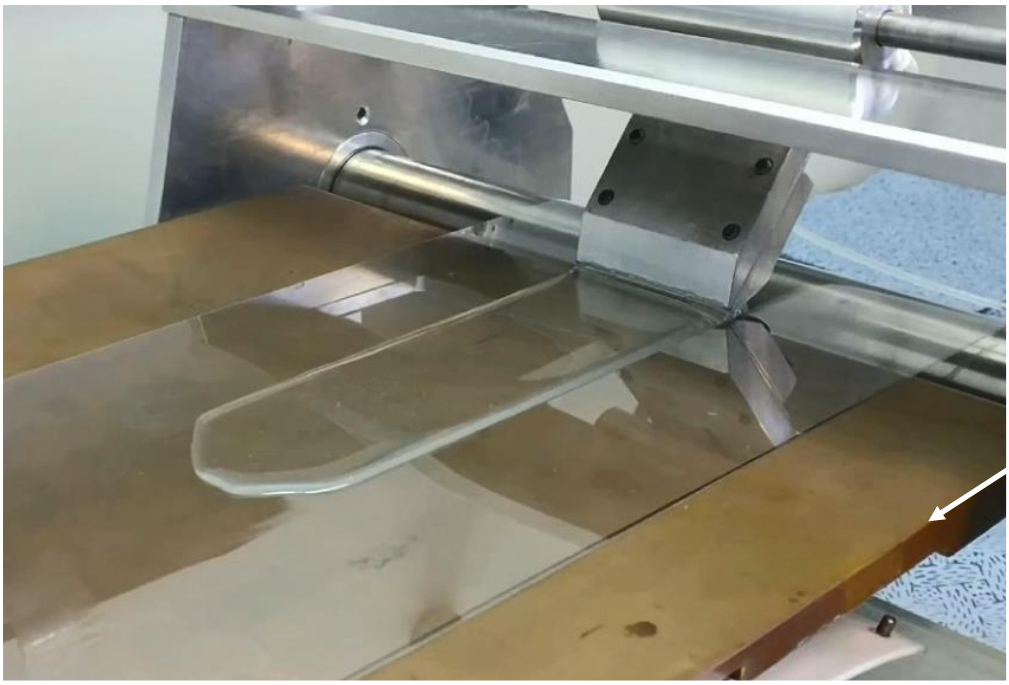


Figure 4.2: A photograph of slot-die roll to roll machine shown depositing a Chi-TEOS IPN hydrogel onto a PET substrate over a hotplate.

4.2.2 The preparation of chitosan-based hydrogels

Based on the information available from the literature [10, 11, 20] the chitosan chosen for this work was lower molecular weight (50000 – 190000 Da, Sigma Aldrich Ireland) with a DD of 75-85% to help facilitate the dissolving of the crystalline solid in aqueous acid solution. Tetraethyl-orthosilicate (≥99%), glutaraldehyde solution (25%), Hydrochloric acid (37%), acetic acid (≥99%) and ethanol (≥99%) were purchased from Sigma-Aldrich (Ireland). Millipore deionised water (18 MΩ) was used to prepare aqueous solutions. All materials were used as received. Three types of chitosan-based hydrogel were synthesised and used as the precursors to (a), chitosan-only films, (b), chitosan-TEOS IPNs and (c), chitosan-glutaraldehyde cross-linked films. The synthesis of all these types of films have been reported previously in the literature [16, 21-26] and so they serve as benchmarks for the evaluation of the performance of the slot-die approach described here.

For all films studied, the dissolution of the chitosan was initially performed as follows: low molecular weight chitosan (50000-190000 Da, 0.005 mol, 1.04 g) was dissolved in Millipore deionized H_2O (65 ml and acetic acid (0.32 ml, 1%wt), covered with Parafilm and left to continuously stir at room temperature overnight. The chitosan solid began to dissolve once the acid was added as a result of protonation of the amine groups on the chitosan, scheme 4.1 below:

$$Chi - NH_2 + H_3O^+ \leftrightarrow Chi - NH_3^+ + H_2O \qquad \text{Scheme 4.1}$$

The resulting hydrogel solution was used directly with the slot-die apparatus to form the chitosan-only films.

For the synthesis of the chitosan-TEOS IPN films (Chi-TEOS) hydrogels were prepared in mildly acidic conditions to facilitate cationic polymerisation. The procedure is based on that described by Park et al. [27] TEOS (≥99%, 0.005 mol, 1.11 mL) was dissolved in filtered ethanol (15 mL) and allowed to continuously stir at room temperature for 30 minutes. Next HCl (0.0274 mL), filtered ethanol (10 mL) and Millipore deionised water (25 mL) were added to a beaker and allowed to stir continuously at room temperature for 30 minutes. After 30 minutes the HCl solution was slowly added to the TEOS solution, dropwise, with continuous stirring. The mixture was covered with Parafilm and allowed to continuously stir at room temperature for 24 hours. The acidic TEOS solution was then slowly added to the chitosan solution dropwise, with continuous stirring. The resulting mixture was covered with Parafilm and allowed to continuously stir at room temperature for a further 48 hours. The mixture was observed to become viscous after 48 hours. The hydrogel was then stored in a fridge until removed for use.

It is known that this process results in the formation of an IPN between the chitosan and the siloxane polymer that forms when TEOS is hydrolysed. [21, 28, 29] The first step involves the hydrolysis of the TEOS. Figure 4.3 shows the accepted mechanism of the formation of the siloxane polymer via the hydrolysis and condensation of TEOS, based on the mechanism presented in [30]:

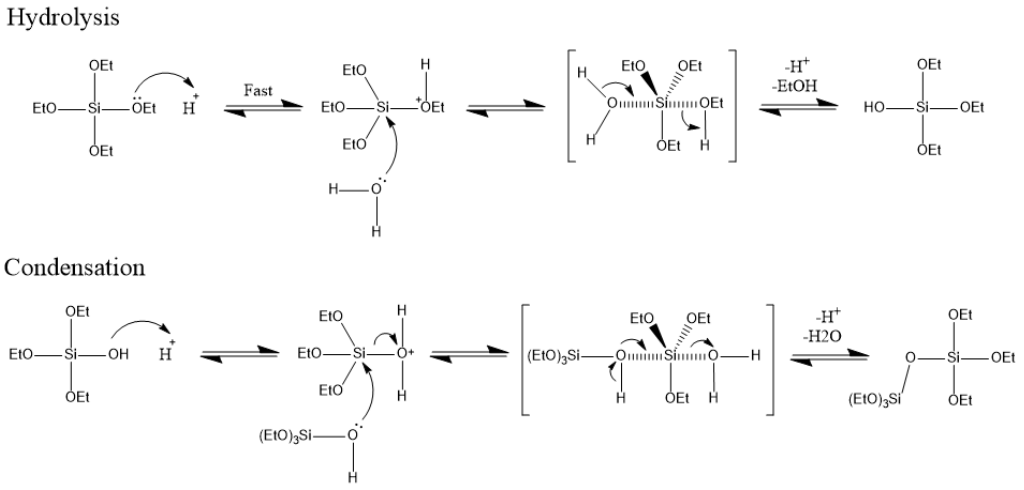


Figure 4.3: Hydrolysis and condensation reactions of TEOS precursors to form a siloxane polymer chain and subsequent network. [30]

The chitosan network itself is held together with hydrogen bonds as shown in figure 4.1. When this solution is added to the solution containing the siloxane polymer mixing occurs and the chitosan chains form their hydrogen-bonded network around the covalently bonded siloxane chains. The cross-linking between the two components thus occurs non-covalently by intermolecular hydrogen bonding in the polymer networks between the polar hydroxyl and amino functional groups of the chitosan polymer network and the polar hydroxyl groups of the TEOS network, figure 4.4:

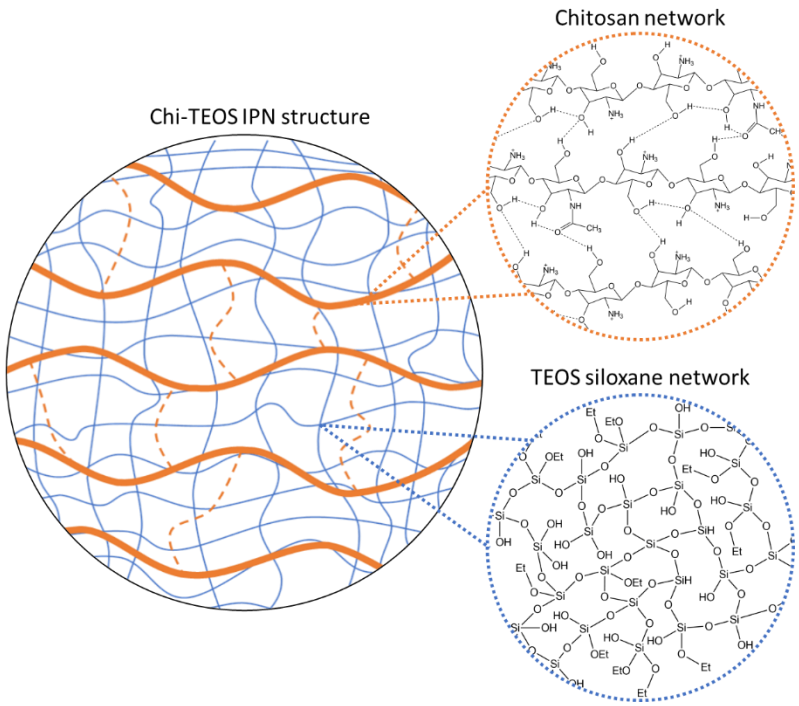


Figure 4.4: A schematic representation of the formation of a Chi-TEOS IPN

For the synthesis of the chitosan-glutaraldehyde cross-linked hydrogels glutaraldehyde solution (GA) (25%, 0.12 mL) was mixed with filtered ethanol (15 mL) and allowed to continuously stir at room temperature for 30 minutes. Next, HCl (0.0274 mL), filtered ethanol (10 mL) and Millipore deionised water (25 mL) were added to a beaker and allowed to stir continuously at room temperature for 30 minutes.

After 30 minutes the two solutions were mixed slowly, dropwise, with continuous stirring. The resulting mixture was then covered with Parafilm and allowed to continuously stir at room temperature for 24 hours, before being added slowly, dropwise to the chitosan solution, with continuous stirring. The resulting mixture was covered with Parafilm and allowed to continuously stir at room temperature for a further 48 hours. The mixture was observed to become viscous. The hydrogel was stored in a fridge at 4°C prior to use.

Unlike the formation of the Chi-TEOS IPN, the reaction cross-linking the chitosan chains with glutaraldehyde molecules is a single step process in which the chitosan hydrogel is first prepared and then glutaraldehyde is added to the gel, which subsequently undergoes a covalent Schiff base reaction. Schiff bases are synthesised from an aliphatic or aromatic amine and a carbonyl compound by nucleophilic addition, followed by a dehydration to generate an imine [31], as shown schematically in figure 4.5 below:

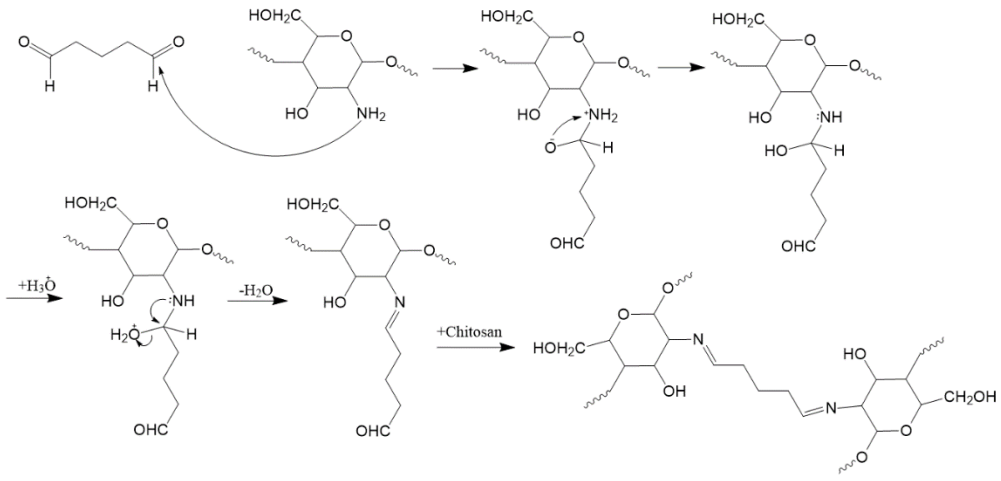


Figure 4.5: The formation of glutaraldehyde-based cross-links between chitosan chains via the formation of Schiff base imine functionalities. The chitosan polymer chains are chemically bonded by Schiff base imine bridges via cross-linking, creating a sterically more rigid structure. [32]

The ratio of (8:1) was chosen based on a previous study whereby the range of possible Chi-GA ratios were tested. It was found that the hydrogels that had higher concentrations of glutaraldehyde were unsuitable for the slot-die apparatus due to the increased viscosity and faster cross-linking reaction times. Glutaraldehyde has a high degree of reactivity with the amine groups of chitosan. [33] The slot-die process takes about 30 minutes to fully deposit the gel (approximately 20 – 25 mL) onto the substrate, but the reaction between chitosan and glutaraldehyde is very fast and for the higher concentrations of glutaraldehyde used it was observed that a solid gel formed in approximately 5 minutes, which could not be deposited via the syringe pump as currently configured.

4.2.3 Tensile strength tests

An Instron 5565 Universal Testing Machine was used to carry out tensile strength tests. The Instron is calibrated periodically using a set of reference weights that are certified annually by the National Metrology Lab, Dublin. In terms of standardising the tensile strength tests performed using this type of instrument, there is no material with a known stress strain graph that can be used repeatedly without suffering fatigue itself. Such a material would make the calibration temperature sensitive as it would be likely to exhibit different stress strain characteristics at different ambient temperatures. Therefore, the only standards measured for the Instron are force, displacement, and time. This factor was taken into consideration when collecting the tensile strength data.

The thin films were cut using a rotary cutter into strips 40 mm to 10 mm in dimension. The samples were clamped in between PDMS supports giving a gauge length of 20 mm. The strips were pulled apart along the 20 mm edge until breaking cleanly in the middle. [34] Test conditions at room temperature included a load of 5 kN, clamp speed of 0.5 $mm.min^{-1}$ and data acquisition rate of 10 Hz.

For the evaluation of possible anisotropy in the mechanical strength of the films in relation to the direction of travel of the film, strips were cut both parallel and at perpendicular right angles to this direction.

4.3 Results

4.3.1 Slot-die film casting

The films produced from the slot-die roll to roll casting method were found to possess relatively uniform thickness throughout the middle section of the strip (approximately 5 cm in width), with thickness varying over the range 20 µm to 25 µm as measured using a 293-185 -MITUTOYO Quantumike digital micrometer. However, as might be expected, a greater variation in thickness was found towards the edges of the strips, where the thickness ranged from 25 µm to 40 µm. The average dimensions for each film sample grown was 5 cm x 25 cm but it is important to note that the method is not inherently limited to the production of samples of this size and much longer strips could easily be produced. The chitosan and Chi-TEOS films were translucent in appearance with a slight yellow colour. The Chi-GA film also displayed a translucent appearance but with a more vibrant yellow colour, as has been reported previously. [35, 36] Each film was thin and flexible to varying degrees, with little or no bubbles being observable by eye. Figure 4.6 shows photographs of some of the films produced by the slot-die apparatus described here:

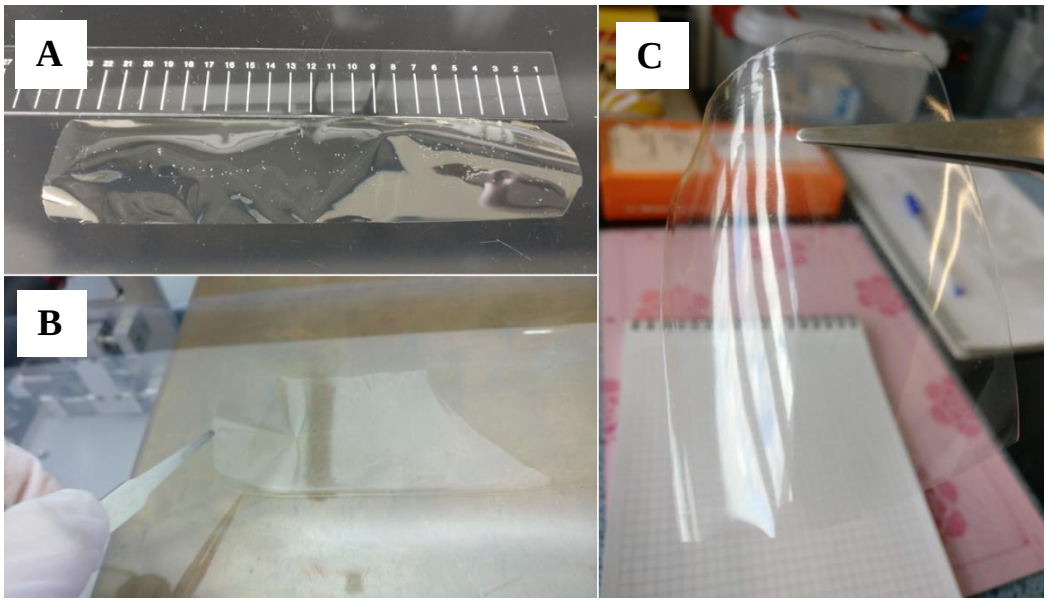


Figure 4.6: Photographs of the dry Chi-TEOS films approximately 23-24 cm in length (A), being peeled off the PET substrate on the slot-die apparatus (B) and a focus of a fragment demonstrating the transparency of the films (C)

4.3.2 Tensile strength tests

For all three materials multiple tensile strength tests were performed until breakage and the displacement of force was recorded for each. Chitosan and Chi-TEOS films were tested 20 times while the Chi-GA films were tested 15 times. The reduced sample number for the Chi-GA films was due to the very brittle nature of these films relative to that of the chitosan and Chi-TEOS films, making them more difficult to handle. The median stress-strain graphs for each material calculated from all measurements taken are shown below, figure 4.7:

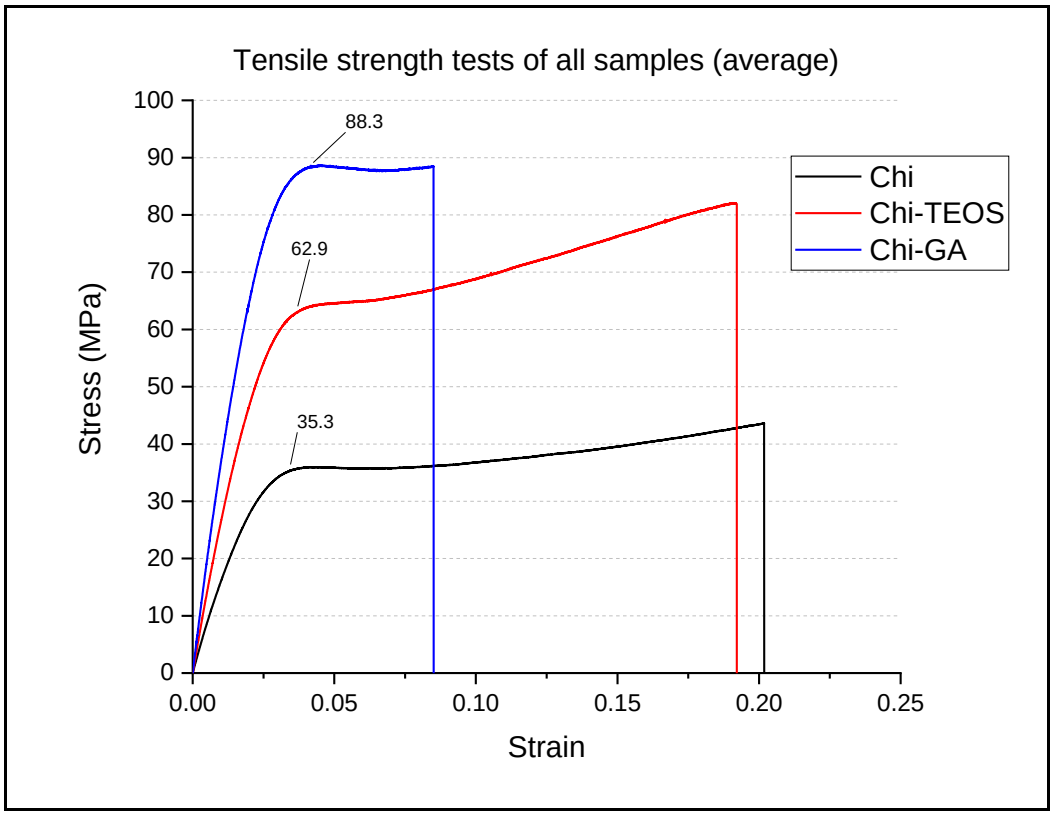


Figure 4.7: median values of stress vs strain for all samples studied.

It was found that there was a considerable sample-to-sample variation in the position of the break point for all samples studied. However, the position of the initial yield point for the samples was remarkably consistent for each material examined. The yield point is the limit of the elastic region of the material i.e., any strain applied to the material after the yield point will result in permanent deformation. During the plastic phase of the stress-strain curve it is difficult to predict the breakage point due to this permanent deformation, so the yield point of the graphs was used as a more accurate

metric for comparison. As well as the yield point, the overall shape of the graph shows the type of material the films are, plastic or elastic.

Based on the initial yield point of the tensile tests it appears that the strongest film is the Chi-GA with an average yield point value of 88.3 MPa and a stress breaking point of 8.5 %. The shape of the graph also shows that this material is much more brittle than the Chi-TEOS and plain chitosan samples which was noted during the testing.

The average strain yield point for the plain chitosan films was 35.3 MPa with a stress breaking point of 20.1 %. In this case, the shape of the graphs indicates that material is more ductile than the Chi-GA samples.

The average strain yield point for the Chi-TEOS films was 62.9 MPa with a stress breaking point of 19.2 %. Again, the shape of the graphs indicates that material is ductile and as an illustration of this it was observed that a high degree of 'necking' occurred during the testing.

For the plain chitosan samples, mechanical testing was performed using strips cut both parallel to and at 90 degrees to the direction of travel of the film, figure 4.8.

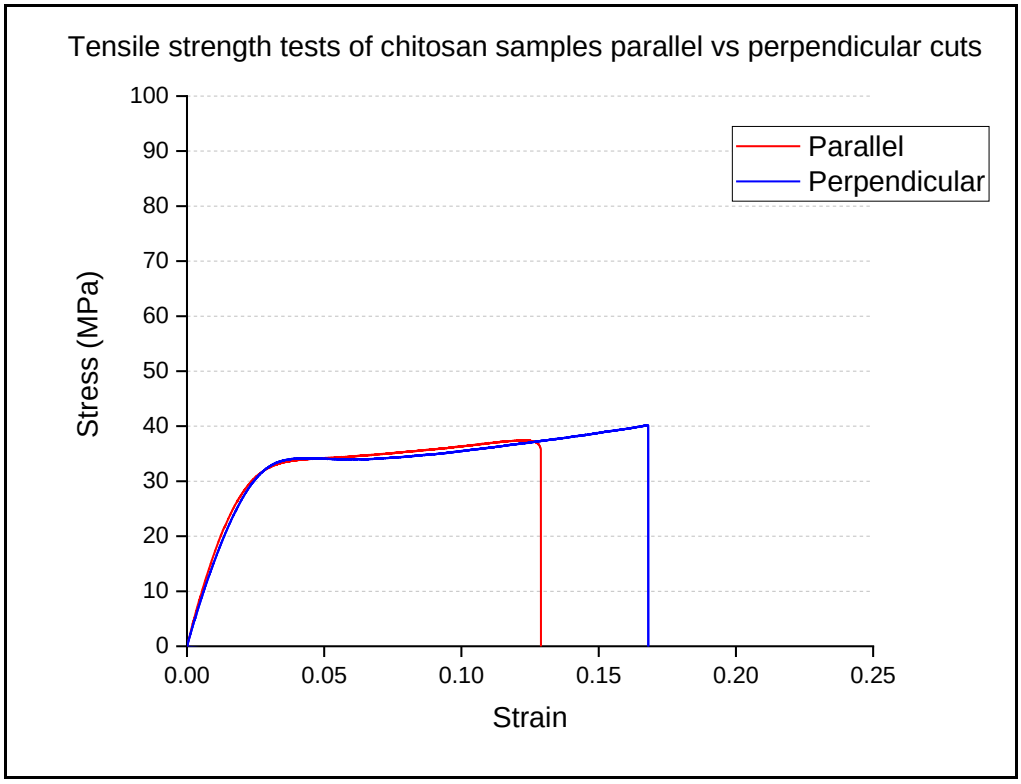


Figure 4.8: Median values for chitosan stress vs strain samples cut parallel and perpendicular to the slot-die casting direction.

From figure 4.8 it may be seen that there are no significant differences that can be discerned from the data obtained for the samples studied. As can be seen from figure 8 no significant differences were observed between samples cut parallel to or perpendicular to the direction of travel.

4.4 Discussion

The slot-die technique described here demonstrates that a range of chitosan-based films can be synthesized rapidly and with a reasonable degree of consistency using a simple laboratory-built coating system. This is a very encouraging finding which clearly suggests that with some development the rapid production of highly reproducible chitosan-based films could be achieved in the high volumes needed for manufacturing.

In the work presented here the average time required for a film to be cast, dried, and removed from the substrate was around 1.5 – 2 hours but it is easy to envisage that this time could be shortened by use of a vacuum pump in a sealed environment. The combination of the hotplate and the extractor fan provided adequate conditions for the formation of solid chitosan-based films while the use of the slot-die method ensured that the dimensions of the films in terms of length, width and thickness could all be controlled to a degree.

The mechanical properties of the films in relation to their structure will be discussed in more detail in a forthcoming publication. However, from the data shown in figure 4.7 it is apparent that, as expected, the plain chitosan film is shown to be the most ductile out of the three samples. With an average yield point value of 35.3 MPa, it is noted that this value compares very favourably with other data in the literature. [6, 37, 38]

Considering the molecular structure of chitosan, it can be seen that it consists of long polymer chains with a high degree of sterical flexibility. From figure 4.7 it is seen that the data for the chitosan sample adopts the appropriate shape of the stress: strain curve for such a material. The initial elastic region shows a linear relationship between stress and strain implying that the film would retain its original shape if it were freed from stress. As the stress reaches the initial lower yield point, the material shifts to the plastic region and further elongation is now permanent. The graph plateaus from here on with increasing strain, culminating to the higher yield point due to the necking phenomenon where the material becomes harder and thinner. At this point the material reaches its physical limit and breaks. This behaviour is typical for an elastic material. [34, 39]

The Chi-TEOS sample displays a higher yield point value than chitosan with a steeper elastic region, indicating that the material is more brittle. This is also shown in the higher degree of necking with a much steeper plastic deformation region indicating that the material can withstand more stress before it breaks. Based on the molecular structure of the Chi-TEOS samples it still maintains the inherent chitosan appearance but with the TEOS siloxane network wrapped intermolecularly by hydrogen bonds. This explains how the material can withstand more stress than plain ductile chitosan but still retain some elasticity. According to the literature, raising the concentration of TEOS in a thin film membrane increases the mechanical strength. As was the case for Yu et al. who made polyvinylidene fluoride–silica composite hollow fibre ultrafiltration membranes, a higher concentration of TEOS increased the rigidness of the films. [40] This is also seen by Ryan et al. who made chitosan-based hybrid composites with silica and polystyrene nanoparticles and measured an average breaking point of 75 MPa for their Chi-TEOS (1:1) films. [29] They also found that with increased TEOS concentration, their chitosan based composite films became more brittle. [28]

The Chi-GA film data shows that material is brittle with a very steep elastic region and higher yield point. The film breaks at lower strain values than the other two materials studied, which indicates the brittle nature and lack of flexibility in these films and suggests that these films would not be suitable for applications where considerable flexing of the material is required although of course, subsequent studies using smaller amounts of glutaraldehyde may produce films that could overcome this limitation. The higher stress values plateau for a short amount of time before shattering, which is typical behaviour for a more rigid material. On the molecular level, the glutaraldehyde Schiff base bridges chemically bond the chitosan polymer network into a tight, sterically restricted structure as shown in figure 4.4. As a result, the material is unable to stretch or bend like chitosan or Chi-TEOS, but it can withstand higher stress levels. The average yield point for the Chi-GA sample was 88.3 MPa which is comparable with those presented in the literature. [41]

Indeed these results are in accord with those obtained by Arianita et al. who found that adding glutaraldehyde to chitosan-cellulose materials increases the tensile strength, boosting the effect with higher concentrations of glutaraldehyde to a limit of 2-3%. [42]

Interestingly the preliminary examination of the samples in terms of possible directional anisotropy in the mechanical properties revealed little or no differences between the two directions sampled. The implication here is that the mechanical stress imposed on the hydrogel as a result of forcing it through the slot-die on the apparatus does not appreciably influence the structure of the films. Hence it may be concluded that the deposition process itself does not appear to influence the structure and measured mechanical properties of the films which means that the films produced using the slot-die approach should be directly comparable to those produced by other methods, although more data is clearly required before this can be shown to be the case, unequivocally.

4.5 Conclusions

In this work it has been shown that reproducible chitosan-based films may be readily produced using a simple slot-die technique that could easily be up-scaled to enable the commercial production of such films. It has been demonstrated the use of this method for films consisting of chitosan alone, chitosan combined with TEOS to produce a true IPN in which the two polymeric networks are intimately mixed but possess only hydrogen bonding links between them and finally a cross-linked material based on chitosan in which glutaraldehyde is added to create Schiff base links between the amine groups of neighbouring chitosan chains. In addition, preliminary mechanical properties of all three types of films produced using the slot-die apparatus have been measured and shown to be comparable to the properties of chemically similar films that were prepared using different methods, exhibiting no obvious dependence on the direction of travel of the film in relation to the extrusion of the hydrogel through the slot.

It is suggested that the approach described here open the potential to prepare a range of chitosan-based films using high-volume, continuous manufacturing methods and that therefore, new or improved products will emerge based on chitosan which may find application in the medical device industry in areas such as wound dressings, controlled-release drug patches and other important applications.

In addition, this work opens the possibility of using chitosan-based films or indeed other films made from cheap, readily available materials such as cellulose, to produce biodegradable replacements for plastics and packaging, thereby helping to address one of the major problems facing society at the present time.

References

1. Rinaudo, M., *Chitin and chitosan: Properties and applications.* Progress in Polymer Science, 2006. **31**(7): p. 603-632.
2. Kong, X., et al., *Synthesis and characterization of a novel MPEG–chitosan diblock copolymer and self-assembly of nanoparticles.* Carbohydrate Polymers, 2010. **79**(1): p. 170-175.
3. Leedy, M.R., et al., *Use of Chitosan as a Bioactive Implant Coating for Bone-Implant Applications*, in *Chitosan for Biomaterials II*, R. Jayakumar, M. Prabaharan, and R.A.A. Muzzarelli, Editors. 2011, Springer Berlin Heidelberg: Berlin, Heidelberg. p. 129-165.
4. Mahmoudzadeh, M., et al., *Physicochemical, pharmaceutical and biological approaches toward designing optimized and efficient hydrophobically modified chitosan-based polymeric micelles as a nanocarrier system for targeted delivery of anticancer drugs.* Journal of Drug Targeting, 2013. **21**(8): p. 693-709.
5. Y N, S., et al., *Miscibility Studies of Chitosan and Starch Blends in Buffer Solution.* Journal of Macromolecular Science, 2013. **49**.
6. Ma, B., et al., *Structure and properties of chitin whisker reinforced chitosan membranes.* International Journal of Biological Macromolecules, 2014. **64**: p. 341-346.
7. Jayakumar, R., et al., *Biomaterials based on chitin and chitosan in wound dressing applications.* Biotechnology Advances, 2011. **29**(3): p. 322-337.
8. Khor, E. and L.Y. Lim, *Implantable applications of chitin and chitosan.* Biomaterials, 2003. **24**(13): p. 2339-2349.
9. Yusof, N.L.B.M., et al., *Flexible chitin films as potential wound-dressing materials: Wound model studies.* Journal of Biomedical Materials Research Part A, 2003. **66A**(2): p. 224-232.
10. Kanke, M., et al., *Appilcation of Chitin and Chitosan to Pharmaceutical Preparations. I. : Film Preparation and in Vitro Evaluation.* CHEMICAL & PHARMACEUTICAL BULLETIN, 1989. **37**(2): p. 523-525.
11. Wan Ngah, W.S., L.C. Teong, and M.A.K.M. Hanafiah, *Adsorption of dyes and heavy metal ions by chitosan composites: A review.* Carbohydrate Polymers, 2011. **83**(4): p. 1446-1456.

12. Tripathi, S., G. Mehrotra, and P. Dutta, *Chitosan based antimicrobial films for food packaging applications.* e-Polymers, 2008. **8**.
13. Liang, S., et al., *Preparation of single or double-network chitosan/poly(vinyl alcohol) gel films through selectively cross-linking method.* Carbohydrate Polymers, 2009. **77**(4): p. 718-724.
14. Decher, G., *Fuzzy Nanoassemblies: Toward Layered Polymeric Multicomposites.* Science, 1997. **277**(5330): p. 1232.
15. Pavinatto, F.J., L. Caseli, and O.N. Oliveira, *Chitosan in Nanostructured Thin Films.* Biomacromolecules, 2010. **11**(8): p. 1897-1908.
16. Ligler, F.S., et al., *Development of Uniform Chitosan Thin-Film Layers on Silicon Chips.* Langmuir, 2001. **17**(16): p. 5082-5084.
17. Allum, J., et al., *Interlayer bonding has bulk-material strength in extrusion additive manufacturing: New understanding of anisotropy.* Additive Manufacturing, 2020. **34**: p. 15.
18. Hmeidat, N.S., et al., *Mechanical anisotropy in polymer composites produced by material extrusion additive manufacturing.* Additive Manufacturing, 2020. **34**: p. 12.
19. Batterman, S.D. and J.L. Bassani, *YIELDING, ANISOTROPY, AND DEFORMATION PROCESSING OF POLYMERS.* Polymer Engineering and Science, 1990. **30**(20): p. 1281-1287.
20. Tripathi, S., G.K. Mehrotra, and P.K. Dutta, *Chitosan based antimicrobial films for food packaging applications.* E-Polymers, 2008.
21. Park, S.B., et al., *A novel pH-sensitive membrane from chitosan - TEOS IPN; preparation and its drug permeation characteristics.* Biomaterials, 2001. **22**(4): p. 323-330.
22. Silva, G.S., et al., *Chitosan/Siloxane Hybrid Polymer: Synthesis, Characterization and Performance as a Support for Immobilizing Enzyme.* Journal of the Brazilian Chemical Society, 2011. **22**(8): p. 1407-1417.
23. Rashidova, S.S., et al., *Bionanocompositional chitosan-silica sorbent for liquid chromatography.* Journal of Chromatography B-Analytical Technologies in the Biomedical and Life Sciences, 2004. **800**(1-2): p. 49-53.
24. Dragan, E.S., *Design and applications of interpenetrating polymer network hydrogels. A review.* Chemical Engineering Journal, 2014. **243**: p. 572-590.

25. Tripathi, S., G.K. Mehrotra, and P.K. Dutta, *Physicochemical and bioactivity of cross-linked chitosan-PVA film for food packaging applications.* International Journal of Biological Macromolecules, 2009. **45**(4): p. 372-376.
26. Tual, C., et al., *Transport properties of chitosan membranes: Influence of cross-linking.* Journal of Polymer Science Part B-Polymer Physics, 2000. **38**(11): p. 1521-1529.
27. Park, S.-B., et al., *A novel pH-sensitive membrane from chitosan — TEOS IPN; preparation and its drug permeation characteristics.* Biomaterials, 2001. **22**(4): p. 323-330.
28. Ryan, C.C., et al., *Silica-based photonic crystals embedded in a chitosan-TEOS matrix: preparation, properties and proposed applications.* Journal of Materials Science, 2016. **51**(11): p. 5388-5396.
29. Ryan, C.C., M. Bardosova, and M.E. Pemble, *Structural and mechanical properties of a range of chitosan-based hybrid networks loaded with colloidal silica and polystyrene particles.* Journal of Materials Science, 2017. **52**(13): p. 8338-8347.
30. Lofgreen, J. and G. Ozin, *Controlling morphology and porosity to improve performance of molecularly imprinted sol-gel silica.* Chemical Society reviews, 2013. **43**.
31. Ostrowska-Czubenko, J., M. Pieróg, and M. Gierszewska, *State of water in noncross-linked and cross-linked hydrogel chitosan membranes - DSC studies.* Progr. Chem. Appl. Chitin Deriv., 2011. **16**: p. 147-156.
32. Luk, C., et al., *A Comprehensive Study on Adsorption Behaviour of Direct, Reactive and Acid Dyes on Cross-linked and Non-cross-linked Chitosan Beads*. 2014.
33. Sampath, U.G.T.M., et al., *Preparation and characterization of nanocellulose reinforced semi-interpenetrating polymer network of chitosan hydrogel.* Cellulose, 2017. **24**(5): p. 2215-2228.
34. Gauthier, M.M. and A.I.H. Committee, *Engineered Materials Handbook, Desk Edition*. 1995: Taylor & Francis.
35. de Oliveira, A.C.S., J.C. Ugucioni, and S.V. Borges, *Effect of glutaraldehyde/glycerol ratios on the properties of chitosan films.* Journal of Food Processing and Preservation, 2021. **45**(1): p. 11.

36. Pavoni, J.M.F., et al., *Impact of acid type and glutaraldehyde cross-linking in the physicochemical and mechanical properties and biodegradability of chitosan films.* Polymer Bulletin, 2021. **78**(2): p. 981-1000.
37. Nunthanid, J., et al., *Physical Properties and Molecular Behavior of Chitosan Films.* Drug Development and Industrial Pharmacy, 2001. **27**(2): p. 143-157.
38. Bonilla, J., et al., *Physical, structural and antimicrobial properties of poly vinyl alcohol–chitosan biodegradable films.* Food Hydrocolloids, 2014. **35**: p. 463-470.
39. Swallowe, G.M., *Mechanical Properties and Testing of Polymers: An A–Z Reference*. 2013: Springer Netherlands.
40. Yu, L.-Y., et al., *Preparation and characterization of PVDF–SiO2 composite hollow fiber UF membrane by sol–gel method.* Journal of Membrane Science, 2009. **337**(1): p. 257-265.
41. Da Silva, R., et al., *Preparation and characterisation in simulated body conditions of glutaraldehyde cross-linked chitosan membranes.* Journal of materials science. Materials in medicine, 2004. **15**: p. 1105-12.
42. Arianita, A., et al., *Effect of glutaraldehyde to the mechanical properties of chitosan/nanocellulose.* Journal of Physics: Conference Series, 2019. **1317**: p. 012045.

5. A Study of the Adsorption of $^{99m}TcO_4^-$ ions on Chitosan-based Films

This work was carried out in the Faculty of Natural Sciences, Comenius University in Bratislava with the assistance of Dr Olga Rosskopfová and Andrea Hamárová.

5.1 Introduction

5.1.1 Heavy metal pollution

Pollution by heavy metals is an ongoing issue for our environment. The main contributors to heavy metal pollution are the rapid development of industry and agriculture. [1, 2] Heavy metals can discharge into the environment where they can threaten fragile ecosystems and humans through the food chain. [3] In general, living organisms require trace amounts of some heavy metals, e.g., iron, copper, cobalt, and zinc, as they are essential to maintain the metabolism. However, at higher concentrations these metals can be poisonous. They become toxic when they are not metabolized by the body and accumulate in the soft tissues. Other heavy metals, such as mercury, cadmium and lead are highly poisonous while some may even be radioactive. Heavy metals can enter the bodies of humans via the food chain, drinking water, air or absorption through the skin. [4]

Radioactive metal isotopes, such as ^{99m}Tc (where m indicates a metastable radionuclide), and ^{137}Cs are artificially produced in large quantities by the nuclear fission of ^{235}U during both nuclear weapons tests and reactor operation. [5] ^{99m}Tc is a gamma emitter with a half-life on the order of 6 hours. ^{137}Cs is a beta emitter with a half-life of around 30.17 years but it decays to yield ^{137m}Ba which is a gamma emitter. It is particularly dangerous since it may easily embed into biochemical cycles as a chemical counterpart of potassium and sodium. [6]

The methods for removing heavy metals include electrolysis, [7] precipitation, [8] photocatalysis, [9] film filtration, [10] ion exchange [11] and adsorption. [12] Adsorption is considered an ideal method of removing heavy metals, as it is inexpensive, efficient, and non-toxic. [3]

5.1.2 Chitosan-based materials for heavy metal adsorption

Chitosan-based materials can facilitate the removal of dangerous heavy metals from the environment. Adsorption is considered an effective and economical method of removing high concentrations of pollutants due to its potential reversibility. [13, 14] Therefore, over the past decade there has been considerable interest in finding sorbents with high adsorption capacities, fast adsorption/desorption rates, and easy separation and regeneration. [15, 16]

For the materials that are the focus of this thesis, the main factors which influence the adsorption capacity on chitosan-based IPNs, and hydrogels are pH, sorbent dosage, temperature, and the initial concentration of solute. Interference with other ionic species should be also considered. As described earlier in section 2.1, in addition to the formation of IPNs, chitosan may be successfully combined with many other species to create potentially useful thin films. Examples of these include the Chi-GA and Chi-PAM films described in this work. Films of these types of materials can also be used to exploit the adsorptive properties of chitosan. [17-19]

Chitosan is potentially an ideal compound to be used for the adsorption of dyes, heavy metals, and radioactive metal isotopes due to the presence of the active amino and hydroxyl sites. The amino groups can be partially protonated in acidic media, after which they can absorb anionic dyes by strong electrostatic attractions. However, even though some heavy metals ions form cations in aqueous solutions, they can also be absorbed by chitosan through chelation in basic media via the unprotonated amine groups. In addition, it is known that some heavy metal ions can form anionic species in solution, such as the pertechnetate ion, TcO_4^- [20, 21] In this case absorption may occur via the same mechanism as that seen for the anionic dyes. It is this dual mechanism for the adsorption of both anionic and cationic species that makes chitosan a formidable compound in adsorptive material research. Figure 5.1 attempts to illustrate the chemical adsorption mechanism of heavy metals onto chitosan cross-linked by glutaraldehyde. The mechanism shows that the hydroxyl and amine groups of chitosan-based adsorbents are key sites for the chelation of heavy metals. [22]

Chauhan and Mahajan [23] have studied the adsorption of metal ions from aqueous solutions on semi-IPN composite hydrogels. Wang *et al*. [24] have reported the preparation of semi-IPN hydrogels made from chitosan and gelatine, which have very

high adsorption capacities for Pb^{2+} and Cu^{2+}. The enhanced mechanical strength also allows the sorbent to be reused. [25]

In this present study we examine the use of chitosan and chitosan-based IPNs formed with tetraethyl orthosilicate silane (TEOS), which is also known as tetraethoxy silicate, 3-aminopropyltriethoxy silane (APTES), glutaraldehyde (GA), and polyacrylamide (PAM) for the adsorption of radioactive $^{99m}TcO_4^-$ ions from aqueous solution. Swelling and TcO_4^- adsorption studies are reported, and comments are made as to the suitability of each material synthesised for the removal or TcO_4^- ions from aqueous solution.

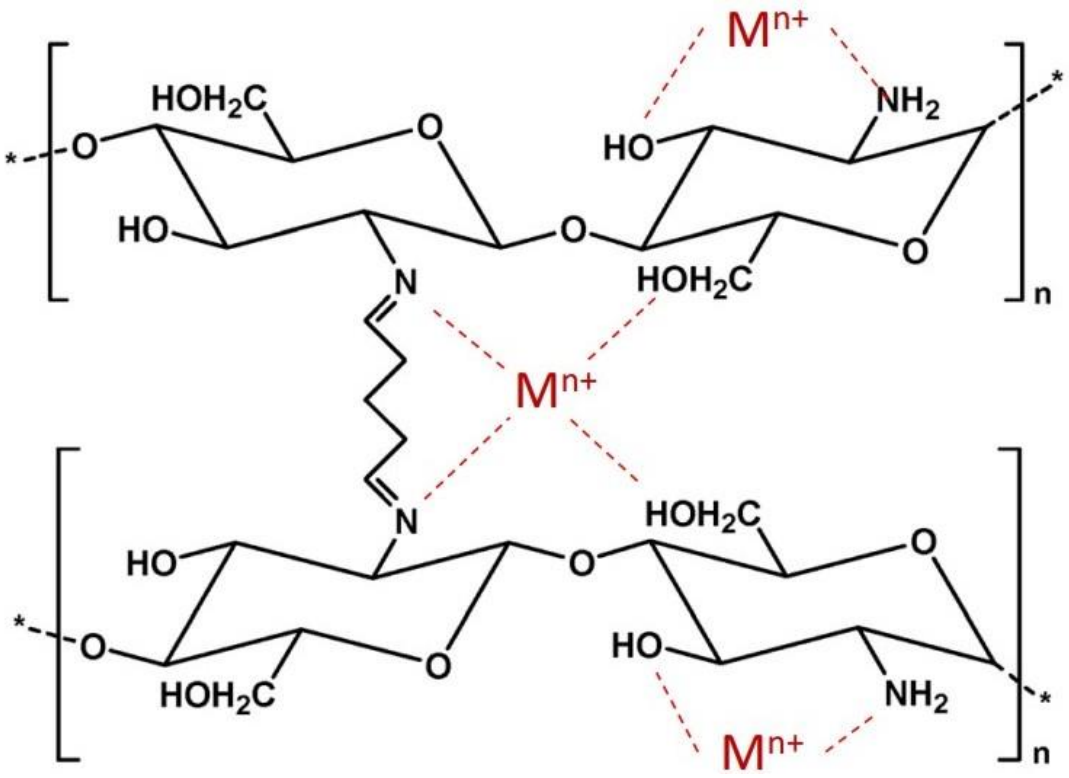


Figure 5.1: Adapted from Briao et al. [22] The mechanism of monolayer chemical adsorption of heavy metal ions onto a chitosan-based adsorbent. Where M^{n+} represents a toxic heavy metal species in aqueous solution.

5.2 Methods

All chemicals used were of analytical grade by Lachema n.p., Czech Republic and by SLAVUS Ltd., Slovak Republic. Analysis of films by gamma spectroscopy was provided by the Faculty of Natural Sciences, Comenius University, Bratislava, Slovak Republic.

5.2.1 Swelling characteristics

To determine the swelling capacity of the chitosan-based films, they were cut into 2 cm^2, 3 cm^2, 4 cm^2 and 5 cm^2 samples, and weighed before and after swelling in an acidic aqueous solution. The films were immersed in H_2O, that was adjusted to pH 4 with 0.1 N NaOH and 0.1 N HCl, for 30 minutes. The weight of the water before and after swelling was also recorded. After 30 minutes the samples were removed, dried, and immediately weighed on analytical scales. The percentage of swelling – Q_{eq} (%) was calculated based on the following equation (Eqn. 5.1): [26, 27]

$$Q_{eq} = \frac{m_1 - m_{01}}{m_1} \times 100 \qquad \text{Eqn. 5.1}$$

Where:

m_{01} is the initial mass of the films before swelling, and m_1 is the mass of the films after swelling and centrifuging for 10 minutes.

5.2.2 Adsorption experiments

Adsorption experiments were performed by a batch method in a static arrangement under aerobic conditions at laboratory temperature. Technetium (IV) chloride $TcCl_4.xH_2O$ solutions over a range of concentrations were prepared in 50 mL tubes with deionised water. The concentration range was 10^{-1}, $5x10^{-2}$, 10^{-2}, $5x10^{-3}$, 10^{-3}, $5x10^{-4}$, 10^{-4}, $5x10^{-5}$ and 10^{-5} M. Radio-indicator $^{99m}TcO_4^-$ solution was prepared using a DRYTEC technetium-99m generator [28] where the metastable isotope ^{99m}Tc of technetium is prepared from a decaying sample of molybdenum-99.

^{99m}Tc only has a short half-life of 6 hours, so long-term storage is impossible. It must be generated from ^{99}Mo, which has a half-life of 66 hours, for it to be handled in the lab. ^{99}Mo in the form of molybdate is absorbed onto acid alumina in a lead shielded column and allowed to decay into pertechnetate TcO_4^-. Flushing the column with

saline solution elutes the soluble ^{99m}Tc resulting in a solution of ^{99m}Tc with a sodium counterion. [29]

Samples (25 µL) of the $^{99m}TcO_4^-$ solution were added to each tube and mixed. Nine samples of 1 cm^2 squares of chitosan-based film were placed in separate test tubes and 2 mL of the technetium solution was added to each. The ratio of the solid and liquid phases was 1:100. The solution/sample combinations were then mixed in a Multi Bio RS-24 laboratory extractor at a rate 35 rpm for 60 minutes. After adsorption the samples were centrifuged 10 minutes at 6000 rpm in a Hettich EBA 20 type centrifuge. Aliquot volumes of the supernatant were extracted and sent for analysis. A series of blank solutions without chitosan film samples was also prepared and sent for analysis. The measurements recorded here are not significantly affected by isotope decay.

Adsorption analysis was performed on a 1470 Wizard Perkin Elmer automated gamma counter. The effects of the contact time, pH, sample size, and isotherms were analysed with a relative measurement error of < 5%. The adsorption properties of the chitosan-based films; distribution coefficient (Eqn. 5.2), adsorption percentage (Eqn. 5.3), adsorption capacity (Eqn. 5.4), and equilibrium concentration (Eqn. 5.5) were calculated by the following equations: [26, 27, 30]

$$K_D = \frac{c_0 - c_{eq}}{c_{eq}} \times \frac{V}{m} = \frac{a_0 - a}{a} \times \frac{V}{m} \; ; [dm^3 \cdot g^{-1}] \qquad \text{Eqn. 5.2}$$

$$R = \frac{100 \times K_D}{K_D + (\frac{V}{m})} \; ; [\%] \qquad \text{Eqn. 5.3}$$

$$\Gamma = K_D \cdot c_{eq} \; ; [mol \cdot g^{-1}] \qquad \text{Eqn. 5.4}$$

$$c_{eq} = \frac{c_0 \cdot a}{a_0} \; ; [mol \cdot dm^{-3}] \qquad \text{Eqn. 5.5}$$

Where:

c_0 is initial concentration [mol·dm^{-3}], c_{eq} is equilibrium concentration [mol·dm^{-3}], V is volume of aqueous phase [ml], m is mass of sorbent [g], a_0 is volume activity of initial solution [Bq·ml^{-1}, where Bq is the activity in [Becquerel], and a is equilibrium volume activity of solution [Bq·ml^{-1}].

The Langmuir and Freundlich isotherm models were used to evaluate the data obtained for the adsorption of $^{99m}TcO_4^-$ onto the chitosan-based films.

The Langmuir isotherm (Eqn. 5.6) is a theoretical model used to describe a particular type of adsorption system. It is applied to monolayer adsorption on a homogeneous surface with no interactions between adsorbed species: [30, 31]

$$\Gamma = \frac{\Gamma_{max} \cdot b c_{eq}}{1 + b \cdot c_{eq}} \qquad \text{Eqn. 5.6}$$

Where:

Γ is the adsorption capacity ($mol \cdot g^{-1}$), Γ_{max} is the maximum of the adsorption capacity corresponding to site saturation ($mol \cdot g^{-1}$), c_{eq} is equilibrium concentration ($mol \cdot dm^{-3}$) and b is the ratio of adsorption/desorption rates.

The Freundlich isotherm (Eqn. 5.7) is an experimental model that can account for multilayer adsorption on a heterogeneous surface, accompanied by interaction between adsorbed molecules and is usually expressed as follows: [30]

$$\Gamma = K_F \cdot c_{eq}^n \qquad \text{Eqn. 5.7}$$

Where:

K_F is the Freundlich constant. c_{eq} is the equilibrium concentration ($mol.dm^{-3}$), and n is a power that represents degree of dependence of adsorption on the equilibrium concentration.

5.3 Results

5.3.1 Evaluation of swelling characteristics

In this work, the swelling properties of the chitosan-based films were characterized apart from the chitosan-only films, which were not sufficiently robust to withstand soaking in acidic media. The swelling was based on percentage mass gain, and not size increase of the samples. The swelling was determined by an immersion method in H_2O at pH 4 and ran for 30 minutes at room temperature. The percentage of swelling Q_{eq} is high in all cases. The dependence of swelling of the films on their growing area was determined, a full summary of the results can be found in the appendix section A.2.

From figure 5.2, it may be seen that for Chi-TEOS (1:1), the film average percentage swelling across all samples is over 90%. This value is about the same for the Chi-GA (8:1) samples while the values for Chi-APTES (2:1) and Chi-PAM (1:1) samples are slightly lower. It may therefore be concluded that for all samples studied the percentage swelling recorded is very significant, being between 80 and 95% and while the variation between samples may be significant to a first approximation all samples behave essentially the same.

A statistical analysis was performed using Pearson's *r* correlation coefficient (Eqn. 5.8) in order to examine any possible correlations that might exist between the mass gain data and the sample size used. The results of this analysis are shown in table 5.1 below.

$$r = \frac{\sum(x-\bar{x})(y-\bar{y})}{\sqrt{\sum(x-\bar{x})^2 \sum(y-\bar{y})^2}} \qquad \text{Eqn. 5.8}$$

Where:

x is the values of the x-variables in a sample

y is the values of the y-variables in a sample

$\overline{x}$ is the mean of the values of the x-variable

$\overline{y}$ is the mean values of the y-variable

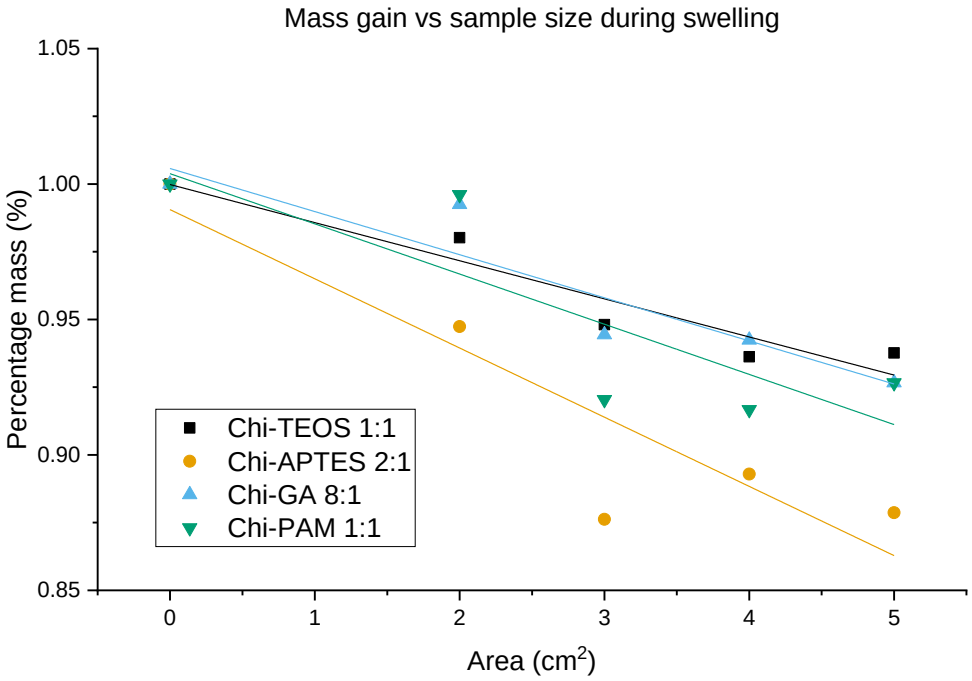


Figure 5.2: Dependence of film size to percentage mass gain during swelling at pH 4

Film type	Pearson's *r* factor	STD intercept
Chi-TEOS (1:1)	-0.95479	0.00831
Chi-APTES (2:1)	-0.91624	0.02119
Chi-GA (8:1)	-0.93251	0.01169
Chi-PAM (1:1)	-0.84357	0.02238

Table 5.1: Calculated Pearson's *r* factors for the potential correlation between % swelling as measured by mass gain and sample area (size). Straight line Pearson's plots can be found in the appendix sections A.2.1, A.2.2, A.2.3, and A.2.4.

Pearson's correlation coefficient (*r*) is a measure of the linear association of two variables, in this case, mass gain and sample size during swelling. Correlation analysis usually starts with a graphical representation of the relation of data pairs using a scatter diagram. The values of correlation coefficient vary from –1 to +1. [32]

From figure 5.2 and table 5.1 above, it may be seen that for all samples a linear plot is produced when % mass gain is plotted against sample area. However, analysis of these

data sets revealed that all samples gave rise to negative Pearson *r* values, near to -1, which implies a negative correlation which in turn implies that as one parameter increases the other decreases. In other words, this analysis suggests that as sample area increases the % mass gain decreases and *vice versa*.

Thus, it may be concluded that the swelling characteristic as measured using the percentage approach may be influenced by the apparent sample area, as might be expected for samples where variations in thickness might occur.

With this in mind it is perhaps useful to point out that despite this, for the larger area samples it would be expected that the measured variation in sample mass determined before and after immersion would be the largest, and so given that the analytical balances employed could typically measure to 0.1 mg, the error associated with the swelling percentage values will decrease as sample area increases.

5.3.2 Evaluation of the optimum pH for the $^{99m}TcO_4^-$ adsorption process

Initial adsorption tests for ^{99m}Tc showed that the optimal contact time was less than 30 - 60 minutes because the films began to degrade if left any longer. Furthermore, from the data depicted in figure 5.3 below it is proposed that the adsorption ability of all films is most efficient at pH 4. This could be due to increasing the chelation effect by protonating the amino functional groups. The positively charged amino groups interact with TcO_4^- ions and capture them within the chitosan network by chelation, thus allowing them to be removed from the water sample. A figure has been produced which shows schematically how the pertechnetate ions might be chelated between the chitosan chains (Figure 5.1). However, at a more acidic pH, the protonation of the amino groups is so high, the active sites are unavailable for metal chelation. The H^+ compete with the metal ions for the same binding site. [33]. The protonation of the amine groups induces electrostatic repulsion which decreases with a higher pH value. [34]

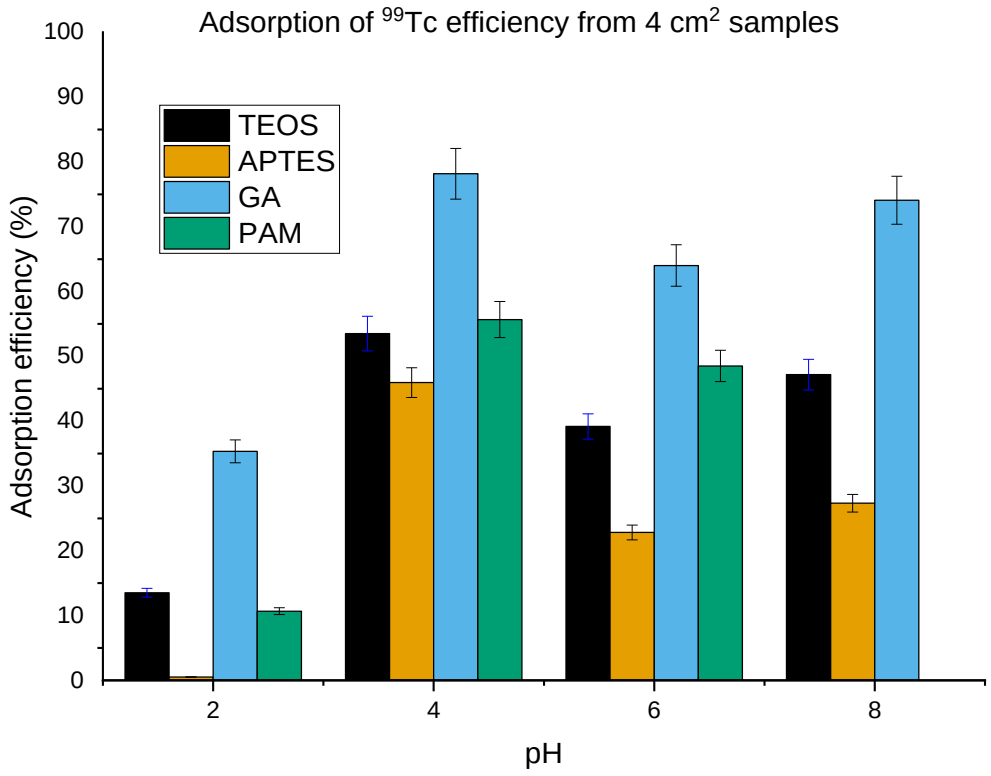


Figure 5.3: Adsorption efficiency R%, of $^{99}TcO_4^-$ ions on chitosan-based films (Chi-TEOS IPN (1:1), Chi-APTES (2:1), Chi-GA (8:1) and Chi-PAM (1:1) at a pH range of 2-8 for samples of surface area of 4 cm^2, after immersion for 30 minutes. Adsorption efficiency graphs for 2 cm^2 and 6 cm^2 can be found in the appendix section A.3.

These initial results suggested that the most efficient type of chitosan film is that formed by cross-linking with glutaraldehyde with adsorption efficiency R% values as high as 80% at pH 4 for the samples of apparent surface area 4 cm^2, figure 5.3.

Interestingly at this pH there is no obvious dependence upon the surface area of the sample in terms of the adsorption efficiency R%, see figure 5.4.

5.3.3 Adsorption of pertechnetate ions

After further sample optimization, the effect of the size-area of the chitosan-based films on the percentage adsorption efficiency R% of the samples when immersed in the pertechnetate ion solution was studied at the initial pH 4 for a contact time of 60 minutes, tables 5.2 and 5.3 below:

K_D	2 cm^2	3 cm^2	4 cm^2	5 cm^2	STD
Chi-TEOS	2.81	1.81	1.16	0.84	0.75
Chi-APTES	0.74	0.81	0.86	0.59	0.10
Chi-GA	44.46	25.34	25.5	20.74	9.12
Chi-PAM	1.38	5.23	5.31	2.26	1.75

Table 5.2: The effect of area of films on the pertechnetate diffusion coefficient K_D

R%	2 cm^2	3 cm^2	4 cm^2	5 cm^2	STD
Chi-TEOS	65.18	64.45	60.83	58.21	2.82
Chi-APTES	33.09	44.74	53.41	49.39	7.61
Chi-GA	96.74	96.21	97.14	97.19	0.39
Chi-PAM	47.87	83.94	87.62	78.97	15.73

Table 5.3: The effect of area of films on the pertechnetate adsorption efficiency R%

The data in Table 5.2 show the calculated distribution coefficient values which characterize the mobility of the pertechnetate between the aqueous phase and the solid phase. Low K_D values indicate that the pertechnetate ions prefer to be in the aqueous phase. Conversely, high distribution coefficients indicate that the pertechnetate ions prefer to be chelated onto the chitosan-based films. [35] This analysis highlights very effectively why the Chi-GA films are consistently more able to chelate the TcO_4^- ions, as evidenced by the fact that the average K_D values for these samples are 10-20 times larger than the K_D values obtained for the other samples.

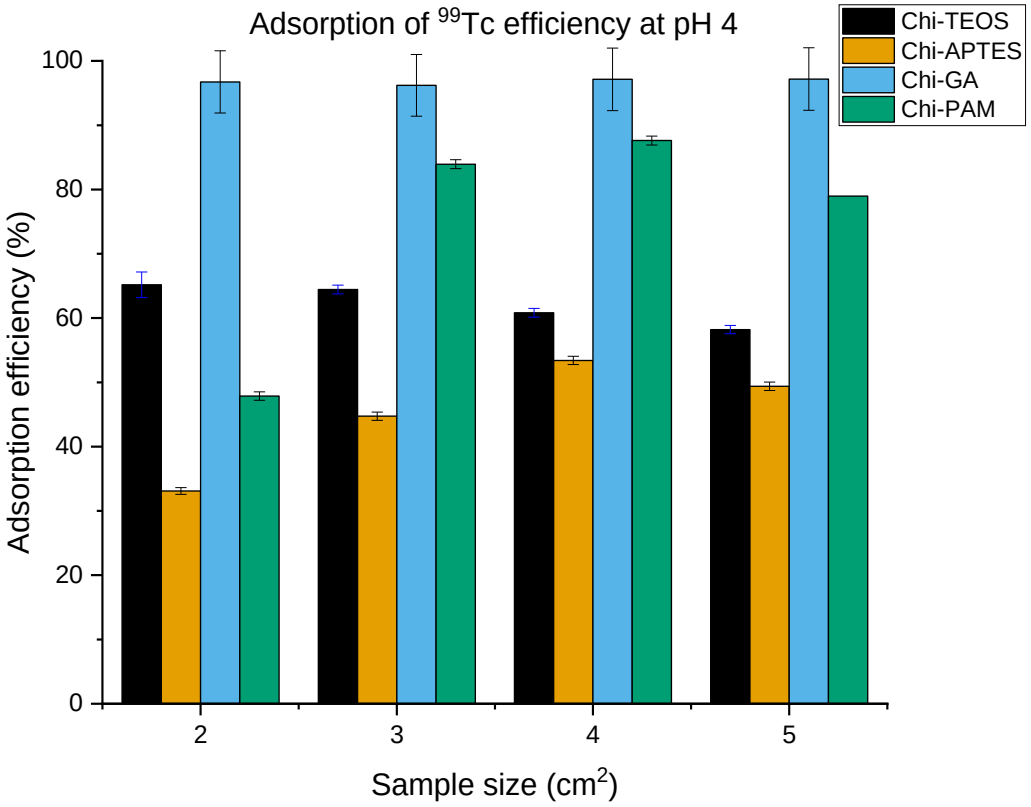


Figure 5.4: Summary of the adsorption efficiency R%, of $^{99}TcO_4^-$ ions on chitosan-based films Chi-TEOS IPN (1:1), Chi-APTES (2:1), Chi-GA (8:1), and Chi-PAM (1:1) at pH 4 for a range of sample sizes. Samples recorded after swelling for 60 minutes immersion time.

The adsorption efficiencies for 4cm^2 samples in figure 5.3 are larger than that of figure 5.4. This discrepancy is due to the fact that the samples were immersed for 60 minutes and had a longer time to adsorb the $^{99}TcO_4^-$ ions.

From table 5.3, in the case of the Chi-TEOS films, as the size of the sample increases there is a very slight decrease in the values of R%, which range from 65.18% to 58.21%. In contrast from Chi-TEOS, for Chi-APTES, it appears that as the sample size increases so the values of R% also increase although there is more variation in the values for these samples. The values R% for Chi-APTES were in a range from 33.09% to 53.41%. Interestingly, from table 5.3, the R% values for the Chi-GA sample are more convincingly independent of sample size but these samples also represent the highest vales of R% achieved, around 96%, indicating that these films are the most

efficient in terms of the adsorption of TcO_4^- ions. In the case of the Chi-PAM films from table 5.3, as for Chi-APTES and Chi-GA, as sample size increases so the R% values also increase, but again there is considerable scatter in these data. What can be said is that from the R% values alone these films are second only to the Chi-GA films in terms of their adsorptive abilities towards the TcO_4^- ions. The lowest R% values were for the films with area of 2 cm^2 was 47.87%. Chi-PAM with size-areas 3 - 5 cm^2 had the adsorption percentages as high as 87.62%.

Overall, it may be concluded that that the ability to adsorb $^{99}TcO_4^-$ anions on the chitosan-based films studied here decreases in the order of Chi-GA > Chi-PAM ≈ Chi-TEOS >Chi-APTES.

The structure of the cross-linked Chi-GA polymer contains a cyclic ring with the chitosan chain and bridging imine functional groups. The empty space in between is an ideal site for chelation of heavy metal species that contain anionic ligands. Protonated amino groups can chelate with the ligands and the polymer chain may naturally fold around and capture the whole heavy metal species. [36, 37] Figure 5.5 below shows how the $^{99m}TcO_4^-$ ions may be trapped within the Chi-GA matrix:

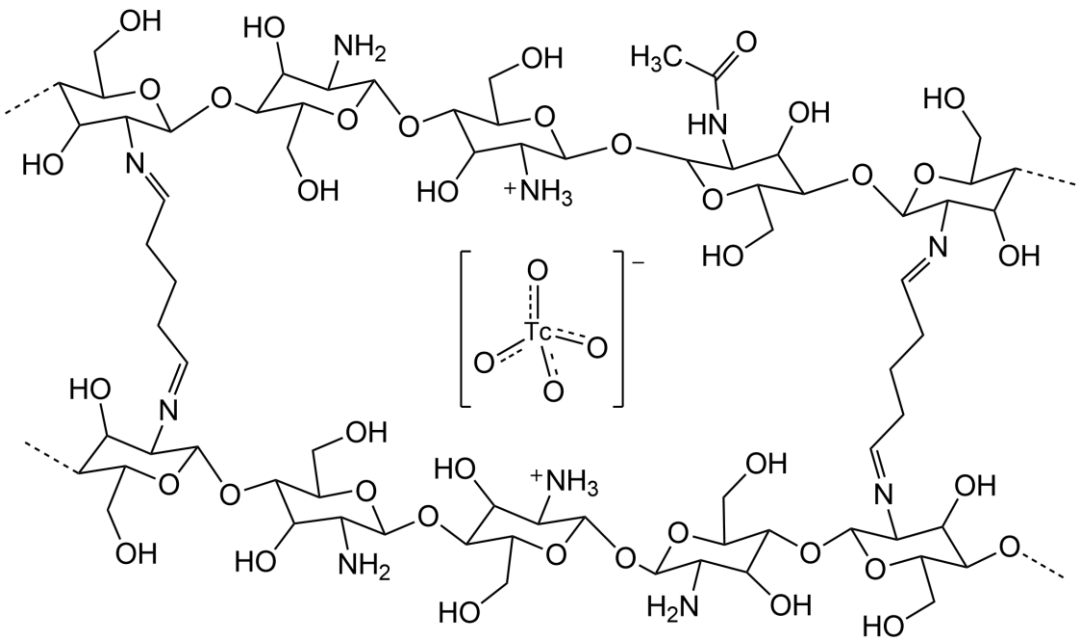


Figure 5.5: Molecular representation of a Chi-GA cross-linked blend showing the chelation mechanism for pertechnetate anions.

The adsorption process studied here is for a specific occurrence of technetium present as TcO_4^-. However, not all heavy metals have an anionic form in nature and yet they are affected by the adsorption properties of chitosan-based thin films. The proposed mechanism of adsorption for cationic heavy metal ions is as follows: [38]

The kinetics of adsorption is controlled by both mass transport of the adsorbate to the active centre and the mechanism of attachment onto the substrate. The amine groups on chitosan are the main active sites that interact with metal ions although there will also be some other potential linkages possible through –OH groups for example. The amine groups may interact with metal ions through different mechanisms depending on the metal and the pH. The lone pair on the nitrogen may bind with metal cations in basic, neutral, or very weakly acidic pH. [38] The protonation of amine groups to NH_3^+ makes the polymer cationic and consequently increases the potential for attracting metal (oxo) anions. [38] In an acidic medium the protonation of the amine groups will prevent them binding to cations and so it is to be expected that cations will be preferentially chelated under very weakly acidic or neutral pH conditions while metal (oxo) anions will be preferentially chelated under more acidic conditions.

The following equation shows the generic mechanism for the chelation of di-cationic metals such as Pb(II) and Cd(II), under conditions where the amine groups are not protonated:

$$M^{2+} + 2RNH_2 \rightarrow M(RNH_2)_2^{2+} \qquad \text{Eqn. 5.9}$$

Similarly for metal (oxo) anions such as the pertechnetate species studied here, the following generic process might account for their trapping on the films surfaces under more acidic conditions where a significant proportion of the amine groups are protonated:

$$MO^{x-} + xRNH_3^+ \rightarrow MO(RNH_3)_x \qquad \text{Eqn. 5.10}$$

5.3.4 Adsorption Isotherms and possible adsorption mechanisms

Additional adsorption experiments were carried out using a solution of pertechnetate ions at pH 5.5 with an initial concentration of aqueous phase ranging from 1.10^{-5} to 1.10^{-1} mol·dm^{-3} and the percentage of pertechnetate was measured with the pertechnetate tracer. The results were plotted in terms of the real (data points) and idealized (solid lines) expected variation in coverage vs solution concentration obtained for both Langmuir and Freundlich adsorption models (Figures 5.6 and 5.7).

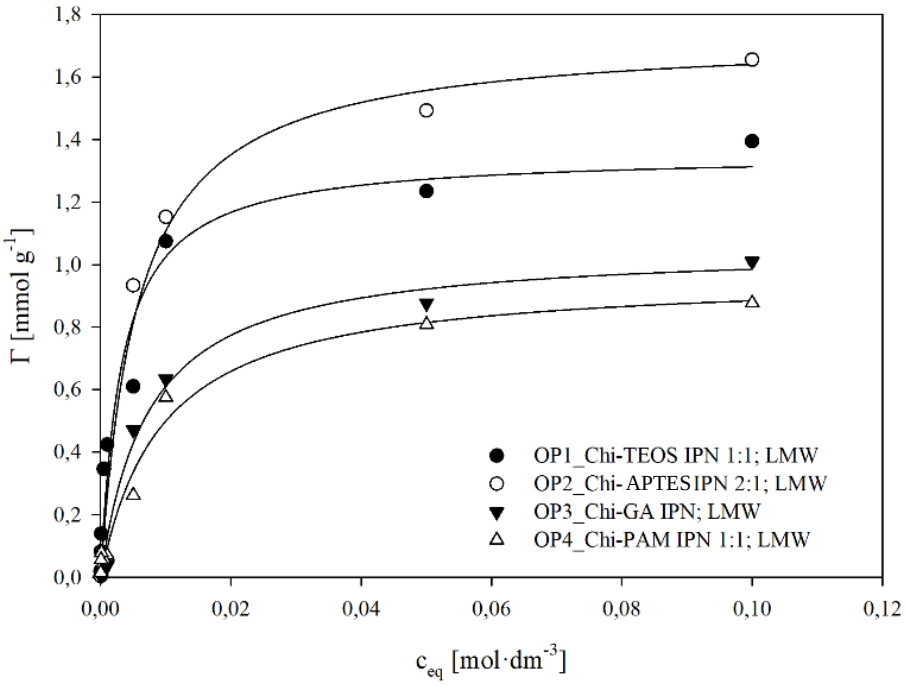


Figure 5.6: Isotherms obtained by fitting the data obtained for the range of chitosan-based thin films studied here to a Langmuir model.

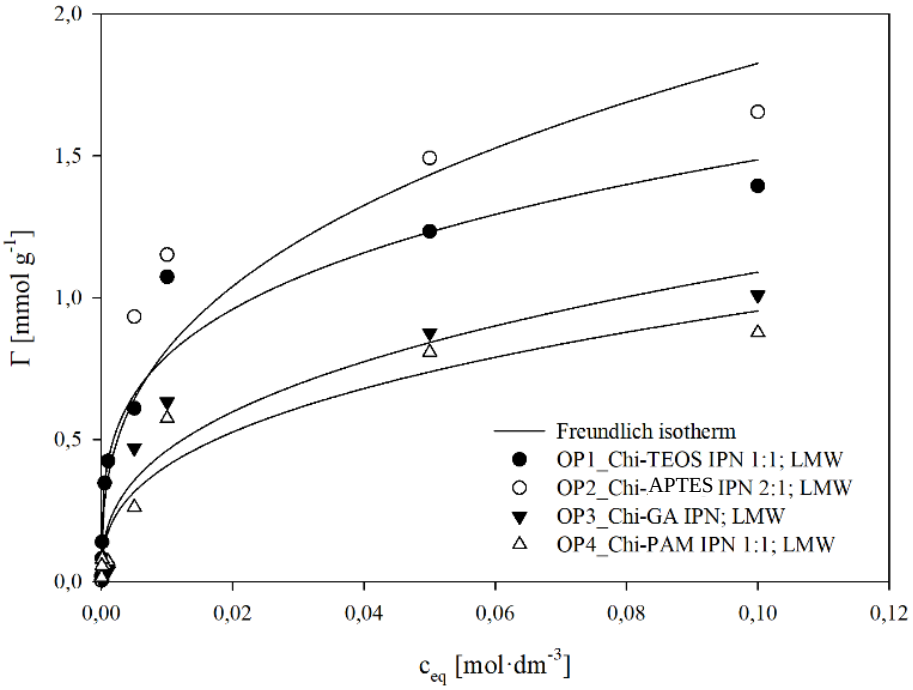


Figure 5.7: Isotherms obtained by fitting the data obtained for the range of chitosan-based thin films studied here to a Freundlich model.

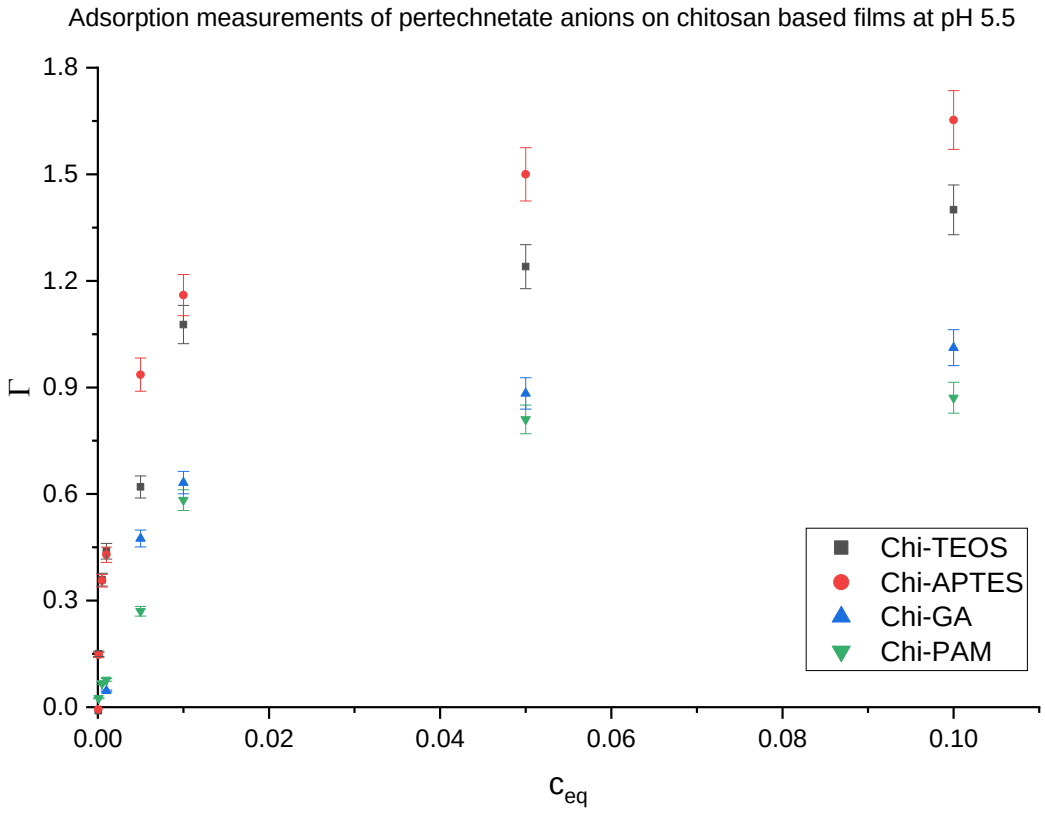


Figure 5.8: Adsorption measurements of pertechnetate anions on chitosan films at pH 5.5. Analysed with a relative measurement error of < 5%.

From figures 5.6 and 5.7 above it may be seen that by eye the ‘best fit’ of the data seems to be for the Langmuir-type process, where the coverage is seen to increase from zero until it reaches a plateau above which there is no further increase. Contrast this with the ‘best fit’ for a Freundlich-type process where the data points show a greater degree of scatter about the best fit line, which does not seem to reach a plateau. This indicates the coverage continuing to increase with increasing solution concentration. The measured data points remain the same for each isotherm, but the linear fit of the lines differ.

In order to quantify the quality of the fit, the straight-line versions of both equations were generated, the quality of the fit now being assessed using linear regression, the R^2 values.

5.3.4.1 Langmuir Isotherm straight-line plot derivation

As discussed in section 5.2.2, the Langmuir isotherm may be written as follows:

$$\Gamma = \frac{\Gamma_{max} \cdot bc_{eq}}{1+b \cdot c_{eq}} \qquad \text{Eqn. 5.11}$$

Rearranging this formula as follows, gives the linear version:

$$\frac{\Gamma}{\Gamma_{max}} = \frac{\Gamma_{max} \cdot bc_{eq}}{1+b \cdot c_{eq}} \qquad \text{Eqn. 5.12}$$

Multiplying both sides by $1+b \cdot c_{eq}$ yields

$$\frac{\Gamma}{\Gamma_{max}} + \frac{\Gamma . bc_{eq}}{\Gamma_{max}} = bc_{eq} \qquad \text{Eqn. 5.13}$$

Now dividing by Γ yields

$$\frac{1}{\Gamma_{max}} + \frac{bc_{eq}}{\Gamma_{max}} = \frac{bc_{eq}}{\Gamma} \qquad \text{Eqn. 5.14}$$

Finally, dividing by b yields the linearised version of the Langmuir adsorption isotherm,

$$\frac{1}{b\Gamma_{max}} + \frac{c_{eq}}{\Gamma_{max}} = \frac{c_{eq}}{\Gamma} \qquad \text{Eqn. 5.15}$$

Since for a given material both Γ_{max} and b are constants, plotting

$$\frac{c_{eq}}{\Gamma} \text{ vs } c_{eq}$$

gives a straight-line plot, where:

$\frac{1}{\Gamma_{max}}$ = slope $\qquad\qquad$ $\frac{1}{b\Gamma_{max}}$ = intercept

5.3.4.1 Freundlich Isotherm straight-line plot derivation

Similarly, the Freundlich isotherm, Eqn. 5.16 below, may be rearranged to form a linear version:

$$\Gamma = K_F \cdot c_{eq}^{n} \qquad \text{Eqn 5.16}$$

Taking logs, we obtain

$$\log \Gamma = \log K_F + n\log C_{eq} \qquad \text{Eqn 5.17}$$

Since K_F is constant a graph of

$$\log \Gamma \ vs \ \log C_{eq}$$

yields a straight-line plot where:

n = slope

The adsorption data were fitted to both a Langmuir and a Freundlich type isotherms as shown by the solid lines presented on the graphs in appendix section A.4. The data obtained from these graphs are presented in Table 5.4 below:

Model		Adsorbents				STD
		Chi-TEOS	Chi-APTES	Chi-GA	Chi-PAM	
Langmuir fitting parameters	Γ_{max}	1.35	1.73	1.06	0.97	0.30
	b	310.64	177.38	136.41	106.67	77.97
	R^2	0.99	0.99	0.97	0.99	0.01
Freundlich fitting parameters	K_F	2.78	4.08	2.57	2.23	0.70
	n	0.27	0.34	0.37	0.37	0.04
	R^2	0.94	0.95	0.78	0.96	0.07

Table 5.4. Langmuir and Freundlich isotherm parameters obtained via the fitting the measured data to the appropriate equations over the range of chitosan-based films studied. In this table Γ_{max} is the calculated maximum theoretical coverage as expressed as number of filled sites divided by the number of actual sites and b is the Langmuir adsorption constant, while K_F and n are constants associated with the fit obtained to the Freundlich isotherm, Eqn. 5.16. The R^2 values describe the efficacy of the linear regression fit of the data to the equations.

From Table 5.4 it may be seen that the experimental results for pertechnetate fit the theoretically-derived Langmuir isotherm model (R^2 – from 0.97 to 0.99) better than the more empirical Freundlich isotherm model (R^2 – from 0.78 to 0.96). This proposes that the uptake of $^{9m}TcO_4^-$ ions occurs on a homogeneous surface by monolayer adsorption. [39] Further, Ustynyuk et al. [40] proposed that the pertechnetate anion forms an asymmetric hydration shell of water molecules in aqueous solutions. This suggests that the adsorption of $^{9m}TcO_4^-$ occurs on the unprotected side of the anion, leaving a shell of water molecules facing outwards, which may contribute to monolayer adsorption over multilayer adsorption.

The calculated fits for both types of isotherm using these R^2 values suggest that the adsorption in question is best described by a Langmuir-type adsorption process although for the Chi-TEOS films there is no real distinction between the two processes based on the R^2 value alone. For this particular material the calculated value of Γ_{max} for the Langmuir isotherm is >> 1, suggesting that multilayer adsorption can occur. Thus, it is possible that for this material, the true adsorption mechanism is likely to be

a hybrid mechanism, perhaps dominated by initial monolayer formation. Clearly further studies are required to fully evaluate the true nature of this process.

Despite this uncertainty, one may speculate the meaning of this data. It is interesting to examine the data for the Chi-GA samples which in contrast to other data presented here have been shown to be the most active in terms of TcO_4^- ion adsorption. For Chi-GA samples, R^2 is 0.97 as compared to the values of 0.99 obtained for the other samples.

Accordingly, while the isotherm data suggest that a Langmuir-type process being applicable for all films studied, there is still degree of uncertainty regarding the true nature of the adsorption process.

An important implication of this finding which was not properly tested here is that the adsorption process would be reversible if either type of isotherm was in operation. This would be a critical factor in determining the efficacy of using these films as a means of extracting heavy metal ions from solution while also being able to regenerate the films after use. With this in mind it is recognised that extensive further studies would be necessary before this point can be firmly established.

5.4 Conclusions

This work has demonstrated that a range of chitosan-based films can be made simply and cheaply and then used to extract TcO_4^- ions from aqueous solutions. The film which showed the greatest ability to adsorb the pertechnetate ions at pH4 was that made by cross linking chitosan with glutaraldehyde. This work also demonstrates that the films produced here might also be suitable for the extraction of other large, negatively charged ions from aqueous solutions. This could include other metal oxoanions or even negatively charged organic ions that may be formed following water contamination with metal-organic salts.

As demonstrated in Chapter 3 these particular films show the highest mechanical strength but do tend to be somewhat brittle. Furthermore, as shown in Chapter 6, as a result of their composition and structure these films do not appear to possess any appreciable anti-bacterial activity in comparison with the other films studied. Since some antimicrobial activity could also be reflected in the film being less likely to exhibit fouling due to the formation of biofilms, the ability of these films to adsorb pertechnetate ions must be offset against such considerations when evaluating their efficacy to be used as filters.

All films are shown to nearly double in mass as a result of swelling in aqueous solution of pH 4 which is relevant not only to adsorption studies but also potentially for drug delivery applications. Models are presented which account for the efficacy of the films in terms of TcO_4^- ion adsorption which invoke the proposed structural models for the films and their likely behaviour towards oxo anions of this type under mildly acidic conditions. The films have been ranked according to their percentage swelling as measured by mass gain and adsorption efficiency towards aqueous TcO_4^- ions. Finally, preliminary isotherm studies suggest that a Langmuir type adsorption process is the preferred mode of adsorption for all films, but further experimentation is required in order to be able to properly confirm or deny this finding. It is interesting that the data seem to favour the Langmuir, monolayer-type model over the Freundlich model. This finding does need further clarification, but it may be that the chitosan network is sufficiently open on a scale comparable to the size of the ions in question, that it effectively presents an extended surface over which monolayer adsorption dominates. In addition, there is little evidence in the literature to suggest that oxo-anions could

adsorb on top of sites already occupied by another oxo-anion and thus monolayer adsorption would be expected to dominate as a result.

References

1. Suarez-Serrano, A., et al., *Procambarus clarkii as a bioindicator of heavy metal pollution sources in the lower Ebro River and Delta.* Ecotoxicology and Environmental Safety, 2010. **73**(3): p. 280-286.
2. Briffa, J., E. Sinagra, and R. Blundell, *Heavy metal pollution in the environment and their toxicological effects on humans.* Heliyon, 2020. **6**(9).
3. Wu, S.S., et al., *Facile preparation of magnetic sodium alginate/carboxymethyl cellulose composite hydrogel for removal of heavy metal ions from aqueous solution.* Journal of Materials Science, 2021. **56**(23): p. 13096-13107.
4. CIS, *Metals In Basics of Chemical Safety.* International Occupational Safety and Health Information Centre, 1999. **Chapter 7**(Geneva: International Labour Organization).
5. Yoshihara, K., *Technetium in the environment.* Technetium and Rhenium: Their Chemistry and Its Applications, 1996. **176**: p. 17-35.
6. Tokar, E., et al., *Development and practical evaluation of the scheme for Cs-137 concentrating from seawater using chitosan and mixed ferrocyanides of Zn-K and Ni-K.* Journal of Radioanalytical and Nuclear Chemistry, 2020. **325**(2): p. 567-575.
7. Belkacem, M., M. Khodir, and S. Abdelkrim, *Treatment characteristics of textile wastewater and removal of heavy metals using the electroflotation technique.* Desalination, 2008. **228**(1-3): p. 245-254.
8. Ku, Y. and I.L. Jung, *Photocatalytic reduction of Cr(VI) in aqueous solutions by UV irradiation with the presence of titanium dioxide.* Water Research, 2001. **35**(1): p. 135-142.
9. Gao, X.Y. and X.C. Meng, *Photocatalysis for Heavy Metal Treatment: A Review.* Processes, 2021. **9**(10).
10. Landaburu-Aguirre, J., et al., *The removal of zinc from synthetic wastewaters by micellar-enhanced ultrafiltration: statistical design of experiments.* Desalination, 2009. **240**(1-3): p. 262-269.
11. Papadopoulos, A., et al., *Nickel uptake from a wastewater stream produced in a metal finishing industry by combination of ion-exchange and precipitation methods.* Separation and Purification Technology, 2004. **39**(3): p. 181-188.

12. Pillay, K., E.M. Cukrowska, and N.J. Coville, *Multi-walled carbon nanotubes as adsorbents for the removal of parts per billion levels of hexavalent chromium from aqueous solution.* Journal of Hazardous Materials, 2009. **166**(2-3): p. 1067-1075.
13. Crini, G. and P.-M. Badot, *Application of chitosan, a natural aminopolysaccharide, for dye removal from aqueous solutions by adsorption processes using batch studies: A review of recent literature.* Progress in Polymer Science, 2008. **33**(4): p. 399-447.
14. Wan Ngah, W.S., L.C. Teong, and M.A.K.M. Hanafiah, *Adsorption of dyes and heavy metal ions by chitosan composites: A review.* Carbohydrate Polymers, 2011. **83**(4): p. 1446-1456.
15. Dalaran, M., et al., *Study on a novel polyampholyte nanocomposite superabsorbent hydrogels: Synthesis, characterization and investigation of removal of indigo carmine from aqueous solution.* Desalination, 2011. **279**(1): p. 170-182.
16. Huang, X.-Y., et al., *Chemical modification of chitosan by tetraethylenepentamine and adsorption study for anionic dye removal.* Carbohydrate Research, 2011. **346**(10): p. 1232-1240.
17. Atangana, E. and P.J. Oberholster, *Mathematical modeling and stimulation of thermodynamic parameters for the removal for Cr6+ from wastewater using chitosan cross-linked glutaraldehyde adsorbent.* Alexandria Engineering Journal, 2020. **59**(4): p. 1931-1939.
18. Cao, J., et al., *Novel complex gel beads composed of hydrolyzed polyacrylamide and chitosan: An effective adsorbent for the removal of heavy metal from aqueous solution.* Bioresource Technology, 2010. **101**(7): p. 2558-2561.
19. Zhao, S., et al., *Removal of anionic dyes from aqueous solutions by adsorption of chitosan-based semi-IPN hydrogel composites.* Composites Part B: Engineering, 2012. **43**(3): p. 1570-1578.
20. Buzetzky, D., et al., adsorption *of pertechnetate anion by cation modified bentonites.* Journal of Radioanalytical and Nuclear Chemistry, 2019. **322**(3): p. 1771-1776.
21. Pivarciova, L., et al., adsorption *of pertechnetate anions on chitosan.* Journal of Radioanalytical and Nuclear Chemistry, 2016. **308**(1): p. 93-98.

22. Briao, G.D., et al., *Removal of toxic metals from water using chitosan-based magnetic adsorbents. A review.* Environmental Chemistry Letters, 2020. **18**(4): p. 1145-1168.
23. Chauhan Ghanshyam, S. and S. Mahajan, *Use of novel hydrogels based on modified cellulosics and methacrylamide for separation of metal ions from water systems.* Journal of Applied Polymer Science, 2002. **86**(3): p. 667-671.
24. Wang, W.-B., et al., *One-step in situ fabrication of a granular semi-IPN hydrogel based on chitosan and gelatin for fast and efficient adsorption of Cu2+ ion.* Colloids and Surfaces B: Biointerfaces, 2013. **106**: p. 51-59.
25. Pivarciova, L., et al., adsorption *of technetium on glutaraldehyde crosslinked chitosan.* Journal of Radioanalytical and Nuclear Chemistry, 2016. **309**(3): p. 1251-1256.
26. da Silva, R.M.P., et al., *Poly(N-isopropylacrylamide) surface-grafted chitosan membranes as a new substrate for cell sheet engineering and manipulation.* Biotechnology and Bioengineering, 2008. **101**(6): p. 1321-1331.
27. Mi, F.-L., S.-S. Shyu, and C.-K. Peng, *Characterization of ring-opening polymerization of genipin and pH-dependent cross-linking reactions between chitosan and genipin.* Journal of Polymer Science Part A: Polymer Chemistry, 2005. **43**(10): p. 1985-2000.
28. Kitson, S., *Amersham radiochemistry to GE Healthcare.* Journal of Labelled Compounds and Radiopharmaceuticals, 2007. **50**: p. 737-745.
29. GEHealthcare, *DRYTEC Technetium Tc99m Generator*. 2015, https://www.accessdata.fda.gov/drugsatfda_docs/label/2015/017693s029lbl.pdf: GE Healthcare, Medi-Physics, Inc.
30. Matovic, L., et al., *Removal of pertechnetate from aqueous solution using activated pyrolytic rubber char.* Journal of Radioanalytical and Nuclear Chemistry, 2017. **314**(2): p. 897-905.
31. Pivarciova, L., et al., adsorption *of nickel on chitosan.* Journal of Radioanalytical and Nuclear Chemistry, 2014. **300**(1): p. 361-366.
32. Ly, A., M. Marsman, and E.J. Wagenmakers, *Analytic posteriors for Pearson's correlation coefficient.* Statistica Neerlandica, 2018. **72**(1): p. 4-13.
33. Sankararamakrishnan, N., A.K. Sharma, and R. Sanghi, *Novel chitosan derivative for the removal of cadmium in the presence of cyanide from*

electroplating wastewater. Journal of Hazardous Materials, 2007. **148**(1-2): p. 353-359.

34. Heidari, A., et al., *Selective adsorption of Pb(II), Cd(II), and Ni(II) ions from aqueous solution using chitosan-MAA nanoparticles.* International Journal of Biological Macromolecules, 2013. **61**: p. 251-263.
35. Sedeno-Diaz, J.E., et al., *Distribution Coefficient and Metal Pollution Index in Water and Sediments: Proposal of a New Index for Ecological Risk Assessment of Metals.* Water, 2020. **12**(1).
36. Hernandez, R.B., O.R. Yola, and A.L.R. Merce, *Chemical equilibrium in the complexation of first transition series divalent cations Cu2+, Mn2+ and Zn2+ with chitosan.* Journal of the Brazilian Chemical Society, 2007. **18**(7): p. 1388-1396.
37. McIlwee, H.A., et al., *Thin chitosan films as a platform for SPR sensing of ferric ions.* Analyst, 2008. **133**(5): p. 673-677.
38. Guibal, E., *Interactions of metal ions with chitosan-based sorbents: a review.* Separation and Purification Technology, 2004. **38**(1): p. 43-74.
39. Baran, A., et al., *Comparative studies on the adsorption of Cr(VI) ions on to various sorbents.* Bioresource Technology, 2007. **98**(3): p. 661-665.
40. Ustynyuk, Y.A., et al., *Hydration of the pertechnetate anion. DFT study.* Journal of Molecular Liquids, 2021. **342**.

6. A preliminary study on the antibacterial properties of selected chitosan-based films

6.1 Introduction

This work was performed by Oliver James Pemble together with Ms Rebecca Quinlan and Dr David Clarke of the Department of Microbiology at University College Cork.

Bacterial contamination is a subject that is of great concern in a variety of areas, such as healthcare products, medical devices, food packaging, and hospital sanitation. [1] In particular, medical device bacterial contamination is a major problem to many medical disciplines that employ biomaterials. [2] Thus, researchers in relevant fields are attempting to develop diverse approaches to synthesise antibacterial materials for medical use. [3] The need for new materials that are resistant to microbial colonisation and biofilm attachment is apparent.

In this present work we set out to perform a preliminary assessment of the antibacterial activity of the selected chitosan-based films studied here. The four film types prepared via the drop cast method; chitosan and tetraethyl-orthosilicate (Chi-TEOS), chitosan and 3-aminopropyltriethoxysilane (Chi-APTES), chitosan and polyacrylamide (Chi-PAM), and chitosan and glutaraldehyde (Chi-GA) each display unique compositional properties that may affect bacterial cells. Each film was tested for their ability to inhibit bacterial growth and attachment over a period of 24 hours. The molecular chemistry of the films was assessed with regards to their interactions with bacteria and several mechanisms of the interactions are proposed.

6.1.1 Bacteria

Bacteria may be defined as single-celled microorganisms that inhabit virtually all environments including water, soil, organic matter, and other living organisms. [4] They are an example of one of the two type of living cells in nature. The two basic cell types are prokaryotes and eukaryotes, with prokaryotes predating eukaryotes for billions of years on earth. [5] Bacteria are prokaryotes, while animals, plants and fungi are eukaryotes. The name “prokaryote” means “pre-nucleus”, while eukaryotes possess a true nucleus, so one of the major differences between bacterial cells and mammalian cells is the presence of a defined nucleus containing the genetic

information. Bacteria have a plasma membrane and cell wall to protect them against changes in osmotic pressure and control the uptake of beneficial molecules/ions. [6] Some species of bacteria can live under extreme conditions of pressure or temperature, [7] and others are important for facilitating biochemical cycles and recycling nutrients in organic matter. [8]

6.1.1.1 Bacterial growth and attachment

Bacterial attachment or adhesion is the term commonly used to describe the ability of bacteria to grow on a surface and is the first step in bacterial colonisation, see figure 6.1. The initial phase is driven by electrostatic interactions between the bacteria and the surface, so it can be reversed by simple washing. The final phase of bacterial attachment is the formation of a biofilm through stronger intermolecular forces such as hydrogen bonds. [9] The key factors that affect bacterial attachment are the surface chemistry, the surface topology, temperature, pH, and other competing bacteria. [10] These factors must all be considered when designing antibacterial materials.

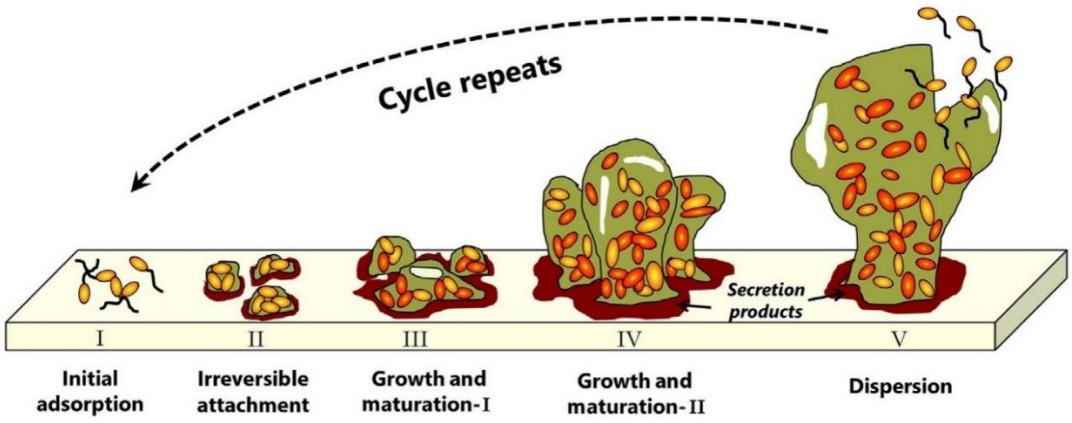


Figure 6.1: Schematic illustration of the five stages of the biofilm formation process. (I) initial adsorption, (II) irreversible attachment, (III)-(IV) growth and maturation stages, and (V) evolution into bacterial biofilms. [10]

Bacterial growth refers to a complex process of reactions that synthesise and breakdown bacterial cell constituents and metabolites. Ultimately, under ideal conditions, these reactions lead to cell division. Typically, to understand the growth of bacteria, the cells are placed in a liquid nutrient medium under controlled environmental parameters. The increase in bacterial mass can be measured as a function of time to obtain a growth curve. Distinct phases can be observed within the

growth curve, the lag phase, the exponential phase, the stationary phase, and the death phase, see figure 6.2. [11]

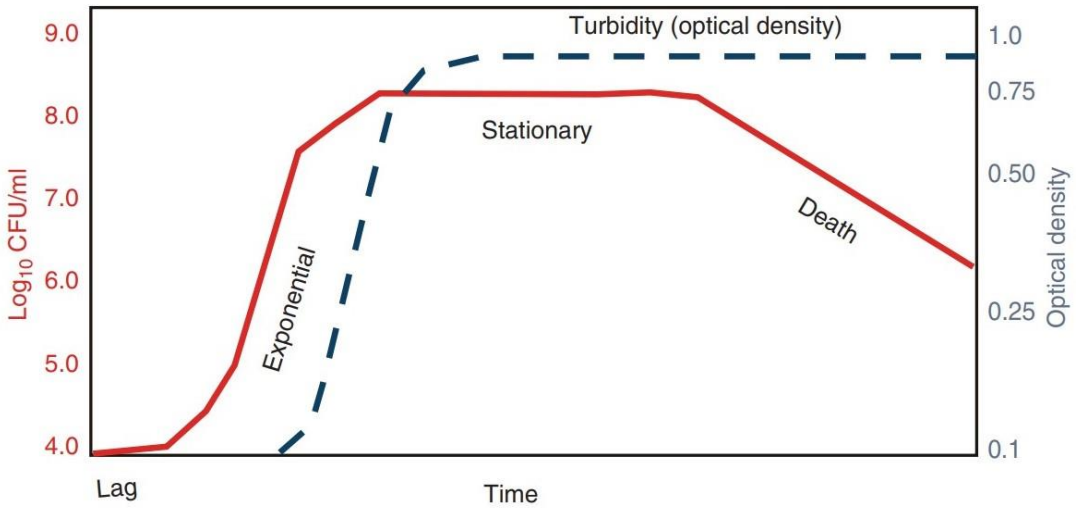


Figure 6.2: Typical growth curve for bacterial population [7].

In figure 6.2 CFU/mL refers to colony-forming unit per mL, which measures viable cells by calculating the number of colonies as factors of the dilution and volume of culture plate. [11] It should be noted that the way in which the bacterial growth is measured can influence the shape of the graph. For example, if optical density (OD) is used to measure the turbidity of bacteria in suspension, the onset of the death phase is not apparent due to the dead cells remaining and affecting the turbidity.

6.1.1.2 Bacteria subgroups

Bacteria are divided into two major subgroups, Gram-positive and Gram-negative. As per the Gram stain test, a colour change from a dye can distinguish between the two types; dark blue for Gram-positive bacteria and pink for Gram-negative bacteria. [12]

Gram positive bacteria are surrounded by a thick cell wall containing peptidoglycan which consists of alternating N-acetylglucosamine and N-acetylmuramic acid chains. These chains are chemically cross-linked by binding proteins to provide rigidity to the wall. Figure 6.3 shows the molecular structure of the peptidoglycan cell wall which is negatively charged due to the carboxyl groups. [6] *Listeria monocytogenes* and *Staphylococcus aureus* or *S. aureus* are examples of Gram-positive bacteria. [13]

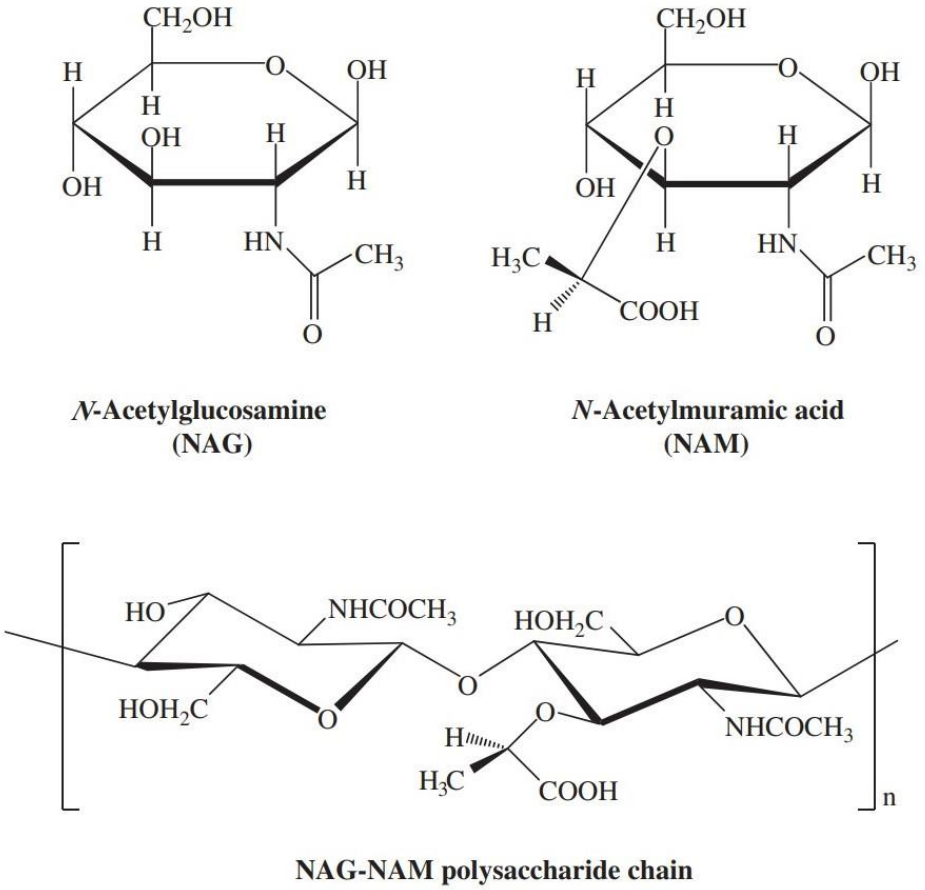


Figure 6.3: Structure of the alternating N-acetylglucosamine and N-acetylmuramic acid polysaccharide chains present in peptidoglycan. [6] Note the similarity in structure to the chitosan molecule, which comprises N-acetylglucosamine and glucosamine alternating units.

The cell wall of Gram-negative bacteria is much thinner than that of Gram-positive bacteria, but Gram-negative bacteria have two membranes (an inner membrane and an outer membrane) of negatively charged phospholipids and proteins. The phospholipids provide a barrier for the uptake of any hydrophilic molecules and the proteins create pores that allow certain molecules to diffuse through. [6] *Salmonella enteritidis* and *Escherichia coli* or *E. coli* are examples of Gram-negative bacteria. [13].

In this work both *S. aureus* and *E. coli* have been utilised. Figure 6.4 and figure 6.5 below show magnified images of these bacteria.

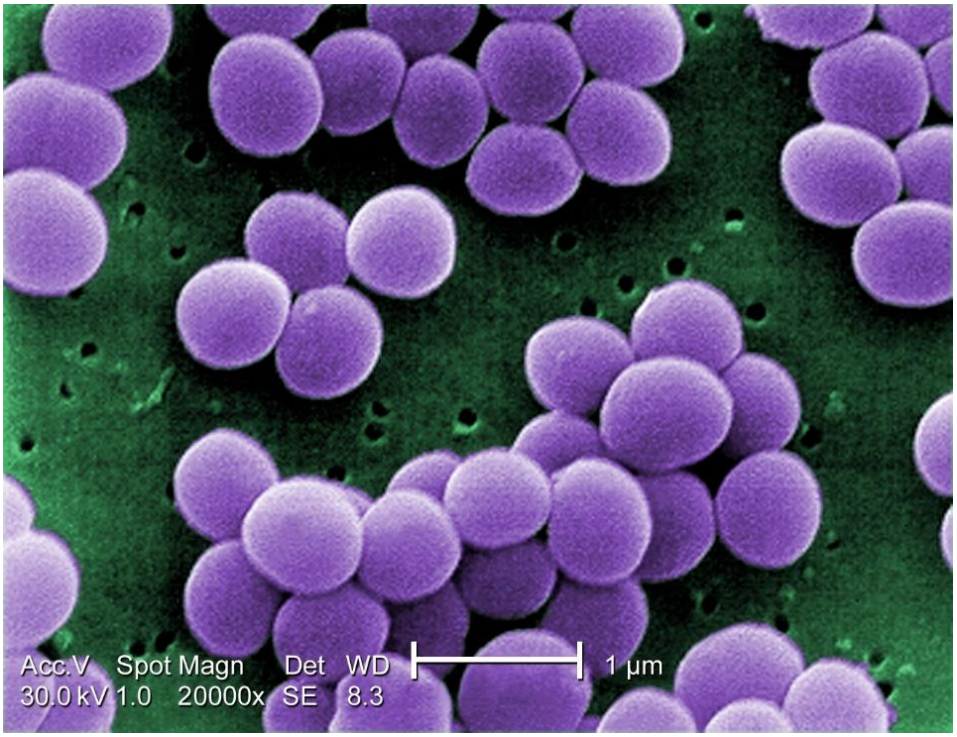


Figure 6.4: SEM image of *S. aureus* cells. [14]

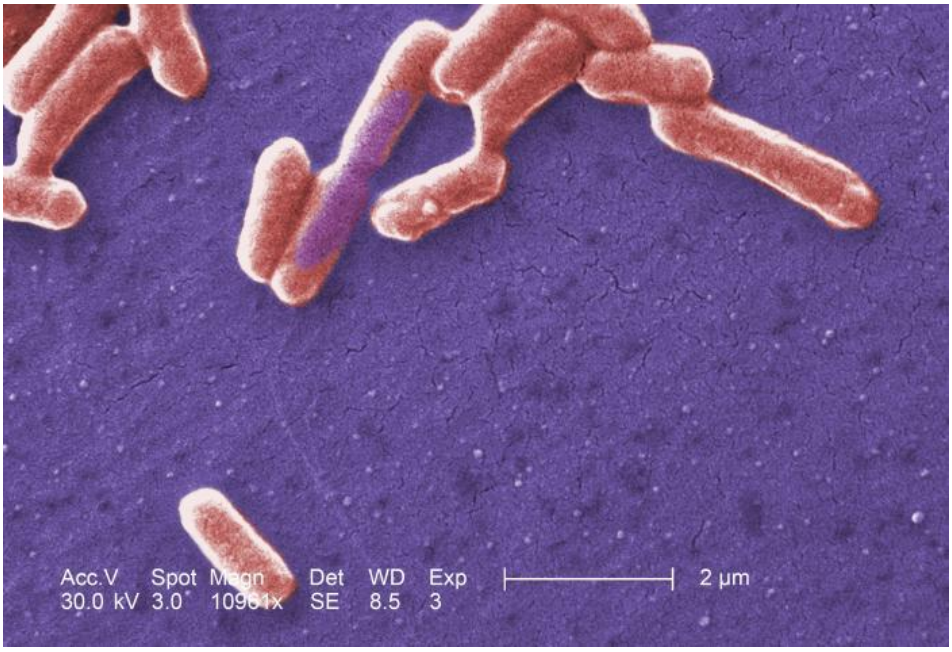


Figure 6.5: SEM image of *E. coli* cells. [15]

6.1.2 Antibacterial materials

Silver, specifically silver nanoparticles, are very promising antibacterial materials due to their broad spectrum of antibacterial activity, killing a variety of bacterium types including some that are antibiotic resistant. [16, 17] Nanomaterials in particular play an important role in antibacterial applications due to their large surface area and size dependant physiochemical properties. [18, 19] Via the introduction of silver nanoparticles into a material or on the surface of a material, silver ions can interact with the bacterial cell wall, membranes, and DNA by binding to the negatively charged surface and disabling the oxygen metabolising enzymes. [20] Generally, Gram-positive bacteria are less susceptible to silver nanoparticles than Gram-negative bacteria, most likely due to the thicker peptidoglycan cell wall forming a dense network, reducing silver ion permeation. [21] Specific care should be taken before using silver nanoparticles as antibacterial agents as they have been reported to be toxic to certain mammalian cells. [22, 23] To address this issue, biocompatible polymeric materials are widely used to reduce the toxic effects of nanomaterials.

Antibacterial polymers have a lot of potential in medical device research. They may be incorporated into biomedical applications such as sterile wound dressings (as discussed in Chapter 7) or disinfectants. For example, antimicrobial surgical gowns and antifungal coatings on surfaces utilize polymers to minimise the release of pathogenic microbes. [24] Polymeric antimicrobial materials have an advantage in that they can be non-volatile, chemically stable and do not permeate through human skin. They can reduce losses associated with volatilisation and decomposition that remain a significant challenge to certain medical implants. [25, 26] Infection is the most common case of biomaterial implant failure in modern medicine and antibacterial polymers may play an important role in reducing the incidences of that failure. [27]

A bio passive polymer layer ensures minimum protein adsorption on the surface thereby preventing bacterial adhesion. These materials do not actively kill bacteria; the hydrophilic polymers merely prevent the bacteria from forming a biofilm. A wide variety of polymers including poly (ethylene glycol), phosphobetaine, phospholipid polymers with a phosphorylcholine group, [28, 29] and polysaccharides have been examined as bio passive polymers. [30, 31] Bioactive polymers are polymers functionalised with antimicrobial agents, typically in the form of quaternary ammonium compounds (QAC) or antibiotics and have been demonstrated to kill

bacteria. QACs are among the most common antimicrobial coatings, utilising cationic functionality that interact with bacterial cell walls. [27] However, use of QACs have been known to have negative environmental impact as they become more widely used as the active ingredient for disinfectants. [32, 33] Chitosan is a bioactive polymer that interacts with bacteria using the same mechanism as QACs but has the benefit of being biodegradable and environmentally friendly. [34-36]

6.1.3 Chitosan antibacterial activity

The antibacterial properties of chitosan can be affected by many factors, including the molecular weight of chitosan, [37, 38] the degree of deacetylation of chitosan, [39, 40] the pH value, [41, 42] the type of microorganism, [43, 44] temperature, [43] and cell growth phase. [43] Chitosan is most active on the surface of the bacterial cell where the interactions are considered to be electrostatic. [45] As discussed in section 1.6.2.1, the positive charge of a protonated amino group in chitosan can interact with the negatively charged molecules or functional groups on the bacterial cell surface. The permeability of the cell increases, causes leakage of the intracellular material, leading to bacterial death. [46, 47] Some research results show that chitosan may also affect DNA expression by binding to the nucleic acid in a bacterial cell, but chitosan must first penetrate the bacterial membrane in order for this to occur. [48]

Chitosan displays different antibacterial effects on Gram-positive and Gram-negative bacteria. Fernandez-Saiz et al. [49] measured the antibacterial properties of chitosan acetate films against the growth of *Salmonella* and evaluated the effect of bacterial type on the films. They found that Gram-positive bacteria were more sensitive to chitosan due to their cell walls consisting of peptidoglycan and highly negatively charged polymers called teichoic acids. These acids, which are anionic polymers consisting of 20-30 repeat units of polyglycerol phosphates, [50] can interact electrostatically with chitosan. The Gram-negative bacteria cell wall is surrounded by a phospholipid membrane which is less anionic than that of Gram-positive bacteria and thus it was concluded that Gram-positive bacteria are more sensitive to chitosan as an antibacterial agent than Gram negative. [49] However, contrary to these results, Devlieghere et al. explored the suitability of chitosan films as a food preservative by measuring the growth of a number of different bacterium types. They found that the Gram-negative bacteria were more susceptible to the films than Gram-positive bacteria, the results of which varied greatly. [51]

The amino groups in the chitosan chain are essential for the antibacterial activity, but they can only have a relatively weak positive charge, limiting their effectiveness. Increasing the amino positive charge can improve the antibacterial activity of chitosan. [52] This has led to researchers modifying chitosan to form derivatives with improved solubility and antimicrobial properties. [53-55] Abbasipour et al. developed an advanced cotton gauze composite from chitosan modified with silver and zinc oxide. The results obtained illustrated that treating the chitosan-Ag-ZnO nanocomposite increased the antibacterial efficiency greatly for both *E. coli* and *S. aureus*. [56] A more detailed discussion of the effectiveness of chitosan as a material for wound dressings is described in chapter 7.

6.2 Methods

6.2.1 Basic methodology for antimicrobial studies

The methods employed during these experiments are described in detail in Chapter 2, section 2.2.4.

Briefly, isolated colonies of *E. coli* and *S. aureus* were grown by inoculating agar plates with pure cultures of the bacteria and incubating them for 24 hours at 37 °C. After the incubation period, a single colony of each bacterium was transferred to 5 mL of liquid nutrient broth (Lysogeny Broth (LB) for *E. coli* and Brain Heart Infusion (BHI) broth for *S. aureus*) and incubated overnight with shaking at 37 °C and 30 °C, respectively. 1 mL of the overnight cultures was withdrawn and centrifuged at 14000 RPM for 2-5 minutes and the resulting cell pellet was re-suspended in Phosphate Buffered Saline (PBS). The absorbance or optical density (OD) of the bacterial colonies were measured at a wavelength of 600 nm using a spectrophotometer (Shimadzu UVmini-1240 model) and adjusted to give an OD_{600}=1.0.

The chitosan film samples were placed in a 9 cm sterile plastic Petri dish and flooded with the respective nutrient medium broths (5 mL) and inoculated with the re-suspended cultures (50 µL) to create a 1:100 dilution (equivalent to OD_{600nm} = 0.01). The Petri dishes were placed in a humidified airtight container and incubated for 24 hours (37 °C for *E. coli* and 30 °C for *S. aureus*). Control samples were prepared by inoculating with sterile PBS.

6.2.2 Determination of bacteriological activity using Optical Density measurements

Optical Density measurements were employed in order to quantify the growth of the bacterial cells in the medium and the attachment of the bacterial cells to the chitosan film. After incubation on the chitosan films, the broth was removed and an OD_{600} reading was taken to measure the growth of bacteria in the broth. The films were then repeatedly washed with distilled water to remove loose cells before staining with crystal violet (CV) for 15 min to measure the attached biomass. The CV was solubilised in ethanol and the OD_{595} was taken as a quantitative measurement of bacterial attachment on the chitosan films. OD_{595} was used for the crystal violet assay because crystal violet has a maximum absorbance of 595 nm, and it is common practice for measuring biofilm formation assays. [57, 58]

6.3 Results and discussions

While the antibacterial activity of chitosan is well known, [59] the specific antibacterial mechanism has not been definitely established. Research indicates that the pH, temperature, and ionic strength strongly influence the antibacterial activity of chitosan. [43, 60] An acidic pH (pH < 6) and high temperature (25 – 37 °C) can increase the ionic strength and improve the sterilizing effect of chitosan. [61] These factors and influences were considered when analysing the results of this study.

6.3.1 pH of bacterial cultures

A pH probe was used to measure the pH of the bacterial cultures after allowing them to grow for 24 hours. The results are displayed in table 6.1 below. In this table both control samples contained sterile growth medium (i.e., either LB or BHI broth).

Sample	**OD_{600}**	**pH**
E. coli control	-0.07	7.0
E. coli 1	2.10	7.5
E. coli 2	2.06	7.5
E. coli 3	2.06	7.5
STD E. coli	0.018	0
S. aureus control	0.07	7.0
S. aureus 1	1.91	6.5
S. aureus 2	1.69	6.5
S. aureus 3	1.94	6.5
STD S. aureus	0.112	0

Table 6.1: Optical Density and pH measurements of *E. coli* and *S. aureus* overnight cultures. Control samples had no bacteria present.

No chitosan-based films were present in these initial experiments. From table 6.1 it may immediately be seen that the two types of bacteria generate environments which are similar, but which lie either side of the neutral point on the pH scale. Since the control samples were all adjusted to pH 7, it may be seen that the pH achieved is affected by either the growth of the bacteria or the growth medium broth.

6.3.2 Optical Density measurements

The optical density tables may be found in the appendix section A.5. From these tables the following observations may be made:

- Introducing the chitosan-based films causes a variation in pH as compared to the control experiments
- Chi-TEOS (1:1) had an average attachment for *E. coli* of 0.47 ± 0.25 and an average attachment for *S. aureus* of 0.37 ± 0.03. The average growth for *E. coli* was 0.01 ± 0.01 and the average growth for *S. aureus* was 0.37 ± 0.06.
- Chi-APTES (2:1) had an average attachment for *E. Coli* of 1.70 ± 0.32 and no attachment for *S. Aureus*. The average growth for *E. Coli* was 1.36 ± 0.42 and there was no growth for *S. Aureus*.
- Chi-PAM (1:1) had an average attachment for *E. Coli* of 0.19 ± 0.05 and no attachment for *S. Aureus*. The average growth for *E. Coli* was 0.08 ± 0.01 and the average growth for *S. Aureus* was 0.16 ± 0.06.
- Chi-GA (8:1) had an average attachment for *E. Coli* of 1.53 ± 0.86 and an average attachment for *S. Aureus* of 0.66 ± 0.58. The average growth for *E. Coli* was 2.05 ± 0.02 and the average growth for *S. Aureus* was 1.69 ± 0.05.
- There was growth in the control samples for Chi-PAM, suggesting that contamination had taken place. Because of this, the interpretation of the results may not accurately reflect the antibacterial properties of the films.

6.3.3 Bacterial attachment

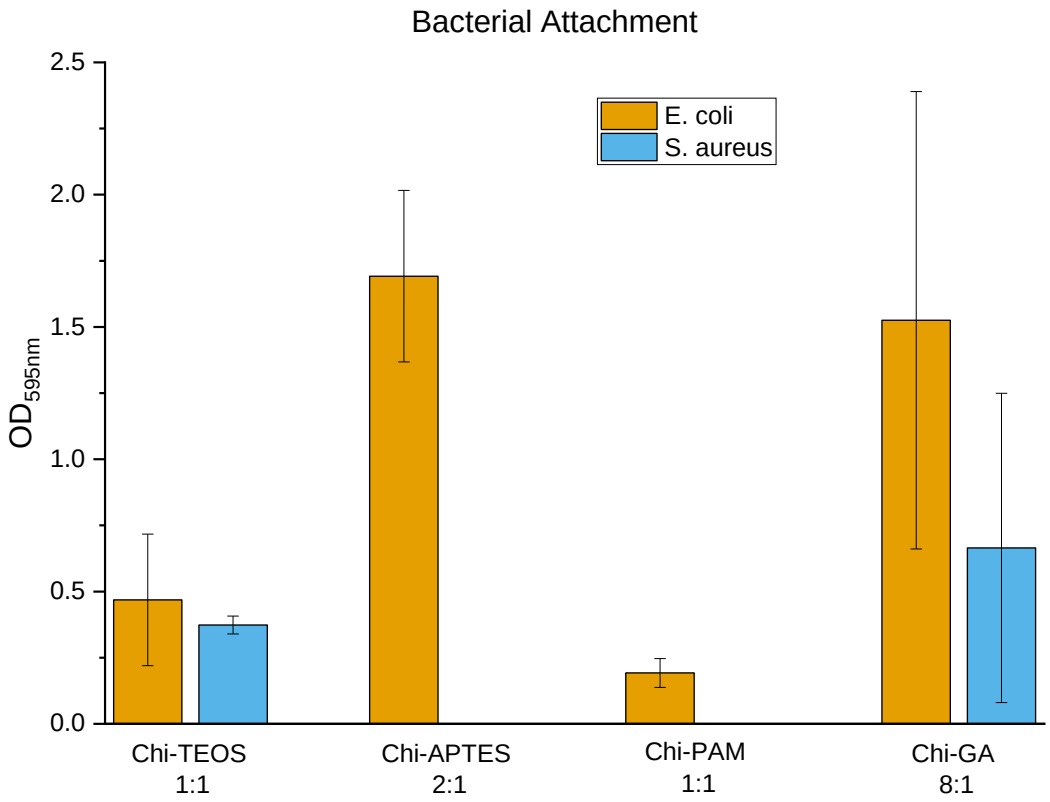


Figure 6.7: OD_{595nm} values for bacterial attachment on all samples

The attachment activity of *E. coli* on all films was higher than that of *S. aureus*. This may be attributed to the difference in cell wall structure or the presence of a second membrane. *E. coli* is a Gram-negative bacterium, the cell wall of which is made up of a thin membrane of peptidoglycan and an outer membrane constituted of proteins and phospholipids. Chitosan and its large molecular weight derivatives can be expected to coat the cell surface and prevent the leakage of intracellular components. [62] Helander et al. [63] found that chitosan disrupted the barrier properties of the outer membrane of Gram-negative bacteria via electrostatic forces. The amino groups in chitosan are protonated in acidic conditions, and the carboxyl and phosphate groups of the bacterial surface are anionic and offer potential sites for electrostatic binding. [64] On the other hand, *S. aureus*, a Gram-positive bacterium, has a thicker cell wall composed mainly of peptidoglycan, which may prevent the formation of a surface layer of chitosan. The thickness of the cell wall for *E. coli* is 7-8 nm, while the cell wall for *S. aureus* is 20-80 nm thick. [65]

The attachment of *S. aureus* was relatively low for all samples compared to *E. coli*, with Chi-APTES (2:1) displaying no attachment at all of S. aureus. Comparing Chi-TEOS (1:1) and Chi-APTES (2:1), it may be that the presence of an extra $-NH_2$ group on the APTES siloxane chain contributes to an enhancement of the electrostatic interactions between the samples and the *E. coli* bacteria cell surface. Further, the ratio of chitosan to siloxane polymer is larger in Chi-APTES (2:1) compared to Chi-TEOS (1:1), providing more $-NH_2$ active sites to be protonated. The Chi-GA (8:1) samples are chemically bound by Schiff base cross-linked bridges via the $-NH_2$ groups on chitosan, giving the polymer a rigid structure. This dense network is very mechanically resilient, see section 3.3.2, and resistant against bacterial enzymes. [66] One may expect reduced bacterial attachment due to the enhanced properties of a chitosan glutaraldehyde cross-linked structure. [67]

A proposed mechanism for the antibacterial attachment activity for all chitosan-based films is quorum sensing inhibition. Quorum sensing (QS) is a mechanism of communication between microorganisms that leads to the process of biofilm formation. It is dependent on the constant secretion of signalling molecules into the bacterial environment. QS is a primary function that is vital for the regulation of cell processes such as the formation of biofilms or virulence factors. [68, 69] The increment in the resistance of microbes to antibiotics has led to research into other antimicrobial therapies such as reagents that block QS communication between microbes. [70] Based on this approach, cationic chitosan molecules have the ability to interact with the negatively charged surfaces of bacterial cell walls and inhibit the communication signalling molecules. This would lead to a delay in the formation of biofilms and reduced bacterial attachment. [71, 72]

6.3.4 Bacterial growth

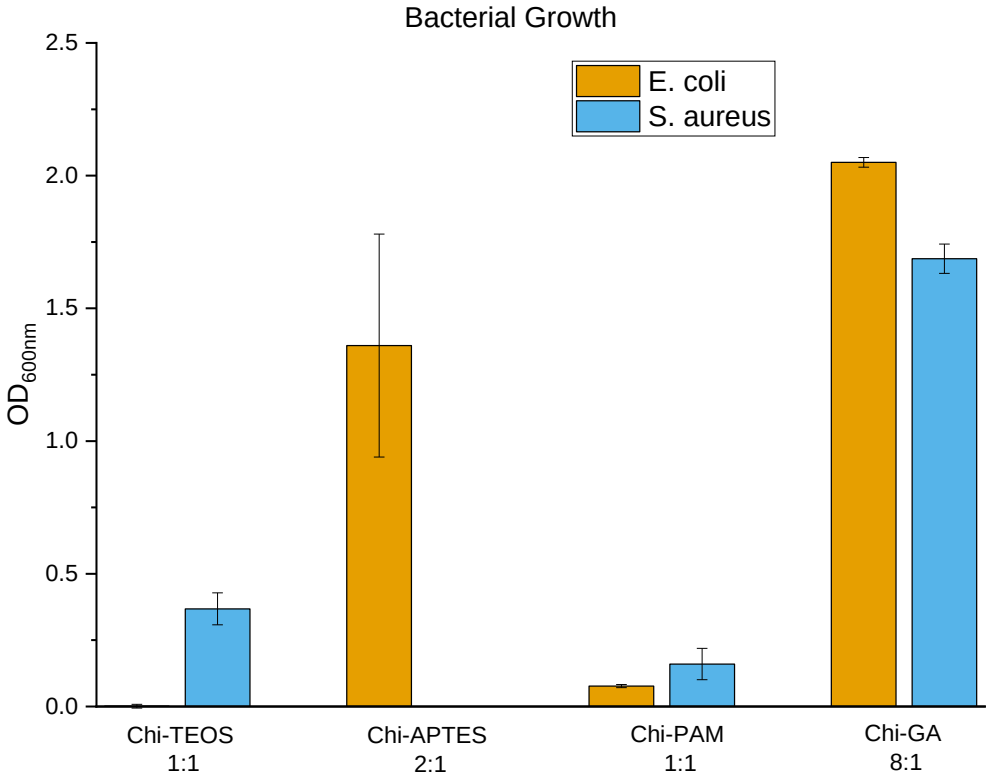


Figure 6.8: OD_{600nm} values for bacterial growth on all samples

For all cases with an acid aqueous medium, we can expect the -NH_2 groups in chitosan to be protonated to -NH_3^+ cations to some extent. The electrostatic interactions between the -NH_3^+ group and the polysaccharides on the cell membrane of *E. Coli* or the teichoic acids on the cell wall of *S. Aureus* will lead to an uneven distribution of negative charge on the bacteria. [73] This results in an imbalance between cell wall synthesis and dissolution, causing the cell membrane to become deformed, leading to rupture via osmotic pressure and eventual cell lysis or death. [74] The Chi-APTES (2:1) and Chi-GA (8:1) samples were in basic aqueous mediums for *E. Coli* specifically. This factor accounts for the high OD values for *E. Coli* in both attachment and growth studies, and the high degree of variability in the data. With no cationic interactions between the bacteria and the samples, the *E. Coli* is free to thrive in the basic medium, as indicated by the pH measurements of bacterial cultures in section 6.3.1.

The most bacterial growth occurred on the Chi-GA samples, for which an explanation of the behaviour of the *E. Coli* samples is given above. The high degree of bacterial growth for the *S. Aureus* samples may be explained by the inert nature of the chitosan glutaraldehyde cross-linked polymer blend. While the antibacterial activity of glutaraldehyde is well known, [75-77] the chemical structure changes when it cross-links with chitosan. [78]

For the Chi-TEOS (1:1) samples, while both *E. Coli* and *S. Aureus* mediums were acidic, the *E. Coli* pH was 6.5 and the *S. Aureus* pH was 5.5. The difference in acidity may have affected the bacterial growth in the presence of the films. From the pH studies in section 6.3.1, it may be seen that *S. Aureus* metabolises a lower pH than *E. Coli*. In fact, *S. Aureus* is able to survive in many different acidic environments. [79] In an acidic environment, a chitosan-based film is expected to swell as the chitosan molecules become uncoiled and assume a more elongated shape. [80] However, the TEOS siloxane polymer has a rigid frame and does not swell in accordance with pH. The combination of the two polymer networks allows the composite to swell and shrink with increased structural integrity. Park et al. [81] reported that the swelling of a chitosan-TEOS network caused the chitosan to block the pores of the TEOS network, reducing drug permeability through the membrane. They do, however, acknowledge that film permeation may also increase with swelling at an acidic pH. [82] The decrease in permeability in a more acidic pH may account for the higher rate of growth for *S. Aureus* than *E. Coli* on the Chi-TEOS (1:1) films due to less film surface area having access to bacterial cells. This is one explanation, but an equally plausible explanation may simply be related to the thicker cell walls of the Gram-positive bacteria having more of a resistance against the electrostatic forces from the $-NH_3^+$ groups present on chitosan, as discussed earlier.

6.4 Conclusions

While the results are consistent with the proposed structure of the composite films, more experiments are needed to strengthen the quality statistics of the data. The work carried out was preliminary and serves as an indication of the potential antibacterial and/or anti-attachment activity of the 4 chitosan-based films against *E. coli* and *S. aureus*.

The most likely mechanism for the antibacterial/anti-attachment activity of the chitosan-based films are electrostatic interactions between protonated -NH_2 groups from the chitosan chain, and the negatively charged bacterial cell walls. This is predicted to cause an imbalance of charge density across the cell surface, leading to cell rupture from osmotic pressure and eventual cell death. [60]

The Chi-TEOS (1:1) films displayed promising anti-attachment and anti-growth properties. Excluding the results for the Chi-PAM films, the Chi-TEOS were the most effective.

The Chi-PAM (1:1) films appeared to be the most effective against both bacteria, but the occurrence of bacterial growth in the control samples suggests it was contaminated. As such, the Chi-PAM (1:1) films cannot be properly evaluated and further work is needed to accurately test the antibacterial properties of the material.

The Chi-APTES (2:1) films displayed good antibacterial properties against *S. aureus* but not *E. coli*. The *E. coli* samples were in a basic solution, preventing the protonation of the -NH_2 groups and reducing the electrostatic interactions between the films and the bacterial cell walls. The pH of the solution will therefore need to be carefully monitored and corrected as necessary, in future experiments.

The Chi-GA (8:1) film experiments may also have suffered from the basic pH solution described for Chi-APTES. Specifically, the *E. coli* samples had a pH of 8 so the potential antibacterial activity would have been reduced. The low level of attachment but high level of growth for *S. aureus* may be attributed to Schiff base linkages occupying the active -NH_2 sites and reducing electrostatic interactions.

As discussed in section 6.1.2, many different antibacterial materials exist. For future studies, it may be effective to incorporate these materials into the chitosan film synthesis, with a focus on toxicity and mechanical strength. Combining silver

nanoparticles with chitosan is a promising approach to the development of antibacterial films. The -NH_2 groups on chitosan could coordinate with the silver metal ions and create multilayers of silver nanoparticles. [83] By pairing the antibacterial properties of both chitosan and silver ions, and fine-tuning the mechanical strength with cross-linking agents, the development of antibacterial chitosan-based films could play an important role in future biomedical applications.

References

1. Patel, M.B., et al., *Synthesis, characterization, and antimicrobial activity of acrylic copolymers.* Journal of Applied Polymer Science, 2003. **89**(4): p. 895-900.
2. Ranucci, E. and P. Ferruti, *NEW BASIC MULTIFUNCTIONAL POLYMERS .5. POLY(ESTERTHIOETHERAMINE)S BY POLYADDITION OF 2,2'-ALKYLENEDIIMINO DIETHANETHIOLS TO BISACRYLIC AND BISMETHACRYLIC ESTERS.* Polymer, 1991. **32**(15): p. 2876-2879.
3. Luo, H., et al., *Polymeric antibacterial materials: design, platforms and applications.* Journal of Materials Chemistry B, 2021. **9**(12): p. 2802-2815.
4. Alberts, B. and I. National Center for Biotechnology, *Molecular Biology of the Cell*. 2004: Garland.
5. GM, C., *The Origin and Evolution of Cells*, in *The Cell: A Molecular Approach*. 2000, Sunderland (MA): Sinauer Associates: https://www.ncbi.nlm.nih.gov/books/NBK9841/.
6. Anderson, R., et al., *Antibacterial Agents: Chemistry, Mode of Action, Mechanisms of Resistance and Clinical Applications*. 2012: Wiley.
7. Rothschild, L.J. and R.L. Mancinelli, *Life in extreme environments.* Nature, 2001. **409**(6823): p. 1092-1101.
8. Hayat, R., et al., *Soil beneficial bacteria and their role in plant growth promotion: a review.* Annals of Microbiology, 2010. **60**(4): p. 579-598.
9. Sant'Ana, A.S., et al., *FRUITS AND VEGETABLES | Introduction*, in *Encyclopedia of Food Microbiology (Second Edition)*, C.A. Batt and M.L. Tortorello, Editors. 2014, Academic Press: Oxford. p. 972-982.
10. Rowthu, S. and P. Hoffmann, *Chapter 3 - Versatile micro- and nanotexturing techniques for antibacterial applications*, in *Functional Nanostructured Interfaces for Environmental and Biomedical Applications*, V. Dinca and M.P. Suchea, Editors. 2019, Elsevier. p. 27-62.
11. Maier, R.M., *Chapter 3 - Bacterial Growth*, in *Environmental Microbiology (Second Edition)*, R.M. Maier, I.L. Pepper, and C.P. Gerba, Editors. 2009, Academic Press: San Diego. p. 37-54.

12. Snyder, L.R., et al., *Molecular Genetics of Bacteria*. ASM Books. 2014: Wiley.
13. Kim, J.H., et al., *Gram-negative and Gram-positive bacterial extracellular vesicles.* Seminars in Cell & Developmental Biology, 2015. **40**: p. 97-104.
14. contributors, W.C. *File:Staphylococcus aureus VISA 2.jpg*. 2020 26 April 2022 15:13 UTC]; https://commons.wikimedia.org/w/index.php?title=File:Staphylococcus_aureus_VISA_2.jpg&oldid=511845454].
15. contributors, W.C. *File:Scanning electron micrograph of an E. coli colony.jpg*. 2020 26 April 2022 15:19 UTC]; https://commons.wikimedia.org/w/index.php?title=File:Scanning_electron_micrograph_of_an_E._coli_colony.jpg&oldid=498593775].
16. Mauter, M.S., et al., *Antifouling Ultrafiltration Membranes via Post-Fabrication Grafting of Biocidal Nanomaterials.* Acs Applied Materials & Interfaces, 2011. **3**(8): p. 2861-2868.
17. Liong, M., et al., *Antimicrobial Activity of Silver Nanocrystals Encapsulated in Mesoporous Silica Nanoparticles.* Advanced Materials, 2009. **21**(17): p. 1684-+.
18. Rai, M.K., et al., *Silver nanoparticles: the powerful nanoweapon against multidrug-resistant bacteria.* Journal of Applied Microbiology, 2012. **112**(5): p. 841-852.
19. Duncan, T.V., *Applications of nanotechnology in food packaging and food safety: Barrier materials, antimicrobials and sensors.* Journal of Colloid and Interface Science, 2011. **363**(1): p. 1-24.
20. Kim, J.S., et al., *Antimicrobial effects of silver nanoparticles.* Nanomedicine-Nanotechnology Biology and Medicine, 2007. **3**(1): p. 95-101.
21. Shrivastava, S., et al., *Characterization of enhanced antibacterial effects of novel silver nanoparticles.* Nanotechnology, 2007. **18**(22).
22. AshaRani, P.V., et al., *Cytotoxicity and Genotoxicity of Silver Nanoparticles in Human Cells.* Acs Nano, 2009. **3**(2): p. 279-290.
23. Kim, Y.S., et al., *Twenty-eight-day oral toxicity, genotoxicity, and gender-related tissue distribution of silver nanoparticles in Sprague-Dawley rats.* Inhalation Toxicology, 2008. **20**(6): p. 575-583.

24. Worley, S.D. and G. Sun, *Biocidal polymers.* Trends in Polymer Science, 1996. **4**(11): p. 364-370.
25. Baveja, J.K., et al., *Furanones as potential anti-bacterial coatings on biomaterials.* Biomaterials, 2004. **25**(20): p. 5003-5012.
26. Jiang, H.Q., et al., *Plasma-enhanced deposition of silver nanoparticles onto polymer and metal surfaces for the generation of antimicrobial characteristics.* Journal of Applied Polymer Science, 2004. **93**(3): p. 1411-1422.
27. Kenawy, E.R., S.D. Worley, and R. Broughton, *The chemistry and applications of antimicrobial polymers: A state-of-the-art review.* Biomacromolecules, 2007. **8**(5): p. 1359-1384.
28. Yoshimoto, K., et al., *Non-Fouling Character of Poly 2-(methacryloyloxy)ethyl Phosphorylcholine -Modified Gold Surfaces Fabricated by the 'Grafting to' Method: Comparison of its Protein Resistance with Poly(ethylene glycol)-Modified Gold Surfaces.* Macromolecular Rapid Communications, 2009. **30**(24): p. 2136-2140.
29. Ishihara, K., et al., *REDUCED THROMBOGENICITY OF POLYMERS HAVING PHOSPHOLIPID POLAR GROUPS.* Journal of Biomedical Materials Research, 1990. **24**(8): p. 1069-1077.
30. Krishnan, S., C.J. Weinman, and C.K. Ober, *Advances in polymers for anti-biofouling surfaces.* Journal of Materials Chemistry, 2008. **18**(29): p. 3405-3413.
31. Magin, C.M., S.P. Cooper, and A.B. Brennan, *Non-toxic antifouling strategies.* Materials Today, 2010. **13**(4): p. 36-44.
32. Xiang, L., et al., *Related Environmental Problems and Research Progresses of Quaternary Ammonium Compounds (QACs).* Progress in Chemistry, 2016. **28**(5): p. 727-736.
33. Hora, P.I., et al., *Increased Use of Quaternary Ammonium Compounds during the SARS-CoV-2 Pandemic and Beyond: Consideration of Environmental Implications.* Environmental Science & Technology Letters, 2020. **7**(9): p. 622-631.
34. Bourtoom, T. and M.S. Chinnan, *Preparation and properties of rice starch-chitosan blend biodegradable film.* Lwt-Food Science and Technology, 2008. **41**(9): p. 1633-1641.

35. Rathinam, K., et al., *An environmentally-friendly chitosan-lysozyme biocomposite for the effective removal of dyes and heavy metals from aqueous solutions.* Carbohydrate Polymers, 2018. **199**: p. 506-515.
36. Ngah, W.S.W., L.C. Teong, and M. Hanafiah, *Adsorption of dyes and heavy metal ions by chitosan composites: A review.* Carbohydrate Polymers, 2011. **83**(4): p. 1446-1456.
37. Zheng, L.Y. and J.A.F. Zhu, *Study on antimicrobial activity of chitosan with different molecular weights.* Carbohydrate Polymers, 2003. **54**(4): p. 527-530.
38. Kingkaew, J., et al., *Effect of molecular weight of chitosan on antimicrobial properties and tissue compatibility of chitosan-impregnated bacterial cellulose films.* Biotechnology and Bioprocess Engineering, 2014. **19**(3): p. 534-544.
39. Younes, I., et al., *Influence of acetylation degree and molecular weight of homogeneous chitosans on antibacterial and antifungal activities.* International Journal of Food Microbiology, 2014. **185**: p. 57-63.
40. Mellegard, H., et al., *Antibacterial activity of chemically defined chitosans: Influence of molecular weight, degree of acetylation and test organism.* International Journal of Food Microbiology, 2011. **148**(1): p. 48-54.
41. Meng, X.T., et al., *Molecular weight and pH effects of aminoethyl modified chitosan on antibacterial activity in vitro.* International Journal of Biological Macromolecules, 2012. **50**(4): p. 918-924.
42. Li, J.H., Y.G. Wu, and L.Q. Zhao, *Antibacterial activity and mechanism of chitosan with ultra high molecular weight.* Carbohydrate Polymers, 2016. **148**: p. 200-205.
43. Kong, M., et al., *Antimicrobial properties of chitosan and mode of action: A state of the art review.* International Journal of Food Microbiology, 2010. **144**(1): p. 51-63.
44. Ma, Z.X., A. Garrido-Maestu, and K.C. Jeong, *Application, mode of action, and in vivo activity of chitosan and its micro and nanoparticles as antimicrobial agents: A review.* Carbohydrate Polymers, 2017. **176**: p. 257-265.
45. Krajewska, B., P. Wydro, and A. Janczyk, *Probing the Modes of Antibacterial Activity of Chitosan. Effects of pH and Molecular Weight on Chitosan*

Interactions with Membrane Lipids in Langmuir Films. Biomacromolecules, 2011. **12**(11): p. 4144-4152.

46. Costa, E.M., et al., *Evaluation and insights into chitosan antimicrobial activity against anaerobic oral pathogens.* Anaerobe, 2012. **18**(3): p. 305-309.
47. Liu, H., et al., *Chitosan kills bacteria through cell membrane damage.* International Journal of Food Microbiology, 2004. **95**(2): p. 147-155.
48. Marquez, I.G., et al., *Disruption of protein synthesis as antifungal mode of action by chitosan.* International Journal of Food Microbiology, 2013. **164**(1): p. 108-112.
49. Fernandez-Saiz, P., J.M. Lagaron, and M.J. Ocio, *Optimization of the biocide properties of chitosan for its application in the design of active films of interest in the food area.* Food Hydrocolloids, 2009. **23**(3): p. 913-921.
50. Silhavy, T.J., D. Kahne, and S. Walker, *The Bacterial Cell Envelope.* Cold Spring Harbor Perspectives in Biology, 2010. **2**(5).
51. Devlieghere, F., A. Vermeulen, and J. Debevere, *Chitosan: antimicrobial activity, interactions with food components and applicability as a coating on fruit and vegetables.* Food Microbiology, 2004. **21**(6): p. 703-714.
52. Xiao, B., et al., *Preparation and characterization of antimicrobial chitosan-N-arginine with different degrees of substitution.* Carbohydrate Polymers, 2011. **83**(1): p. 144-150.
53. Runarsson, O.V., et al., *Antibacterial activity of N-quaternary chitosan derivatives: Synthesis, characterization and structure activity relationship (SAR) investigations.* European Polymer Journal, 2010. **46**(6): p. 1251-1267.
54. El-Shafei, A.M., et al., *Antibacterial activity of cationically modified cotton fabric with carboxymethyl chitosan.* Journal of Applied Polymer Science, 2008. **110**(3): p. 1289-1296.
55. Shanmugam, A., K. Kathiresan, and L. Nayak, *Preparation, characterization and antibacterial activity of chitosan and phosphorylated chitosan from cuttlebone of Sepia kobiensis (Hoyle, 1885).* Biotechnology Reports, 2016. **9**: p. 25-30.
56. Abbasipour, M., et al., *Coated Cotton Gauze with Ag/ZnO/chitosan Nanocomposite as a Modern Wound Dressing.* Journal of Engineered Fibers and Fabrics, 2014. **9**(1): p. 124-130.

57. Kesari, R. and V.K. Gupta, *A sensitive spectrophotometric method for the determination of dithiocarbamate fungicide and its application in environmental samples.* Talanta, 1998. **45**(6): p. 1097-1102.
58. Hou, X.X., et al., *Effects of Bleaching Associated with Er:YAG and Nd:YAG Laser on Enamel Structure and Bacterial Biofilm Formation.* Scanning, 2021. **2021**.
59. Zivanovic, S., et al., *Physical, mechanical, and antibacterial properties of chitosan/PEO blend films.* Biomacromolecules, 2007. **8**(5): p. 1505-1510.
60. Rabea, E.I., et al., *Chitosan as antimicrobial agent: Applications and mode of action.* Biomacromolecules, 2003. **4**(6): p. 1457-1465.
61. Tsai, G.J. and W.H. Su, *Antibacterial activity of shrimp chitosan against Escherichia coli.* Journal of Food Protection, 1999. **62**(3): p. 239-243.
62. Zhong, Z.M., et al., *Synthesis of acyl thiourea derivatives of chitosan and their antimicrobial activities in vitro.* Carbohydrate Research, 2008. **343**(3): p. 566-570.
63. Helander, I.M., et al., *Chitosan disrupts the barrier properties of the outer membrane of Gram-negative bacteria.* International Journal of Food Microbiology, 2001. **71**(2-3): p. 235-244.
64. Mohamed, N.A. and N.A. Abd El-Ghany, *Synthesis, Characterization, and Antimicrobial Activity of Carboxymethyl Chitosan-Graft-Poly(N-acryloyl, N '-cyanoacetohydrazide) Copolymers.* Journal of Carbohydrate Chemistry, 2012. **31**(1-3): p. 220-240.
65. Eaton, P., et al., *Atomic force microscopy study of the antibacterial effects of chitosans on Escherichia coli and Staphylococcus aureus.* Ultramicroscopy, 2008. **108**(10): p. 1128-1134.
66. McConnell, E.L., S. Murdan, and A.W. Basit, *An investigation into the digestion of chitosan (noncross-linked and cross-linked) by human colonic bacteria.* Journal of Pharmaceutical Sciences, 2008. **97**(9): p. 3820-3829.
67. Li, B., et al., *Synthesis, Characterization, and Antibacterial Activity of Cross-Linked Chitosan-Glutaraldehyde.* Marine Drugs, 2013. **11**(5): p. 1534-1552.
68. Defoirdt, T., *Quorum-Sensing Systems as Targets for Antivirulence Therapy.* Trends in Microbiology, 2018. **26**(4): p. 313-328.

69. Papenfort, K. and B.L. Bassler, *Quorum sensing signal-response systems in Gram-negative bacteria.* Nature Reviews Microbiology, 2016. **14**(9): p. 576-588.
70. Paluch, E., et al., *Prevention of biofilm formation by quorum quenching.* Applied Microbiology and Biotechnology, 2020. **104**(5): p. 1871-1881.
71. Muslim, S.N., et al., *Chitosan extracted from Aspergillus flavus shows synergistic effect, eases quorum sensing mediated virulence factors and biofilm against nosocomial pathogen Pseudomonas aeruginosa.* International Journal of Biological Macromolecules, 2018. **107**: p. 52-58.
72. Rubini, D., et al., *Extracted chitosan disrupts quorum sensing mediated virulence factors in Urinary tract infection causing pathogens.* Pathogens and Disease, 2019. **77**(1).
73. Kassem, A., G.M. Ayoub, and L. Malaeb, *Antibacterial activity of chitosan nano-composites and carbon nanotubes: A review.* Science of the Total Environment, 2019. **668**: p. 566-576.
74. Li, Z.H., F. Yang, and R.D. Yang, *Synthesis and characterization of chitosan derivatives with dual-antibacterial functional groups.* International Journal of Biological Macromolecules, 2015. **75**: p. 378-387.
75. King, J.A., W. Woodside, and P.V. McGucken, *RELATIONSHIP BETWEEN PH AND ANTIBACTERIAL ACTIVITY OF GLUTARALDEHYDE.* Journal of Pharmaceutical Sciences, 1974. **63**(5): p. 804-805.
76. Wu, M.C., et al., *Graphene-Based Photothermal Agent for Rapid and Effective Killing of Bacteria.* Acs Nano, 2013. **7**(2): p. 1281-1290.
77. Imazato, S., *Antibacterial properties of resin composites and dentin bonding systems.* Dental Materials, 2003. **19**(6): p. 449-457.
78. Schiffman, J.D. and C.L. Schauer, *Cross-linking chitosan nanofibers.* Biomacromolecules, 2007. **8**(2): p. 594-601.
79. Zhou, C.Y. and P.D. Fey, *The acid response network of Staphylococcus aureus.* Current Opinion in Microbiology, 2020. **55**: p. 67-73.
80. Kim, J.H., et al., *Properties and swelling characteristics of cross-linked poly(vinyl alcohol)/chitosan blend membrane.* Journal of Applied Polymer Science, 1992. **45**(10): p. 1711-1717.

81. Park, S.B., et al., *A novel pH-sensitive membrane from chitosan - TEOS IPN; preparation and its drug permeation characteristics.* Biomaterials, 2001. **22**(4): p. 323-330.
82. Singh, D.K. and A.R. Ray, *Controlled release of glucose through modified chitosan membranes.* Journal of Membrane Science, 1999. **155**(1): p. 107-112.
83. Yuan, W.Y., et al., *Self-assembled chitosan/heparin multilayer film as a novel template for in.* Colloids and Surfaces B-Biointerfaces, 2010. **76**(2): p. 549-555.

7. Demonstration of a Chitosan-Based, pH-Responsive, Smart Material for Potential Wound Dressing Applications

7.1 Introduction

This chapter describes work that was performed by Oliver James Pemble together with Dr Tomas Kohoutek, at the National Institute for Materials Science (NIMS) in Tsukuba under the direction of Professor Hiroshi Fudouzi. The aim of this work was to utilise chitosan-based films of the type described elsewhere in this thesis, together with flexible photonic crystals made using fluoro-rubber substrates combined with polystyrene spheres made at NIMS, to produce a prototype device capable of showing a visual colour change in response to a change in pH. It is proposed that this type of device could be of particular use as a sensor in the monitoring of chronic wounds, in so-called 'smart' wound dressings, which are described in the following sections.

7.2 Introduction to smart wound dressings

Wound dressing development has become a billion-dollar enterprise around the world as medical technology advances in many promising ways. [1, 2] A wound dressing can be classified as a material that covers a wound to protect it from damage and promote healing. [3] To date, many different wound dressings have been developed for various specific wounds, [4-6] but they are still limited with regards to functionality. For example, most current clinical wound dressings cannot adjust their properties as the wound condition changes and redressing prematurely can cause more damage to the affected area. Any abnormal changes that may occur in the wound healing process can lead to the development of chronic wounds. [7] Smart wound dressings can in principle, not only detect, but also treat these issues, and there is a growing need to reduce the burden chronic wounds can have on a patient's quality of life. [8]

7.2.1 What are smart wound dressings?

Smart wound dressings can interact with, sense, and react to the wound condition or environment via the use of built-in sensors or smart materials. The different stages of the wound healing process each display specific characteristics and physiological reactions. [7, 9] Smart wound dressings are expected to take care of the needs of each stage and give an effective response to these reactions. A number of different types of smart wound dressing, such as monitoring, [10, 11] self-healing, [12] stimuli response, [13] and biomechanical [14] have been developed over the years. In particular, a pH sensitive smart wound dressing would be very effective in detecting the condition of chronic wounds. [15] There is a clear need for smart wound dressings equipped with physical and/or biochemical sensors that can determine and communicate the wound status in a cost effective and non-invasive manner. [16]

7.2.2 Chronic wounds

In chronic wounds, the physiological balance between tissue degradation and tissue regeneration is lost. As a result, destructive catabolic metabolism predominates, and proteolytic enzymes continue to break down protein in the tissue, hindering the healing process. Eventually when the healing is allowed to progress, the physiological balance is restored and the enzyme activity diminishes. [17] As a chronic wound heals, the pH of the affected area and surrounding tissue can fluctuate, prolonging the injury and causing discomfort for the individual. Figure 7.1 summarises the current data for the pH environment of chronic wounds. [17]

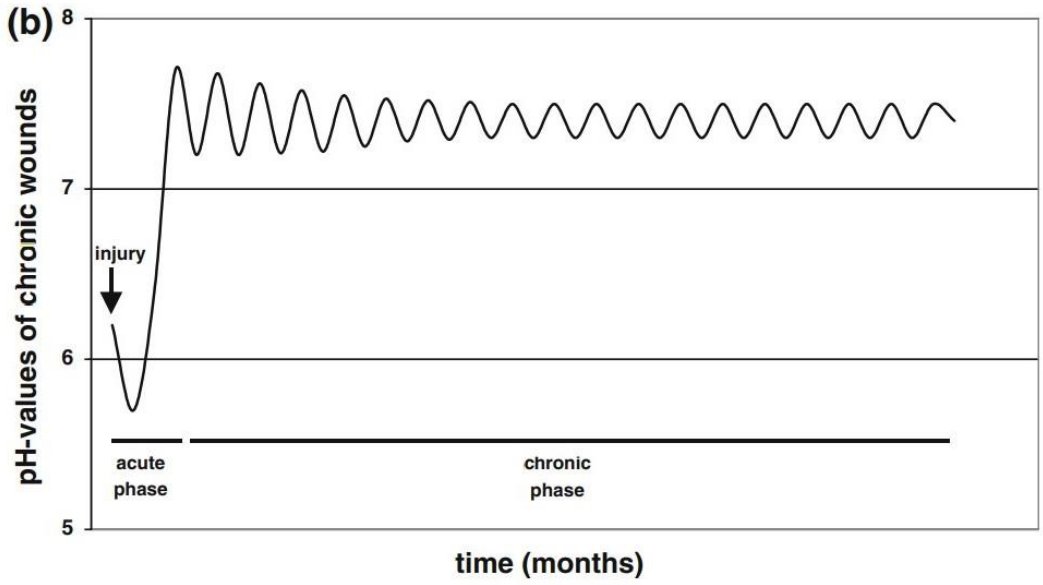


Figure 7.1: Typical variations in the pH environment ranging from healthy skin (4-6 pH) [18] to chronic wounds (7-8 pH). The pH value is a rapidly dynamic factor in chronic wounds that can change with therapeutic interventions such as cleaning or removing infected or nonviable tissue. [17]

Although there is still some debate on the pH of wounds, the widely accepted concept is that chronic wounds have a pH higher than 7, [19] but there are still a few studies that suggest the initial acute phase of the injury have a pH closer to 5.5. [20] In any case, since the pH at the wound site is different to that of the surrounding skin, researchers have made use of this pH difference to develop various pH responsive wound dressings. [13, 20-22] A simple and cost-effective method for determining pH is by using indicator dyes that absorb different wavelengths of visible light depending on the pH value. However, a challenge in using these dyes in close proximately to open wounds is that they must not leach harmful substances into the affected area. [23] Generally, pH-change-responsive wound dressings that can respond to slight variations are desirable. Hydrogels are ideal materials for detecting pH changes as they have the natural ability to swell in different pH conditions. [24] The pH responsive behaviour of hydrogels is caused by ionisable active sites in the polymer backbone. [25] When exposed to an aqueous solution of an appropriate pH, the active sites ionise resulting in the build-up of a fixed charge along the polymer chain. The generation of electrostatic repulsive forces causes water to either be absorbed or expelled, hence pH dependant swelling. [26, 27] It is this swelling principle that is the inspiration for the

use of hydrogels as pH sensitive indicators in wound dressings. Two particular examples of this approach are described briefly here.

Sridhar et al. [28] developed a continuous pH monitor designed to be embedded into a wound dressing. The device uses a pair of wire coils which sandwiched a pH-sensitive poly(vinyl alcohol)–poly(acrylic acid) hydrogel. As the hydrogel swells and de-swells with pH, the distance between the two coils changes, resulting in a change of inductance which is picked up by a wireless link. Wang et al. [13] developed a pH responsive wound dressing using a pH-switchable antimicrobial hydrogel fabricated from peptides. The hydrogel would release antibacterial peptides into the wound at an acidic pH, reducing chronic inflammation and promoting healing. This was based on the understanding that the pH of chronic wounds drastically changes when it has been infected. [29, 30]

7.2.3 Ideal properties of smart wound dressings

A smart wound dressing needs to be robust, flexible, and biocompatible. [31] Wounds often provide an ideal environment for the growth of bacteria and microorganisms. [32] To improve the process of wound healing, a wound dressing needs to provide conditions that are unfavourable for microorganism growth. In general, dressings can protect the wound from the outside world and act as a barrier from further bacterial infections, but the composition of the dressing plays a major role in maintaining a stable healing environment. [33] Oxygen delivery is a critical element in the healing of wounds, as it is an essential nutrient for cell metabolism. Thus, a desirable characteristic of wound dressings would be effective gaseous exchange of both air and water. [34] The retention of moisture may help accelerate the healing process as moisture facilitates the production of vital health defences in the body such as macrophages. An added benefit of a moist wound environment is reduced pain during rest. [35] The mechanical properties must be compatible to the topical application of dressings while at the same time providing an environment that can adapt to the healing processes of inflammation, regeneration, and remodelling. The material should not cause a toxic response when coming into contact with the skin and should be easily metabolised and cleared from the body. [36] The functions and important characteristics of wound dressings and wound healing devices are summarised in figure 7.2.



Figure 7.2: Functions and ideal characteristics of wound dressings and devices. [37]

7.2.4 Scope of this work

The scope of this work is to design and test a proof-of-concept pH sensor with chitosan-based films, using the principle of photonic crystal colour changes as an indicator for pH changes in proximity of a chronic wound. Chitosan was chosen as an ideal hydrogel polymer with many biocompatible properties. These properties are discussed in section 1.6.

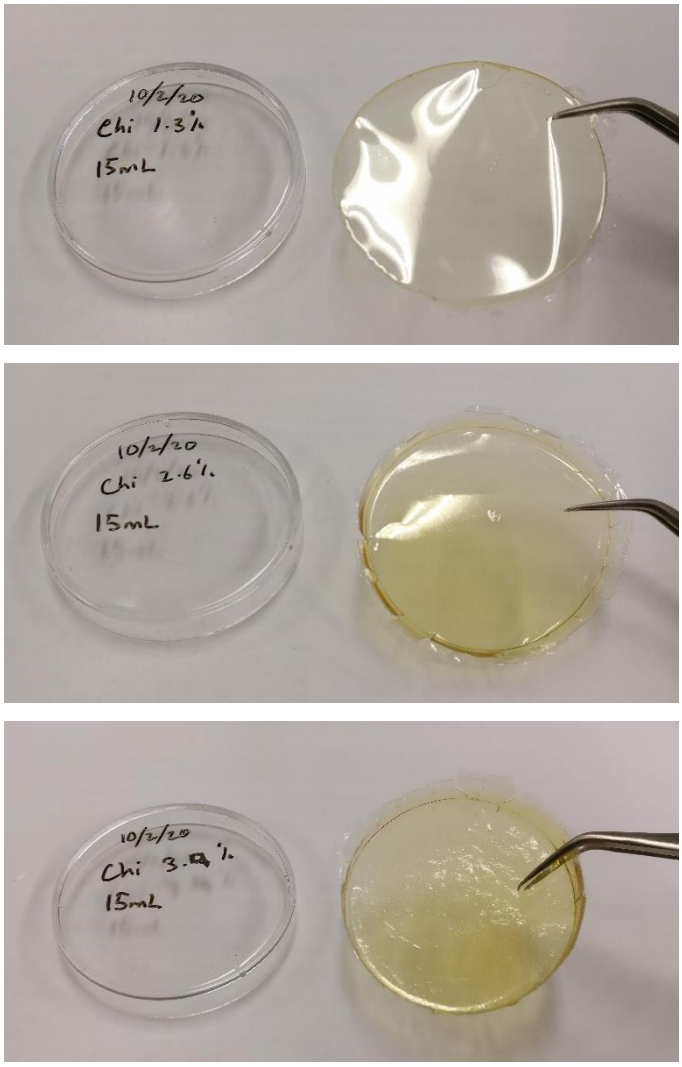
Chitosan is a natural polysaccharide with bacteriostatic, haemostatic and fungistatic properties that are very suitable for medical applications. Animal studies and human clinical trials have found that wounds treated with chitosan healed faster than wounds treated with chitosan-free dressings. [38-41] Indeed, the presence of chitosan on the surface of a wound can encourage collagen and hyaluronic acid formation as well as cell proliferation. [42] These biocompatible properties twinned with chitosan's natural swelling ability make it the most desirable material for smart wound dressing design.

Sadri et al. [43] used electrospinning to make a polymeric nanofiber of chitosan/polyethylene oxide with green tea extract and investigated its antibacterial activity as a wound dressing. Although chitosan generally has poor mechanical properties, combining it with polyethylene oxide enhanced the strength and made it suitable for a wound dressing material. [44]

In this work chitosan films were tested in neutral pH swelling experiments as part of a preliminary design for smart chronic wound dressing sensors. As well as plain chitosan, two other chitosan-based films which represent different polymer blend mechanics were tested in pH dependant swelling experiments. Both films displayed improved mechanical properties and higher tensile strength than plain chitosan films, as discussed in section 3.2.2. Chi-APTES is an example of a chitosan polymer blend in which hydrogen bonds attract the 3-aminopropyltriethoxysilane siloxane polymer chain to the chitosan polymer chain, creating a cross-linked electrostatic network. [45, 46] As well as the improved mechanical properties over chitosan, Chi-APTES membranes have promising gas permeability properties due to the disturbance of chitosan intramolecular hydrogen bonding. The introduction of the APTES siloxane chain breaks some hydrogen bonds in chitosan to form new ones, thus increasing the amorphous regions of the membrane and also the gas permeability. [47] Chi-GA is a chitosan polymer blend with cross-linked glutaraldehyde forming chemical Schiff base bonds between amino groups on the chitosan polymer. [48, 49] The chemical Schiff base bonds gives the cross-linked Chi-GA superior tensile strength over plain chitosan, [50, 51] and also may contribute to the improved hydrophobicity of the resulting material. [52]

7.3 Synthesis and characterisation of the chitosan films

The prepared chitosan hydrogel was cast and dried to produce thin free-standing films. The films were pale yellow/brown in colour, transparent and flexible, see figure 7.3.



OP1-A: Chitosan 1.3% w/v

Thickness = 90 µm ± 4.5

OP1-B: Chitosan 2.6% w/v

Thickness = 190 µm ± 9.6

OP1-C: Chitosan 3.9% w/v

Thickness = 330 µm ± 16.4

Figure 7.3: Photographs of the physical appearance of each chitosan film made with different concentrations and their average thicknesses.

As the concentration of the hydrogel increased, the colour of the film intensified, and the surface roughness appeared to be less uniform. The average film thickness appeared to have a linear relationship with the concentration of the hydrogel used to make the film, see figure 7.4. As stated in Chapter 2, any hydrogel with a concentration higher than 3.9 % w/v was deemed inappropriate for film casting due to high viscosity and non-homogeneity.

Initial concentration swelling tests were carried out on chitosan-only films. Chitosan-APTES (2:1) and chitosan-GA (8:1) films were also synthesised via the same method described in section 2.1.1 and drop cast for pH-based swelling tests.

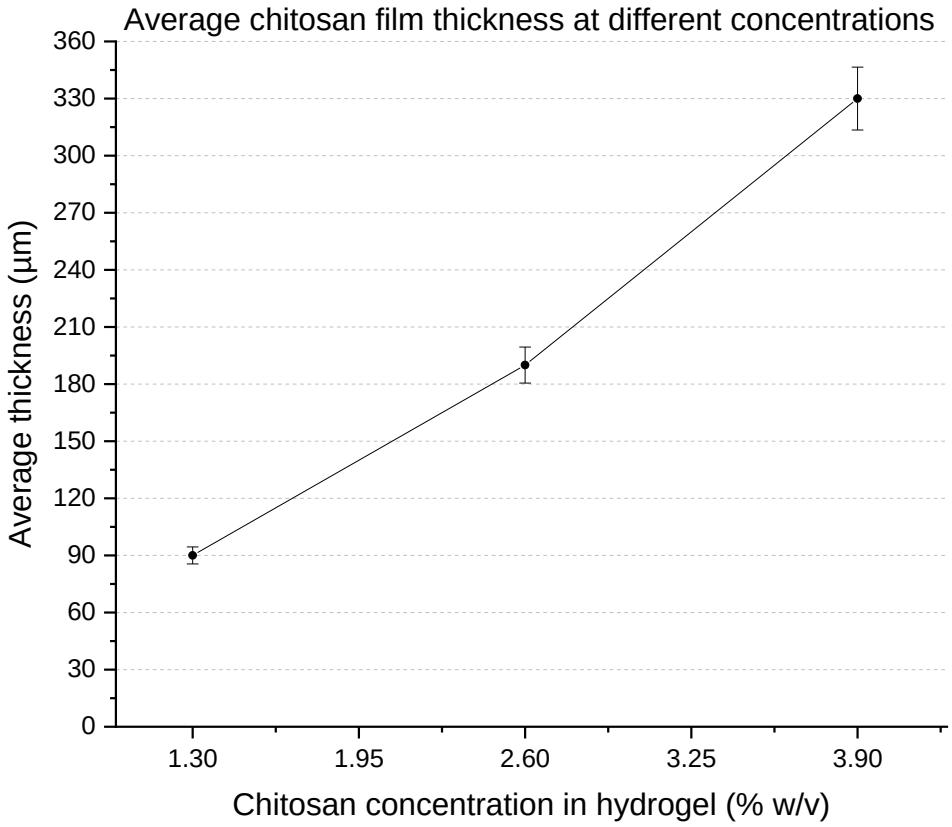


Figure 7.4: Graph of the average chitosan film thicknesses at three different concentrations: 1.3 % w/v, 2.6 % w/v, and 3.9 % w/v. Each film was measured 20 times using 293-185 -MITUTOYO Quantumike digital micrometer.

7.3.1 Swelling tests of free-standing drop-cast films

The concentration of chitosan 2.6% w/v was chosen to be the default for all films tested as it showed the most durability with a relatively flat surface area. Initial swelling studies were carried out on a loose sample cut to 1 cm x 1cm. The square sample was weighed and placed in a glass Petri dish and covered with water and left to swell for 10 minutes. The sample was weighed again after swelling and observations were recorded.

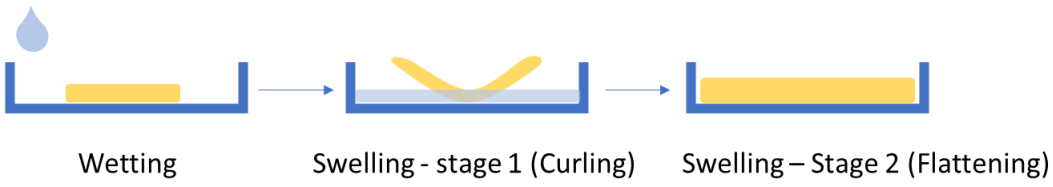


Figure 7.5: Schematic of initial swelling procedure on a free-standing chitosan film

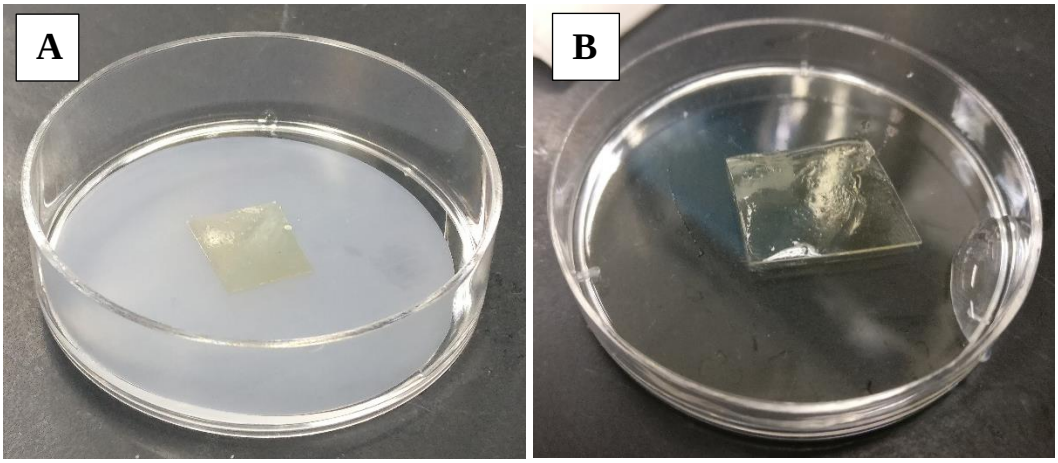


Figure 7.6: Square sample of 2.6% w/v chitosan film before swelling and dry (A) and after 10 minutes of swelling in water (B)

It was observed that the film began to curl inwards as it absorbed the water but then laid flat in the Petri dish once it had finished swelling. The dry weight of the sample before swelling was 0.017 g (thickness ~190 µm) and the weight after swelling was 0.096 g (thickness ~400 µm). The degree of deacetylation for the chitosan used was 75-85 %, which was sufficient to allow the formation of a flexible film, but not too much so the film crystallises and reduces swelling ability.

The swelling of the chitosan film is a very important factor when considering medical device applications. A higher degree of swelling can cause a decrease in elasticity and tensile strength, whereas a lower degree of swelling would limit the functionality of the critical component of the device. The swelling behaviour refers to when water molecules enter the material and bind with the hydrophilic groups in the material's molecular structure, in chitosan's case, the -NH_2 and -OH groups. The content of hydrophilic groups and the intermolecular forces are the two main factors that influence a material's swelling properties. With an increase in the degree of deacetylation (DD), more amino groups are available for water interactions, thus increasing the swelling ability. [53] However, higher numbers of intermolecular hydrogen bonds prevent water from entering the crystal regions of the material, the water content present in dry chitosan is found to be lower with a higher DD. [54] It has been well reported in literature that the swelling capacity and tendency to aggregate is dependent on the DD of chitosan. [55-57] Therefore, when performing swelling experiments on chitosan-based materials, it is important to consider the DD as it may affect the swelling efficiency. For the sake of simplicity in this current work, only one type of chitosan (lower molecular weight) with a DD of 75–85 % was used, as this was found to be optimal for thin film synthesis from a previous study. [58]

7.3.2 Synthesis of the flexible polystyrene colloidal photonic crystal films

The polystyrene (PS) colloidal photonic crystal films were synthesised via the method described in section 2.2.6.2 and left to dry on a flexible fluoro-rubber sheet (figure 7.9). Monodisperse 210 nm PS particles were synthesised by emulsion polymerisation of a styrene monomer in the presence of sodium dodecyl sulfate (SDS) as a surfactant. The full procedure is outlined by Furumi et al. [59] The PS colloid suspension was vertically deposited onto the flexible rubber substrate and covered with silicone oil to make a polystyrene photonic crystal film. The closely packed PS particles were spaced out by additional filling and curing with PDMS elastomer to allow for reversible structural colour change by elastic deformation, see figure 7.7.

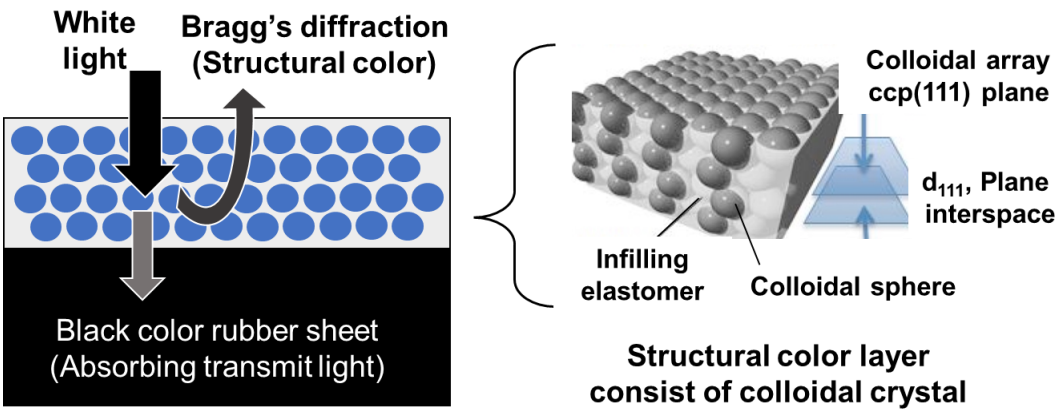


Figure 7.7: Diagram of the cubic close packed (CCP) polystyrene particles deposited on the fluoro-rubber substrate and infilled with a PDMS elastomer to expand the space between particles to allow for structural colour change by elastic deformation. Taken from work of Fudouzi et al. [60]

7.3.3 Proposed mechanism of colour change, flexible photonic crystals

The mechanism in which the colloidal photonic crystal films change colour as the chitosan-based part of the film swells is as follows:

A photonic crystal is a material that influences the propagation of photons. [61] Depending on the angle at which the light hits a material, some wavelengths cannot propagate through the material and are reflected, this is the colour that is seen. Other wavelengths may propagate, but at different angles the colour looks different.

Briefly, the wavelength of the light that is reflected by the material, which is known as the stop band or photonic band gap, is governed by the Bragg-Snell equation, (Eqn. 7.1)

$$n\lambda_s = 2D\,(\eta_{eff}^2 - \sin^2\theta)^{1/2} \qquad \text{Eqn. 7.1}$$

As implied by its name, this equation can be derived by considering a combination of Bragg's Law which may be used to describe diffraction of light under various circumstances and Snell's Law, which describes the relationship between angle of incidence and angle of refraction as light passes from one medium to another.

In this equation, n is the order of diffraction, λ_s is the wavelength of the stop band which corresponds to the observed colour of the film, η_{eff} is the effective or average refractive index estimated from a weighted combination of the refractive indices of the material that the particles are made of and the material in between the particles, θ is the angle of incidence of the light as measured from a normal to the film's surface and D is the spacing between the particles making up the film, which for a close-packed array of particles is related to the diameter of the particles d, by the simple geometric relationship D = 0.86d.

Thus, it may be seen that at any given angle of incidence, there are two factors that may influence the position of the stop band – the effective refractive index and the value of D.

The device constructed in this work consisted of a polystyrene-based colloidal photonic crystal made on a flexible rubber material, which was held in a rigid frame. A chitosan-based film was then attached to the flexible film in an arrangement where the device thus formed could be immersed in aqueous solutions of varying pH. Since it is known that under certain condition of pH the chitosan-based films would swell, this process was used to deform the flexible photonic crystal. This deformation then manifested itself as a colour change arising from a change in the position of the stop band.

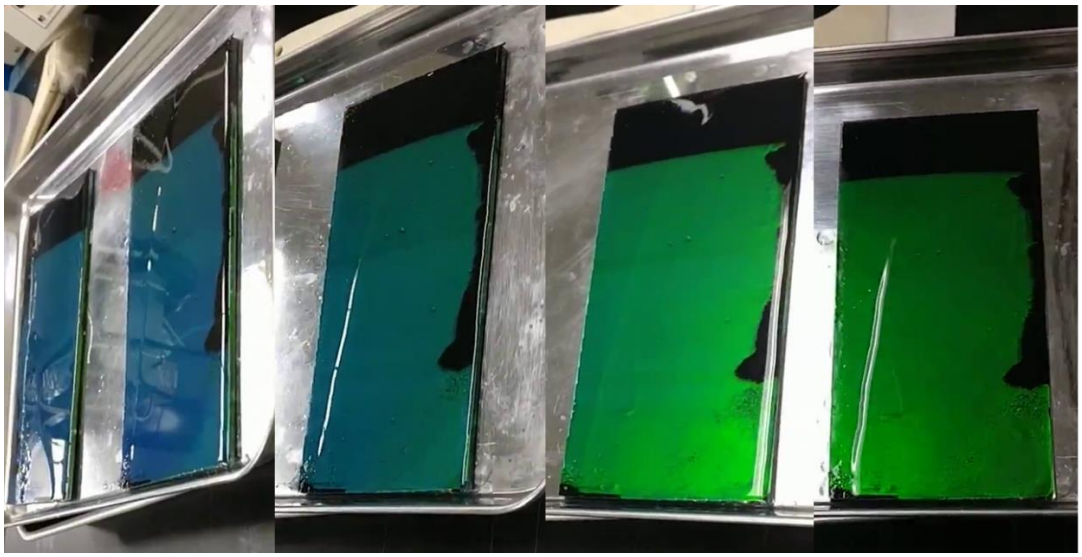


Figure 7.8: 210 nm polystyrene on a flexible rubber substrate at different angles to show the variation in the position of the stop band as a function of varying the angle of observation.

The effects of deforming these materials may be easily seen by observing the behaviour of the flexible photonic crystal when being stretched, figure 7.9 below:

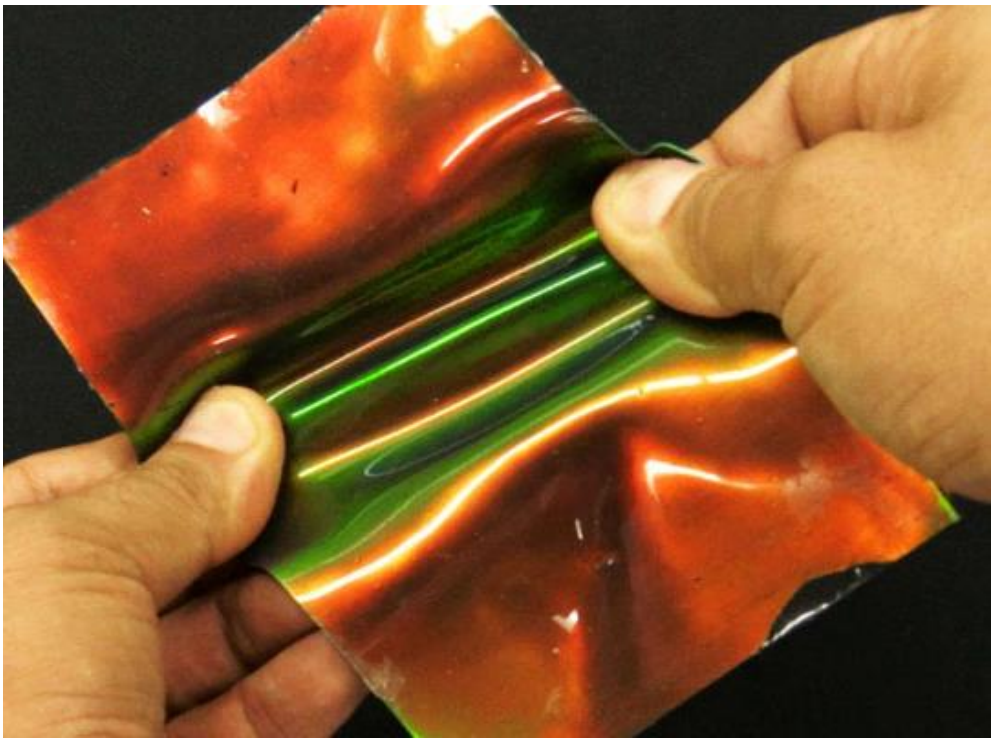


Figure 7.9: Polystyrene colloidal film successfully infilled with PDMS and dried on the flexible rubber sheet. The PDMS layer protects the colloidal film, and it can be handled without damaging the photonic crystal. Note the colour change observed from red to green as the material is being stretched which arises from the fact that the spacing between the colloidal polystyrene particles embedded in the flexible rubber decreases due to the compression resulting from the stretching. Credit: Professor Hiroshi Fudouzi, NIMS, Tsukuba, Japan.

It is the dependence of the position of the stop band of the photonic crystal on the swelling process of the underlying chitosan-based film that forms the basis of the sensor design used here. Since the swelling is pH dependent, the change in swelling associated with a change in pH can, in principle, be detected by a simple visual colour change that requires no electrical power or external sensing device.

For wound dressing applications, it is known that the pH of a wound changes when an infection sets in as described earlier. [17, 62, 63] Thus, a device of the type proposed here could provide a simple, visual indication of the presence of an infection in a wound.

7.3.4 Characterisation of the test structures

SEM was used to examine the nature of the polystyrene photonic crystal made using the approach developed at NIMS, figure 7.10 below:

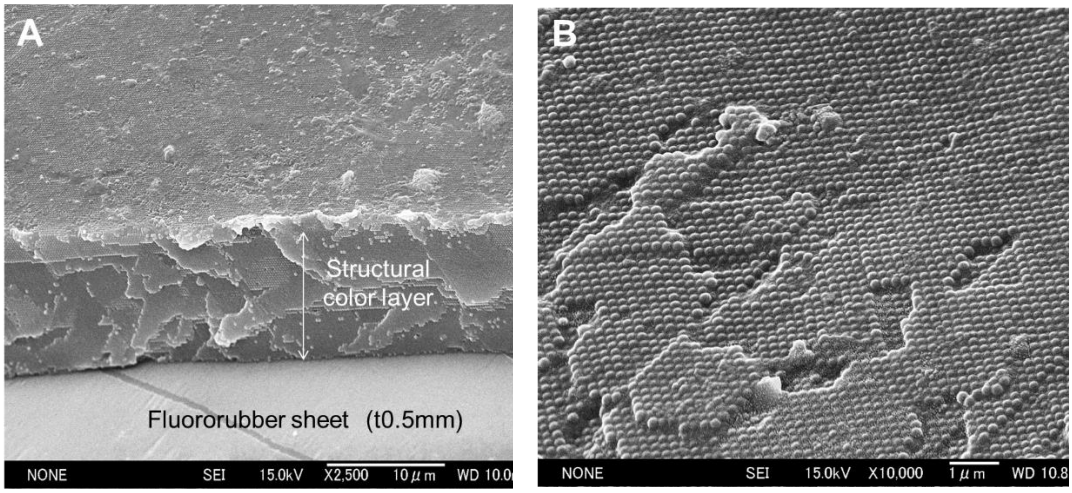


Figure 7.10: SEM images of the polystyrene colloidal film on the fluoro-rubber sheet, recorded at NIMS Professor Hiroshi Fudouzi

A hard plastic mesh served as the frame for the sensor design, which was devised by Dr Tomas Kohoutek. A framed bi-layer of 210 nm polystyrene photonic crystals on a rubber substrate and the chitosan film were fixed into the plastic mesh and stapled together, figure 7.11.

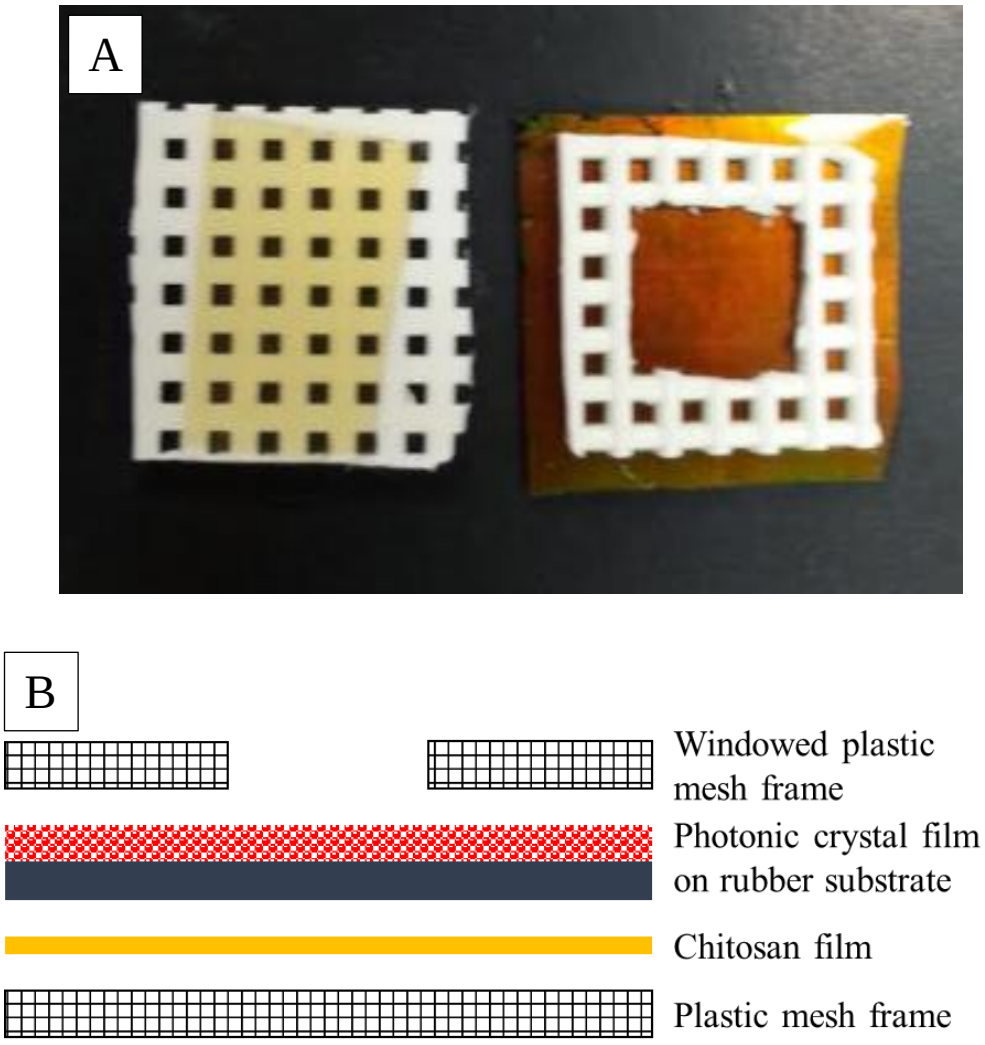


Figure 7.11: (A) The rigid plastic mesh frame with window as initial sensor design. 210 nm polystyrene photonic crystals on flexible rubber substrate with PDMS protective layer was pinned to a chitosan film in the rigid mesh frame. (B) Schematic of a cross sectional diagram of the sensor design.

7.4 Sensor testing

The sensor was allowed to swell in a glass Petri dish with water for 10 minutes. The purpose of the rigid frame was to force the chitosan film to swell in only a vertical direction and warp the photonic crystal layer, causing the colour to change.

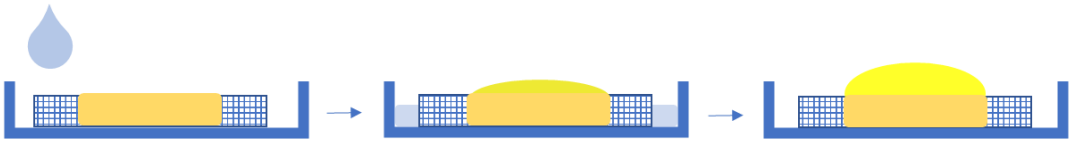


Figure 7.12: Schematic of initial swelling procedure of framed chitosan film sample with 210nm polystyrene photonic crystals on flexible rubber substrate.



Figure 7.13: Framed sample of 210 nm polystyrene photonic crystals on flexible rubber substrate with PDMS protective layer pinned to a chitosan film before swelling (left) and after swelling (right)

The framed sample began to bulge out of the frame window as it absorbed the water. The colour change from gold to green acts as an indicator that the chitosan layer was swelling, putting the flexible photonic crystal under compression in the frame, resulting in the stop band of the photonic crystal shifting from red to green due to an effective decrease in spacing between the polystyrene spheres, D, and the change in effective refractive index (see Eqn. 7.1)

7.4.1 Optical spectroscopy

Optical spectroscopy performed with a fibre-optic reflection probe was used to characterize the structural colour change of the soft colloidal crystal film during the swelling process. A photograph of the experimental set-up used in shown in figure 7.14 below:

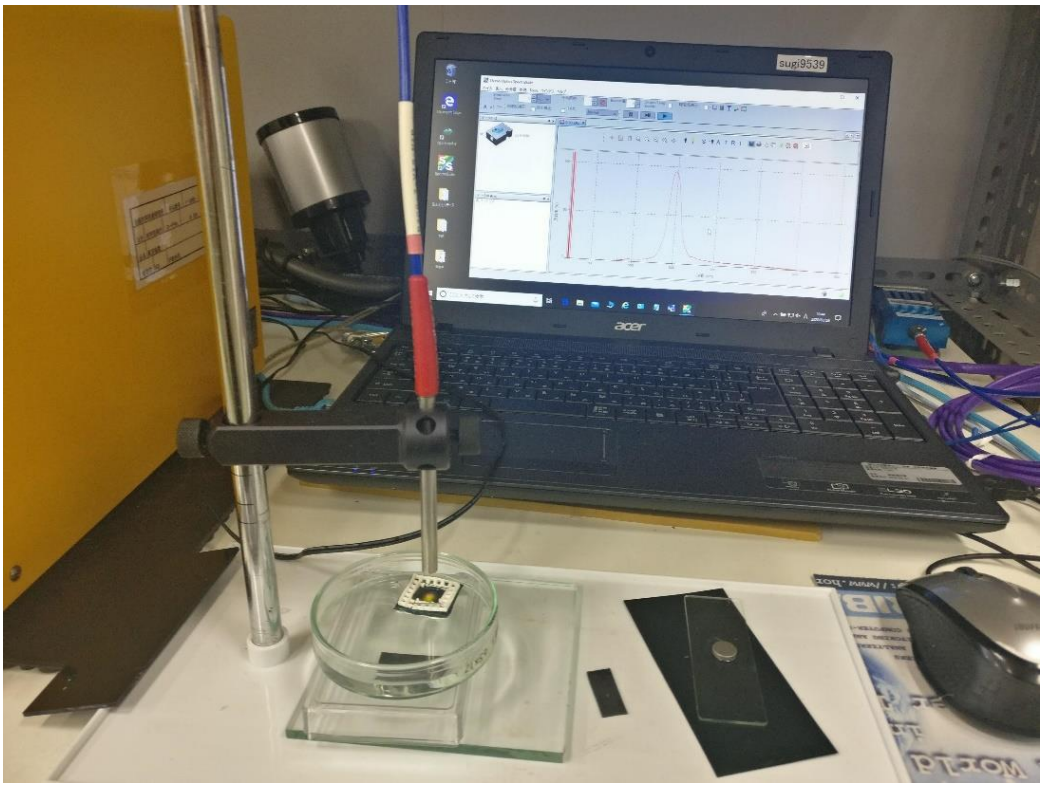


Figure 7.14: Fibre-optic reflection probe set-up with spectrometer and optical spectroscopy software.

The prototype sensor with the bi-layer of the chitosan film and 210 nm polystyrene photonic crystal film on a rubber substrate was placed in a petri dish and the stop-band peak centre on a single point was measured using the reflection probe. Water was then poured into the dish and as the film began to swell, the stop-band peak centres were measured in 5-minute intervals for 2 hours. The sensor was also tested using Chi-APTES (2:1) films and Chi-GA (8:1) films at different pH levels. A pH buffer was used to change the pH of the water for swelling.

7.5 Results – Observed variations in stop band

7.5.1 Chitosan films – neutral pH

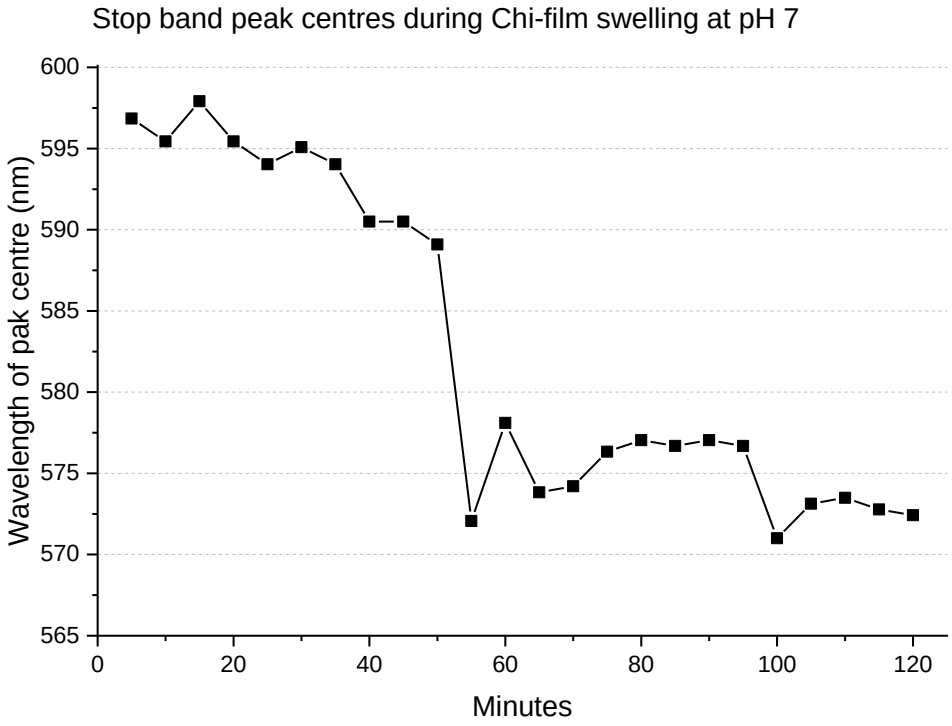


Figure 7.15: Stop-band peak centres of a 2.6% w/v chitosan film with 210 nm polystyrene photonic crystal layer on rubber substrate swelling in water over 2 hours.

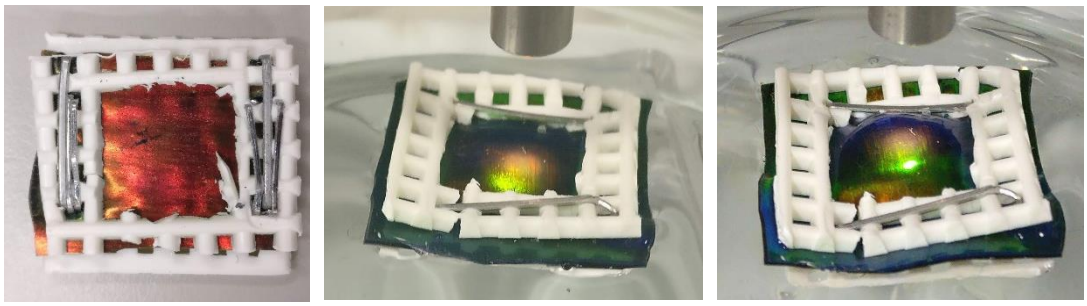


Figure 7.16: Photographs of the sensor during different periods of swelling. As the film began to swell, the centre of the sensor began to bulge out and warp the rubber substrate with photonic crystal layer.

The stop band peak centres were measured as a relative effect on a single point on the sample. Visually the swelled sample appeared to have a range of colour changes depending on the angle in which it was viewed. To avoid human error and as a way of reliably measuring a quantifiable colour change, the reflection probe measured the

stop band peak centres over the course of 2 hours. The graph in figure 7.17 shows the wavelength of light as measured by the reflection probe decreasing over the period of 2 hours from 596 nm to 572 nm. This change can be attributed to the chitosan film absorbing the water and swelling the photonic crystal layer. The colour change observed from red to green is caused by the spacing between the colloidal polystyrene particles decreasing as they are compressed by the bulging chitosan film. They are allowed to move in this manner because of the infilling of the PDMS elastomer after the photonic crystal synthesis process.

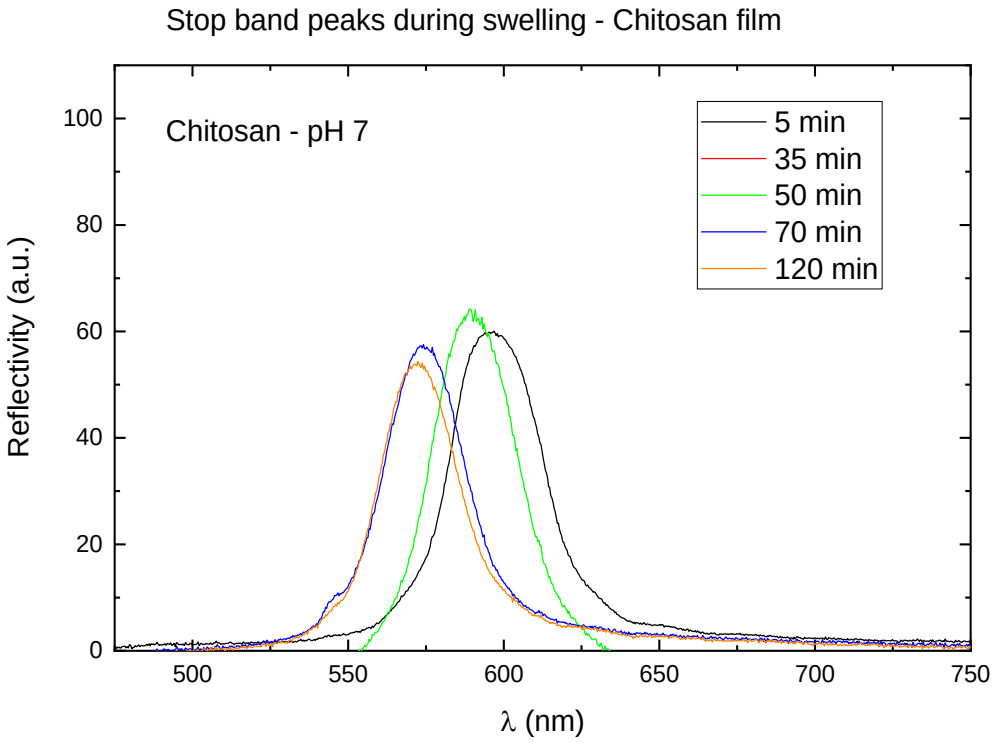


Figure 7.17: Stop band peak centres of the plain chitosan film swelling in water over a period of 2 hours.

A full list of all the stop-band peak centre graphs can be found in the appendix section A.6.

7.5.2 Chi-APTES (2:1) – variation in stop band position as a function of pH

The Chi-APTES (2:1) films were tested for their swelling ability at different pH conditions from 4.01 to 10.9. The stop band peak centres were measured over a period of 2 hours, see figure 7.18. To determine the overall swelling ability of the films, the stop band peak centres at 0 minutes and 120 minutes were recorded and the difference between the two values was classified as the swelling factor for that film, see figure 7.19.

The swelling ability for the Chi-APTES (2:1) films was found to be highest at pH 8.13 with a swelling factor of 21.88 and lowest at pH 10.9 with a swelling factor of 6.33. The chitosan films are hydrophilic so we can expect a degree of swelling to occur at neutral pH. At pH 6.86 the swelling factor was 14.09, which increased to 16.56 at pH 5.55, as expected. The $-NH_2$ groups were ionised at an acidic pH and repelled each other, causing the film to swell. The swelling factor at the lower pH value of 4.01 decreased to 15.87, which may be attributed to the shielding effect of excess H^+ ions in solution. [64] The high swelling factor at pH 8.13 may be a result of the film contracting from the deprotonation of the $-NH_3^+$ groups causing the photonic crystal layer to shrink. As the space between the particles decreases, the stop band peak centres shift to a lower wavelength. The swelling factor was affected by the films both swelling and contracting, either bulging and pushing the colloidal particles together, or shrinking and pulling them closer to each other. The same shift to a lower wavelength was observed in both scenarios, which explains the high swelling factor recorded at a basic pH value. Similarly, the very low swelling factor at pH 10.9 may be attributed to the reduction of H^+ ions, thus having little to no effect on the swelling mechanism, either contracting or bulging.

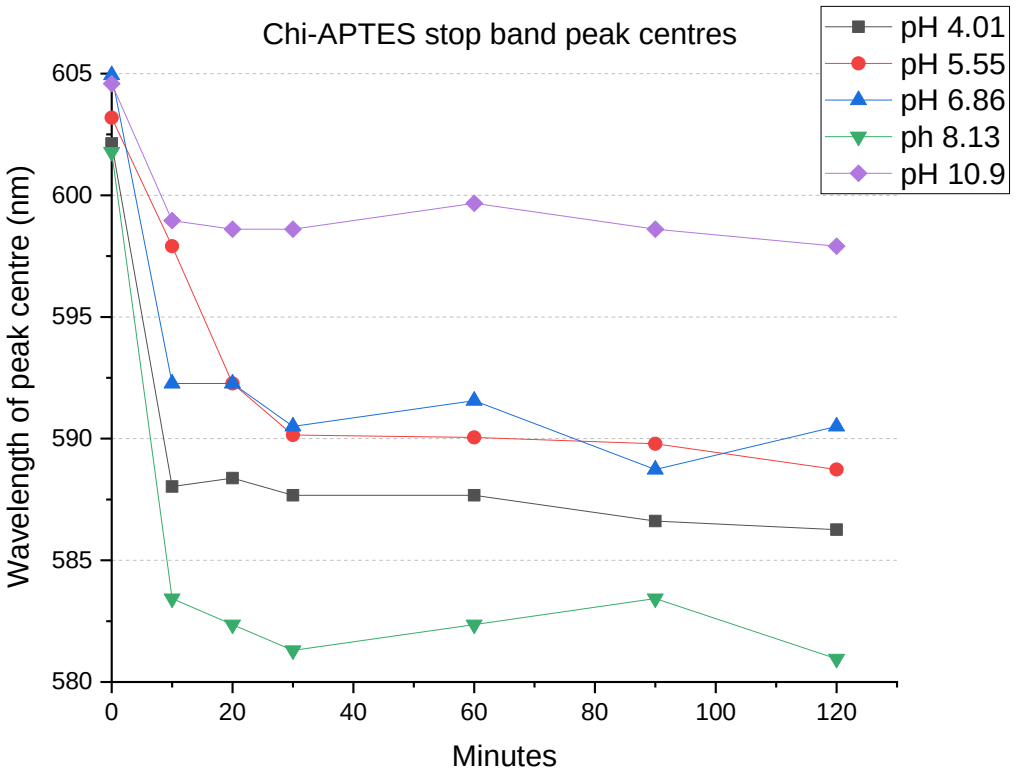


Figure 7.18: Chi-APTES (2:1) stop band peak centres during swelling at varying pH

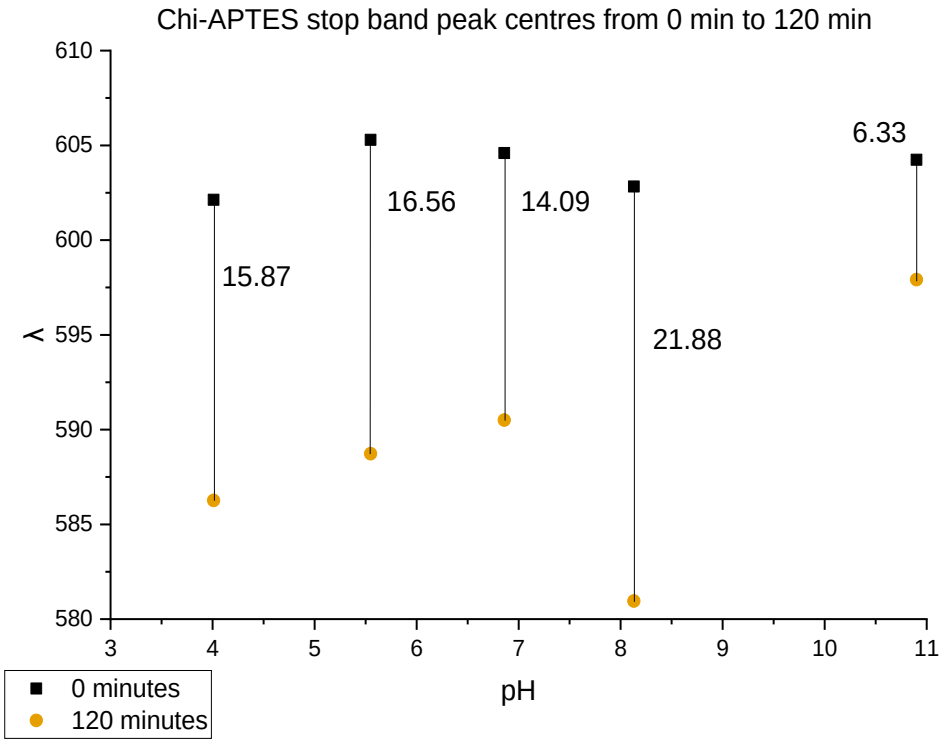


Figure 7.19: The swelling abilities of Chi-APTES (2:1) films, at different pH values, recorded from 0 minutes to 120 minutes, in order to determine the swelling factors.

7.5.3 Chi-GA (8:1) – variation in stop band position as a function of pH

The Chi-GA (8:1) films were tested for their swelling ability at different pH conditions from 4.01 to 8.13. The stop band peak centres were measured over a period of 2 hours, see figure 7.21. To determine the overall swelling ability of the films, the stop band peak centres at 0 minutes and 120 minutes were recorded and the difference between the two values was classified as the swelling factor for that film, see figure 7.22.

The swelling ability for the Chi-GA (8:1) films was found to be highest at pH 5.5 with a swelling factor of 28.37 and lowest at pH 4.01 with a swelling factor of 19.74. The same pattern of swelling for Chi-APTES can be observed in the Chi-GA samples. Again, the films are hydrophilic so some swelling at a neutral pH is expected. At pH 6.86 the swelling factor was 20.11, which increased to 28.37 at pH 5.55. The swelling factor at the lower pH value of 4.01 decreased to 19.74, which again may be attributed to the shielding effect of excess H^+ ions in solution. [64] Based on figure 7.21, it is likely that the film swelling at pH 10.9 was erroneous due to the linear decline of the wavelengths. This may have been due to a fault in the equipment, human error, or the strong basic environment breaking down the Chi-GA film. For this reason, the data for pH 10.9 is omitted from figure 7.22.

The covalent cross-linking between chitosan and glutaraldehyde form Schiff base bridges on the primary amino groups of chitosan. The apparent increase in the film swelling observed as compared to chitosan only or Chi-APTES (2:1) films can be related to the fact the cross-linking reaction promotes the chemical interconnection between chitosan polymer chains, decreasing the material mobility and hence the outward swelling degree. [65] As discussed in section 7.3.3 and section 7.5.1, the wavelengths of the stop band peak centres were decreasing due to the colloidal particles being compressed by the bulging chitosan film. Chi-GA is a tightly packed network due to the Schiff base bridges between chains so its “swelling” ability may be attributed to compression instead. In addition, cross-linking in Chi-GA (8:1) reduces the amount of free amino groups, decreasing the chitosan ability to form hydrogen bonds with water molecules and subsequently the swelling ability. [66]

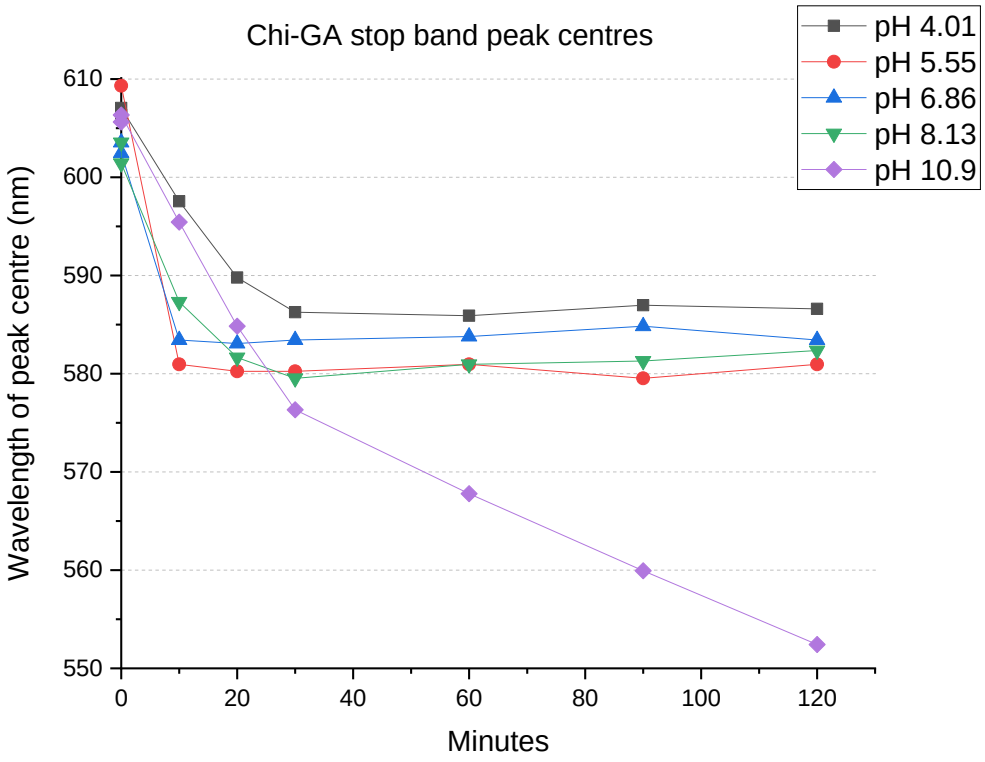


Figure 7.21: Chi-GA (8:1) stop band peak centres during swelling at varying pH.

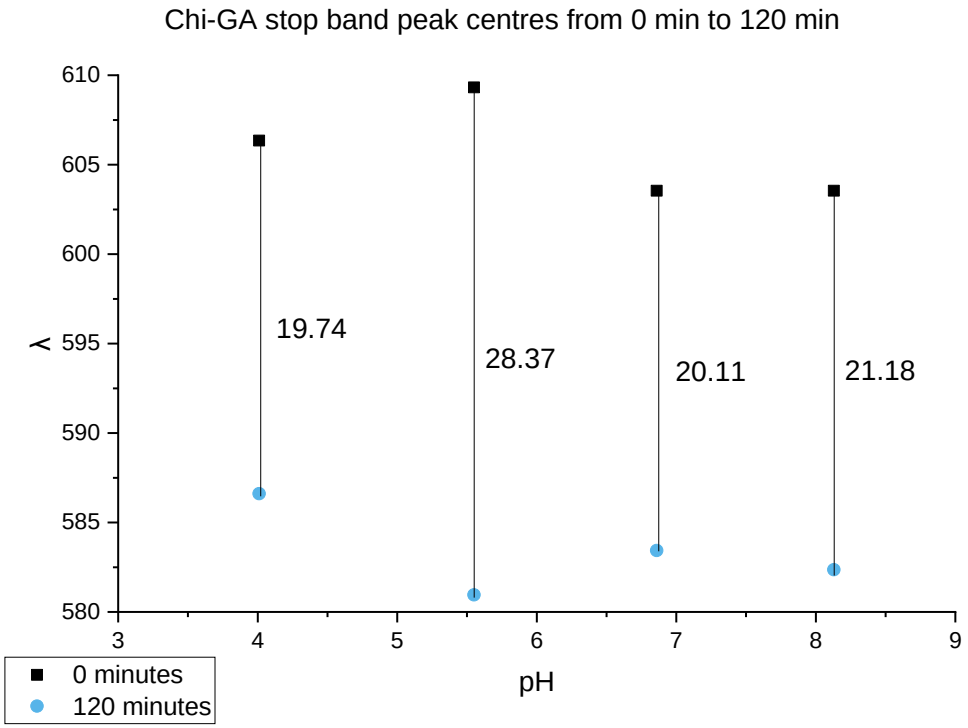


Figure 7.22: The swelling abilities of the Chi-GA (8:1) films at different pH values, recorded from 0 minutes to 120 minutes, in order to determine the swelling factors.

7.6 Conclusions

The required proof-of-concept has been achieved in that prototype device materials have been fabricated which may be used as visual indicators for pH changes. The measured response is in the form of a clear colour change while the device requires no external power supply or electronic sensors to operate.

It has been demonstrated that in the fabricated devices different film types react differently to pH which has been accounted for by considering the differences in chemistry between the films. These differences in chemistry could now be used to fine-tune the properties of the devices for a range of potential applications, including smart wound dressings but also potentially being extended to other areas where the simple, visual monitoring of pH could be beneficial, including other medical devices such as drug-release skin patches and the monitoring of water quality and pollution.

Concerning the target application underpinning this work, that of smart wound dressings to deal with chronic wound situations, it is known that the real state of chronic wounds is complex, and the pH changes observed are often quite subtle and so more research will be needed to fine tune the chitosan-based films – film thickness, concentration, cross-linkers, and photonic crystal size.

References

1. Farokhi, M., et al., *Overview of Silk Fibroin Use in Wound Dressings.* Trends in Biotechnology, 2018. **36**(9): p. 907-922.
2. Kim, H.S., et al., *Advanced drug delivery systems and artificial skin grafts for skin wound healing.* Advanced Drug Delivery Reviews, 2019. **146**: p. 209-239.
3. Derakhshandeh, H., et al., *Smart Bandages: The Future of Wound Care.* Trends in Biotechnology, 2018. **36**(12): p. 1259-1274.
4. Yergoz, F., et al., *Heparin mimetic peptide nanofiber gel promotes regeneration of full thickness burn injury.* Biomaterials, 2017. **134**: p. 117-127.
5. Zhu, Y.X., et al., *Potent laminin-inspired antioxidant regenerative dressing accelerates wound healing in diabetes.* Proceedings of the National Academy of Sciences of the United States of America, 2018. **115**(26): p. 6816-6821.
6. Hajilou, H., M.R. Farahpour, and H. Hamishehkar, *Polycaprolactone nanofiber coated with chitosan and Gamma oryzanol functionalized as a novel wound dressing for healing infected wounds.* International Journal of Biological Macromolecules, 2020. **164**: p. 2358-2369.
7. Rodriguez-Quintero, J.H., E.A. Marquez-Gutierrez, and J. Morales-Maza, *Application of a paste-type acellular dermal matrix for coverage of chronic ulcerative wounds.* Archives of Plastic Surgery-Aps, 2019. **46**(3): p. 285-286.
8. Pal, A., et al., *Early detection and monitoring of chronic wounds using low-cost, omniphobic paper-based smart bandages.* Biosensors & Bioelectronics, 2018. **117**: p. 696-705.
9. Rodrigues, M., et al., *WOUND HEALING: A CELLULAR PERSPECTIVE.* Physiological Reviews, 2019. **99**(1): p. 665-706.
10. He, J.H., et al., *Anti-oxidant electroactive and antibacterial nanofibrous wound dressings based on poly(epsilon-caprolactone)/quaternized chitosan-graft-polyaniline for full-thickness skin wound healing.* Chemical Engineering Journal, 2020. **385**.
11. Zhu, Y.N., et al., *A Multifunctional Pro-Healing Zwitterionic Hydrogel for Simultaneous Optical Monitoring of pH and Glucose in Diabetic Wound Treatment.* Advanced Functional Materials, 2020. **30**(6).

12. Li, S.X., et al., *Rapid Fabrication of Self-Healing, Conductive, and Injectable Gel as Dressings for Healing Wounds in Stretchable Parts of the Body.* Advanced Functional Materials, 2020. **30**(31).
13. Wang, J.H., et al., *pH-Switchable Antimicrobial Nanofiber Networks of Hydrogel Eradicate Biofilm and Rescue Stalled Healing in Chronic Wounds.* Acs Nano, 2019. **13**(10): p. 11686-11697.
14. Li, Q., et al., *Perspective on theoretical methods and modeling relating to electro-catalysis processes.* Chemical Communications, 2020. **56**(69): p. 9937-9949.
15. Schreml, S., et al., *The impact of the pH value on skin integrity and cutaneous wound healing.* Journal of the European Academy of Dermatology and Venereology, 2010. **24**(4): p. 373-378.
16. Mehmood, N., et al., *Applications of modern sensors and wireless technology in effective wound management.* Journal of Biomedical Materials Research Part B-Applied Biomaterials, 2014. **102**(4): p. 885-895.
17. Schneider, L.A., et al., *Influence of pH on wound-healing: a new perspective for wound-therapy?* Archives of Dermatological Research, 2007. **298**(9): p. 413-420.
18. Schmid-Wendtner, M.H. and H.C. Korting, *The pH of the skin surface and its impact on the barrier function.* Skin Pharmacology and Physiology, 2006. **19**(6): p. 296-302.
19. Percival, S.L., et al., *The effects of pH on wound healing, biofilms, and antimicrobial efficacy.* Wound Repair and Regeneration, 2014. **22**(2): p. 174-186.
20. Ninan, N., et al., *Antibacterial and Anti-Inflammatory pH-Responsive Tannic Acid-Carboxylated Agarose Composite Hydrogels for Wound Healing.* Acs Applied Materials & Interfaces, 2016. **8**(42): p. 28511-28521.
21. Kiaee, G., et al., *A pH-Mediated Electronic Wound Dressing for Controlled Drug Delivery.* Advanced Healthcare Materials, 2018. **7**(18).
22. Ahmadian, Z., et al., *A Hydrogen-Bonded Extracellular Matrix-Mimicking Bactericidal Hydrogel with Radical Scavenging and Hemostatic Function for pH-Responsive Wound Healing Acceleration.* Advanced Healthcare Materials, 2021. **10**(3).

23. Dargaville, T.R., et al., *Sensors and imaging for wound healing: A review.* Biosensors & Bioelectronics, 2013. **41**: p. 30-42.
24. Hennink, W.E. and C.F. van Nostrum, *Novel cross-linking methods to design hydrogels.* Advanced Drug Delivery Reviews, 2012. **64**: p. 223-236.
25. Gupta, P., K. Vermani, and S. Garg, *Hydrogels: from controlled release to pH-responsive drug delivery.* Drug Discovery Today, 2002. **7**(10): p. 569-579.
26. Sharpe, L.A., et al., *Therapeutic applications of hydrogels in oral drug delivery.* Expert Opinion on Drug Delivery, 2014. **11**(6): p. 901-915.
27. Peppas, N.A., et al., *Hydrogels in pharmaceutical formulations.* European Journal of Pharmaceutics and Biopharmaceutics, 2000. **50**(1): p. 27-46.
28. Sridhar, V. and K. Takahata, *A hydrogel-based passive wireless sensor using a flex-circuit inductive transducer.* Sensors and Actuators a-Physical, 2009. **155**(1): p. 58-65.
29. Saghazadeh, S., et al., *Drug delivery systems and materials for wound healing applications.* Advanced Drug Delivery Reviews, 2018. **127**: p. 138-166.
30. Tamayol, A., et al., *Flexible pH-Sensing Hydrogel Fibers for Epidermal Applications.* Advanced Healthcare Materials, 2016. **5**(6): p. 711-719.
31. Lin, S.T., et al., *Stretchable Hydrogel Electronics and Devices.* Advanced Materials, 2016. **28**(22): p. 4497-4505.
32. Singer, A.J. and R.A.F. Clark, *Mechanisms of disease - Cutaneous wound healing.* New England Journal of Medicine, 1999. **341**(10): p. 738-746.
33. Falanga, V., *OCCLUSIVE WOUND DRESSINGS - WHY, WHEN, WHICH.* Archives of Dermatology, 1988. **124**(6): p. 872-877.
34. Kalliainen, L.K., et al., *Topical oxygen as an adjunct to wound healing: a clinical case series.* Pathophysiology, 2003. **9**(2): p. 81-87.
35. Parsons, D., et al., *Silver antimicrobial dressings in wound management: A comparison of antibacterial, physical, and chemical characteristics.* Wounds-a Compendium of Clinical Research and Practice, 2005. **17**(8): p. 222-232.
36. Lloyd, A.W., *Interfacial bioengineering to enhance surface biocompatibility.* Medical device technology, 2002. **13**(1): p. 18-21.
37. Mayet, N., et al., *A Comprehensive Review of Advanced Biopolymeric Wound Healing Systems.* Journal of Pharmaceutical Sciences, 2014. **103**(8): p. 2211-2230.

38. Azuma, K., et al., *RETRACTION: Chitin, Chitosan, and Its Derivatives for Wound Healing: Old and New Materials (Retraction of Vol 6, Pg 104, 2015).* Journal of Functional Biomaterials, 2018. **9**(2).
39. Moura, L.I.F., et al., *Chitosan-based dressings loaded with neurotensin-an efficient strategy to improve early diabetic wound healing.* Acta Biomaterialia, 2014. **10**(2): p. 843-857.
40. Jayakumar, R., et al., *Biomaterials based on chitin and chitosan in wound dressing applications.* Biotechnology Advances, 2011. **29**(3): p. 322-337.
41. Ng, V.W.L., et al., *Antimicrobial hydrogels: A new weapon in the arsenal against multidrug-resistant infections.* Advanced Drug Delivery Reviews, 2014. **78**: p. 46-62.
42. Koehler, J., F.P. Brandl, and A.M. Goepferich, *Hydrogel wound dressings for bioactive treatment of acute and chronic wounds.* European Polymer Journal, 2018. **100**: p. 1-11.
43. Sadri, M., et al., *New wound dressing polymeric nanofiber containing green tea extract prepared by electrospinning method.* Fibers and Polymers, 2015. **16**(8): p. 1742-1750.
44. Abrigo, M., S.L. McArthur, and P. Kingshott, *Electrospun Nanofibers as Dressings for Chronic Wound Care: Advances, Challenges, and Future Prospects.* Macromolecular Bioscience, 2014. **14**(6): p. 772-792.
45. Kayani, A., et al., *Effect of Varying Amount of Polyethylene Glycol (PEG-600) and 3-Aminopropyltriethoxysilane on the Properties of Chitosan based Reverse Osmosis Membranes.* International Journal of Molecular Sciences, 2021. **22**(5).
46. Salmah, H., A. Faisal, and H. Kamarudin, *Chemical Modification of Chitosan-Filled Polypropylene (PP) Composites: The Effect of 3-Aminopropyltriethoxysilane on Mechanical and Thermal Properties.* International Journal of Polymeric Materials, 2011. **60**(7): p. 429-440.
47. Zargar, V., M. Asghari, and M. Afsari, *Gas separation properties of swelled nanocomposite chitosan membranes cross-linked by 3-aminopropyltriethoxysilane.* International Journal of Environmental Science and Technology, 2019. **16**(1): p. 37-46.
48. Uragami, T., et al., *STRUCTURE OF CHEMICALLY-MODIFIED CHITOSAN MEMBRANES AND THEIR CHARACTERISTICS OF PERMEATION AND*

SEPARATION OF AQUEOUS-ETHANOL SOLUTIONS. Journal of Membrane Science, 1994. **88**(2-3): p. 243-251.

49. Nematidil, N., et al., *Synthesis and characterization of Schiff-base based chitosan-g-glutaraldehyde/NaMMTNPs-APTES for removal Pb2+ and Hg2+ ions.* Carbohydrate Polymers, 2019. **222**.
50. Sivaselvi, K. and P. Ghosh, *Characterization of modified Chitosan thin film.* Materials Today-Proceedings, 2017. **4**(2): p. 442-451.
51. Pemble, O.J., et al., *A Slot-Die Technique for the Preparation of Continuous, High-Area, Chitosan-Based Thin Films.* Polymers, 2021. **13**(10): p. 13.
52. Beppu, M.M., et al., *Cross-linking of chitosan membranes using glutaraldehyde: Effect on ion permeability and water absorption.* Journal of Membrane Science, 2007. **301**(1-2): p. 126-130.
53. Cao, W.L., et al., *Effects of the degree of deacetylation on the physicochemical properties and Schwann cell affinity of chitosan films.* Journal of Biomaterials Applications, 2005. **20**(2): p. 157-177.
54. Ahmed, S.I.S., *Chitosan : derivatives, composites and applications.* 2017.
55. Ottoy, M.H., K.M. Varum, and O. Smidsrod, *Compositional heterogeneity of heterogeneously deacetylated chitosans.* Carbohydrate Polymers, 1996. **29**(1): p. 17-24.
56. Olsen, R., et al., *in Chitin and Chitosan: Sources, Chemistry, Biochemistry, Physical Properties and Applications" edited by G. Skjak-Brack, T. Anthonsen and PA Sandford*. 1989, Elsevier Applied Science, New York.
57. Sanford, P. and G. Hutchings, *Chitosan--a natural, cationic biopolymer: commercial applications.* Progress in biotechnology, 1987.
58. Ryan, C., *The design, synthesis and characterization of chitosan-based interpenetrating polymer networks and thin film systems*, M.E. Pemble and M. Bardosova, Editors. 2018, University College Cork: College of Science, Engineering and Food Science, University College Cork.
59. Furumi, S., H. Fudouzi, and T. Sawada, *Dynamic photoswitching of micropatterned lasing in colloidal crystals by the photochromic reaction.* Journal of Materials Chemistry, 2012. **22**(40): p. 21519-21528.
60. Fudouzi, H., et al. *Smart photonic coating as a new visualization technique of strain deformation of metal plates*. in *Conference on Sensors and Smart*

Structures Technologies for Civil, Mechanical, and Aerospace Systems. 2012. San Diego, CA.

61. Pemble, M.E. and M. Bardosova. *Colloidal Photonic Crystal Architectures for Advanced Light Management Applications*. in *Nanomaterials and Nanoarchitectures*. 2015. Dordrecht: Springer Netherlands.
62. Jones, E.M., C.A. Cochrane, and S.L. Percival, *The Effect of pH on the Extracellular Matrix and Biofilms.* Advances in Wound Care, 2015. **4**(7): p. 431-439.
63. Dissemond, J., et al., *pH values in chronic wounds. Evaluation during modern wound therapy.* Hautarzt, 2003. **54**(10): p. 959-965.
64. Karaaslan, A.M., M.A. Tshabalala, and G. Buschle-Diller, *WOOD HEMICELLULOSE/CHITOSAN-BASED SEMI-INTERPENETRATING NETWORK HYDROGELS: MECHANICAL, SWELLING AND CONTROLLED DRUG RELEASE PROPERTIES.* Bioresources, 2010. **5**(2): p. 1036-1054.
65. Frick, J.M., et al., *Influence of Glutaraldehyde Cross-linking and Alkaline Post-treatment on the Properties of Chitosan-Based Films.* Journal of Polymers and the Environment, 2018. **26**(7): p. 2748-2757.
66. Tasselli, F., et al., *Mechanical, swelling and adsorptive properties of dry-wet spun chitosan hollow fibers cross-linked with glutaraldehyde.* Reactive & Functional Polymers, 2013. **73**(1): p. 218-223.

8. Conclusions and suggestions for further work

8.1 Summary of work presented, and conclusions drawn

The work presented in this thesis provides an insight into the ease with which chitosan may be incorporated into a range of films using additional reagents designed to modify certain properties of the films including mechanical strength, sorptive behaviour and anti-microbial properties. In doing so, the thesis has shown the potential for the use of chitosan-based films in a range of important industrial and environmental applications. As examples, the thesis shows how certain types of films could be used to extract dangerous metal ions from solution and also presents a new type of pH sensor based on a combination of the properties of chitosan films combined with those of colloidal photonic crystals. Overall, it is hoped that the thesis may inspire others to study chitosan-based films with similar types of applications in mind.

The material chitosan is a commercially available polysaccharide that is non-toxic and biodegradable. It may be produced via the deacetylation of chitin, sourced from crustacean shells or fungi, using chemical or enzymatic industrial processes. With an active -NH_2 group, it is acid soluble and may interact with other electrostatic species both cationically and anionically. These electrostatic interactions are the core mechanisms on which this material may be used in sorption, antibacterial and swelling applications. The amino group also allows the molecule to form Interpenetrating Polymer Networks (IPNs) and polymer blends with other materials. By combining chitosan with another polymer, the properties may be improved to enhance mechanical strength, absorption ability or antibacterial activity. Chitosan has been used in many biomedical and environmental fields and is one of the most versatile natural macromolecules due to its amphiphilic nature.

One of the most popular ways to prepare samples of chitosan is in a film from a hydrogel base. As it is soluble in mildly acidic aqueous solutions, it can easily be combined with other soluble polymers or reagents such as tetraethyl-orthosilicate (TEOS), glutaraldehyde solution (GA), 3-aminopropyltriethoxysilane (APTES) and polyacrylamide solution (PAM). For TEOS and APTES, they must undergo a hydrolysis and condensation reaction to form a siloxane polymer network, then combine with chitosan via hydrogen bonds to produce an IPN. The reaction of cross-linking chitosan with GA is a single step process called a covalent Schiff base reaction.

Schiff bases are synthesized from an aliphatic or aromatic amine and a carbonyl compound by nucleophilic addition, followed by a de-hydration to generate an imine. This results in a Schiff base bridge between chitosan chains. Chitosan and PAM form a polymer blend by simple mixing the two compounds in a mildly acidic solution. Crosslinking these materials together can change and improve the base mechanical properties of chitosan, allowing it to be applied in different fields.

The mechanical strengths and ductility of these films were ranked and equated directly with their proposed structure as interpreted from the FT-IR analysis. Not surprisingly, the chitosan-GA films were found to possess the highest initial yield points suggesting that cross-linking does increase the robustness of the films while also decreasing their ductility, making them somewhat brittle. The next highest mean yield strengths are those associated with chitosan-TEOS IPN and the polymer blend, chitosan-PAM, with these samples showing essentially identical average behaviour in terms of mean yields strength, being consistent with an overall increase in robustness that arises from the mixing of two polymeric systems. Next in this series comes the IPN chitosan-APTES which might be expected to have reduced cross linking between the siloxane chains as a result of replacing an ethoxy group with an aminopropoxy ligand. With the improvement of the mechanical properties of the chitosan-based films, the next step was to develop a method of producing these films quickly and cheaply without affecting the chemistry. The usual drop cast method of synthesising films takes approximately one day to complete.

A stand-alone study which has been published in the journal Polymers (A slot-die technique for the preparation of continuous, high-area, chitosan-based thin films, Oliver J Pemble, Maria Bardosova, Ian M Povey, Martyn E Pemble, 2021/5/13, Polymers, Volume 13, Issue, 10, Pages 1566) was presented to addresses the potential of mass production. The high-volume manufacturability of the various chitosan-based films was achieved via a novel slot-die casting technique. Chitosan hydrogel blends were extruded through a doctor blade nozzle onto a PET substrate and dried within 1 or 2 hours. Although the equipment used to produce these films in a manner which would be suitable for roll-to-roll applications has not been optimised, this study serves to provide the proof-of-concept that chitosan-based films could be made more efficiently. Interestingly in this simple study, no evidence of the influence of the

direction of travel of the films during deposition on mechanical properties was observed, suggesting that such properties arise on the much smaller molecular level.

The first application study of the films produced here, namely that of the ability (or otherwise) of the chitosan-based films to adsorb radioactive technetium pertechnetate $^{99m}TcO_4^-$ ions from solution was the focus of chapter 5. Performed in collaboration with colleagues from the Faculty of Natural Sciences, Comenius University in Bratislava, this study highlights the issues associated with dangerous radioactive materials that can find their way into water supplies after being released as by-products from the nuclear industry. The chitosan-glutaraldehyde films showed the greatest ability to adsorb the technetium pertechnetate ions at pH4. As demonstrated in Chapter 3, these particular films show the highest mechanical strength but tend to be somewhat brittle. Using models based on the Langmuir and Freundlich isotherms, the data for the uptake of the $^{99m}TcO_4^-$ ions from solution were evaluated and it was concluded that while it was most likely that a Langmuir-type, monolayer-based adsorption process was in operation, a multilayer (Freundlich-type) process could not be ruled out.

The next application presented was a preliminary antimicrobial study performed together with colleagues from the Microbiology Department at University College Cork. This study was chosen since one of the emerging applications of chitosan-based films at the time of writing is that of wound dressings, where bacteriological control would be paramount. Both Gram-positive and Gram-negative bacterial attachment and growth were studied. It was concluded that the results were very pH-dependent but overall, in terms of both attachment and growth, the chitosan-tetraethyl-orthosilicate IPN was the most active material. Furthermore, as a result of their composition and structure the chitosan-glutaraldehyde films do not appear to possess any anti-bacterial activity in comparison with the other films studied. Since some antimicrobial activity could also be reflected in the film being less likely to exhibit fouling due to the formation of biofilms, the ability of these films to adsorb the technetium pertechnetate ions must be offset against such considerations when evaluating their efficacy to be used as filters, as the mechanisms of ion adsorption and antibacterial activity are similar. Indeed, the anionic surface of a bacterial cell wall may act similarly to a pertechnetate anion when interacting with positively charged chitosan.

Finally the last study builds on some of the ideas discussed in chapters 3, 5 and 6 to produce a prototype would dressing material which shows the ability to respond visually to a change in pH. A fluctuating pH is a common occurrence for chronic wounds specifically. This work, performed in the laboratories of Prof Hiroshi Fudouzi at NIMS, Tsukuba, Japan, uses photonic crystal technology to produce a visual colour change when the films are distorted as a consequence of pH-induced swelling. With considerable assistance provided by Dr Tomas Kohoutek, the various films produced here were shown to give a distinct red to green colour change which required no externally applied power supply to be seen. Thus, the required proof-of-concept has been achieved and the prototype devices have been fabricated which may be used as visual indicators for pH changes. While again also a preliminary study, the potential of such layered structures based on photonic crystals and chitosan-based films has been clearly demonstrated by this work.

8.2 Suggestions for further work

As chitosan is such a diverse material, it can be combined with many different types of reagents. For future studies, it would be interesting to create more composite films from materials with varied functional groups and study their properties. Mechanical strength, solubility, adsorption efficiency, antibacterial activity and swelling capacity may be improved by creating new polymer blends or IPNs.

For the slot-die technique, scaling up the procedure to become a true roll-to-roll method would increase the production of films rapidly. Factors such as temperature and pressure may be altered to dry the films more efficiently. Optimising the formulation of the chitosan hydrogel to set faster without sacrificing the mechanical stability of the final product would also be a viable option for industrial implementation.

A wider range of toxic materials should be studied as to their ability to be adsorbed onto chitosan-based films. Testing true water samples from a contaminated environment would provide interesting results for the adsorption efficiency of chitosan. In addition, re-useable chitosan-based filters should be evaluated for a range of toxic dyes and heavy metals in water samples.

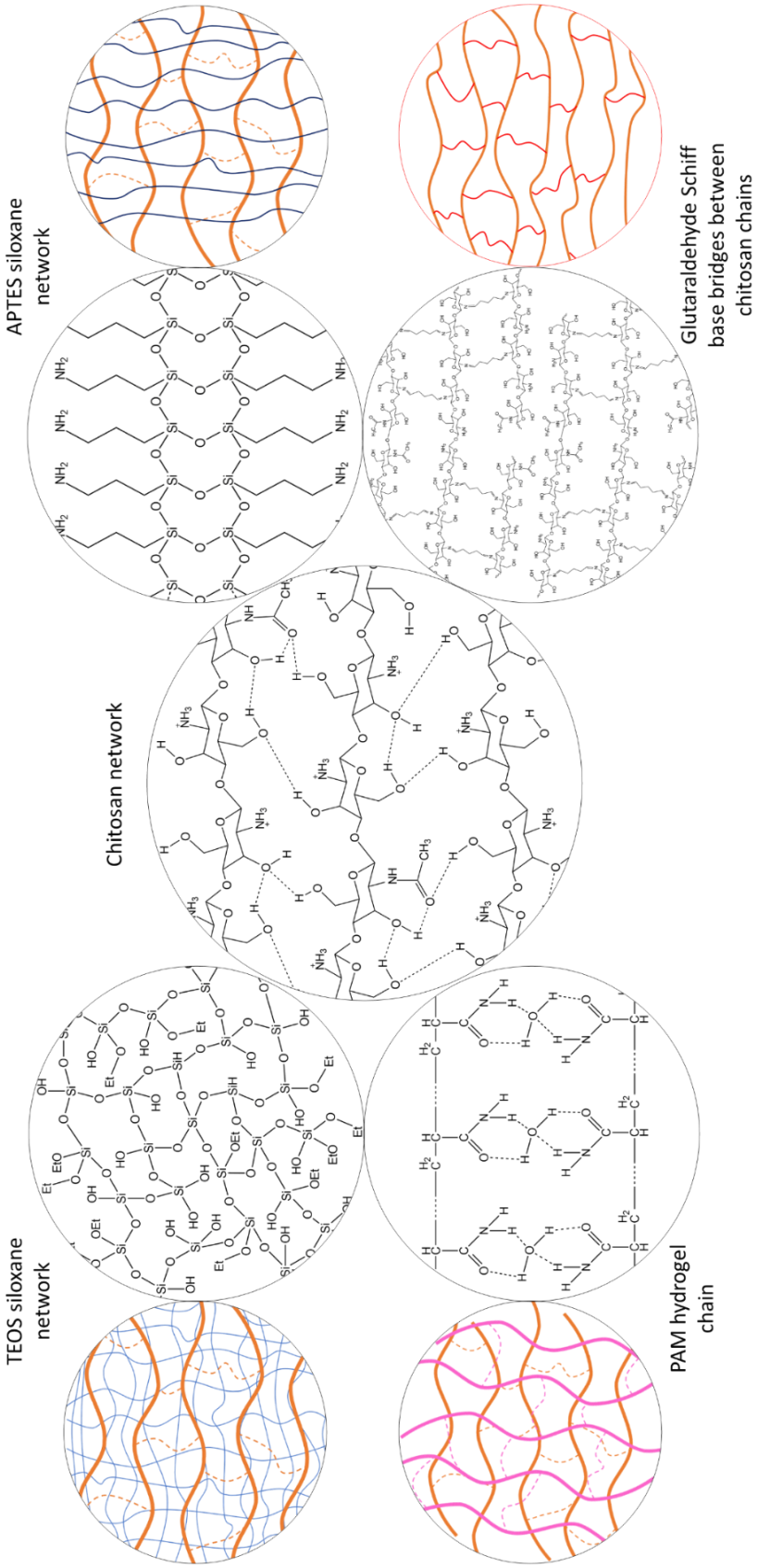
A more detailed antimicrobial study must be performed on chitosan samples combined with known bacteriostatic agents. The environment of the bacterial growth must also

be considered. It would be beneficial for bacterial growth to be supressed in areas relating to food packaging, medical device production or infection control situations.

The wound dressing prototype may be improved through a number of different approaches. The ability to tune the colour changes that can be induced by distorting the photonic crystals should be thoroughly evaluated. The photonic crystal stop band may be controlled by altering the size of the particles, spacing between particles and infilling material. The type of chitosan polymer blend can be altered to maximise the swelling ability of the dry film. The design of the sensor device could be modified to cause a bigger stop band peak centre variation, allowing for easier reading of the colour change. Additionally, these factors must consider what the final product may appear like, as a wearable medical device.

Appendix

A.1 Chapter 2: Schematic of all chitosan film composites



A.2 Chapter 5: Swelling percentages

Individual plots of percentage swelling as measured by mass gain vs sample area (size) showing the statistical parameters calculated.

	S [cm^2]	m_{01} [g]	m_1 [g]	m_{02} [g]	m_2 [g]	Q_{eq} [%]
Chi-TEOS 1:1	2	9.8311	9.6366	0.0052	0.1754	98.02
	3	9.9234	9.4082	0.005	0.1121	94.81
	4	9.9492	9.3148	0.0059	0.2833	93.62
	5	9.9285	9.3095	0.0092	0.1998	93.77
	S [cm^2]	m_{01} [g]	m_1 [g]	m_{02} [g]	m_2 [g]	Q_{eq} [%]
Chi-APTES 2:1	2	9.8276	9.3106	0.0069	0.5038	94.74
	3	9.9608	8.7277	0.0065	0.6478	87.62
	4	9.9085	8.8473	0.0061	0.6589	89.29
	5	9.9332	8.7282	0.0178	0.6314	87.87
	S [cm^2]	m_{01} [g]	m_1 [g]	m_{02} [g]	m_2 [g]	Q_{eq} [%]
Chi-GA 8:1	2	9.848	9.7738	0.0076	0.0636	99.25
	3	9.9437	9.3909	0.0102	0.0337	94.44
	4	9.9082	9.3381	0.0129	0.0479	94.25
	5	9.9438	9.2143	0.0186	0.062	92.66
	S [cm^2]	m_{01} [g]	m_1 [g]	m_{02} [g]	m_2 [g]	Q_{eq} [%]
Chi-PAM 1:1	2	9.8518	9.8134	0.001	0.0143	99.61
	3	9.9228	9.1328	0.0118	0.2434	92.04
	4	9.9908	9.1586	0.0115	0.1966	91.67
	5	9.9309	9.2022	0.0098	0.2209	92.66

Table A.1: Data obtained for the calculation of percentage swelling Q% for all samples following immersion into a solution of pH = 4 for 60 minutes. Where m_{01} is the weight of H_2O before swelling, m_{02} is the mass of the films before swelling, m_1 is the weight of H_2O after swelling, and m_2 is the mass of swelled films.

A.2.1 Chi-TEOS (1:1)

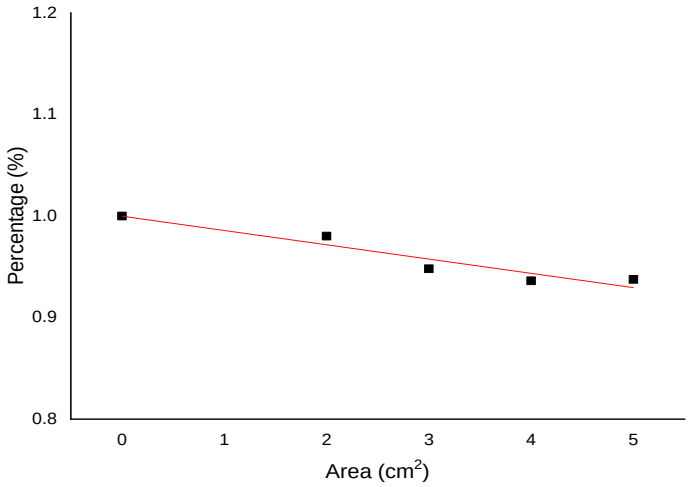
Equation	y = a + b * x		
Weight	Non		
Residual sum of Squares	0.000284		
Pearson's r	-0.95479		
R-Square	0.91163		
		Value	**Standard Error**
Chi-TEOS 1:1	**Intercept**	0.99983	0.00831
	Slope	-0.01407	0.00253

Table A.2: Swelling percentage verses area of film sample for Chi-TEOS (1:1)

A.2.2 Chi-APTES (2:1)

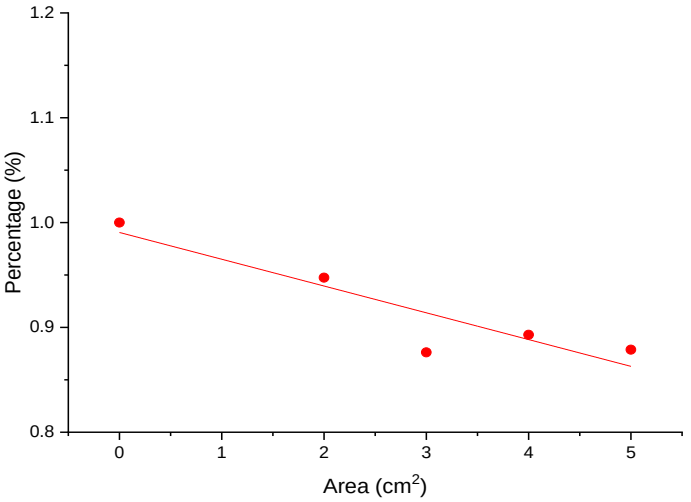
Equation	y = a + b * x		
Weight	Non		
Residual sum of Squares	0.00185		
Pearson's r	-0.91624		
R-Square	0.8395		
		Value	**Standard Error**
Chi-APTES 2:1	**Intercept**	0.99057	0.02119
	Slope	-0.02555	0.00645

Table A.3: Swelling percentage verses area of film sample for Chi-APTES (2:1)

A.2.3 Chi-GA (8:1)

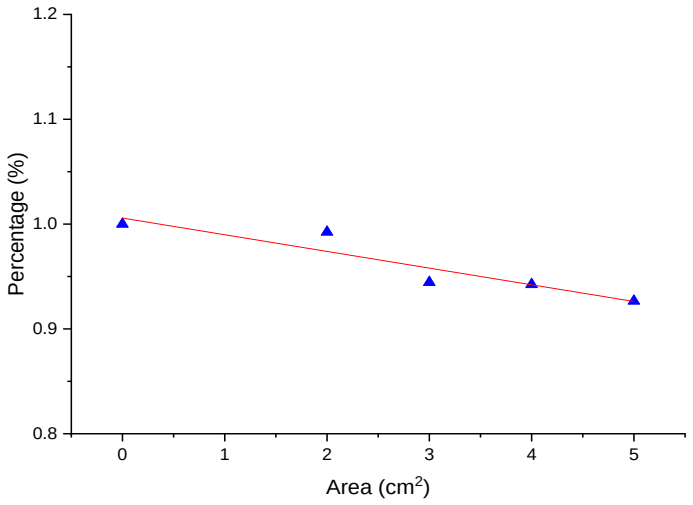
Equation	y = a + b * x		
Weight	Non		
Residual sum of Squares	0.000562		
Pearson's r	-0.93251		
R-Square	0.86957		
		Value	**Standard Error**
Chi-GA 8:1	**Intercept**	1.00575	0.01169
	Slope	-0.01591	0.00365

Table A.4: Swelling percentage verses area of film sample for Chi-GA (8:1)

A.2.4 Chi-PAM (1:1)

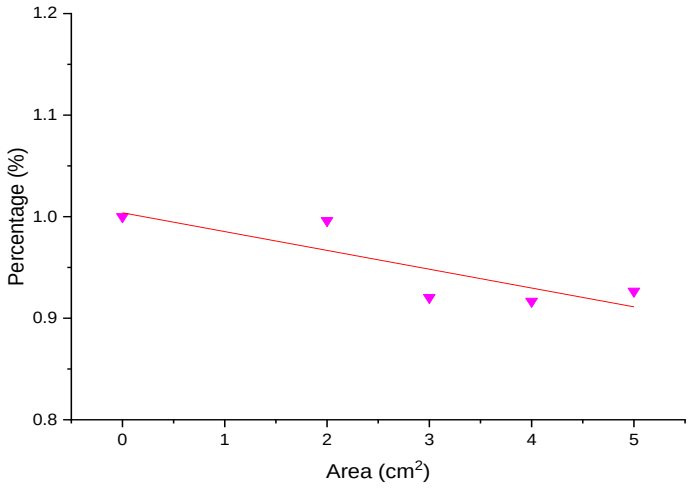
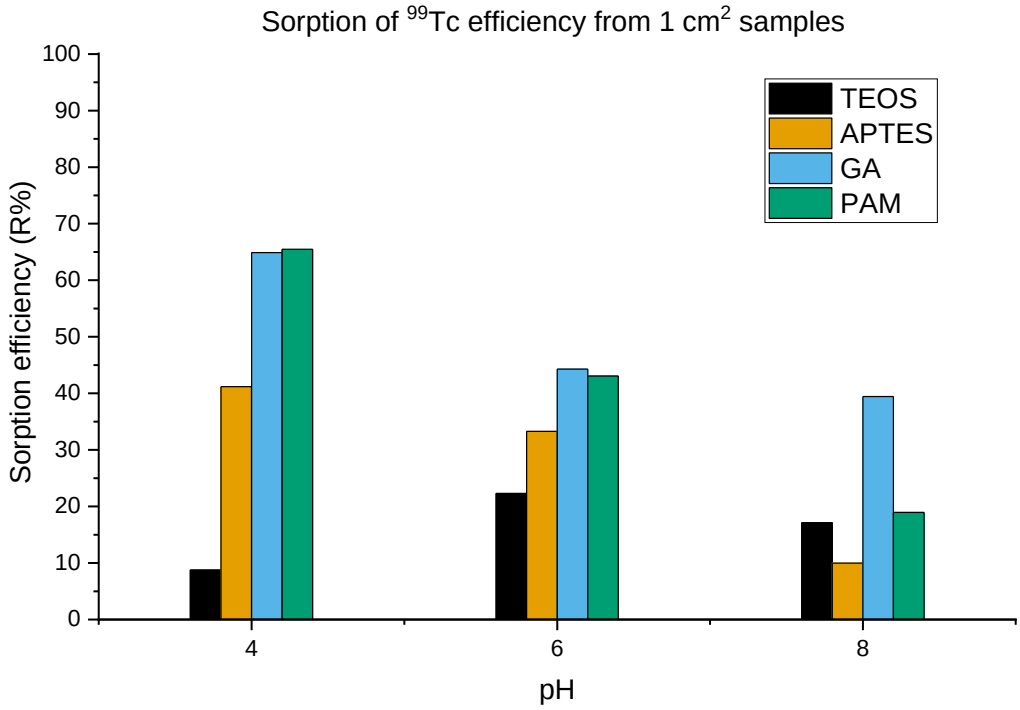
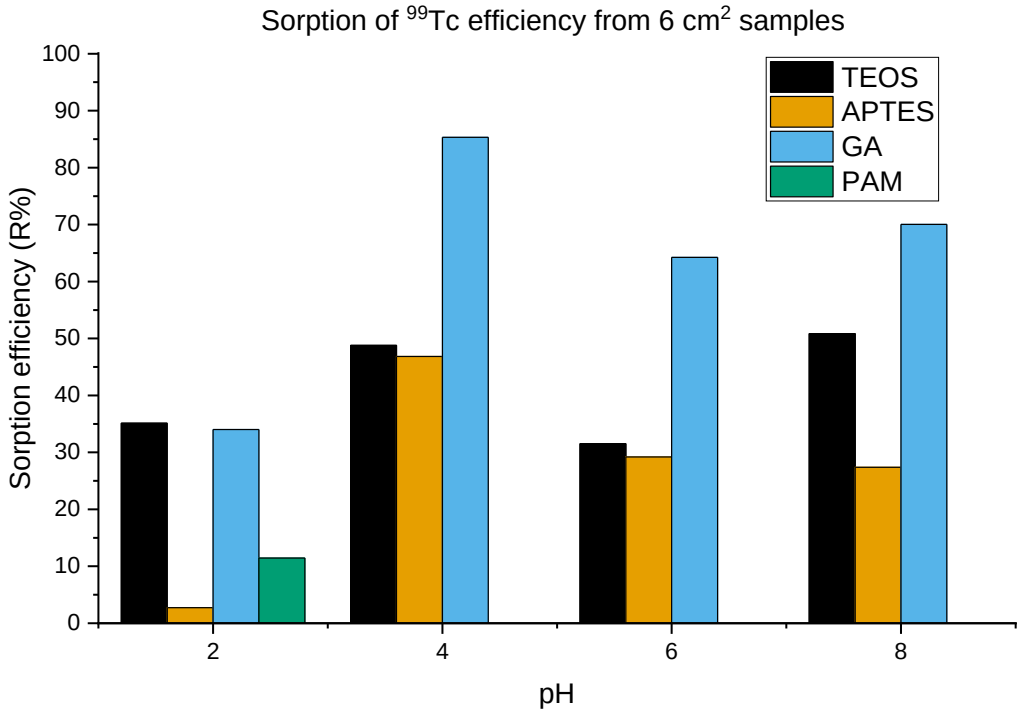
Equation	y = a + b * x		
Weight	Non		
Residual sum of Squares	0.00206		
Pearson's r	-0.84357		
R-Square	0.71162		
		Value	**Standard Error**
Chi-PAM 1:1	**Intercept**	1.00384	0.02238
	Slope	-0.01853	0.00681

Table A.5: Swelling percentage verses area of film sample for Chi-PAM (1:1)

A.3 Chapter 5: Sorption efficiency on sample size and pH

A.3.1 Sample size

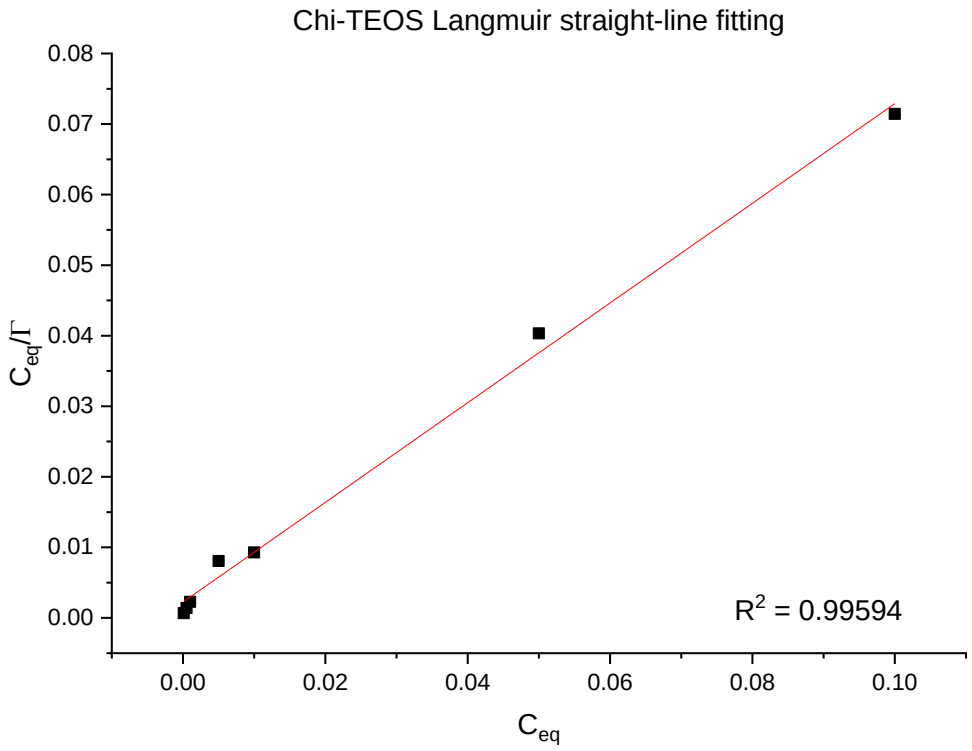




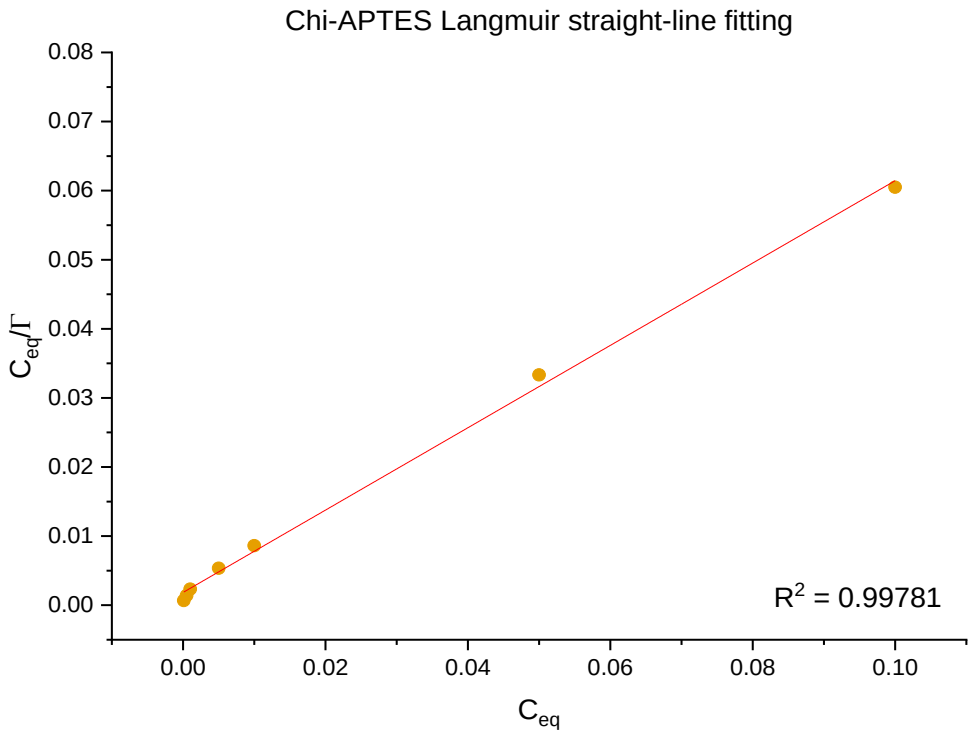
A.4 Chapter 5: Langmuir and Freundlich straight-line graphs

A.4.1 Langmuir straight-line graphs

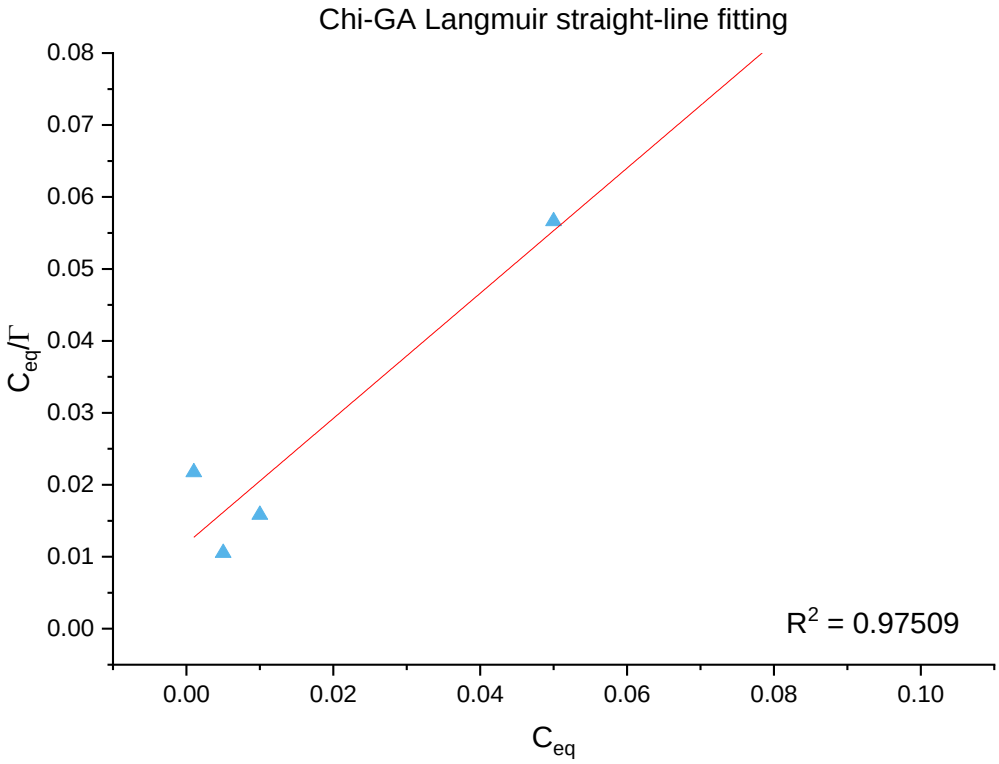
A.4.1.1 Chi-TEOS



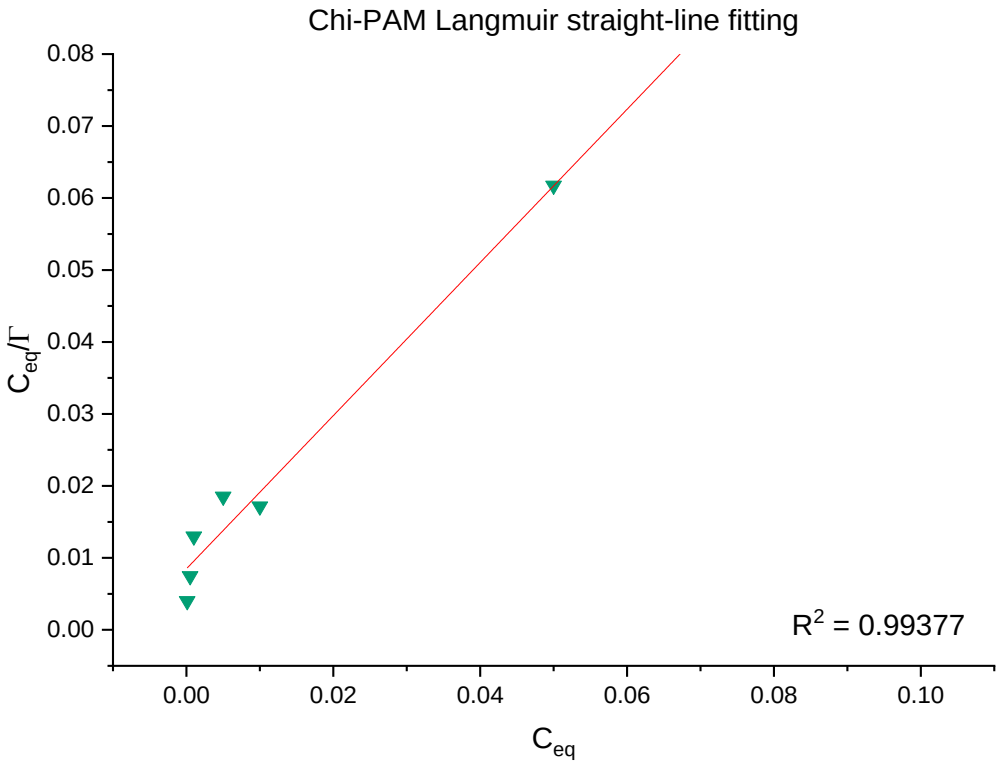
A.4.1.2 Chi-APTES



A.4.1.3 Chi-GA

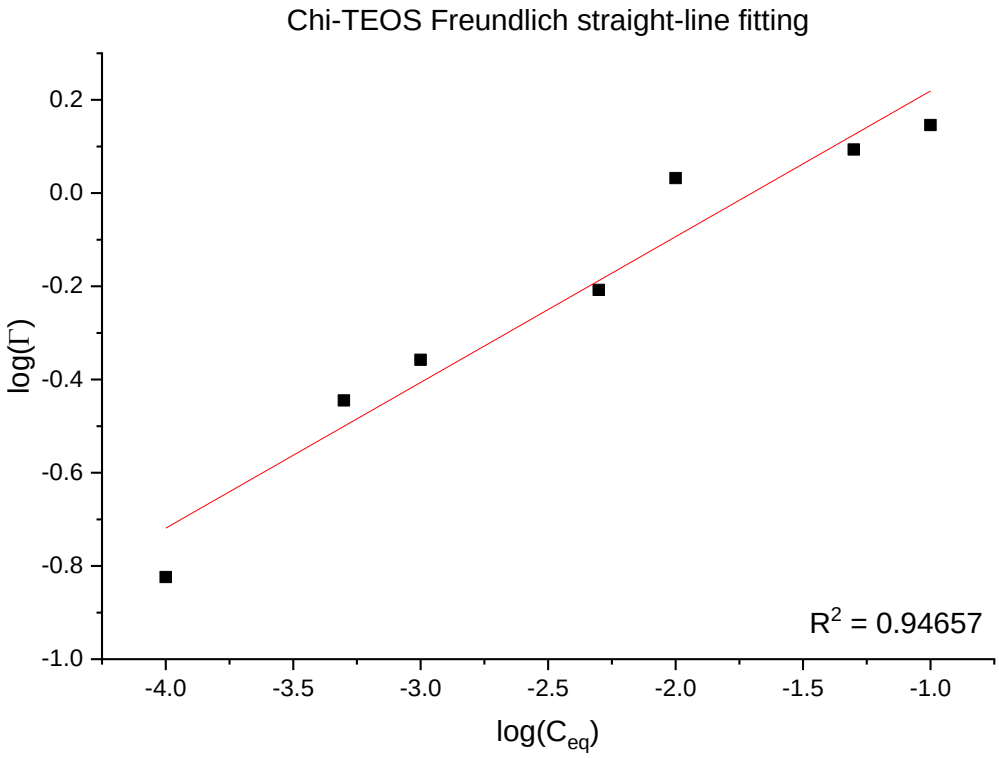


A.4.1.4 Chi-PAM

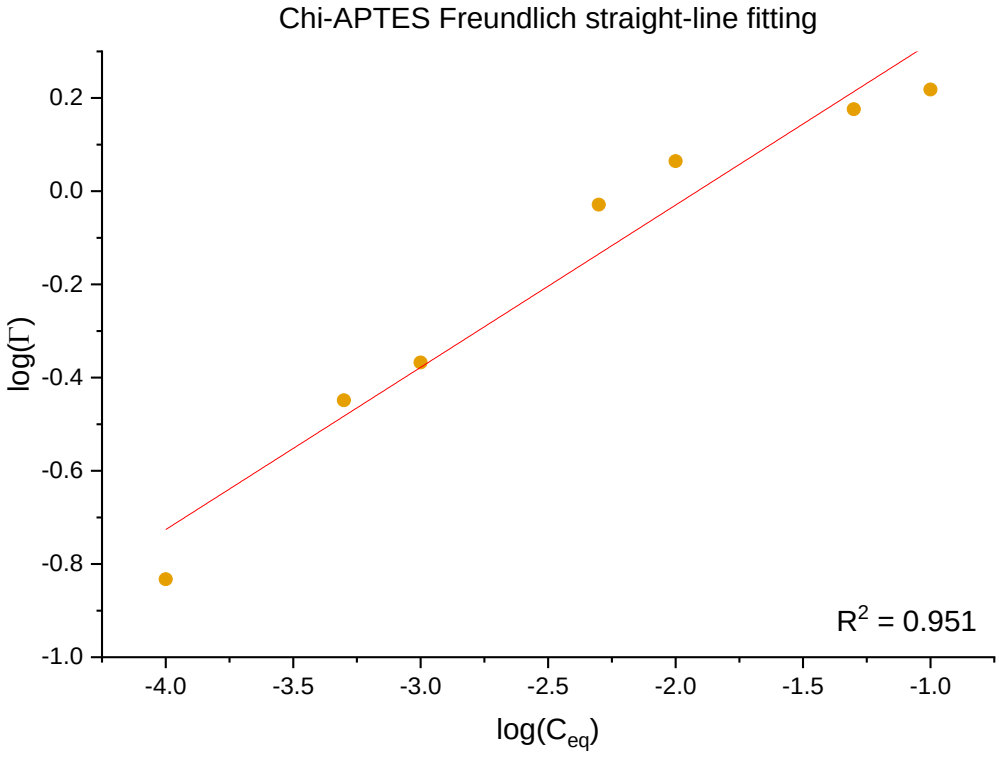


A.4.2 Freundlich straight-line graphs

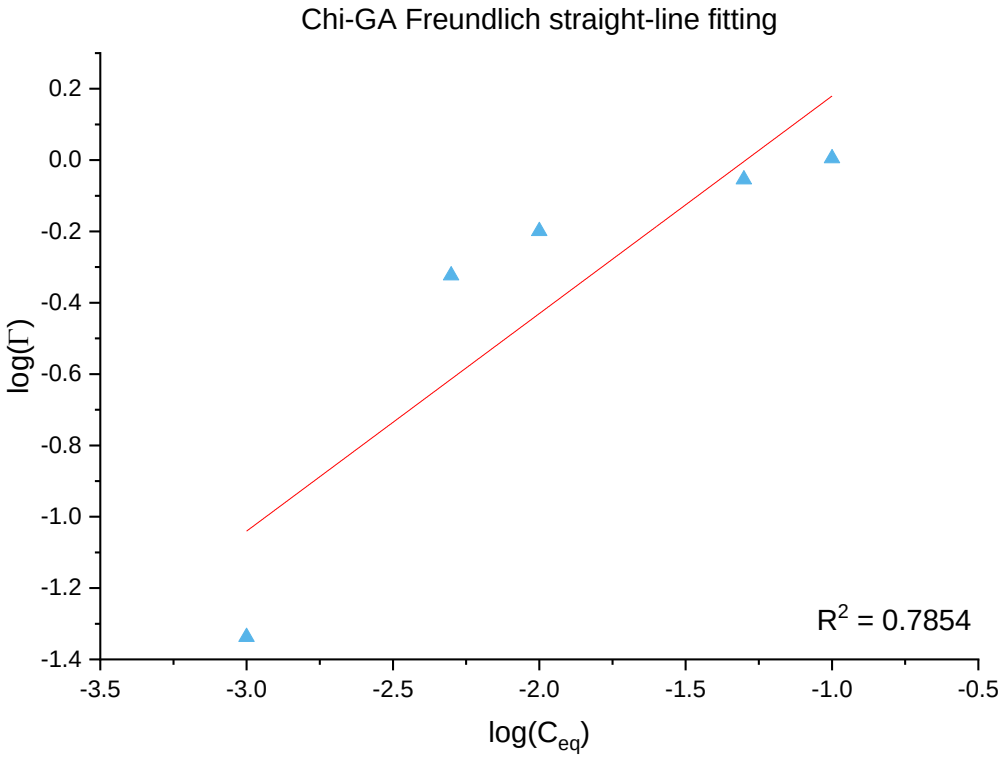
A.4.2.1 Chi-TEOS



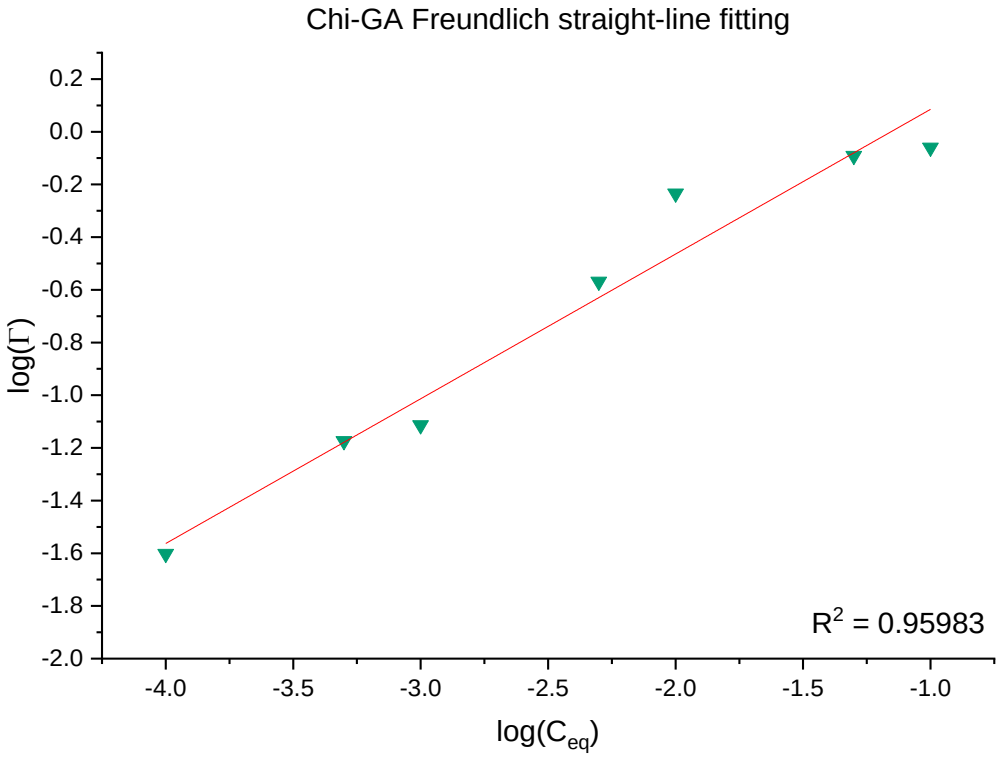
A.4.2.2 Chi-APTES



A.4.2.3 Chi-GA



A.4.2.4 Chi-PAM



A.5 Chapter 6: Optical Density measurements

A.5.1 Chi-TEOS 1:1

Bacteria	Sample	Growth OD_{600}	Growth corrected	Attachment OD_{595}	Attachment corrected	pH
E. Coli	Control	0.018	-	0.749	-	6.5
	Sample 1	0.019	0.001	1.511	0.717	6.5
	Sample 2	0.005	-0.013	1.014	0.220	6.5
	STD	0.007	0.007	0.248	0.248	0
S. Aureus	Control	0.018	-	0.911	-	7.0
	Sample 1	0.446	0.428	1.251	0.340	5.5
	Sample 2	0.326	0.308	1.318	0.407	5.5
	STD	0.060	0.060	0.033	0.033	0

A.5.2 Chi-APTES 2:1

Bacteria	Sample	Growth OD_{600}	Growth corrected	Attachment OD_{595}	Attachment corrected	pH
E. Coli	Control	0.061	-	0.240	-	7.0
	Sample 1	1.844	1.783	2.256	2.016	8.0
	Sample 2	1.011	0.95	1.608	1.368	8.0
	STD	0.416	0.416	0.324	0.324	0
S. Aureus	Control	-0.043	-	1.061	-	7.0
	Sample 1	0.000	0	0.766	-0.295	6.5
	Sample 2	0.004	0	0.955	-0.106	6.5
	STD	0.002	0	0.095	0.095	0

A.5.3 Chi-PAM 1:1

Bacteria	Sample	Growth OD_{600}	Growth corrected	Attachment OD_{595}	Attachment corrected	pH
E. Coli	Control	0.311	-	1.077	-	6.0
	Sample 1	0.243	-0.068	1.215	0.138	6.0
	Sample 2	0.234	0.077	1.324	0.247	6.0
	STD	0.004	0.004	0.054	0.054	0
S. Aureus	Control	0.668	-	1.077	-	6.5
	Sample 1	0.771	0.103	1.031	-0.046	6.5
	Sample 2	0.892	0.224	0.977	-0.100	6.5
	STD	0.061	0.061	0.027	0.027	0

A.5.4 Chi-GA 8:1

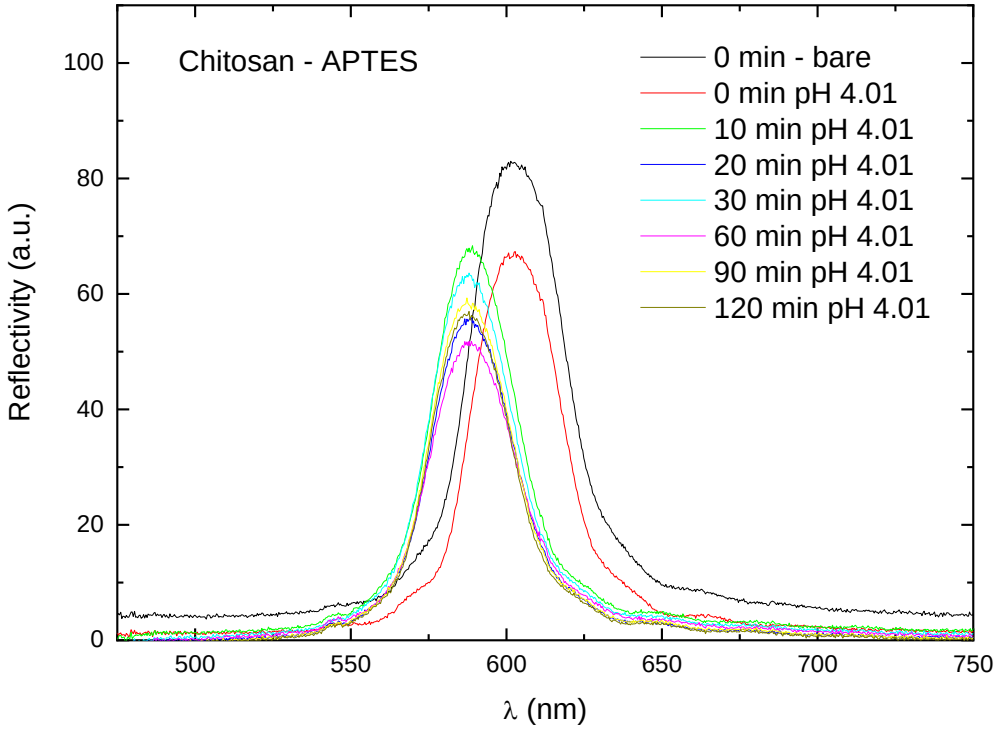
Bacteria	Sample	Growth OD_{600}	Growth corrected	Attachment OD_{595}	Attachment corrected	pH
E. Coli	Control	-0.005	-	0.042	-	6.0
	Sample 1	2.079	2.079	0.703	0.661	8.0
	Sample 2	2.032	2.032	2.432	2.390	8.0
	STD	0.024	0.024	0.865	0.865	0
S. Aureus	Control	-0.036	-	0.158	-	7.0
	Sample 1	1.632	1.632	1.409	1.251	6.0
	Sample 2	1.742	1.742	0.240	0.082	6.0
	STD	0.055	0.055	0.585	0.585	0

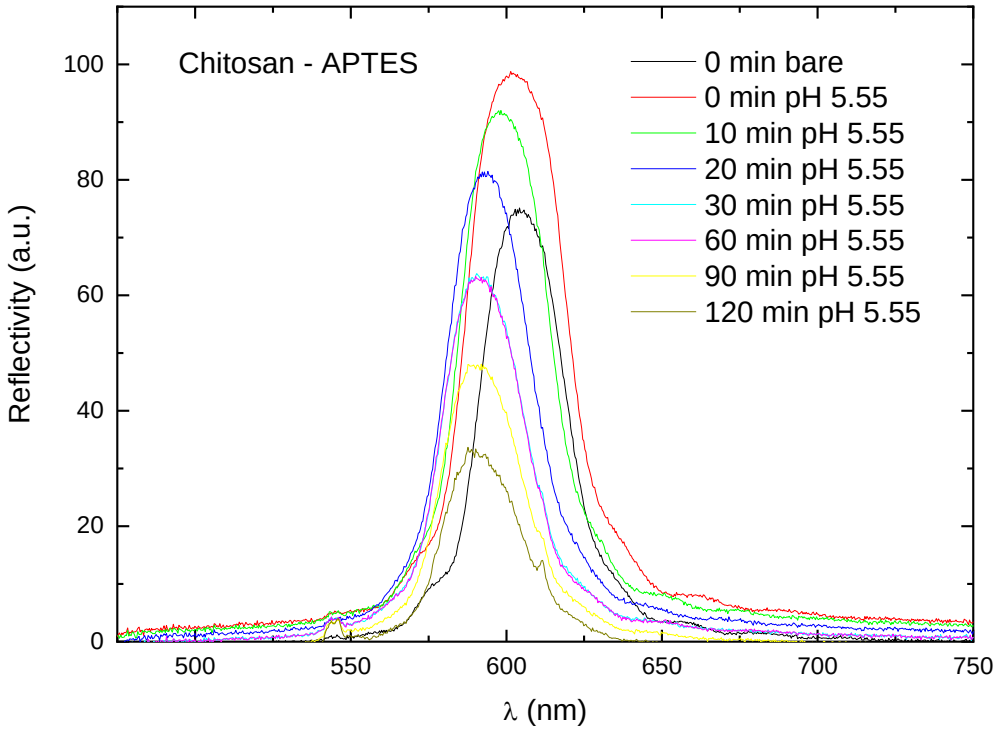
Note: the corrected values are calculated by:

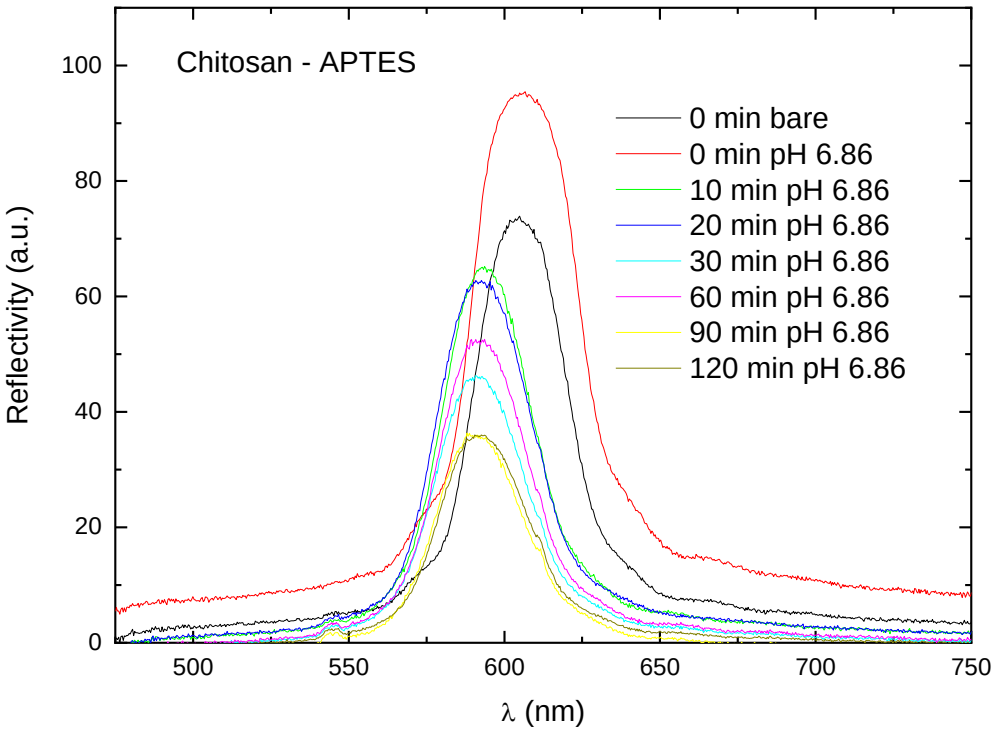
Attachment/Growth (sample) – Attachment/Growth (control)

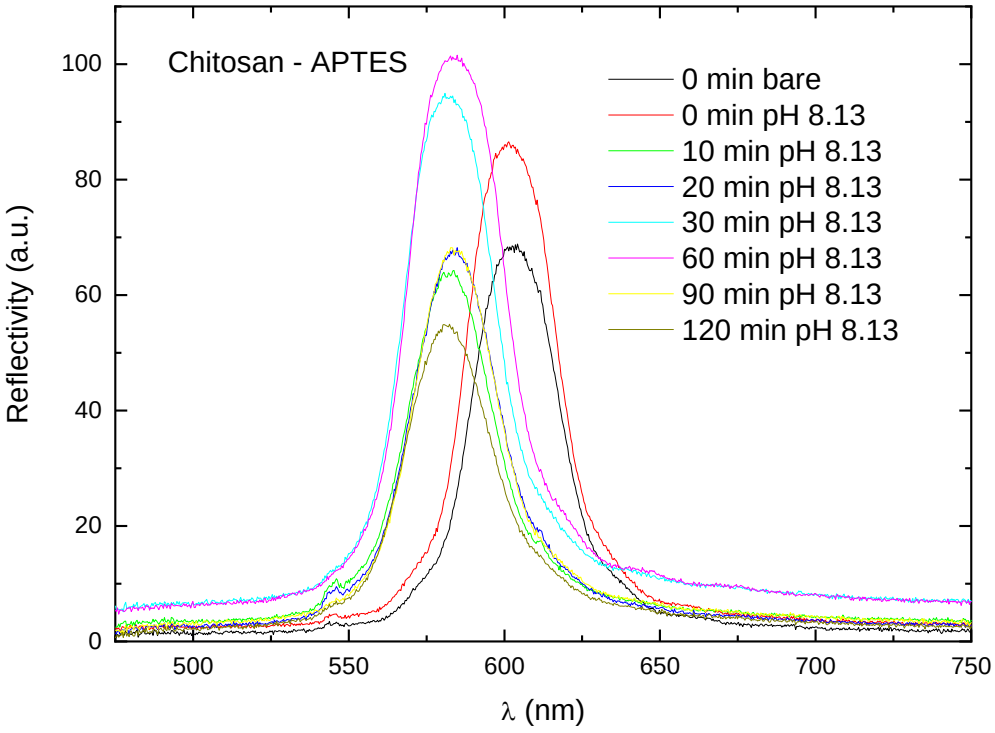
A.6 Chapter 7: Stop band peak centres

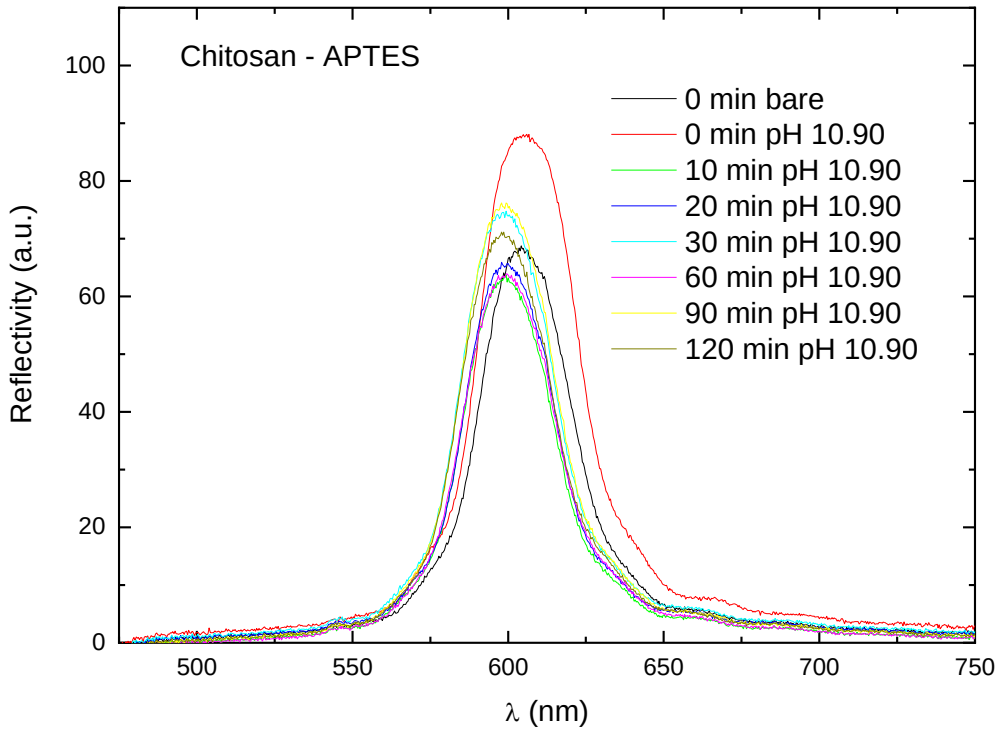
A.6.1 Chi-APTES



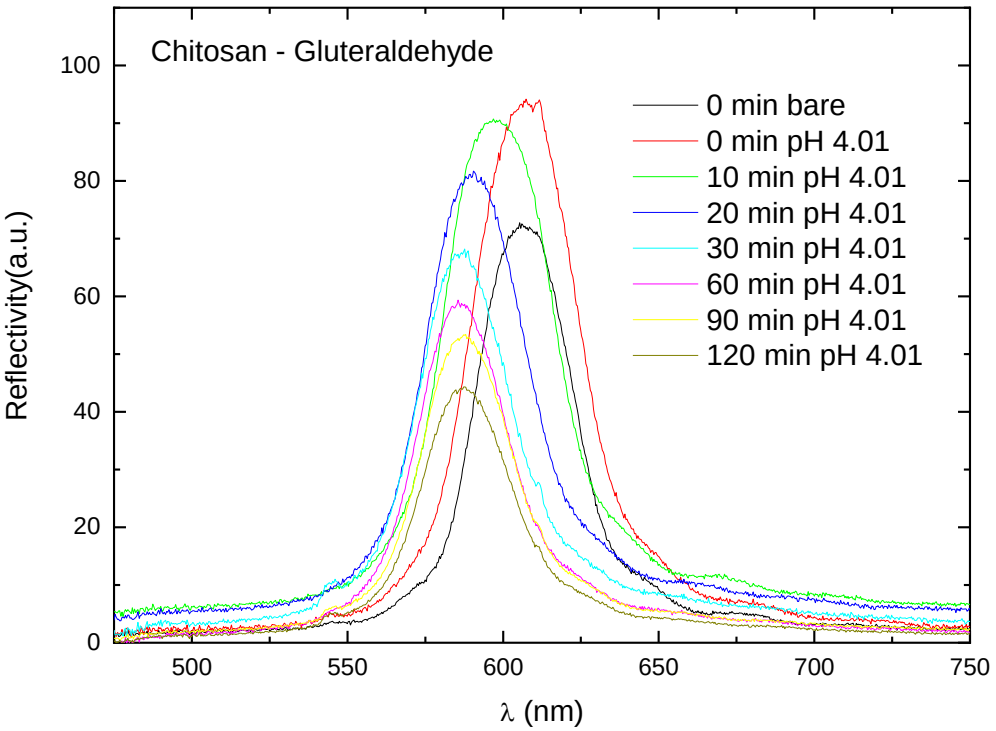


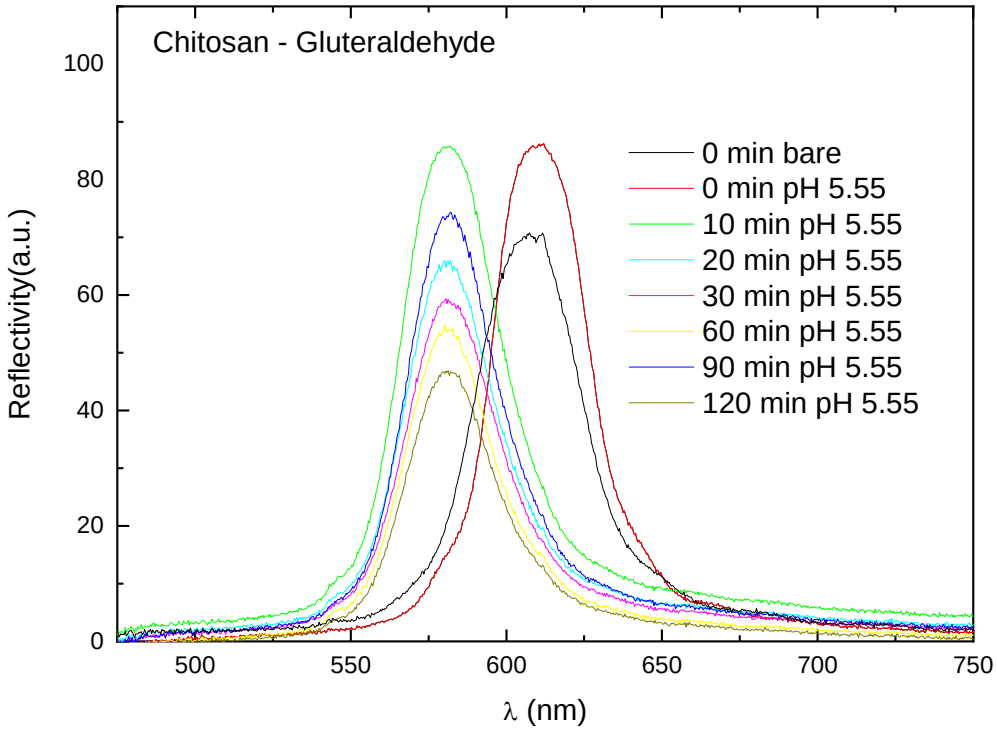

Chitosan - APTES
0 min bare
0 min pH 6.86
10 min pH 6.86
20 min pH 6.86
30 min pH 6.86
60 min pH 6.86
90 min pH 6.86
120 min pH 6.86
Reflectivity (a.u.)
λ (nm)
0
20
40
60
80
100
500
550
600
650
700
750

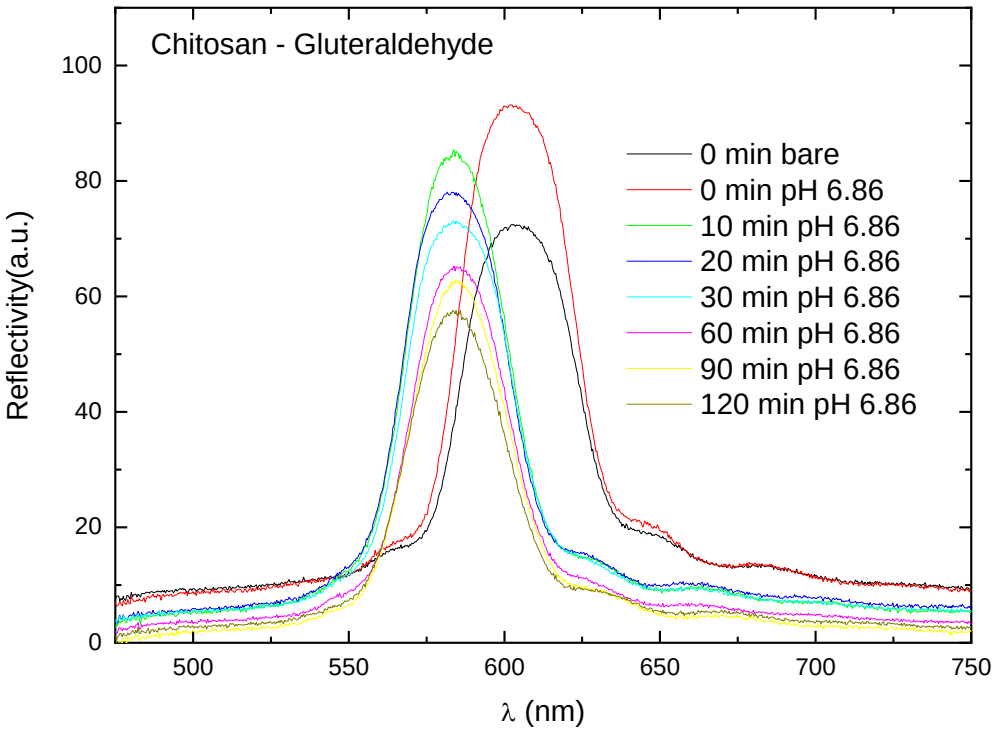

Chitosan - APTES
0 min bare
0 min pH 8.13
10 min pH 8.13
20 min pH 8.13
30 min pH 8.13
60 min pH 8.13
90 min pH 8.13
120 min pH 8.13
Reflectivity (a.u.)
λ (nm)
0
20
40
60
80
100
500
550
600
650
700
750

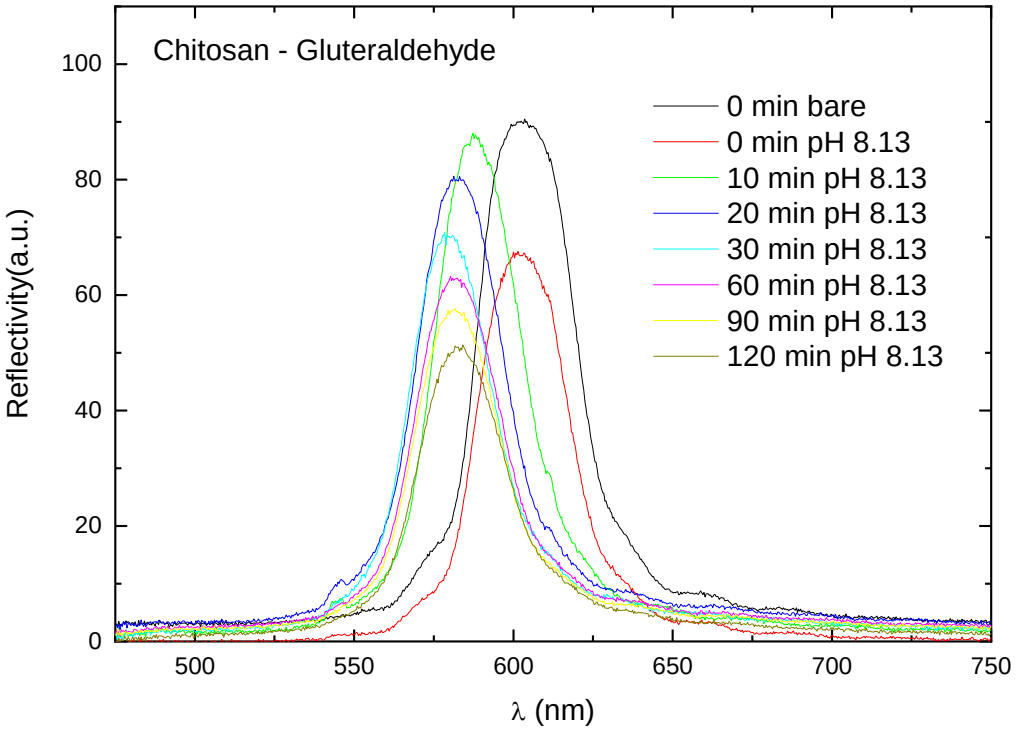

Chitosan - APTES
0 min bare
0 min pH 10.90
10 min pH 10.90
20 min pH 10.90
30 min pH 10.90
60 min pH 10.90
90 min pH 10.90
120 min pH 10.90
Reflectivity (a.u.)
λ (nm)
0
20
40
60
80
100
500
550
600
650
700
750

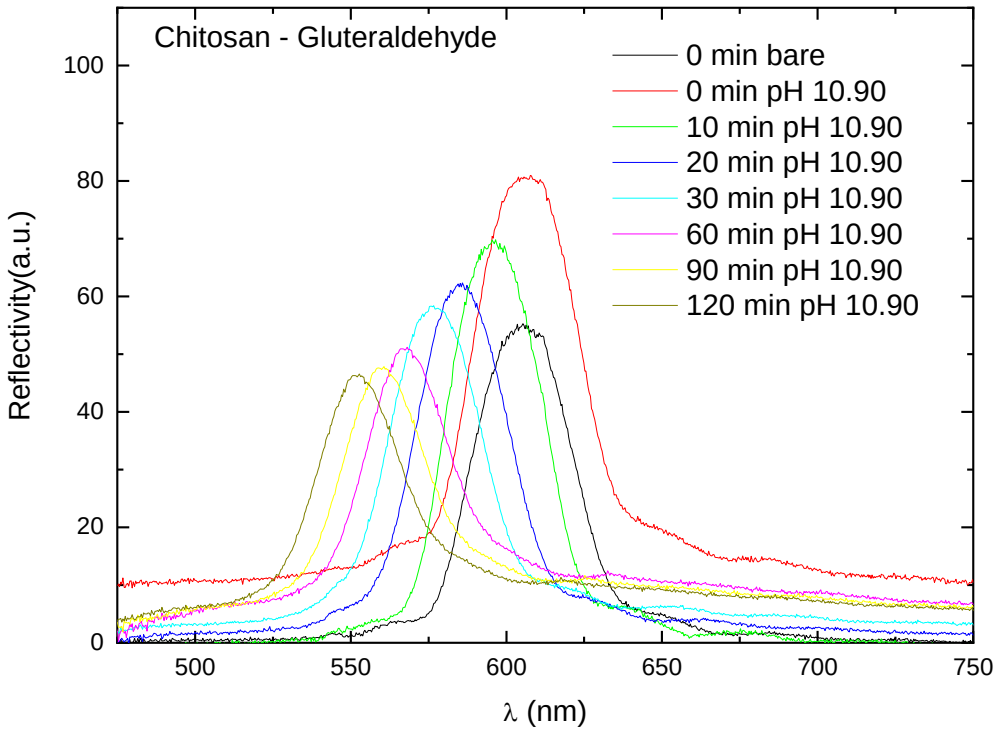
A.6.2 Chi-GA


Chitosan - Gluteraldehyde
0 min bare
0 min pH 4.01
10 min pH 4.01
20 min pH 4.01
30 min pH 4.01
60 min pH 4.01
90 min pH 4.01
120 min pH 4.01
Reflectivity(a.u.)
λ (nm)
0
20
40
60
80
100
500
550
600
650
700
750


Chitosan - Gluteraldehyde
0 min bare
0 min pH 5.55
10 min pH 5.55
20 min pH 5.55
30 min pH 5.55
60 min pH 5.55
90 min pH 5.55
120 min pH 5.55
Reflectivity(a.u.)
λ (nm)
0
20
40
60
80
100
500
550
600
650
700
750


Chitosan - Gluteraldehyde
Reflectivity(a.u.)
λ (nm)
0 min bare
0 min pH 6.86
10 min pH 6.86
20 min pH 6.86
30 min pH 6.86
60 min pH 6.86
90 min pH 6.86
120 min pH 6.86


Chitosan - Gluteraldehyde
Reflectivity(a.u.)
λ (nm)
0 min bare
0 min pH 8.13
10 min pH 8.13
20 min pH 8.13
30 min pH 8.13
60 min pH 8.13
90 min pH 8.13
120 min pH 8.13


Chitosan - Gluteraldehyde
0 min bare
0 min pH 10.90
10 min pH 10.90
20 min pH 10.90
30 min pH 10.90
60 min pH 10.90
90 min pH 10.90
120 min pH 10.90
Reflectivity(a.u.)
λ (nm)
0
20
40
60
80
100
500
550
600
650
700
750